Global impacts of aircraft emissions on air quality and nitrogen deposition

Domingos de Azevedo Quadros, F.

DOI
10.4233/uuid:b54561bd-1141-429f-83e3-a94b966c7a07

Publication date
2024

Document Version
Final published version

Citation (APA)
Domingos de Azevedo Quadros, F. (2024). *Global impacts of aircraft emissions on air quality and nitrogen deposition*. [Dissertation (TU Delft), Delft University of Technology]. https://doi.org/10.4233/uuid:b54561bd-1141-429f-83e3-a94b966c7a07

Important note
To cite this publication, please use the final published version (if applicable).
Please check the document version above.

Global impacts of aircraft emissions on air quality and nitrogen deposition

Global impacts of aircraft emissions on air quality and nitrogen deposition

Dissertation

for the purpose of obtaining the degree of doctor
at Delft University of Technology,
by the authority of the Rector Magnificus prof. dr. ir. T.H.J.J. van der Hagen,
chair of the Board for Doctorates,
to be defended publicly on
Wednesday 17 January 2024 at 12:30 o'clock

by

Flávio DOMINGOS DE AZEVEDO QUADROS

Master of Science in Aeronautical and Mechanical Engineering,
Instituto Tecnológico de Aeronáutica, Brazil,
born in São Paulo, Brazil.

This dissertation has been approved by the promotors.

Composition of the doctoral committee:

Rector Magnificus,	chairperson
Prof. dr. ir. M. Snellen,	Delft University of Technology, promotor
Dr. I.C. Dedoussi,	Delft University of Technology, copromotor
Independent members:	
Prof. dr. N. Bellouin	Sorbonne Université, France, University of Reading, United Kingdom
Prof. dr. V. Grewe,	Delft University of Technology, German Aerospace Center (DLR), Germany
Prof. dr. ir. H.W.J. Russchenberg,	Delft University of Technology
Dr. R.P. Dwight,	Delft University of Technology
Dr. ir. B.F. Lopes dos Santos,	Delft University of Technology

Keywords: Aviation, air quality, air pollution, aircraft emissions, nitrogen deposition, intercontinental pollution, public health, atmospheric chemical transport model

An electronic version of this dissertation is available at
http://repository.tudelft.nl/.

Tell me what it's like to live without
curiosity, without awe. To sail
on clear water, rolling your eyes
at the kelp reefs swaying
beneath you, ignoring the flicker
of mermaid scales in the mist,
looking at the world and feeling
only boredom. To stand
on the precipice of some wild valley,
the eagles circling, a herd of caribou
booming below, and to yawn
with indifference. To discover
something primordial and holy.
To have the smell of the earth
welcome you to everywhere.
To take it all in, and then,
to reach for your knife.

Letter to the Person Who Carved His Initials into
the Oldest Living Longleaf Pine in North America

Matthew Olzmann

Contents

Summary

Global passenger air traffic has doubled in the 13 years prior to 2019, and is expected to double again over the next 20 years or so. Growing demand for aviation is met by a corresponding increase in jet fuel being burned by aircraft, releasing multiple pollutants into the atmosphere. Besides disturbing the Earth's radiative balance, these emissions also lead to excessive deposition of reactive nitrogen, and to a degradation of air quality. Anthropogenic nitrogen deposition damages vulnerable ecosystems, while degraded air quality is associated with increases in human mortality rates. These last two environmental impacts can be very localized, but, owing to the high altitude of emissions, they also occur over intercontinental distances. This thesis aims to evaluate the magnitude of air quality and nitrogen deposition due to emissions from civil fixed-wing aircraft at a global scale, and how these impacts might change in the coming decades.

This is achieved by estimating present-day aircraft emissions globally, projecting them into future using the latest industry forecasts, then using a chemical transport model (namely GEOS-Chem) to simulate atmospheric processes leading to impacts at the ground-level. Simulations were performed for the years 2005, 2019, and 2040 considering multiple scenarios for aircraft emissions, non-aviation emissions, and meteorological fields. By using a consistent methodology across simulations, this thesis presents a complete picture of how much aircraft emissions impact air quality and nitrogen deposition globally in the present, and how different variables internal and external to aviation can change that impact in the future.

A spatially resolved bottom-up global inventory of aircraft emissions in the years 2017–2020 was created using a list of flights provided by both a commercial and an open network of telemetry receivers. This improved on the then most recently available inventory which was for the year 2005. Another improvement was the use of actually realized flights, as opposed to previous inventories which were largely built on flight schedule databases with only localized radar data being incorporated. The produced inventory had a total amount of NO_x emissions ($NO + NO_2$) for the year 2019 that was 59% and 72% higher compared to two previous estimates for 2005. This work also enabled the first assessment of COVID-19 pandemic impacts on global aircraft emissions, finding that 48% less fuel was burned in 2020 than what was forecast before the pandemic.

Present-day aircraft emissions were projected up to the year 2050 using technology and region-specific air traffic forecasts from the aviation industry. Despite technological and operational improvements, all scenarios considered had continuously increasing fuel burn and NO_x emissions, including a 113% NO_x increase between 2018 and 2050 for the baseline scenario. Contributing to this is the expectation that the observed trend of increasing engine pressure ratios continues, driven by designs optimizing for fuel efficiency.

Air quality impacts of aircraft emissions were first investigated by a set of atmospheric simulations for 2005, in which these emissions were perturbed alternatively in different world regions. This allowed, for the first time, to isolate the extent to which multiple re-

gional factors drive the air quality responses to aircraft emissions. Global health impacts of emissions released over Europe were found to be 45% and 50% larger than those of the same amount of emissions released over Asia and North America, respectively. This was associated both with atmospheric composition favorable to $PM_{2.5}$ formation over Europe and with prevailing winds directing ground-level impacts of cruise emissions towards highly populated regions in Asia. The intercontinental character of air pollution from aircraft was underscored by the finding that 73% and 88% of health impacts from emissions over Europe and North America, respectively, occur outside the region of emission.

The newly produced aircraft emissions inventories were then used in a series of simulations in the atmospheric chemical transport model, quantifying air quality and health impacts for the years 2019 and 2040. The effects of different future non-aviation emissions and meteorology were evaluated by a set of atmospheric simulations with different input parameters, enabling an estimation of the uncertainty in future projections of aviation's air quality impacts associated with these factors. Aircraft emissions in 2019 were estimated to lead to a total of 33 900, 79 500, and 2700 additional premature deaths that year due to $PM_{2.5}$, ozone, and NO_2, respectively. This is a higher estimate compared to previous studies, due to a combination of more recent (and thus higher) aircraft emissions, large sensitivity of ground-level ozone to cruise altitude NO_x emissions, and a stronger association between long-term ozone exposure and mortality according to recent epidemiological estimates. Health impacts increase overall in the year 2040, by 76% relative to 2019 in the baseline future scenario, and by 28% (low) and 135% (high) when considering different projections of 2040 aircraft emissions. Changing population and non-aviation emissions from the baseline SSP2-4.5 scenario to six other future scenarios resulted in -1% to +5% global aircraft-attributable mortality.

The atmospheric chemical transport model was also used to quantify for the first time the reactive nitrogen deposition attributed to aircraft emissions at a global scale. Simulations performed for the years 2005 and 2019 showed that aircraft-attributable nitrogen deposition increased globally by 76% between the two years. In 2019, aircraft represented 1.2% of total nitrogen deposition worldwide from all sources, with the average values over Asia, Europe, and North America being 0.66%, 1.13%, and 1.61%, respectively. Landing and takeoff emissions were responsible for 8% of aircraft-attributable deposition globally, and between 16–32% over most land in regions with high aviation activity. Impacts from full-flight emissions were spatially widespread, as suggested by the figure of 56% of aircraft-attributable deposition occurring over water.

In conclusion, the modeling studies described in this thesis provide further evidence that aircraft emissions are increasing globally, and that those emissions have a significant impact on air quality, leading to increased mortality, as well as contributing to excessive nitrogen deposition. New insights were gained by isolating the effects of several variables on these impacts, such as non-aviation emissions, large-scale atmospheric transport patterns, population spatial distribution, and spatial and temporal changes in global aircraft emissions. With the goal of mitigating impacts to make air travel more sustainable, future research efforts should continue to update the estimates of aviation's environmental impacts at a global scale, incorporating improvements — as they become available — concerning aircraft emissions quantification, atmospheric modeling and epidemiological understanding of pollution.

Samenvatting

Het globale passagiersluchtverkeer is van 2006 tot 2019 verdubbeld en zal naar verwachting de komende twintig jaar nogmaals verdubbelen. Als gevolg van deze groeiende vraag naar luchtvaart wordt er meer brandstof verbrand door vliegtuigen, waardoor meerdere verontreinigende stoffen in de atmosfeer terechtkomen. Deze emissies verstoren niet alleen de stralingsbalans van de aarde, maar leiden ook tot overmatige afzetting van reactieve stikstof en tot een verslechtering van de luchtkwaliteit. Antropogene stikstofdepositie beschadigt kwetsbare ecosystemen, terwijl een verminderde luchtkwaliteit gepaard gaat met een stijging van de menselijke sterftecijfers. Deze milieueffecten kunnen zeer lokaal zijn, maar vanwege de grote hoogte van de emissies vinden ze ook plaats over intercontinentale afstanden. Dit proefschrift evalueert de omvang van de luchtkwaliteit en stikstofdepositie als gevolg van de uitstoot van civiele vliegtuigen met vaste vleugels op wereldschaal te evalueren, en ook hoe deze gevolgen de komende decennia zouden kunnen veranderen.

Dit wordt bereikt door de huidige vliegtuigemissies wereldwijd te schatten, deze in de toekomst te projecteren met behulp van de nieuwste industriële voorspellingen en vervolgens een chemisch transportmodel (namelijk GEOS-Chem) te gebruiken om atmosferische processen te simuleren die tot effecten op grondniveau leiden. Er zijn simulaties uitgevoerd voor de jaren 2005, 2019 en 2040, waarbij meerdere scenario's voor vliegtuigemissies, niet-luchtvaartemissies en meteorologische velden zijn overwogen. Door een consistente methodologie te gebruiken voor alle simulaties dit proefschrift een compleet beeld van hoeveel vliegtuigemissies de luchtkwaliteit en stikstofdepositie wereldwijd in het heden beïnvloeden, en hoe verschillende variabelen binnen en buiten de luchtvaart die impact in de toekomst kunnen veranderen.

Voor de jaren 2017–2020 wordt er een globaal inventaris van vliegtuigemissies opgesteld met behulp van een lijst met vluchten die werden aangeboden door zowel een commercieel als een open netwerk van telemetrieontvangers. Dit is een verbetering ten opzichte van de toen meest recent beschikbare inventaris uit het jaar 2005. Een andere verbetering was het gebruik van daadwerkelijk gerealiseerde vluchten, in tegenstelling tot eerdere inventarissen die grotendeels waren gebaseerd op databases met vluchtschema's waarin alleen gelokaliseerde radargegevens waren verwerkt. De geproduceerde inventaris had een totale hoeveelheid NO_x-emissies ($NO + NO_2$) voor het jaar 2019 die 59% en 72% hoger was dan de twee voormalige schattingen uit 2005. Dit werk maakte ook de eerste beoordeling mogelijk van de gevolgen van de COVID-19-pandemie voor de globale vliegtuigemissies, bevinding dat er in 2020 48% minder brandstof werd verbrand dan vóór de pandemie werd voorspeld.

De huidige vliegtuigemissies zijn geprojecteerd tot het jaar 2050 met behulp van technologie en regiospecifieke luchtverkeersvoorspellingen uit de luchtvaartindustrie. Ondanks technologische en operationele verbeteringen hadden alle beschouwde scenario's een voortdurend toenemend brandstofverbruik en een toename van de NO_x-emissies, waaronder een toename van de NO_x-uitstoot met 113% tussen 2018 en 2050 voor het basisscenario. Hiertoe draagt bij dat de verwachting is dat de waargenomen trend van toenemende motordrukverhoudingen, aangedreven door ontwerpen die de brandstofefficiëntie optimaliseren, zich voortzet.

De gevolgen voor de luchtkwaliteit door vliegtuigemissies werden voor het eerst onderzocht door een reeks atmosferische simulaties voor 2005 waarbij deze emissies afwisselend in verschillende delen van de wereld werden gepeturberen. Dit maakte het voor het eerst mogelijk om de mate waarin meerdere regionale factoren de luchtkwaliteitsreacties op vliegtuigemissies bepalen. De globale gevolgen voor de gezondheid van de emissies die in Europa vrijkomen blijken 45% en 50% groter te zijn dan die van dezelfde hoeveelheid emissies die respectievelijk in Azië en Noord-Amerika vrijkomen. Dit hield zowel verband met de atmosferische samenstelling die gunstig is voor $PM_{2.5}$-vorming in Europa als met de heersende winden die de effecten van cruise-emissies op grondniveau naar dichtbevolkte regio's in Azië. Het intercontinentale karakter van de luchtverontreiniging door vliegtuigen werd onderstreept door de bevinding dat 73% en 88% van de gezondheidseffecten van emissies in respectievelijk Europa en Noord-Amerika buiten het emissiegebied plaatsvinden.

De nieuw geproduceerde inventarissen van vliegtuigemissies werden vervolgens gebruikt in een reeks simulaties in het atmosferische chemische transportmodel, waarbij de gevolgen voor luchtkwaliteit en volksgezondheid voor de jaren 2019 en 2040 werden gekwantificeerd. De effecten van verschillende toekomstige niet-luchtvaartemissies en meteorologie werden geëvalueerd door een reeks van atmosferische simulaties met verschillende inputparameters. Hierdoor wordt een schatting mogelijk van de onzekerheid in toekomstige projecties van de gevolgen voor de luchtkwaliteit van de luchtvaart die met deze factoren samenhangen. De uitstoot van vliegtuigen in 2019 zou naar schatting leiden tot in totaal 33 900, 79 500 en 2700 extra voortijdige sterfgevallen dat jaar als gevolg van respectievelijk $PM_{2.5}$, ozon en NO_2. Dit is een hogere schatting dan volgt uit eerdere studies, als gevolg van een combinatie van recentere (en dus hogere) vliegtuigemissies, de grote gevoeligheid van ozon op grondniveau voor emissies op kruishoogte, en een sterker verband tussen langdurige blootstelling aan ozon en sterfte volgens recente epidemiologische schattingen. De gevolgen voor de gezondheid nemen in het jaar 2040 over het geheel genomen toe, met 76% ten opzichte van 2019 in het toekomstige basisscenario, en met 28% (laag) en 135% (hoog) als we verschillende projecties van de vliegtuigemissies in 2040 in ogenschouw nemen. De veranderende bevolkings- en niet-luchtvaartemissies van het basisscenario SSP2-4.5 naar zes andere toekomstscenario's resulteerden in een globale, aan vliegtuigen toe te schrijven sterfte veranderde met -1% tot +5%.

Het atmosferische chemische transportmodel werd ook gebruikt om voor het eerst de reactieve stikstofdepositie te kwantificeren die wordt toegeschreven aan vliegtuigemissies op wereldschaal. Uit simulaties, uitgevoerd voor de jaren 2005 en 2019, blijkt dat de door vliegtuigen veroorzaakte stikstofdepositie tussen de twee jaren wereldwijd met 76% is toegenomen. In 2019 vertegenwoordigden vliegtuigen 1,2% van de totale stikstofdepositie uit alle bronnen wereldwijd, waarbij de gemiddelde waarden over Azië, Europa en Noord-Amerika respectievelijk 0,66%, 1,13% en 1,61% bedroegen. De emissies van landen en opstijgen waren verantwoordelijk voor 8% van de door vliegtuigen veroorzaakte depositie wereldwijd, en voor tussen de 16 en 32% depositie boven land in regio's met veel luchtvaartactiviteit. De gevolgen van emissies tijdens de volledige vlucht waren ruimtelijk wijdverspreid, zoals blijkt uit het cijfer dat 56% van de door vliegtuigen veroorzaakte depositie op water plaatsvindt.

In conclusie leveren de modelleringsstudies die in dit proefschrift worden beschreven verder bewijs dat de emissies van vliegtuigen wereldwijd toenemen en dat deze emissies een aanzienlijke impact hebben op de luchtkwaliteit, wat leidt tot verhoogde sterfte en bijdraagt aan overmatige stikstofdepositie. Nieuwe inzichten werden verkregen door het isoleren van de effecten van verschillende variabelen op deze effecten, zoals niet-luchtvaartemissies, grootschalige atmosferische transportpatronen, ruimtelijke verdeling van de bevolking en ruimtelijke en temporele veranderingen in de globale vliegtuigemissies. Met als doel gevolgen te verzachten om vliegverkeer duurzamer te maken, moeten toekomstige onderzoeksinspanningen doorgaan met het actualiseren van de schattingen van de milieueffecten van de luchtvaart op globale schaal. Hierbij moeten verbeteringen worden opgenomen — zodra deze beschikbaar komen — met betrekking tot de kwantificering van vliegtuigemissies en atmosferische modellering en epidemiologisch begrip van vervuiling.

Nomenclature

Acronyms and abbreviations

ACTK	Available cargo ton·kilometers
ADS-B	Automatic Dependent Surveillance-Broadcast
AFTK	Available freight ton·kilometers
ALRI	Acute lower respiratory infection
APU	Auxiliary power unit
AQG	Air quality guidelines
ASK	Available seat·kilometers
ATK	Available ton·kilometers
CAEP	(ICAO's) Committee on Aviation Environmental Protection
CASTNET	Clean Air Status and Trends Network
CI	Confidence interval
CLRTAP	Convention on Long-range Transboundary Air Pollution
COPD	Chronic obstructive pulmonary disease
CRF	Concentration-response function
CTK	Cargo ton·kilometers
CTM	Chemical transport model
EANET	Acid Deposition Monitoring Network in East Asia
EI	Emission index, mass ratio between emission and fuel consumed
EMEP	European Monitoring and Evaluation Program
EPA	U.S. Environmental Protection Agency
FL	Flight level
FNR	Formaldehyde to NO_y (or NO_2) ratio
FR24	Flightradar24

FTK	Freight ton·kilometers
GR	Gs ratio
HTAP	(Task Force on) Hemispheric Transport of Air Pollution
IATA	International Air Transport Association
ICAO	International Civil Aviation Organization
ICD	International Statistical Classification of Diseases
IHD	Ischemic heart disease
LTO	Landing and takeoff (operations)
MCC	Multi-City Multi-Country Collaborative Research Network
MDA8	Maximum daily 8-hour average
NAAQS	U.S. National Ambient Air Quality Standards
NADP	National Atmospheric Deposition Program
NCD	Noncommunicable diseases
OAG	Name of a private company that provides travel data, originally Official Aviation Guide, or Official Airline Guides
OPR	Overall pressure ratio
OS	OpenSky
RPK	Revenue passenger·kilometers
RR	Relative risk
WHO	World Health Organization

Pollutants

BC	Black carbon; elemental carbon
Black smoke	Aerosol with a darkening property, usually referring to a measure of particulate matter based on the soiling of a filter
HC	Hydrocarbons
N_r	Reactive nitrogen
nvPM	Nonvolatile particulate matter
$nvPM_m$	Mass of nonvolatile particles

$nvPM_N$	Number of nonvolatile particles
PM	Particulate matter
$PM_{0.1}$	Ultrafine particulate matter, with an aerodynamic diameter ≤0.1 µm
PM_{10}	Coarse particulate matter, with an aerodynamic diameter ≤10 µm
$PM_{2.5}$	Fine particulate matter, with an aerodynamic diameter ≤2.5 µm
Primary	Pollutant directly emitted into the atmosphere
Secondary	Pollutant formed in the atmosphere from previously emitted species
Smog	Combination of smoke and fog, is also used to refer to air conditions of low visibility and foul odor in general
Smoke	Visible volume of air with aerosol affecting opacity
Soot	Elemental carbon with impurities formed by combustion
UFP	Ultrafine particles
vPM	Volatile particulate matter

Symbols

ϵ	Sulfur conversion factor	1
π_{00}	Reference pressure ratio	1
a_1	Logistic function coefficient, describing aircraft retirement rate	1
a_2	Logistic function coefficient, describing aircraft retirement rate	yr^{-1}
C	Mass of fuel burned	kg
D_p	Pollutant mass emitted during a reference landing and takeoff cycle	g
EI	Emission index	$g{\cdot}kg^{-1}$
F_{00}	Rated thrust	kN
FSC	Fuel sulfur content	ppm
k_{op}	Annual fuel burn reduction from operational improvements	%
k_{tec}	Annual fuel burn reduction from technological improvements	%
M	Molecular weight	$g{\cdot}mol^{-1}$
N	Number of aircraft	1

r	Compound annual (RPK or ATK) growth rate	1
ret	Fraction of aircraft that retires in a year	1
T	Passenger (RPK) or cargo (CTK) air traffic metric	RPK | CTK
t	Age of aircraft	yr

Subscripts

$class$	Specific to aircraft class
i	Specific to aircraft type
new	Aircraft entering the fleet in the current year
old	Aircraft already present in the fleet
ref	Reference
rgn	Specific to regional origin-destination pair
t	Of aircraft age t, in years
y	At year y

1

Introduction

Rumack: You'd better tell the Captain we've got to land as soon as we can. This woman has to be gotten to a hospital.

Elaine Dickinson: A hospital?! What is it?

Rumack: It's a big building with patients, but that's not important right now.

Airplane![1]

1.1 Overview and motivation

The Earth's atmosphere connects every human being by the shared need for constant breathable air in order to remain alive, in addition to physically connecting us by being a continuous mass of matter enveloping the planet's surface. Through the vibration of air we communicate, through its transparency we see each other, and through its fluidity we can move towards each other. Modern aircraft take this last point to the extreme by allowing people to travel halfway across the globe with ease and speed that would be unimaginable in pre-industrial times. Propelled by the burning of hydrocarbon fuels, these aircraft release pollution as a byproduct of combustion. This release soils the air with regard to its other human-connecting abilities mentioned and jeopardizes the often delicate balance between the atmosphere, biosphere, hydrosphere, and other Earth systems. While living under a single soup of air brings opportunities transportation-wise, it also causes the pollution that comes with these activities to have impacts that can span the whole world.

[1] 1980 film written by Jim Abrahams, David Zucker, and Jerry Zucker

1

Out of the multiple impacts aviation has on the environment, which include climate change and noise pollution, this thesis concerns specifically the global scale impacts of atmospheric emissions from civil fixed-wing aircraft on air quality and nitrogen deposition. Both of these kinds of environmental impacts are typically regarded as local problems, whereas this thesis focuses on their long-range effects, which are expected to be of greater relative importance for aviation than for other sectors, owing to the higher altitude of emissions. Air quality is covered in the context of the long-term increases in ground-level pollutant concentration that are associated with negative human health impacts.

As a source of ground-level ozone, particulate matter, and NO_2, aviation has been estimated to have a burden on human health due to air quality as an increase in annual nonaccidental mortalities by ~16 000, globally, in the year 2005 [1]. And as aviation activity increases, potentially so does its environmental footprint, and therefore the importance of studying these impacts. Civil aviation is an industry that has steadily grown since the dawn of the jet age, as measured by passenger transport volume, with revenue traffic kilometers having increased at an average rate of 5.2% per year between 1992–2005 [2–4]. This growth in traffic has occurred in parallel with a corresponding increase in fuel consumption, at an average of 2.5% per year in that same period, and 2.6% per year between 2005–2018 [5]. Improvements in technology and operations lead to the better fuel efficiency over time behind the lower growth rates for fuel compared to traffic. But with the latter expected to continue to increase by between 3% and 4% yearly up to 2040, fuel consumption is likely to continue to increase as well [6].

CO_2 emissions, which cause global warming, are largely proportional to fuel usage, but the air quality and nitrogen deposition impacts from aviation result from non-CO_2 emissions. These include oxides of nitrogen (NO_x), oxides of sulfur (SO_x), unburned hydrocarbons, carbon monoxide, and both volatile and nonvolatile particulate matter. The amount of those emissions that are released per mass of fuel burned can vary by orders of magnitude, depending on the specific engine design and operating condition [7]. The requirements for reducing a specific pollutant might also be in conflict with solutions aiming to reduce fuel consumption and CO_2 emissions or overall reducing climate impact, such that it is not a given that technological progress will improve aircraft emission characteristics all-around [8–11].

NO_x emissions are of particular interest because they are likely the main driver of aviation-attributable premature mortality [1, 12], as a precursor of ozone and particulate matter, and as a source of local NO_2. Additionally, as the products formed from NO_x are removed from the atmosphere, they contribute to anthropogenic reactive nitrogen deposition, which can cause an overenrichment of nutrients in the soil and in water bodies, disrupting the local ecological balance [13, 14]. Efforts to limit the environmental damage in areas of natural preservation have driven actions aiming to cap or reduce emissions of reactive nitrogen species. In the Netherlands, the pressure to limit nitrogen emissions due to the country's environmental protection duties within the European Union, and the subsequent struggle between the various emitting sectors affected, including aviation, has started to the so called "nitrogen crisis" in 2019 [13, 15–17].

1.1.1 Research gap

Despite the long-range nature of air travel, its air quality impacts are generally still treated as a local problem near airports, with only emissions up to 3000 ft above ground being considered (altitude representative of the mixing height at midlatitudes) [18–21]. As individual airport owners, operators, and local authorities may conduct environmental impact analyses and compliance checking independently, there is an abundance of studies on air quality impacts from aircraft at specific airports, including both modeling and measurements [22–28]. However, a growing number of studies based on numerical simulation of the atmosphere are suggesting that cruise emissions can have a significant impact on ground-level pollution [1, 29–34]. Multiple test campaigns have been conducted to measure aircraft emissions during flight by directly sampling the plume [35–39], but attributing ground-level pollutant concentrations to specific high altitude emissions remains challenging, hence the use of numerical simulations.

Modeling a system as large and complex as the atmosphere requires the coupling of various physical models, making compromises in complexity and resolution, and involves significant uncertainty. Models are developed by continuously updating their input data to reflect new measurements, new emission scenarios, and new atmospheric conditions, incorporating the results of new analyses and submodels, trying to improve the accuracy of the representation of many output variables which are often interdependent. The challenges and limitations of atmospheric modeling thus call for model intercomparisons and ensemble modeling in order to draw more robust conclusions in fields of research such as air quality [40]. This means that there is a need for additional studies on how high altitude emissions from aviation might affect surface air pollution, with up-to-date aviation emissions and atmospheric background composition being particularly valuable, as anthropogenic emissions change over time. At the start of the research described in this thesis, the most recent openly-available aircraft emissions inventory for use in such modeling was for the year 2005 [41], and a 40% increase in aviation fuel burn has been estimate between then and 2018 [5].

Likewise, nitrogen deposition is studied through a mix of measurements and modeling efforts, at local, regional, and global scales [42–47]. However, to the best of the author's knowledge, there has not been research focused specifically on the contribution of aircraft emissions to global nitrogen deposition. In this thesis, by performing such analysis using the same atmospheric simulations used to assess air quality, a more comprehensive picture of the environmental impacts of aviation is presented, using consistent modeling assumptions.

To reconcile the aviation industry's desired long-term expansion plans with society's aspiration to be more sustainable, the former has offered promises and potential solutions to reduce aviation's various environmental impacts [48–54], including those discussed here. Within this context, this thesis aims to contribute by providing estimates of how much aviation affects air quality and nitrogen deposition at a global scale, as well as how much those impacts might change in the coming decades. In broad terms, this is done by creating inventories of global aircraft emissions, then using a chemical transport model to simulate how these emissions affect air quality and nitrogen deposition.

1

1.2 Research objectives

In a sector such as civil aviation, that is constantly expanding and evolving technologically, the first step of estimating the environmental impacts of its emissions is to quantify them. The spatial heterogeneity of changes in emissions over time require that their quantification be timely, and that future projections take this heterogeneity into account. The environmental impacts of those emissions is also not uniformly distributed, and their magnitude depends on local atmospheric conditions over all the affected areas. Therefore, it is valuable to understand how the sensitivity of impacts to emissions vary spatially. And as the intensity of air travel increases over time, quantifications of both present day and future air quality and nitrogen deposition impacts could serve to support decision-making related to their mitigation. Because the impacts of aircraft emissions depend on conditions affected by emissions from other sectors, assessments of impacts in the future should contemplate multiple (non-aviation) scenarios in order to provide a more useful range of circumstances covered.

The research presented in this thesis aims to contribute in those areas by achieving the following objectives:

- Quantify present-day global civil aircraft emissions, with three-dimensional spatial resolution.
- Project global civil aircraft emissions to the year 2040, maintaining spatial resolution.
- Estimate the differences in the sensitivity of air quality to aircraft emissions according to the source and receptor world regions.
- Quantify the present-day global air quality and associated human health impact of aircraft emissions.
- Compare how different future atmospheric scenarios can be expected to change the global air quality impacts from aircraft emissions.
- Estimate the spatial distribution of present-day global nitrogen deposition that is attributable to aircraft emissions.

1.3 Thesis outline

The thesis starts with some introductory material providing context, a summary of the scientific basis underpinning this work and an overview of current scientific literature on the topic:

- *Chapter 1* is the preamble you are currently reading, containing the motivation, research objectives and thesis outline.
- *Chapter 2* provides the background for this thesis, covering pollution sources from aviation, the basic atmospheric processes leading these pollutants to degrade air quality, how air quality affects human health, and how aviation emissions contribute to nitrogen deposition.

The research conducted to achieve the objectives listed in Section 1.2 is presented in six chapters. First covering aircraft emissions, then their air quality impacts, and finally nitrogen deposition impacts:

- *Chapter 3*: production of an up-to-date, spatially resolved estimate of global aircraft emissions by building a bottom-up inventory from the combination of a list of flights, engine emissions data, and an aircraft performance model.
- *Chapter 4*: how the developed present day estimate of aircraft emissions can be extrapolated to the year 2040, keeping its spatial distribution information, using industry forecasts for air traffic, and for technological and operational efficiency improvements.
- *Chapter 5*: how the sensitivity of air quality and human health impacts to aircraft emissions can vary depending on the source and receptor world region.
- *Chapter 6*: quantification of present day global air quality and human health impacts of aircraft emissions, and estimates of how future atmospheric conditions and aircraft emissions can change those impacts.
- *Chapter 7*: quantification of the contribution of aircraft emissions to nitrogen deposition at a global scale.

Finally, *Chapter 8* recapitulates the conclusions from the research conducted and gives an outlook on future work in the field.

2

Background

We feel that the present condition of our city, enveloped in a continual cloud of smoke, endangers the health of our families, especially those of weak lungs and delicate throats, impairs the eyesight of our school children, and adds infinitely to our labors and our expenses as housekeepers, and is a nuisance no longer to be borne with submission.

Wednesday Club of St. Louis[1]
1892

This chapter provides context supporting the motivation for this thesis, as well as a summary of existing scientific knowledge relevant to air quality, nitrogen deposition, aircraft emissions, and how atmospheric processes lead aircraft emissions to contribute to the issues of air quality and nitrogen deposition. Firstly, some concepts about air quality are defined, evidence for associations between air pollution and human health effects is reviewed, and some influential air quality standards are listed. Secondly, the basic processes behind nitrogen deposition are described, and the environmental problems associated with excessive deposition are reviewed. Thirdly, an overview on which pollutants are emitted by aircraft and how they are formed, an emissions standard applied to aircraft main engines is summarized, and emission sources from aviation other than aircraft turbines are listed. And fourthly, a summary is given on how aircraft emissions form ozone in the atmosphere, how they form secondary particulate matter, and how high-altitude emissions can have long-range effects on air pollution.

[1]Resolution passed by the women's organization, that was engaged in smoke abatement, among other subjects. Apud [55]

2.1 Overview

Section 2.2 describes basic concepts of air quality and their impacts on human health. Section 2.3 discusses excessive nitrogen deposition and the consequent environmental problems. Section 2.4 discusses aviation as a source of air pollution. And Section 2.5 discusses some important atmospheric processes that cause aircraft emissions to impact air quality.

2.2 Air quality and human health

Air pollution may be defined as an anthropogenic increase in the concentration of substances in the atmosphere to the point that there are measurable effects on humans, animals, vegetation, the natural environment at large, or on man-made structures [56]. The concept of air quality adopted in this thesis refers to the degree of direct noxiousness that an atmospheric composition has on breathable organisms, whether caused by anthropogenic pollution or natural processes. This excludes the damage caused indirectly by pollution inducing climate change, or by accidents occurring due to degraded visibility, for example. More specifically, only the impacts of air quality on human health are taken into account in this research, even though the pollutants considered also harm animals and vegetation concomitantly.

2.2.1 Air pollutants

Presently, the main pollutants of concern with regard to air quality and public health are O_3 (ozone), NO_2 (nitrogen dioxide), SO_2 (sulfur dioxide), CO (carbon monoxide), and particulate matter (PM) [57]. The latter is an umbrella term for solid or liquid aerosol particles or any composition, which are typically classified based on their size, as determined by their aerodynamic diameter:

- $\leq 10\,\mu m$: coarse particles, PM_{10}
- $\leq 2.5\,\mu m$: fine particles, $PM_{2.5}$
- $\leq 0.1\,\mu m$: ultrafine particles, $PM_{0.1}$, UFP

These size definitions are based on modes observed in the number and volume distribution of particles per size, due to the chemical and physical processes affecting aerosol formation, growth, coagulation, evaporation and deposition [56]. The processes involved in the physiological response to aerosol pollution also depend on particle size, with evidence suggesting that smaller particles have higher toxicity [58, 59], leading to the number of particles being a useful air quality metric in addition to mass concentration. The chemical composition of aerosol also affects toxicity to humans, with particles with more reactive surfaces believed to be more harmful, although quantitative differentiation of particle toxicity per size and composition remains challenging [58–62]. Particulate matter is also classified based on its composition and origin, with the following terms defined in the Nomenclature being used in the field of air quality[2]: black carbon, soot, black smoke, smog, (non)volatile particulate matter, (in)organic aerosol, primary and secondary aerosol.

[2]Some of these definitions may vary according to source and context.

In addition to the more ubiquitous pollutants mentioned in the previous paragraph, which are related to combustion, there is also concern over more acutely toxic substances that might be released to the atmosphere, desirably in more limited ways. Pb (lead) is one of the most important examples, as use of fuel with leaded additives in piston engines used to be widespread. For this reason, it is regulated in the United States together with the already mentioned pollutants (O_3, NO_2, SO_2, CO, PM), as "criteria pollutants", by the National Ambient Air Quality Standards (NAAQS) [63]. Similarly, the same six pollutants, with the addition of benzene are regulated in the European Union under the same directive (2008/50/EC) [64]. Various other species considered to be toxic contribute to air pollution, for example: mercury, cadmium, chromium, asbestos, arsenic, radionuclides (such as radon), organochlorines, dioxin, toluene, benzene, and a multitude of other organic compounds. As of 2023, the U.S. Environmental Protection Agency has a list of 188 "hazardous air pollutants" which, in addition to the six "criteria pollutants", it is required by law to regulate [65].

2.2.2 Short-term pollution exposure

The quick pace of industrialization and use of coal power in 19th century created a growing problem of air pollution, along with efforts from various groups to mitigate it [55, 66]. Up until the mid-20th century, the motivation for control measures was largely the nuisance in terms of poor visibility, unpleasant odor, eye irritation, crop damage, and material degradation, particularly in cities suffering from chronic air pollution such as Los Angeles, Chicago and St. Louis (among many others, not restricted to the United States) [67–70]. Although health concerns, even if not backed by strong scientific evidence, were already present [55, 66, 70].

Those efforts to study and improve air quality gained impetus in the aftermath of significant acute local air pollution episodes in the 20th century, such as the smog incidents of Meuse Valley in 1930, St. Louis in 1939, Donora in 1948, London in 1952, and New York City in 1966 [67, 71, 72]. Low winds and thermal inversion can cause the pollution that would usually dispersed from highly emitting regions to get trapped near the surface, accumulating to dangerously high concentrations and causing a sharp increase in morbidity and mortality. These incidents provided both a boost in public awareness and the data to strengthen the case for intervention, which still took place locally, at the city level [66]. It was the observed correlation between acute short-term exposure to pollution and hospital visits and mortality rates that provided the first strong evidence that air quality should be regarded as a public health issue [72, 73].

From the more notable smog incidents, a field of studies emerged that quantified the short-term effects of air quality on human health by combining time-series data of both air pollution (from measurement stations) and health indicators (such as hospital visits and deaths) within a location, as reviewed by Refs. [72, 74, 75]. Generalized additive models are used to relate daily health outcomes to daily pollutant concentrations, carefully adjusting for confounding variables such as: weather, season, day of week, unrelated epidemics, pollen count, and trends of improving medical care, population size, smoking and drinking rates. Alternatively, case-crossover studies compare pollution levels when a person is hospitalized to those of other days within a time range, when the person did not experience that outcome.

Research evolved from looking at individual events or specific cities towards combining data from multiple cities in order to obtain more robust results. Landmark studies include the National Morbidity, Mortality, and Air Pollution (NMMAPS) in the United States, and the Air Pollution and Health: European Approach (APHEA) and its follow-up APHEA-2 in Europe. Analysis of data over multiple years in the 1970s, 80s, and 90s from collections of large cities, with combined population in the tens of millions, provided significant correlations of daily PM_{10} concentration with daily mortality and hospitalization rates. The increase in all-cause (nonaccidental) mortality per $10\,\mu g \cdot m^{-3}$ was estimated as 0.51% (95% CI: 0.07–0.93) in NMMAPS [76] and 0.6% (95% CI: 0.4–0.8) in APHEA-2 [77]; significant associations were also found for deaths due to cardiopulmonary disease. NMMAPS found that a $10\,\mu g \cdot m^{-3}$ increase in 2-day mean PM_{10} was associated with the following increases in hospitalization rates (95% CI in parenthesis) of persons over the age of 65 for specific causes: 1.17% (1.01–1.33) for cardiovascular disease, 1.98% (1.49–2.47) for chronic obstructive pulmonary disease (COPD), and 1.98% (1.65–2.31) for pneumonia [78]. Analyses of APHEA-2 also found significant correlations of PM_{10}, black smoke, and SO_2 to hospitalizations due to asthma, cardiac arrest, ischemic heart disease (IHD), cardiovascular diseases, COPD, and respiratory diseases of people of various age groups [79–82].

More recently, the Multi-City Multi-Country (MCC) Collaborative Research Network pooled time-series mortality data from 652 cities in 24 countries between 1986 and 2015, adding to 59.6 million deaths, to evaluate their association with local air quality [83]. By including data from North America, Europe, and Asia, this study covers a wide range of background pollution levels, demographic makeup, and local climates. It was found that a $10\,\mu g \cdot m^{-3}$ increase in the 2-day average PM_{10} was associated with mortality increases of (95% CI in parenthesis): 0.44% (0.39–0.50) for all-cause, 0.36% (0.30–0.43) for cardiovascular diseases, and 0.47% (0.35–0.58) for respiratory diseases. The rates for the same increase in $PM_{2.5}$ were: 0.68% (0.59–0.77) for all-cause mortality, 0.55% (0.45–0.66) cardiovascular, 0.74% (0.53–0.95) respiratory. The analysis also showed stronger associations in places with lower annual mean concentrations and higher ambient temperatures. The mortality response per concentration increase was also stronger for lower concentration values. The MCC has also found that a $10\,\mu g \cdot m^{-3}$ increase in the 2-day average of ozone was associated with an all-cause mortality increase of 0.18% (95%CI: 0.12–0.24) [84].

The World Health Organization (WHO) publishes Air Quality Guidelines (AQG), described further in Section 2.2.4, which are based on systematic reviews and meta analyses of global scientific evidence. For the latest guidelines publication [57], this included reviews performed on the evidence of: effects of short-term exposure to $PM_{2.5}$, PM_{10}, O_3, and NO_2 on cause-specific and all-cause mortality [85]; effects of short-term exposure to SO_2 on respiratory and all-cause mortality [86]; effects of short-term exposure to O_3, NO_2, and SO_2 on hospital visit due to asthma [87]; and effects of short-term exposure to CO on myocardial infarction [88]. The mortality analyses found significant positive effects for all exposure-outcome combinations analyzed except 1-h maximum NO_2 and all-cause mortality, and 24-h average SO_2 and respiratory mortality (Table 2.1). The certainty of evidence of all but three of those exposure-concentration pairs were judged to be high. The review of the association between short-term pollution and hospital visits found pooled relative risk values larger than 1 (positive association) for five of the six exposure-outcome pairs analyzed, with two of them having high certainty of evidence (Table 2.2).

Table 2.1: Association between short-term pollutant exposure and human mortality, according to systematic reviews and meta analyses by Refs. [85, 86]. To improve readability, relative risks are shown as percentages after subtracting 1, such that a value of 0 indicates no expected change in outcome.

Pollutant	Mortality endpoint	Relative risk – 1 [% per 10 µg·m^{-3}]	Certainty of evidence
PM_{10} (24-h mean)	All-cause	0.41 (0.34–0.49)	High
	Cardiovascular	0.60 (0.44–0.77)	High
	Respiratory	0.91 (0.63–1.19)	High
	Cerebrovascular	0.44 (0.22–0.66)	High
$PM_{2.5}$ (24-h mean)	All-cause	0.65 (0.44–0.86)	High
	Cardiovascular	0.92 (0.61–1.23)	High
	Respiratory	0.73 (0.29–1.16)	High
	Cerebrovascular	0.72 (0.12–1.32)	High
NO_2 (24-h mean)	All-cause	0.72 (0.59–0.85)	High
NO_2 (1-h max.)	All-cause	0.24 (−0.05–0.53)	Moderate
O_3 (8-h or 24-h max.)	All-cause	0.43 (0.34–0.52)	High
SO_2 (24-h mean)	All-cause	0.59 (0.46–0.71)	High
	Respiratory	0.67 (0.25–1.09)	Moderate
SO_2 (1-h max.)	All-cause	0.16 (−0.70–1.02)	Low
	Respiratory	0.52 (0.13–0.91)	High

Table 2.2: Association between short-term pollutant exposure and asthma related emergency room visits or hospital admissions, according to a systematic review and meta analysis by Ref. [87]. To improve readability, relative risks are shown as percentages after subtracting 1, such that a value of 0 indicates no expected change in outcome.

Pollutant	Relative risk – 1 [% per 10 µg·m^{-3}]	Certainty of evidence
O_3 (8-h or 24-h)	0.8 (0.5–1.1)	High
O_3 (1-h)	1.7 (−2.7–6.3)	Moderate
NO_2 (24-h)	1.4 (0.8–2.0)	High
NO_2 (1-h)	−0.1 (−3.4–3.3)	Low
SO_2 (24-h)	1.0 (0.1–2.0)	Moderate
SO_2 (1-h)	0.3 (−0.8–1.4)	Moderate

2.2.3 Long-term pollution exposure

As more data on air pollution and health indicator were collected, it became feasible to look for evidence of the effect of air pollution beyond extreme exposure events. In the second half of the 20th century, studies started to investigate the possible long-term health effects of exposure to higher levels of air pollution. These include cross-sectional, cohort, and case control studies [72].

Ecological cross-sectional studies compare health indicators of populations who live in regions with different levels of air quality. By comparing air quality and health outcomes at the same time, this kind of study does not consider the impacts as the cumulative result of a history of exposure, such that temporal changes in exposure at an individual level are not taken into account (either because of a person moving or because of changing air quality at the same location). The focus was first on differences between urban and rural environments [89], but more data and stronger statistical analyses expanded that scope [90–93]. A significant challenge is to correct for all possible confounding variables, as is the case with time-series studies (Section 2.2.2).

Modern cross-sectional studies also utilize satellite sensing and numeric atmospheric models to obtain air pollution values specific to the residence of each individual in an analysis, instead of considering average values for entire cities or districts, although this requires surveying participants, which limits sample size. Examples using this approach include a study in the Netherlands which did not find significant association between NO_2 concentration and type 2 diabetes [94], and a study in China which found that a 41.7 $\mu g \cdot m^{-3}$ increase in $PM_{2.5}$ was associated with an 11% (95%CI: 5%–17%) [95].

Prospective cohort studies follow a cohort of participants over time, which involves better control of personal covariates (such as smoking and level of physical activity) and often higher spatial resolution of pollution exposure metrics (based on the residence address of participants) over time. One of the most influential studies on air quality and human health is the Harvard Six Cities study published in 1993, which included 14–16 years of follow-up on 8111 adults in six American cities to investigate the association between air pollution and mortality [96]. As is (now) standard on this kind of studies, a survival analysis using Cox proportional-hazards regression model was used while controlling for individual risk factors (such as smoking status, sex, age, body mass index, education, etc.). It was found that the ratio of adjusted mortality rates between the most and least polluted cities was 1.26 (95%CI: 1.08–1.47).

Another landmark study from the same era analyzed data for 552,138 persons across 151 U.S. metropolitan areas enrolled in the Cancer Prevention Study II (CPS-II) of the American Cancer Society [97]. The analysis 7 years of mortality resulted in adjusted relative risk ratios of all-cause mortality between most and least polluted areas of: 1.15 (95%CI: 1.09–1.22) and 1.17 (1.09–1.26) when using sulfates and $PM_{2.5}$ as measures of pollution, respectively. Both pollutants were also found to be associated with increased cardiopulmonary and lung cancer mortality.

The strong associations found by the Six Cities and CPS-II studies, particularly for $PM_{2.5}$, were met with criticisms over lack of independent reanalysis and openness of data [98]. Since then, further reanalysis of the original data, extension analysis of the same cohort, and multiple independent cohort studies worldwide have largely validated the original conclusions [98]. Although the need for confidentiality of private information of

participants has created an opening for attempts to disregard the results of these studies by way of concerns about transparency [99, 100].

A further challenge worth mentioning is the potential confounding effect of co-pollutants, as there is usually correlation between pollution levels of different species, and there can be synergisms and antagonisms in the combined health effect of multiple pollutants [75]. Thus a feature on some of these large studies is the evaluation of both single and multi-pollutant models, depending on how the individual variables are included in the regression analysis. Results isolating the effect of individual pollutants are more desirable from the point of view of ease in planning mitigating actions, but pollutant concentrations can be dependent on emissions of various species, complicating air quality management regardless [66].

Some of the main cohorts that have provided evidence of the link between long-term exposure to air pollution and adverse health outcomes include, among others: Harvard Six Cities [101], CPS-II [102–104], California Teachers Study [105], the (female) Nurses' Health Study [106], (male) Health professionals follow-up [107], Women's Health Initiative Observational Study [108], Netherlands Cohort Study on Diet and Cancer [109], Canadian National Breast Screening Study [110], Canadian Census Health and Environment Cohort [111], (Austrian) VHMP&PP [112]. The results from these cohorts are often pooled into larger analyses. One example of them is the European Study of Cohorts for Air Pollution Effects (ESCAPE), which found a 7% (95%CI: 2–13) increase in all-cause mortality with $5\,\mu g{\cdot}m^{-3}$ a increase in $PM_{2.5}$, and a similar 7% (1–13) when considering only exposures below $20\,\mu g{\cdot}m^{-3}$. The positive association even for low levels of pollution served as motivation for the similar Effects of Low-Level Air Pollution: A Study in Europe (ELAPSE), which found the relative risk of all-cause mortality to increase by 5.3% (95%CI: 2.1–8.5) for a $5\,\mu g{\cdot}m^{-3}$ increase in $PM_{2.5}$, 4.4% (1.9–6.9) for a $10\,\mu g{\cdot}m^{-3}$ increase in NO_2, and 3.9% (1.8–5.9) for a $0.5 \cdot 10^{-5}\,m^{-1}$ increase in black carbon, as well as significant associations between these pollutants and cardiovascular, respiratory, and lung cancer mortalities [113]. Unlike results from North American cohorts featuring a wider range of concentrations, this European study found only a weak negative association between ozone single-pollutant models and mortality. This last study also found that $PM_{2.5}$, NO_2, and especially black carbon had stronger effects on the relative risk of mortality at lower concentrations. Another notable meta analysis study was done by Burnett et al., who created the Global Exposure Mortality Model (GEMM) relating long-term $PM_{2.5}$ concentration with various mortality endpoints, building the model from studies covering a wide range of $PM_{2.5}$ concentrations [114]. The modeled nonlinear increase in mortality from noncommunicable diseases (NCD) plus lower respiratory infections (LRI) per $10\,\mu g{\cdot}m^{-3}$ increase in annual $PM_{2.5}$ is 35% at the counterfactual concentration of $2.4\,\mu g{\cdot}m^{-3}$, 7.2% at $25\,\mu g{\cdot}m^{-3}$, and 5.9% at $75\,\mu g{\cdot}m^{-3}$.

A slightly different approach is to use an open cohort, which sacrifices data on individual risk factors but enables a larger sample size, as was the case for an analysis of the Medicare population in the United States [115]. This study analyzed 460 million person-years of data, finding a 7.3% (95%CI: 7.1–7.5) increase in all-cause mortality per $10\,\mu g{\cdot}m^{-3}$ increment of $PM_{2.5}$, and 1.1% (1.0–1.2) per 10 ppb increment of ozone. The $PM_{2.5}$ effect was greater at exposures below $12\,\mu g{\cdot}m^{-3}$: 13.6% (13.1–14.1) per $10\,\mu g{\cdot}m^{-3}$.

Systematic reviews and meta analyses of long-term air quality impacts on human mor-

tality were done in support of the WHO's Air Quality Guidelines published in 2021, covering PM [116] and NO_2 and O_3 [117]. A summary of the results is shown in Table 2.3. Long-term exposure to PM, especially $PM_{2.5}$, is consistently and significantly associated with both all-cause and several cause-specific mortality rates, with the amount of evidence increasing over time, particularly with more data from poorer countries. The confidence interval evaluated for PM_{10} and some cause-specific mortality rates (circulatory, stroke, and COPD) range from negative to positive associations. Also of note is the fact that associations remain — or increase in some studies — at the lower end of PM concentration levels, suggesting that there is no safe limit of exposure, regardless of limits set by standards or guidelines (Section 2.2.4).

The evidence for NO_2 and O_3 is also significant albeit weaker, especially for ozone, with substantial heterogeneity observed across studies and a more limited geographical coverage and lower number of independent cohorts available [117]. Given the seasonality of ozone concentrations in the atmosphere, driven by photochemistry, some studies utilize "peak-season" metrics, which consider concentration averages only over warm months instead of the whole year. The review commissioned by the WHO separated the studies in the meta analysis based on which type of ozone metric was used, and a significant positive association was only found between peak-season ozone and all-cause mortality (Table 2.3). Annual average ozone metrics were not found to be significantly associated either positively or negatively with all-cause or respiratory mortality. The review also noted a lack of studies with multipollutant models.

Table 2.3: Association between long-term pollutant exposure and human mortality, according to systematic reviews and meta analyses by Ref. [116, 117]. To improve readability, relative risks are shown as percentages after subtracting 1, such that a value of 0 indicates no expected change in outcome.

Pollutant	Mortality endpoint	Relative risk – 1 [% per 10 $\mu g \cdot m^{-3}$]	Certainty of evidence
$PM_{2.5}$	All-cause	8 (6–9)	High
	Circulatory	11 (9–14)	High
	IHD	16 (10–21)	High
	Stroke	11 (4–18)	High
	Respiratory	10 (3–18)	Moderate
	COPD	11 (5–17)	High
	ALRI	16 (1–34)	High
	Lung cancer	12 (7–16)	High
PM_{10}	All-cause	4 (3–6)	High
	Circulatory	4 (–1–10)	Moderate
	IHD	6 (1–10)	Moderate
	Stroke	1 (–17–21)	Low
	Respiratory	12 (6–19)	High
	COPD	19 (–5–49)	Moderate
	Lung cancer	8 (4–13)	High
NO_2	All-cause	2 (1–4)	Moderate
	Respiratory	3 (1–5)	Moderate
	COPD	3 (1–4)	High
	ALRI	6 (2–10)	Moderate
O_3 (average)	All-cause	–3 (–7–2)	Low
	Respiratory	–1 (–11–11)	Low
O_3 (peak)	All-cause	1 (0–2)	Moderate
	Respiratory	2 (–1–5)	Low

2.2.4 Air quality standards

As a reaction to the acknowledgment of the deleterious short-term and long-term effects of air pollution, governments throughout the world enact a multitude of measures with the goal of improving air quality. Among these measurements are regulations of specific sectors setting allowable levels of pollutant emissions, like those applicable to aviation (Section 2.4.2). Typically, strategies are organized into an air quality management framework, in which the various measures to reduce emissions are applied and adjusted such that air quality monitoring measurements are in accordance with air quality goals set beforehand [66]. These goals are driven by the concerns of pollution impacts such as those on human health, acid rain, visibility, and biodiversity. As such, the epidemiological studies mentioned in Sections 2.2.2 and 2.2.3 are important in informing the goals and standards set for air quality.

Table 2.4 lists the main air quality standards in effect in the European Union and the United States, as well as the latest WHO guidelines. While it should be recognized that both developing and developed countries have their own air quality standards, the EU and U.S. standards are a strong influence on legislation elsewhere, like they also influence each other [118]. The WHO guidelines do not have any legal power, but their purpose is to serve as a tool to policy-makers, being an influence on discussions around revising regulatory limits [119]. The more stringent limits suggested by the WHO are driven by the findings that air pollution has health impacts even at low levels, and are meant to keep pushing governments towards improving air quality over time.

Table 2.4: Summary of air quality standards defined by European directive 2008/50/EC [64], U.S. National Ambient Air Quality Standards [63], and the WHO Air Quality Guidelines [57], as of 2023. Concentrations in $\mu g \cdot m^{-3}$, except where noted otherwise.

Pollutant	Average[a]	EU	NAAQS	WHO guidelines				
				Interim				AQG
				1	2	3	4	
$PM_{2.5}$	24-h	–	35	75	50	37.5	25	15
	Annual	25[b]	12	35	25	15	10	5
PM_{10}	24-h	50	150	150	100	75	50	45
	Annual	40	–	70	50	30	20	15
O_3	8-h	120[c]	140 (70 ppb)[d]	160	120	–	–	100
	Peak season	–	–	100	70	–	–	60
NO_2	1-h	200	191 (100 ppb)[d]	–	–	–	–	200
	24-h	–	–	120	50	–	–	25
	Annual	40	101 (53 ppb)[d]	40	30	20	–	10
SO_2	1-h	350	200 (75 ppb)[d]	–	–	–	–	–
	24-h	125	–	125	50	–	–	25
CO $[mg \cdot m^{-3}]$	1-h	–	40.8 (35 ppm)[d]	–	–	–	–	35
	8-h	10	10.5 (9 ppm)[d]	–	–	–	–	10
	24-h	–	–	7	–	–	–	4
Pb	3-month	–	0.15	–	–	–	–	–
	Annual	0.5	–	–	–	–	–	–

[a] The EU, U.S., and WHO have different specific criteria for compliance of each limit, such as number of exceedances per period of time, which is an important factor in the severity of a requirement.

[b] There is also a 20 $\mu g \cdot m^{-3}$ "indicative limit" set for an "Average Exposure Indicator" metric based on background measurements in urban areas.

[c] The EU defines the ozone value as a "target" instead of "limits" as for the other pollutants shown here; a target has less strength with regard to a state's obligations in meeting and maintaining it.

[d] Limits defined as (volumetric) ppm or ppb, converted assuming 20 °C at 1 atm.

2.3 Nitrogen deposition

Around 78% of molecules in the Earth's atmosphere are nitrogen gas (N_2), which is therefore constantly breathed in and out of our lungs. Nitrogen atoms (N) are essential to all life forms, as part of proteins and the nucleotides that form DNA and RNA. However, N_2 is largely chemically inert, and thus unavailable to living beings, except for a few species of bacteria and archaea that evolved the ability of nitrogen fixation [120]. Through this process of biological nitrogen fixation, N_2 is converted into ammonia (NH_3) by nitrogenase enzymes and then into other reactive species such as NO, NO_2^-, NO_3^-, N_2O, and NH_2OH [121]. Ammonia is also converted by other enzymes into various forms of organic nitrogen, or biomass, and is thus fundamental to nutrition. Nitrogen content in these organic and inorganic species more reactive than N_2 is referred to as reactive nitrogen (N_r). Biological nitrogen fixation occurs both in the soil, particularly by organisms that are symbiotic with legumes, and in the water [121]. A smaller but still significant natural source of N_r is lightning, as the high temperatures following a strike lead to the production of NO [122]. Figure 2.1 illustrates some of the ways by which nitrogen species are transformed across the atmosphere and soil, as well as some significant anthropogenic sources of N_r.

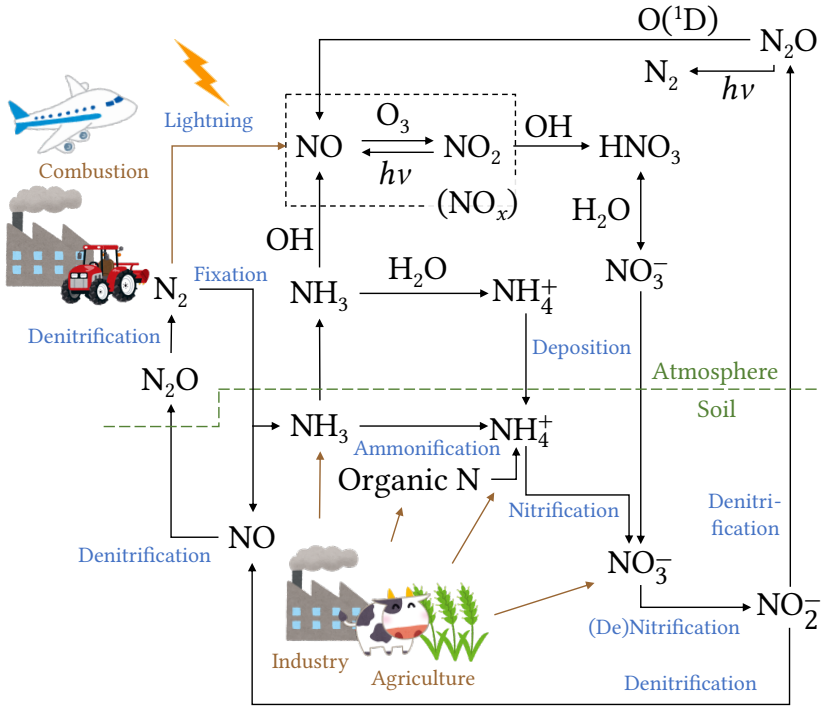

Figure 2.1: Important processes involving nitrogen compounds in the atmosphere and soil.

Human activity has significantly affected the Earth's nitrogen cycle in multiple ways, chiefly due to: fertilizer production, ammonia production for industrial use, cultivation-induced biological N fixation, and fossil-fuel combustion [13, 122]. The discovery of the

Haber-Bosch process in the early 20th century enabled abundant production of ammonia from atmospheric N_2, according to the following simplified global reaction:

$$3\,H_2 + N_2 \longrightarrow 2\,NH_3 \tag{2.1}$$

In addition to supporting the manufacturing of explosives, fibers, plastics, and pharmaceutical products, this process provided a limitless source of nutrients to grow plants [14, 123]. Synthetic fertilizers, primarily those based on nitrogen, became essential in meeting the need for proteins of a growing human population, being responsible for feeding an estimated 48% of humanity in 2008 [123]. As a consequence of this demand, ammonia is one the most produced chemical commodities globally, with over 150 Tg being created annually in 2016, and with an expected growth rate of 1.0% per year [124]. Growing production of reactive nitrogen from fertilizers and legumes is expected to continue in the coming decades, driven by increases in population count (and thus demand for food and fiber crops), per-capita protein consumption, and biofuel demand, including from aviation [14, 123, 125]. Due to a need for hydrogen feedstock, ammonia production is also a significant contributor to another anthropogenic source of reactive nitrogen, as it accounted for ~2% of total energy consumption by the year 2020 [126]. Combustion for energy production is a significant source of anthropogenic reactive nitrogen as NO_x, whose formation is further described within the context of aircraft engines in Section 2.4.1.

Overall, Galloway et al. estimated that human activities were responsible for the creation of 226 Tg N in 2020, compared to estimates of natural fixation of 58–128 Tg N·yr^{-1} [13]. The breakdown of the anthropogenic N_r creation rate by sources was 47% from fertilizers, 19% from industrial Haber-Bosch uses, 19% from cultivation-induced biological fixation, and 15% from fossil-fuel combustion. They also found that both creation and use of N_r increased over time, the latter by 50% between 1990–2020 excluding industrial Haber-Bosch, which is also expected to grow by another 42% between 2020–2050, accounting for both population growth and a continuation of the trend in per-capita use increase.

Anthropogenic atmospheric reactive nitrogen species, whether emitted directly from combustion or indirectly from nitrogen-enriched soil or water, undergo deposition onto the Earth's surface through both wet and dry processes [56]. Wet deposition occurs when a species (gaseous or aerosol) interacts with water (cloud, fog, rain, or snow) and is precipitated to the ground surface. Wet deposition can further be classified into in-cloud scavenging (rainout) and below-cloud scavenging by falling rain or snow (washout). Dry deposition can be defined as the processes of atmospheric deposition not involving water, by which gases and particles are transported to a thin layer of air above the surface, then are transported through this layer towards the surface (by diffusion and Brownian motion), and finally are absorbed or adhered to the surface, possibly reacting chemically to it. Dry deposition is also often reversible, with evaporation, wind and diffusion lifting substances from the surface back to the atmosphere. Figure 2.1 indicates deposition in the form of NH_4^+ and NO_3^-, but it should be noted that gaseous forms of N_r are also deposited directly through dry deposition. Besides atmospheric deposition, other mechanisms transfer N_r species across the boundaries between atmospheric, terrestrial, and aquatic domains, such that the impacts of excessive N_r can spread out, reaching even remote areas. The long range spread of anthropogenic nitrogen deposition is demonstrated by the case of emissions from aircraft, as seen in Chapter 7.

The substantial increase in the amount of N_r released due to human activities causes a subsequent equivalent increase in N_r accumulation in natural reservoirs, having cascading effects over atmospheric, terrestrial, and aquatic domains, leading to several environmental problems [13]. Atmospheric impacts include the formation of tropospheric ozone and particulate matter from NO_x, as described further in Section 2.5. Terrestrial impacts include soil acidification [127], and loss of biodiversity [128]. Excess nutrients in the soil and in human waste enrich groundwater, waterways and surface water bodies [13, 14]. Elevated nitrate levels in drinking water, which can be observed in untreated groundwater affected by excessive nitrogen deposition, have also been associated with negative health impacts, such as methemoglobinemia, colorectal cancer, thyroid disease, and neural tube defects [129]. Water eutrophication leads to a myriad of ecological effects including excessive biomass of phytoplankton and macrophyte vegetation, algal bloom, coral reef decline, fish die-off, reduction in biodiversity, reduction in harvestable aquatic animals, changes in water taste and odor, and oxygen depletion [130]. As water transparency decreases and more algae biomass fuel an increase in microbial respiration, oxygen levels decrease, leading to further environmental effects [131]. The extent of marine and coastal areas suffering from hypoxia, termed "dead zones", has increased over time, driven both by nutrient pollution and climate change [132–134]. Nitrate-rich soil also leads to additional release of N_2O into the atmosphere, where the gas contributes to stratospheric ozone depletion and to the greenhouse effect, with the temperature and precipitation dependence of these emissions having a strong positive feedback with global warming [134, 135]. In the atmosphere, N_2O can be transported into the stratosphere, where it photodissociates back into N_2 or is oxidized into NO_x, leading to HNO_3 and nitrate aerosol, which are then deposited through sedimentation and water precipitation, causing acid rain [56].

From a practical standpoint on impact management, an important concept is that of nitrogen critical loads, defined as the threshold amount of N_r flux that an ecological system can take, beyond which long-term harmful effects are expected to occur [128, 136]. These values have guided policy efforts, particularly in Europe, in limiting environmental damage due to anthropogenic emissions over sensitive natural areas [13, 128]. It should be noted that the complex dynamics of nitrogen across the various Earth systems result in anthropogenic nitrogen deposition impacts that interact with other changes driven by human activity, like global warming, and are nonuniform spatially, such that the net effect in certain areas might be a decrease in N_r available to the local ecosystem [137]. To uphold obligations with regard to water pollution, like those from the "Nitrates Directive" in the European Union [138], some governments implement nitrogen budgets to support planning on fertilizer use and other emitting activities [139]. As discussed further in Section 2.5.3, transport of air pollution can lead to emissions exporting a significant amount of impacts to areas controlled by different states, such that achieving goals related to nitrogen deposition might require international coordination. International scientific collaborations in this area include EANET (Acid Deposition Monitoring Network in East Asia) and EMEP (European Monitoring and Evaluation Programme) [140].

While N_r from combustion sources such as aviation are entirely undesirable, the use of nitrogen in agriculture serves in part valuable purposes which have an increasing demand [141]. As a consequence, efforts to mitigate the environmental problems associated with excess nitrogen deposition also have to contemplate economic and social factors across

multiple segments of society, as evidenced by the "nitrogen crisis" in the Netherlands that erupted in 2019 [13, 16, 17], and by the Sri Lankan policy changes concerning fertilizers in 2021 [142].

2.4 Pollution from aviation

This section presents a review of the major sources of emissions from aviation that contribute to air pollution. Section 2.4.1 describes emissions from aircraft engines, including the species listed in Figure 2.2. Section 2.4.2 summarizes the emissions standards that apply to these engines. And Section 2.4.3 lists additional sources of emission from aviation activities.

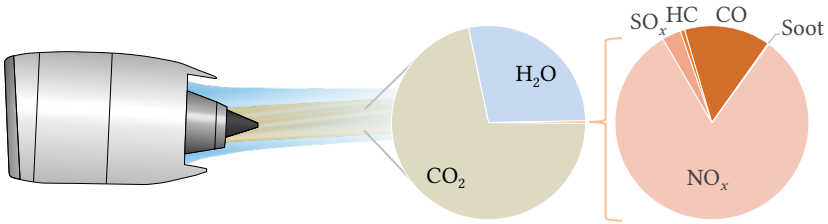

Figure 2.2: Main emission species released by a turbojet engine, with a visual representation of full-flight average mass fractions. For the plot, NO_x is taken in units of mass of NO_2, and hydrocarbons (HC) as mass of CH_4.

2.4.1 Pollutant formation on aircraft engines

Owing to the their higher specific thrust, per frontal area and per mass, gas turbine engines burning kerosene replaced piston engines in the role of powering commercial airplanes starting in the 1950s. Soon, the early turbojets gave way to turbofans, with a trend over time that persists to this day of increasing the ratio of air mass that bypasses the engine core through the fan (bypass ratio), with the goal of putting more of the energy released by combustion into propulsion of the aircraft. Today, around 99% of fuel consumption by civil aviation comes from aircraft powered by turbofans (Chapter 3), with some short regional routes still using turboprop aircraft, in which propulsion comes exclusively from a propeller driven by a turbine engine. Piston aircraft are still used in general aviation, mainly for privates flights and agriculture, making up a negligible amount of fuel use compared to commercial aviation and private jets. These piston engines, for the most part, use aviation gasoline ("avgas"), which is a blend of gasoline that still contain leaded anti-knocking additives.

To avoid the environmental impacts of fossil fuel usage, chiefly climate change, other transportation sectors are transitioning into vehicles powered by alternative means such as electric batteries (automobiles), overhead electric lines (rail vehicles), ammonia and the wind (ships) [143]. However, aviation poses a unique challenge due to the need for a high density energy carrier to achieve flight with similar performance as current aircraft. This constraint has severely limited the options available for aviation to reduce its carbon footprint in the foreseeable future. Sustainable aviation fuels (SAF), i.e. hydrocarbon jet fuel produced from sustainable sources, are being counted on as the main tool to "aspirationally" make flying in civil aviation carbon neutral by 2050 [144, 145]. By that date,

hydrogen and battery electric aircraft are expected to still represent a small share of total energy consumed by aircraft [144]. Consequently, it seems likely that civil aviation flights will continue to be powered by burning hydrocarbons for at least the next three decades.

A brief review of the basics of combustion and pollutant formation is given next, based on Ref. [146]. An idealized model of the stoichiometric combustion of a hydrocarbon with air (21% O_2 and 79% N_2 by volume) is shown in Equation (2.2). Fuel-lean mixtures, i.e. with excess air, can (in this idealized model) result in complete oxidation of the fuel into CO_2 as in Equation (2.2), with additional O_2 going unreacted. Rich mixtures, with excess fuel, will lead to the formation of CO and C.

$$C_xH_y + \left(x + y/4\right)\left(O_2 + 3.76\,N_2\right) \longrightarrow (x)CO_2 + \left(y/2\right)H_2O + \left(x + y/4\right)(3.76)N_2 \tag{2.2}$$

Following the release of energy by the reaction, combustion products will typically have high temperature, and possibly high pressure (as is the case in gas turbines). Under these conditions, the product species included in Equation (2.2) will dissociate, with the products of dissociation undergoing further reactions, forming trace amounts of other species such as H_2, H, OH, CO, O, N, NO. The chemical equilibrium of the product mixture will depend on the atomic makeup of the reactants (the matter available to be rearranged), and the amount of heat released and the heat capacity of the products (affecting the temperature achieved); all of which will depend on the equivalence ratio for a given combination of fuel and oxidizer. The equivalence ratio is the ratio between the actual fuel-oxidizer ratio and the stoichiometric one, such that equivalence ratios greater than 1 indicate fuel-rich mixtures. Figure 2.3 illustrates the basic dependence of flame temperature and pollutant formation rates to the equivalence ratio for the combustion of hydrocarbon and air. The basic mechanisms behind the formation of each of these pollutants is described ahead.

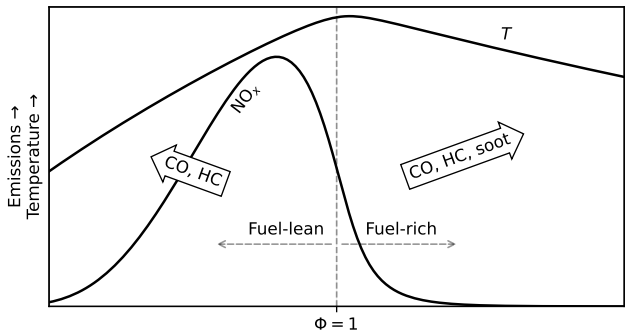

Figure 2.3: Indicative relationship between emissions and flame temperature (T) with equivalence ratio (Φ) in a gas turbine engine. Based on Refs. [147, 148].

Nitrogen oxides (NO_x)

A global reaction like Equation (2.2) is in reality the net result of a multitude of simpler elementary reactions, involving many intermediate species. These include radicals which readily react further, forming a chain of reactions, eventually resulting in more stable products which will react at much slower rates. Going beyond the assumption of equilibrium, a

global reaction such as the combustion of a hydrocarbon can be described by a mechanism of hundreds of reactions, whose kinetics will define the evolution of the overall reaction and the production and destruction of pollutants [149]. Explicit modeling considering an extensive chemical kinetics mechanism is particularly needed for a system such as a gas turbine engine, where combustion occurs within dynamic multiphase flows over complex geometries, with large gradients of temperature and pressure, and short residence time (in which the reactants are in the region of reaction) — and for which there are concerns about efficiency, stability, formation of pollutants, noise and vibration.

Most importantly to this thesis, the N_2 which is largely inert under standard atmospheric conditions, will, under the high temperatures of combustion, break down to form different reactive species containing nitrogen. This includes NO and NO_2, which are quickly interconverted in the atmosphere, and thus are conveniently referred together as the NO_x chemical family [56]; although it will mostly be in NO form during combustion. For fuels with at most trace amounts of nitrogen in their composition, such as aviation kerosene, the most important mechanism for NO_x formation is the "thermal", or Zeldovich mechanism [150]. The triple bond of N_2 is broken by dissociated O and the nitrogen is subsequently oxidized:

$$\begin{aligned} O + N_2 &\rightleftharpoons NO + N \\ N + O_2 &\rightleftharpoons NO + O \\ N + OH &\rightleftharpoons NO + H \end{aligned} \tag{2.3}$$

NO_x formation is thus largely dependent on the temperature reached by the combustion gases, as illustrated in Figure 2.3, as well as the time spent at high temperature. This creates a challenge since high combustion temperatures are desirable to increase specific power, thermodynamic cycle efficiency, and combustion efficiency, therefore decreasing emissions of other pollutants and extracting the most energy out of the fuel [147]. Several solutions in engine design are used to mitigate NO_x formation in aircraft engines, generally with the goals of promoting more uniform combustion throughout the combustor (reducing localized peaks in temperature) and of burning the fuel as much as possible outside of the regime of higher temperatures near stoichiometry.

In the rich-quench-lean combustor architecture, a first stage of combustion occurs in a fuel-rich condition, air is introduced to quickly shift the mixture to a fuel-lean condition, spending as little time as possible at the stoichiometric point before diluting pollutants and achieving the completion of combustion at lean conditions [148, 151]. This strategy is used by most modern engines, e.g. the TALON X combustor designs used by Pratt & Whittney [152]. Alternatively, designs can aim to stay in a lean-burn regime throughout the entire combustion process, e.g. the TAPS design used by General Electric [153]. This introduces issues with flame stability, which can be addressed with a pilot flame stage and improved mixing, such as with lean direct injection and lean premixed prevaporized concepts. Additional stages and more complex injector geometries have the possible downsides of increasing combustor size and pressure drop, and premixing fuel and air carry risks of autoignition and flashback [147, 148, 151]. Even if temperatures spikes are avoided during combustion, improvements in turbine material and cooling technology allow for the temperature at turbine inlet to be high enough to produce NO_x regardless of combus-

tor design, which can potentially become a limiting factor on emissions reduction in the future [148].

As discussed throughout this chapter, NO_x is one of the most important atmospheric pollutants as an oxidizing agent, as a toxicant to humans (Section 2.2) and as a precursor of O_3 (Section 2.5.1), HNO_3, and particulate matter (Section 2.5.2). NO_x and its atmospheric products also have downstream environmental impacts after deposition over land and water (Section 2.3).

Unburned hydrocarbons (HC) and carbon monoxide (CO)

The combustion of hydrocarbons involves the breaking up the fuel molecules into smaller parts, ultimately leading to the formation of CO and then its oxidation into CO_2 [146]. Incomplete combustion results in a certain amount of unburned or partially oxidized hydrocarbons and carbon monoxide remaining as products. In premixed combustion, this can occur if there is a lack of oxidizer, i.e. in a fuel-rich mixture. But even if there is sufficient oxygen overall for complete combustion, some amount of CO_2 will dissociate back into CO at high temperatures.

For the case of a combustor in an aircraft engine, mixing is not perfect, and combustion is not uniform. Locally lean regions have lower temperature and can prevent flame propagation, leaving some amount of fuel partially oxidized [146]. Locally rich regions, in turn, can lead to insufficient amounts of oxidizer being provided for fuel to react with. Overly lean and rich regions are more problematic at low and high thrust levels, respectively, as the equivalence ratio increases with thrust setting. Additionally, lower temperatures result in lower reaction rates, such that the residence time might be short enough for CO to fully oxidize. Higher temperatures in the combustor favor the completeness of combustion through faster reaction rates and sufficient oxidizer supply, thus being desirable for the reduction in the emission of unburned hydrocarbons and carbon monoxide. But higher temperatures are also detrimental in terms of NO_x emissions, as discussed previously.

As described in Section 2.2, CO is noxious to human health, with short-term acute exposures being of particular concern. "Unburned hydrocarbons" on the other hand is an umbrella for a multitude of chemical species which can have different levels of toxicity to humans. Various volatile organic compounds are emitted by aircraft engines, some of which known to be carcinogenic [4]. Both CO and unburned hydrocarbons contribute to tropospheric ozone formation (Section 2.5.1).

Sulfur oxides (SO_x)

Jet fuel being a single hydrocarbon, as in Equation (2.2), is another simplification. In reality it is kerosene distilled from petroleum, yielding a mixture of hydrocarbons with some impurities, and with additives to meet technical requirements, such as those in the standards in Refs. [154, 155]. These standards currently allow up to 3000 ppm (mass) of sulfur content (*FSC*), although typical concentrations have been estimated in 2010 to average between 550–750 ppm in the United States and United Kingdom, with significant variability per sample and per region [156]. 600 ppm has been adopted as a typical value representative of global emissions [157, 158], including in the emissions inventory described in Chapter 3. Local measurements in other studies (i.e. not a broad survey) show similar levels of fuel sulfur content: 700 ppm [159], 490 ppm [160], 500 ppm (200–900) [161]. During combustion, sulfur attached to hydrocarbons forms H_2S, which then oxidizes, primarily

to SO_2 [162]. Some of which is oxidized further into SO_3, which under the presence of water rapidly forms H_2SO_4. A conversion factor (ϵ) can be used to relate the abundance of S^{VI} to total sulfur, with atmospheric studies typically considering all sulfur in the fuel to be emitted in the form of sulfur dioxide, sulfate, or another form of S^{VI} [157]. This is shown in Equation (2.4), where M_i is the molecular weight of species *i*. Estimates of ϵ range between 1–3% [4, 163–166]. The combination of all emissions of oxidized sulfur compounds is referred to as SO_x.

$$\begin{aligned} EI\left(SO_2\right) &= \frac{M_{SO_2}}{M_S} \cdot 10^3 \cdot FSC \cdot (1-\epsilon) \\ EI\left(SO_4^{2-}\right) &= \frac{M_{SO_4^{2-}}}{M_S} \cdot 10^3 \cdot FSC \cdot \epsilon \end{aligned} \tag{2.4}$$

Particulate matter

Particulate matter emitted by aircraft engines consist mostly of ultrafine soot particles, with geometric mean diameter in the tens of nanometers [4, 163, 167, 168]. These particles are mainly composed of elemental carbon (black carbon), with traces of metals from engine components. They are largely nonvolatile (nvPM) and remain as solids despite the high temperatures of the jet exhaust. Soot forms due to localized incomplete combustion, involving complex mechanisms which depend on fuel composition, spray formation, turbulent flow field, and soot oxidation [168]. Some forms of sustainable aviation fuels, proposed to reduce aviation's carbon footprint, have significantly lower concentrations of sulfur and of aromatic species, which can potentially lead to significant reductions in nvPM [35, 39, 160, 163, 168]. A smaller amount of volatile particulate matter is also emitted, primarily in the form of a coating on the soot particles. Possible sources of volatile material are gas-to-particle conversion of volatile organic compounds from incomplete combustion and lubrication oil, and sulfur in the fuel or ambient air [163].

2.4.2 Aircraft engine emissions standards

Turbofan engines used in aircraft for civilian use have to meet the emission requirements defined by the standard in Volume II of Annex 16 to the Convention on International Civil Aviation [7]. This standard applies to engines with a rated thrust >26.7 kN, with a summary of the results from certification tests submitted being published as the ICAO Engine Emissions Databank [169]. While the standard also covers engines for supersonic aircraft, this section describes only the part that applies to engines for subsonic flight. A standard landing and takeoff (LTO) cycle is defined, according to Table 2.5.

For each of the thrust settings listed in Table 2.5, fuel flow rate and emissions at the exhaust are measured and adjusted for temperature, pressure, humidity, and fuel composition (hydrogen/carbon ratio) so as to represent expected values at sea level conditions in the international standard atmosphere with 6.34 g/kg specific humidity. Normalized emission indices (mass ratio between emissions and fuel burned, EI) are then used to quantify the mass of emissions (D_p) for the standard LTO cycle of Table 2.5. The mean values across all tests realized are then adjusted further depending on the number of engines tested, with larger margins applied if fewer engines were tested, yielding values of characteristic emissions. Given the different emission indices and fuel flow rates at each engine thrust setting

Table 2.5: Standard LTO cycle used for engine emissions certification [169].

Mode	Thrust setting F_{00}	Time in mode minutes
Takeoff	100%	0.7
Climb	85%	2.2
Approach	30%	4.0
Taxi / ground idle	7%	26.0

(Figure 2.4), and the defined time at each setting, NO_x compliance is largely determined by performance at 85% and 100% of rated thrust, while CO and hydrocarbons compliance is mostly determined by performance at 7%. The majority of $nvPM_m$ and $nvPM_N$ characteristic emissions can come from any of the four thrust settings, depending on the engine.

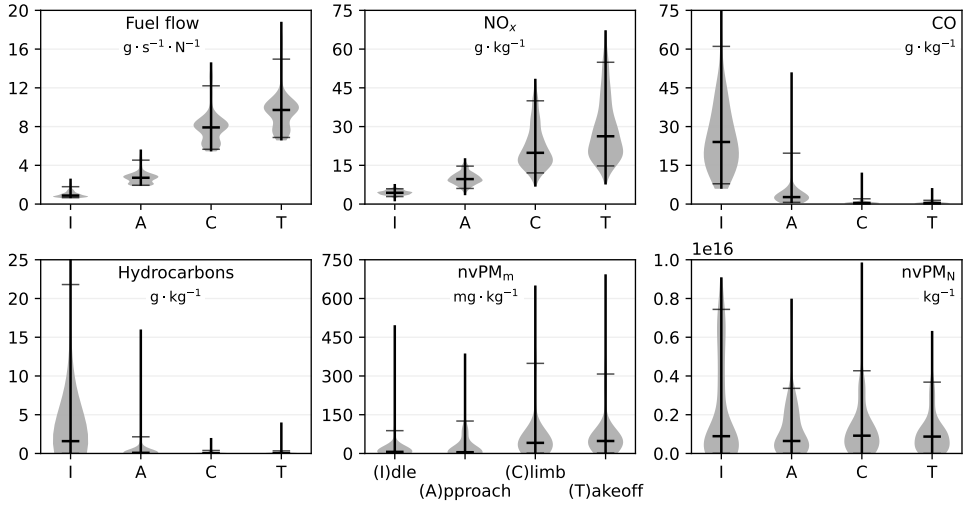

Figure 2.4: Distribution of entries of emission index and fuel flow normalized by rated thrust per thrust setting in the ICAO Engine Emissions Databank, as of June 2023 [169]. 5%, 50%, and 95% quantiles are indicated with horizontal whiskers. Engines that are no longer in production are included. The number of entries, which exclude those with superseded data, is 572 for gaseous emissions and fuel flow, and 185 for nvPM emissions. These distributions are merely for illustration of differences between each thrust setting, as they do not factor in the number of engines produced or the number of engines is use, and thus have a bias towards engine models that happen to have more versions certified.

Limits are set for the allowable characteristic emissions of NO_x, carbon monoxide (CO), unburned hydrocarbons, and nonvolatile particulate matter (mass and number of particles) normalized by rated thrust (D_p/F_{00}). For hydrocarbons, a limit of 19.6 g/kN (base CH_4) applies to engines manufactured on or after January 1, 1984. For CO, engines manufactured on or after July 7, 1997 have a limit of 118 kN. The regulatory limit for NO_x, which is variable with the engine's overall pressure ratio and possibly with rated thrust, has been revised 4 times so far since the original standard, as shown in Figure 2.5. The most recent

NO_x limits apply to engine models that entered into production on or after January 1, 2014 and to engines for use in an aircraft that had its type certificate submitted on or after January 1, 2023 (Table 2.6).

Table 2.6: Maximum allowable characteristic NO_x emissions for aircraft engine modules introduced from 2014, according to reference engine pressure ratio (π_{00}) and rated thrust (F_{00}) [7].

π_{00}	F_{00}	Limit for D_p/F_{00}
≤ 30	26.7 ⋯ 89	$40.052 + 1.5681\,\pi_{00} - 0.3615\,F_{00} - 0.0018\,\pi_{00}\,F_{00}$
	> 89	$7.88 + 1.408\,\pi_{00}$
30 ⋯ 104.7	26.7 ⋯ 89	$41.9435 + 1.505\,\pi_{00} - 0.5823\,F_{00} + 0.005562\,\pi_{00}\,F_{00}$
	> 89	$-9.88 + 2\,\pi_{00}$
≥ 104.7	≥ 26.7	$32 + 1.6\,\pi_{00}$

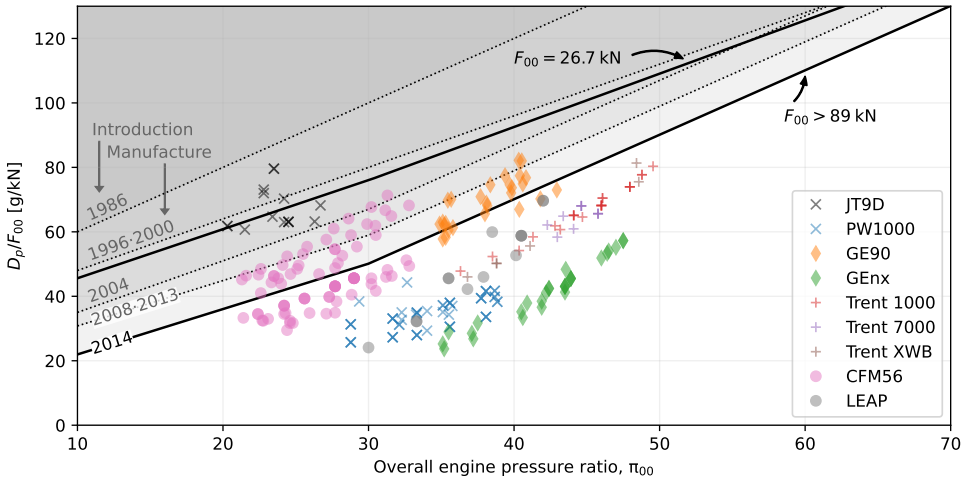

Figure 2.5: Characteristic NO_x emissions for subsonic turbofan engines per rated thrust according to ICAO standard [7]. Black lines indicate limits valid for models produced from (January 1st) 2014, both for a thrust of 26.7 kN and for >89 kN. Dotted lines indicate limits for older engines with thrust >89 kN, based on the year the model was introduced and possibly also the year manufacture of the unit. Certification values for models of a selection of engine families are shown as markers [169].

Long before the creation of ICAO's standard on aircraft emissions, the impact of jet aircraft emissions on visibility was of concern [170]. From its first edition, ICAO's Annex 16 Volume II regulates particulate matter by way of a "smoke number": a dimensionless value on a scale of 0 to 100 determined by a standardized measurement based on the staining of an air filter exposed to the aircraft exhaust. Motivated in part by growing concern about the health impacts of ultrafine particles, direct limits on emissions of nonvolatile particulate matter were introduced in the July 2017 version of ICAO's Annex 16 Volume II. A set of limits on both particle mass ($nvPM_m$) and number ($nvPM_N$), as a function of rated

thrust, are applied to engine models that enter in production on or after January 1, 2023. A more lenient set of limits apply to previously existing models that are manufactured on or after that date, as shown in Figure 2.6. A limit is also set on the mass maximum concentration of nvPM in the exhaust measured at any thrust level, with the same requirement for all engines manufactured from 2023, with the goal of ensuring the exhaust is not visible to the naked eye [171].

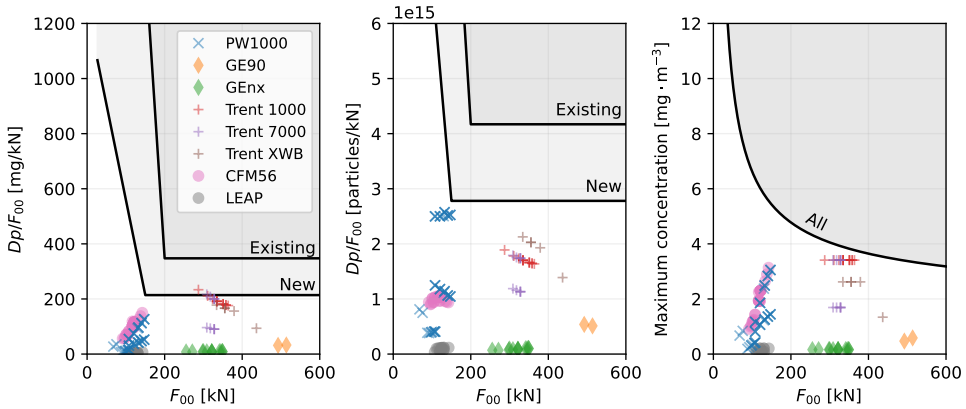

Figure 2.6: Characteristic $nvPM_m$ (left) and $nvPM_N$ (center) emissions and maximum nvPM concentration (right) for subsonic turbofan engines per rated thrust according to ICAO standard [7]. Lines indicate limits valid for models newly introduced from (January 1st) 2023 and units of previously existing models manufactured from that date. Certification values for models of a selection of engine families are shown as markers [169].

2.4.3 Other emissions from aviation

In addition to the exhaust of main engines and APU, aircraft also release emissions due to tire and break wear, and resuspension of particles from the pavement [4, 172]. Besides the fixed-wing aircraft considered in this thesis, large airports might operate rotary-wing aircraft, which are typically powered by turboshaft engines. A number of additional sources of emissions exists in the operation of airports, including: airside vehicles, fuel farms, fire training activities, aircraft engine testing facilities, road traffic and parking, heating, ventilation, and air conditioning equipment, and local transit systems, power generation, water treatment, and food preparation [21, 173, 174]. Airside vehicles are a superset of ground support equipment, that includes catering service trucks, aircraft tractors, hi-loaders, conveyor belt loaders, and other handling equipment. The construction phase of airports also causes a host of emissions [173]. Land use change is also associated with construction or expansion of aviation facilities [175], which might have a net effect on atmospheric emissions. Lastly, life cycle analysis of aviation fuel — be it fossil or different kinds of sustainable fuel — reveals further emissions associated with their production (including land use change), processing, and transportation [176–178].

2.5 Atmospheric processes involved in air quality degradation from aircraft emissions

2.5.1 NO_x cycles and ozone

In this section, relevant aspects of the atmospheric chemistry involving NO_x and ozone are summarized, based on Ref. [56].

During daytime, tropospheric NO_2 is photolyzed into NO, also leading to the formation of O_3, and these products then react to form NO_2 again (Eq. (2.5)). This comparatively fast interchange between NO_2 and NO makes it convenient to treat them as a chemical family, NO_x. Closer to the surface, higher temperatures and higher concentrations of O_3 cause higher ratios of NO_2 to NO than in the upper troposphere, where the last reaction of Equation (2.5) is slower.

$$\begin{aligned} NO_2 &\xrightarrow{h\nu} NO + O \\ O + O_2 &\longrightarrow O_3 \\ O_3 + NO &\longrightarrow NO_2 + O_2 \end{aligned} \tag{2.5}$$

During the day, nitric acid is the main sink for NO_x through the following reaction:

$$OH + NO_2 \longrightarrow HNO_3 \tag{2.6}$$

Without solar radiation at night, NO_x is almost completely in the form of NO_2. The lack of photolysis and NO allows the nitrate radical (NO_3), which is formed by the reaction in Equation (2.7), to be play a more significant role.

$$NO_2 + O_3 \longrightarrow NO_3 + O_2 \tag{2.7}$$

Specifically, more nitrate radicals are available at night to participate in the conversion of NO_2 into N_2O_5, which thermally (and photolitically during the day) decomposes back forming an equilibrium (Eq. (2.8)). Based on this behavior, another chemical family can be defined as $NO_3^* = NO_3 + N_2O_5$. Higher in the troposphere, lower temperatures and higher concentrations of NO_2 cause N_2O_5 levels to be higher.

$$NO_2 + NO_3 \rightleftharpoons N_2O_5 \tag{2.8}$$

N_2O_5 reacts with water on the surface of aerosol particles to form HNO_3, which will subsequently evaporate into the gas phase:

$$N_2O_5 + H_2O(s) \longrightarrow 2\,HNO_3(s) \tag{2.9}$$

Another component in the tropospheric formation of ozone is the HO_x family. The hydroxyl radical (OH) is formed by photolysis of ozone in the presence of water, and, due to its reactivity, is fundamental to the oxidation of all sorts of atmospheric trace species. This includes organic compounds in general, which are progressively broken down into simpler molecules, ending with the oxidation of CO into CO_2. Hydroperoxyl (HO_2) is formed during these oxidation steps (as well as peroxy radicals more generally, referred to as RO_2), and is quickly interconverted with OH, such that both species are referred

together as HO_x. As an alternative to NO being oxidized into NO_2 by ozone, as in the third reaction in Equation (2.5), HO_2 can complete the NO_x cycle as follows:

$$HO_2 + NO \longrightarrow NO_2 + OH \tag{2.10}$$

The consumption of the ozone produced in the photolysis of NO_2 is avoided with this reaction between HO_2 and NO, resulting in a net production of ozone, as shown in the diagram in Figure 2.7. In addition to the processes described, the figure also indicates two important reservoir species: hydrogen peroxide (H_2O_2) and PAN (peroxyacyl nitrates).

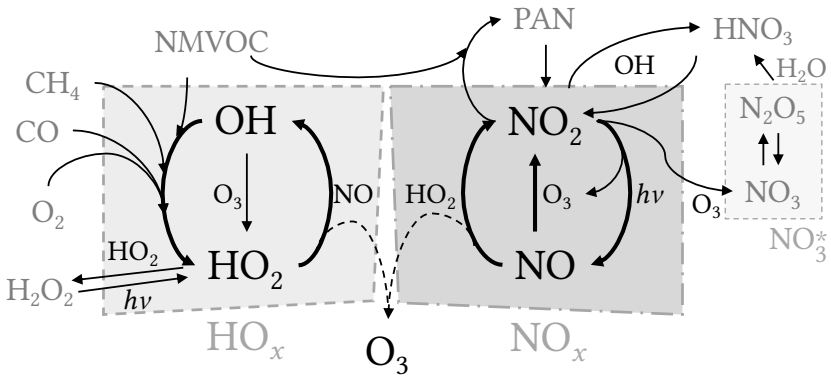

Figure 2.7: Main reactions involved in the tropospheric production of ozone. NMVOC = non-methane volatile organic compounds. PAN = peroxyacyl nitrates. Diagram based on Refs. [56, 179].

Tropospheric ozone production from NO_x thus depends on the presence of peroxy radicals which are intermediates in the oxidation of organic species. This makes air quality, particularly in urban environments, dependent on the balance of emissions of both NO_x and volatile organic compounds (VOC) [56, 180]. At high VOC and low NO_x concentrations, ozone formation is NO_x-limited, such that more emissions of it will lead to more ozone being formed. At low VOC and high NO_x concentrations however, the ozone formation regime might be called VOC-limited or NO_x-saturated, and further NO_x emissions will not result in an ozone increase. And since NO_x and VOC both compete for OH, additional NO_x in this regime slows down VOC oxidation, resulting in a decrease in ozone concentration. This is sometimes called the "weekend ozone effect", as it explains the previously observed increases in ozone over some urban areas in the United States during the weekend, despite lower NO_x emissions due to reduced road traffic [181].

Another aspect to consider is that part of aircraft emissions are released into the stratosphere, where the dynamics between NO_x and ozone are different. About 90% of atmospheric ozone is located in the stratosphere, where it is central to its chemistry. The mixing ratio of ozone is typically a few ppm in the stratosphere, up to around 12 ppm at the peak of the ozone layer at ~25 km [56], compared to tens of ppb at ground-level. Ozone is produced due to photolysis of O_2 into the O radical in the stratosphere, and is itself photolyzed by longer wavelength radiation back into O and O_2. The grouping of O_3 and O is called the O_x, or odd-oxygen family.

NO_x and HO_x cycles are slightly different in the stratosphere, and both chemical families are responsible for catalytic depletion of ozone, keeping its concentration lower than what would be expected solely from photolysis rates. NO_x contributes to ozone destruction by two pathways: Equations (2.11) and (2.12). Most stratospheric NO_x is originated from the photodissociation of N_2O, which is largely inert in the troposphere, and to lesser degree from the reaction of N_2O and oxygen atoms in the excited state $O(^1D)$. Therefore, both anthropogenic emissions of N_2O at ground-level and stratospheric emissions of NO_x by aviation lead to additional ozone depletion.

$$\begin{aligned} NO + O_3 &\longrightarrow NO_2 + O_2 \\ NO_2 + O &\longrightarrow NO + O_2 \end{aligned} \tag{2.11}$$

$$\begin{aligned} NO + O_3 &\longrightarrow NO_2 + O_2 \\ NO_2 + O_3 &\longrightarrow NO_3 + O_2 \\ NO_3 &\xrightarrow{h\nu} NO + O_2 \end{aligned} \tag{2.12}$$

The ozone layer absorbs radiation in the 240–290 nm (UV-C, or "hard ultraviolet") and 290–320 nm (UV-B, "intermediate ultraviolet"), which are damaging to living organisms. While increases in (breathable) tropospheric ozone are noxious to human health, decreases in stratospheric ozone also leads to harm, in the form of increased rates of skin cancer [182]. As most aircraft emissions are released in the upper troposphere and lower stratosphere, they can contribute to both of these effects. Current subsonic aircraft are estimated to result in a net increase in ozone column (combining aircraft-attributable tropospheric production and stratospheric depletion), and thus reduction in ground-level UV-B impacts [32]. Potential (higher-flying) supersonic aircraft are expected to result in a net global decrease in ozone column [183–185].

2.5.2 Secondary particulate matter formation

In addition to directly releasing primary particulate matter (PM), combustion also releases emissions that cause the formation of secondary PM through photochemical processes and physical transformations in the atmosphere. Secondary particular matter vary in particle size, chemical composition, volatility, phase (liquid or solid), and morphology. Important chemical components include sulfate (SO_4^{2-}), bisulfate (HSO_4^-), nitrate (NO_3^-), ammonium (NH_4^+), and a multitude organic species. Several pathways exist between gaseous emissions and aerosol, but in broad terms, NO_2 oxidizes into nitrates, SO_2 oxidizes into sulfates, ammonia (NH_3) converts into NH_4^+, and volatile organic compounds (VOC) oxidize into secondary organic aerosol (SOA). Figure 2.8 illustrates this simplified overview of aerosol formation. Aerosol formation occurs through precipitation of gaseous species into solids, and absorption into water or existing solid particles.

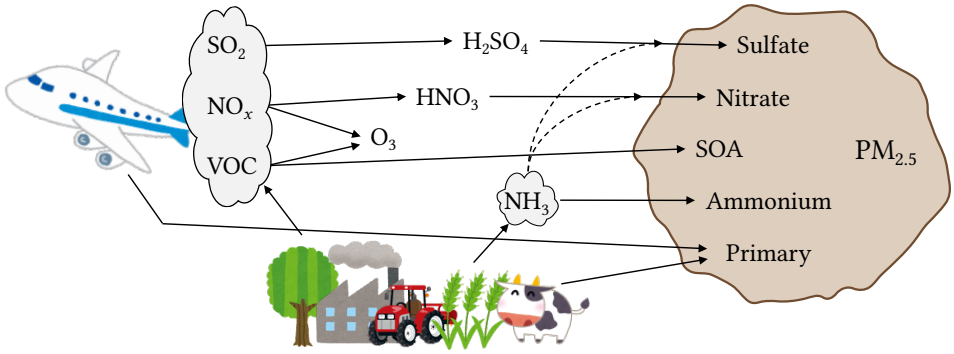

Figure 2.8: Simplified overview of secondary $PM_{2.5}$ formation. Based on Ref. [180].

Atmospheric sulfate is formed through multiple pathways [56, 186]. In the gas phase, sulfur compounds are oxidized mainly by OH, transforming reduced species such as hydrogen sulfide (H_2S) and dimethyl sulfide ($(CH_3)_2S$), as well as SO_2 (oxidation state +4) into sulfuric acid (H_2SO_4), which has an oxidation state of +6. H_2SO_4 dissolves in water, dissociating into HSO_4^- and SO_4^{2-} (plus H^+). SO_2 also dissolves in water subsequently dissociating into HSO_3^- and SO_3^{2-} (plus H^+). Oxidation leading to sulfate takes place in aqueous phase by different pathways, driven by nitrogen oxides, H_2O_2, ozone, organic peroxides, formaldehyde, and O_2 with catalysis by transition metal ions, among other species. Therefore, aircraft contribute to sulfate formation not only by emitting SO_x, but also by its NO_x emissions, which promote the oxidation of already present sulfur-containing compounds through these various mechanisms [187].

Within and around cloud droplets, interactions occur between the components of the ammonia–nitric acid–sulfuric acid–water system, with a thermodynamic equilibrium being reached involving species in the gaseous, solid, and aqueous phases [56]. Besides chemical concentrations, this equilibrium is also dependent on temperature, humidity, and particle pH. Like SO_2 and H_2SO_4, NH_3 and HNO_3 also maintain an equilibrium between gaseous and aqueous phases. Practically all aqueous NH_3 dissociates into $NH_4^+ + OH^-$. Likewise, HNO_3 dissociates into $NO_3^- + H^+$. As the dissolved gases dissociate into ions, their aqueous phase concentration decreases, causing further absorption of the gases into water. If water evaporates and relative humidity lowers, the solutes will precipitate as various forms of crystals. Conversely, increasing relative humidity causes solids to absorb water, forming an aqueous solution. The aforementioned system of interest comprises solid species such as NH_4HSO_4, $(NH_4)_2SO_4$, NH_4NO_3, $(NH_4)_2SO_4 \cdot 2NH_4NO_3$, $(NH_4)_2SO_4 \cdot 3NH_4NO_3$, and $(NH_4)_3H(SO_4)_2$. Overall, a very simplistic representation of inorganic aerosol formation is Equation (2.13); with the additional consideration that, with water, part of sulfates and nitrates will be in the form of ions.

$$\begin{aligned} NH_3(g) + HNO_3(g) &\rightleftharpoons NH_4NO_3(s) \\ 2NH_3(g) + H_2SO_4(g) &\rightleftharpoons (NH_4)_2SO_4(s) \end{aligned} \tag{2.13}$$

Because ammonia will preferentially react with sulfuric acid, nitrate formation depends on the availability of sufficient ammonia to convert H_2SO_4 into sulfate. Different

regimes of PM formation can occur depending the availability of ammonia. When total ammonia (the sum of gas, aqueous, and solid forms) is less than twice the concentration of total sulfates (likewise including gaseous precursors), it is not able to neutralize all sulfate present, causing HNO_3 to remain as a gas [56]. Ansari and Pandis [188] proposed the gas ratio (*GR*), defined by Equation (2.14), as an indicator of which regime is taking place. While other factors are involved in aerosol thermodynamics (such as temperature and relative humidity), $GR < 1$ generally indicates that nitrate production is limited by ammonia availability, and $GR > 1$ indicates that more nitrate is formed with increases in HNO_3.

$$GR = \frac{[NH_3] + [NH_4^+] - 2[SO_4^{2-}]}{[HNO_3] + [NO_3^-]} \tag{2.14}$$

Additionally to these systems, heterogeneous reactions[3] are also significant factors in inorganic aerosol formation. An important heterogeneous reaction is the nightly hydrolysis of N_2O_5 into HNO_3, seen previously in Equation (2.9). Other reactions include the uptake of HNO_3, NO_3^-, N_2O_5, SO_2, H_2SO_4 on dust and sea salt particles [189]. Nitrate formation on coarse particles via heterogeneous chemistry can compete for HNO_3 with pathways that form fine particles ($PM_{2.5}$) [190]. This creates a dependency of inorganic $PM_{2.5}$ formation on other aerosol components like sodium (Na^+), chloride (Cl^-), crustal material (Ca^{2+}, K^+, Mg^{2+}) and organic species, which enable other aerosol formation pathways and affect reactions through the pH of particles [191].

Secondary organic aerosol (SOA) formation is even more complicated, owed to the vast number of species involved [192–194]. In broad terms, SOA is formed through the many steps of gas-phase oxidation of volatile organic compounds (VOC) [56]. Multiple oxidants contribute in this process, such as OH, O_3, and the NO_3 radical. Oxidation leads to species with more functional groups, which tend to have lower volatility and higher solubility, being thus more prone to condensation into aerosol [192]. At the same time, the breaking up of large organic species into smaller ones leads to the formation of species of higher volatility, and ultimately to the oxidation into CO_2. This means that SOA formation depends on the multitude of intermediate species of VOC oxidation, which have different characteristics with regard to reactivity, volatility, photolability, and solubility. As the ability to measure organic species in the atmosphere improved, the importance of lower volatility organic compounds has been explored further, as did the role of various heterogeneous and multiphase reactions, although there remains plenty of open questions about the formation of SOA which are under investigation [192–195]. Aircraft contribute to SOA both by emitting organic species and by contributing to the oxidizing capacity of the atmosphere.

2.5.3 Long range pollution transport

While low-altitude emissions have a direct impact on local air quality, impacts from intercontinental pollution transport are still of concern. The United Nations Economic Commission for Europe (UNECE) directed the creation in 1979 of the Convention on Long-range Transboundary Air Pollution (CLRTAP), with the aim of promoting cooperation to reduce

[3] Heterogeneous reactions refer to those involving a gas against a surface, as opposed to multiphase reactions, which include interactions between gases and liquid volumes.

effects of air pollution between countries in the northern hemisphere. This led to a number of international protocols, including the 1999 Gothenburg Protocol to Abate Acidification, Eutrophication and Ground-level Ozone (revised later in 2012), which covers critical loads of nitrogen deposition and national emission ceilings for sulfur, NO_x, VOCs, and NH_3 [196].

Within CLRTAP, the Task Force on Hemispheric Transport of Air Pollution (TF HTAP) was established in 2004 as an international collaboration to improve scientific understanding of long-range air pollution. HTAP performed studies using an ensemble of atmospheric chemical transport models (CTMs), estimating air quality impacts over the hemisphere due to anthropogenic emissions in four regions for the base year of 2001 [197]. Extra-regional emissions were found to contribute 30% (North America), ≥ 50% (Europe), 20% (South Asia), and 30% (East Asia) of each region's mortality associated with ozone [198]. Likewise, extra-regional emissions were estimated to represent 3–7% of $PM_{2.5}$ mortality in those regions [199]. HTAP also found that between 3–10% of NO_x emissions were deposited as N_r outside the source region [200].

A second phase of HTAP used improved models and updated emission estimates, with different region definitions, for the base year 2010. It was found that the fraction of ozone mortality from anthropogenic emissions that occur outside the source region are 5% (South Asia), 15% (East Asia), 45% (Europe), 46% (North America), 78% (Russia-Belarus-Ukraine), and that more than half of ozone mortality in the last three of those regions come from extra-regional emissions [201]. The same study also found that $PM_{2.5}$ impacts are more localized, with the fraction of mortality in external receptors being 7%, 6%, 19%, 7%, 18%, 68% for regions in the same order. However, because — for the concentration-response functions considered — global health impacts from $PM_{2.5}$ were estimated to be about one order of magnitude larger than from ozone, the magnitude of transboundary health impacts was greater for $PM_{2.5}$.

In these studies using CTMs and focused on ground-level emission sources, several pathways have been identified as contributing to intercontinental pollution transport (Figure 2.9). The higher efficiency of transport at higher altitudes associated with lower temperatures (and thus longer atmospheric lifetimes) and higher wind speeds is particularly relevant to aviation, which impact air quality mostly through NO_x emitted in the upper troposphere and lower stratosphere. As described in Section 2.5.1, NO_x causes production of ozone, which has a lifetime in the free troposphere of weeks or months [56, 197]. Besides being itself toxic to humans, ozone affects $PM_{2.5}$ formation, as described in Section 2.5.2. It has been suggested that aircraft impacts on ground-level $PM_{2.5}$ are largely mediated by ozone [32]. Tropospheric ozone is also affected by exchanges with the stratosphere [202], where concentrations are higher, and where a significant fraction of aircraft cruising takes place. While the atmospheric lifetime of NO_x is only a few days at low altitude, it is about two weeks in the upper troposphere, due to a higher ratio of NO to NO_2 [56]. Additionally, peroxyacyl nitrates (PAN, formula $RC(O)OONO_2$) serve as a significant reservoir for NO_x in the troposphere [56], according to the reversible reaction in Equation (2.15) for the main component of the group, peroxyacetyl nitrate. The main sink of NO_x in the atmosphere is HNO_3, which is also the main driver of nitrate aerosol formation (Section 2.5.2). Given all these contributing factors, before being removed by wet or dry deposition, aircraft NO_x and its products can be transported long distances as illustrated in Figure 2.9.

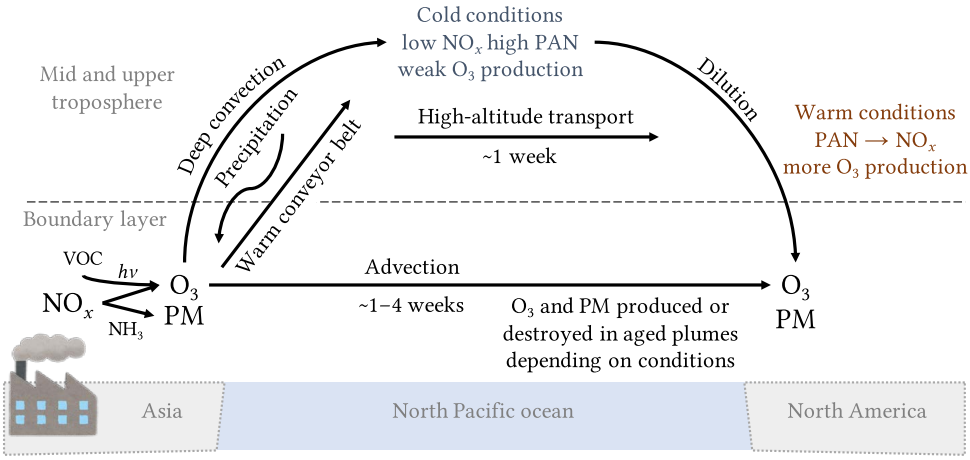

Figure 2.9: Processes involved in intercontinental transport of pollution from ground-level sources, with the north Pacific ocean as an example. Based on Ref. [197].

$$CH_3C(O)O_2 + NO_2 \rightleftharpoons CH_3C(O)O_2NO_2 \tag{2.15}$$

As a result of these long-range transport processes, intercontinental pollution effects tend to follow the global atmospheric circulation patterns, as is also observed in simulations with Lagrangian CTMs [203]. Studies modeling high-altitude aircraft emissions also observe this pattern using both Eulerian [30] and Lagrangian models [204], and this is a key factor in regional differences of air quality sensitivity to aircraft emissions, as discussed in Chapter 5. The westerly prevailing winds in the mid-latitude northern troposphere are particularly important, given the location of human population and emissions, with anthropogenic emissions from all sectors in North America, Europe, and Asia having a more significant impact on air quality and nitrogen deposition in the continent to their east [201, 203, 205]. Policies aiming to reduce effects of air pollution are thus complicated by the interdependency of international trade, emissions from industry and transportation, and long-range pollution transport [206, 207]. The aviation sector has further complications to source apportionment and regulation as approximately 65% of aircraft fuel is burned in international flights [208], with emissions potentially being released over third countries and international waters.

3

Present-day aircraft emissions

You wanna know how to rhyme? You better learn how to add
(...)
Why did one straw break the camel's back?
Here's the secret — the million other straws underneath it

Mathmatics, by Yasiin Bey (Mos Def)[1]

Comprehensive assessments of the environmental impacts of the aviation industry require up-to-date, spatially-resolved, and speciated emissions inventories. In this chapter, the first such estimate of global emissions from aircraft operations for the years 2017–2020 is developed and evaluated. Aircraft activity data, based on flights registered by networks of aircraft Automatic Dependent Surveillance-Broadcast (ADS-B) telemetry receivers, are used together with the Base of Aircraft Data (BADA) 3.15 aircraft performance model and the ICAO Engine Emissions Databank to estimate spatially-resolved fuel burn and emissions of CO_2, H_2O, NO_x ($NO + NO_2$), SO_x ($SO_2 + SO_4^{2-}$), CO, unburned hydrocarbons (HC), and nonvolatile particulate matter (nvPM). It is calculated that 937 Tg of CO_2 and 4.62 Tg of NO_x (base NO_2) were emitted by aircraft in 2019, and the evolution over time of fleet average emission indices is quantified. Owing to impacts from COVID-19, 48% lower fuel burn is estimated for 2020, resulting in 463 Tg less CO_2 and 2.29 Tg less NO_x emitted in that year than what would be otherwise expected. It is concluded that ADS-B is a viable source of data to generate global emissions estimates in a timely and transparent manner for monitoring and assessing aviation's atmospheric impacts.

This chapter was originally published in the Journal of Aircraft. Please cite as shown in the list of peer-reviewed journal articles, item 3.

[1]Written by Dante Smith (Yasiin Bey) and Christopher Martin (DJ Premier).

3.1 Introduction

Atmospheric emissions from aviation contribute to climate change [5] and to degradation of air quality, related to human health effects [4, 209]. Aviation is estimated to have contributed 3.5% of global net anthropogenic effective radiative forcing in 2011 [5], and its associated increase of ground-level fine particulate matter ($PM_{2.5}$) and ozone has been estimated to have led to 16,000 premature deaths globally in 2005 [1]. Such environmental impacts should be considered when evaluating the feasibility and societal benefit of new aircraft technology concepts or policy scenarios [210, 211]. The resulting air quality and climate impacts from aviation depend on the spatial and temporal distribution of the emissions. The air quality impacts of aviation are often regarded and generally regulated as a local air quality issue [19–21], although there is growing evidence suggesting that the majority of human health impacts might result from high altitude (cruise) emissions of oxides of nitrogen (NO_x), which affect ground-level air quality at a hemispheric range [1, 12, 30, 212]. The magnitude of non-local human health impacts from high altitude emissions also depends on the location of emission, due to spatial variations in atmospheric circulation and background composition, as well as population densities [12, 212]. Close to airports, aviation activity can also be a significant source of primary particulate matter, with recent research indicating that emission of high number of ultrafine particles can be particularly problematic [25, 62, 213]. Concerning the climate effects, it is estimated that the non-CO_2 terms—mainly NO_x and contrail cirrus formation—represent 66% of effective radiative forcing from aviation in 2018 [5], and those impacts can be strongly dependent on the altitude [214–216], geographical location [204, 217], and instantaneous atmospheric condition at the site of emission [218–220].

Gross aviation emissions are expected to continue to increase in the foreseeable future, with fuel burn projected to increase by 2.4 to 3.8 times from 2015 to 2045, despite future improvements in aircraft technology and operational efficiency [221, 222], posing a threat to the fulfillment of international climate goals in this century [223]. This growth varies geographically, with Asia growing at twice the rate of Europe and North America [224]. Despite the significant reduction in air traffic that started in 2020 due to the COVID-19 pandemic [225], the aviation industry expects to resume its previously forecast growth after a few years [226]. Recognizing the challenges of more revolutionary aircraft propulsion technologies contributing meaningfully to the reduction of emissions [227], and in order to meet its aspirational goal of carbon neutral growth after 2020 and 50% reduction in carbon emissions by 2050 relative to 2005, the International Civil Aviation Organization (ICAO) is relying on a combination of emissions offset schemes and widespread adoption of sustainable aviation fuels [228, 229]. As both aviation and other sectors change the intensity, location, and make-up of their emissions over the timescale of decades, the setting for air quality and climate impacts changes along with the sensitivity of impacts to each specific activity [11, 230, 231]. The evolving and interconnected nature of this problem requires continuous reanalysis of impacts and up-to-date spatially resolved aviation emissions. As the emissions are an intermediate step in a study—as input to atmospheric, climate, public health, and economic models—there is usually a large time lag between emissions data and assessments of their impact [1, 31, 232]. Tracking progress relative to aviation's environmental goals demands methods of producing global emission inventories with short reporting delays, continuous monitoring, and transparent data sourcing.

Bottom-up emissions estimates can be obtained by summing emissions calculated for every individual flight known to have occurred, which is a necessary complexity to establish the spatial distribution of emissions and obtain the specific contribution of each sector, country, or aircraft type. Unlike CO_2, SO_2 and H_2O, emission of NO_x, CO, hydrocarbons (HC), black carbon (BC), and organic carbon depend not just on the type and amount of fuel burned, but also on the engine's operating conditions, requiring simulation of individual flights. Various bottom-up aviation inventories have been compiled over the years by different institutions, using slightly different data sources and methodologies, by calculating emissions for every aircraft type and flight distance or specific origin-destination pair for a list of all flight movements being considered [233]. A global list of movements is usually obtained from historical flight schedule data sold by private companies which compile them from proprietary information, largely from airlines. Besides potentially missing data for some operators, these sources do not typically capture the portion of civil aviation consisting of general aviation, charter flights, and business flights. To complement these, some studies also use primary radar, air traffic control, or movement data obtained from aviation authorities or airspace control authorities. Alternatively, top-down estimates of emissions can be made from estimates of global aviation fuel production, without distinguishing between individual flights or segments of the industry [5]. Such top-down estimates have been shown to yield larger emissions than bottom-up inventories, consistent with the additional inclusion of fuel for military, charter, and general aviation [234, 235]. Table 3.1 presents an overview of various aviation emissions inventories and their main sources of data.

Automatic Dependent Surveillance-Broadcast (ADS-B) is a telemetry technology used in modern aircraft that automatically transmits unencrypted aircraft identification and state at time intervals ranging from less than a second to a few seconds [236]. The affordability of ADS-B receivers enables monitoring of air traffic by individuals and has led to the creation of online networks of receivers serving data to both commercial and free online services. Modernization of air traffic control is leading its use to become mandatory for commercial aviation and other flights under instrumented flight rules in various parts of the world [237, 238]. The growing availability of telemetry data recorded by ADS-B trackers has motivated their use in estimating aircraft emissions for subsets of regions, aircraft types or chemical species. Liu et al. used such a dataset of flight movements to estimate global CO_2 emissions from aviation by considering a constant value of emissions per kilometer flown, based on a previous bottom-up estimate using flight schedule data [239]. Aircraft position data reported through ADS-B have also been used to provide actually flown trajectories to a flight model to estimate emissions [240–243]. Studies incorporating trajectories recorded by ADS-B have so far been limited to estimating emissions for specific sets of flights for which there is complete tracker coverage, unlike previous inventories based on flight schedule data, which cover all regions of the world. Additionally, ADS-B data have also been used to derive aircraft properties, generating a flight performance model independent of manufacturer-supplied data, which can then be used to estimate emissions for arbitrary flight paths [244].

Table 3.1: Comparison of global civil aviation emission inventories in the literature. APM = aircraft performance model, ATC = air traffic controller.

Inventory	Year	Fuel burn, Tg	Notes	Spatial	Non-CO_2	Open source code	APM	Schedule data	Radar or ATC data
(NASA) [245–247]	1976 1984 1992	64.4 86.6 114	+ charter and general aviation	✓	✓	✘	–	OAG	–
(NASA) [248]	1999	128	Scheduled only	✓	✓	✘	–	OAG	–
(DLR) [249]	1992	112	Scheduled only	✓	✓	✘	–	ABC, ICAO	–
ANCAT/EC2 [249]	1992	114	–	✓	✓	✘	PIANO	ABC, OAG, Aeroflot	Europe
SAGE [250]	2000 2001 2002 2003 2004 2005	181 170 171 176 188 203	No piston	✓	✓	✘	–	OAG	FAA
AEIC [41, 251]	2005	181	Scheduled only	✓	✓	✓	BADA	OAG	–
AEDT [211, 252]	2006 2015	188 240	No general aviation	✓	✓	✘	–	OAG	FAA, EUROCONTROL
QUANTIFY / FAST [234, 253]	1990 2000	105 152	Scheduled only	✓	✓	✘	PIANO	OAG	–
AERO2K [235]	2002	156	–	✓	✓	✘	PIANO	Back Aviation	FAA, EUROCONTROL

Table 3.1 continued from previous page

Inventory	Year	Fuel burn, Tg	Notes	Spatial	Non-CO_2	Open source code	APM	Schedule data	Radar or ATC data
FAST / REACT4C [31]	2006	178	–	✓	✓	✘	PIANO	OAG	Europe and North America
AERO-MS [254]	2006	188	–	✓	✓	✘	BADA	EUROCONTROL	–
APMI [255]	2005 2006 2007 2008 2009 2010 2011	148 152 161 163 158 164 173	Schedule only	✓	✓	✘	BADA	CAPSTATS	–
(EPA) [256]	2015	218	No piston, no small light weight	✘	✘	✘	PIANO	FAA	FAA
(ICCT) [257]	2013 2018 2019	223 286 291	Scheduled only	✓	✘	✘	PIANO	OAG	–
FEAT [258]	2018	257	No freight	✘	✘	?	PIANO	OAG	–

This chapter presents bottom-up estimates of global civil aviation emissions using three sources of flight movements: schedule data for the year 2018 from a market intelligence company (OAG), and activity data derived from ADS-B for the period 2017–2020 both from a commercial service (Flightradar24, data starting on July 2017) and from a non-commercial crowd-sourced platform (OpenSky). An open-source module named openAVEM is developed to calculate full-flight emissions including non-CO_2 components and allocate them into a 3-D grid for every month analyzed. The viability of this method to generate a comprehensive global spatially resolved inventory of civil aviation emissions, using more openly available and traceable data, is established through the comparison of the resulting emissions. Changes in emission totals and their spatial distribution over time are discussed in the context of technological improvements and inherent technological tradeoffs in aircraft engine design, and with regard to the resulting air quality and climate change impacts. This is the first study, to the authors' best knowledge, to produce spatially resolved global estimates of aviation emissions based on ADS-B data, and the first to provide an openly available, spatially resolved and recent inventory of aviation fuel burn, CO_2, and non-CO_2 emissions, which are the drivers of aviation's atmospheric impacts [211]. In addition, it is reported, for the first time, the implications of ICAO's new nonvolatile particulate matter (nvPM) measurement data for global aircraft emissions estimates for both landing and takeoff (LTO) and non-LTO portions of flights. Finally, this model is used to provide the first comprehensive, bottom-up, global emissions quantification of the COVID-19 pandemic restrictions for the aviation sector in 2020. The resulting datasets are made openly available, as described the Appendix.

3.2 Methodology

The framework for creating a bottom-up aircraft emissions inventory is largely similar to the approach used by the Aviation Emissions Inventory Code (AEIC) described by Simone et al. [41], as well as other such bottom-up models [233–235, 252, 254, 257, 258]. The software module developed in this study to calculate emissions (named "Open Aviation Emissions Model" or, in short, openAVEM) is tasked with lists of flights defined by origin-destination pairs for each aircraft type, sourced either from ADS-B or flight schedule data. Input data containing relevant parameters for each airport, aircraft, and engine are loaded into openAVEM, which then simulates each flight. Landing and takeoff (LTO) are modeled by a time-in-mode approach, in which emissions are proportional to the estimated time spent in each aircraft mode of operation, whereas the non-LTO portion is simulated using an aircraft performance model. From the engine's properties and the thrust, fuel burn, and ambient conditions along each flight, emissions of pollutants are calculated. Finally, the emissions of all flights are summed into a 3-D grid of 0.5° latitude × 0.625° longitude × 500 ft altitude resolution. Additionally, the sensitivity of results to changes in various model input parameters is considered by running openAVEM with different configurations.

3.2.1 Origin-destination pairs

The list of flights for which emissions are calculated are obtained from three different sources described in this section. For all three sources of flight data, flights are aggregated into a count of monthly flights for each aircraft type-origin-destination combination.

2018 historic schedule data from OAG are used, consisting of both passenger and cargo scheduled flights based largely on data provided by airlines. Global passenger service data are comprehensive, but three of the largest cargo companies are not included in this dataset: FedEx, UPS, and some of the airlines owned by DHL. A list of individual flights is built from the schedule data, which are condensed by removing duplicate entries due to code-sharing agreements, and multi-leg flights are separated into individual segments. The two other sources of flight movement used consist of two sets of ADS-B telemetry data: one provided by Flightradar24, a commercial service, and another obtained from OpenSky, a nonprofit organization which manages tracker data from a collaborative network of volunteers. Data provided by Flightradar24 start in July 2017 and extends to the end of 2020. Data obtained from OpenSky extend from the start of 2017 to the end of 2020. It is noted that, despite expanding in coverage over time, OpenSky still provides reduced global coverage compared with the other two sources (further discussed in Section 3.3.5). The Flightradar24 data were prepared using the company's proprietary ADS-B and multilateration network, additional data sources, and processing procedures.

The OpenSky ADS-B data were compiled into a list of flights by Strohmeier et al. [259]. Originally, in the latter dataset, flights in which the initial and final trajectories recorded ended at an altitude not higher than 2500 m had those trajectories extrapolated to ground level, and the nearest airport was assigned as the origin or destination of the flight if it lied within 10 km of the extrapolated landing. To account for emissions of flights partially recorded in the data, those conditions are relaxed: origin and destination airports are assigned to all flights regardless of the first or last altitude seen, and airports within a radius of 500 km of the extrapolated landing are considered valid for assignment (Appendix A.1). This reprocessing is done for OpenSky because the main interest here is in the magnitude of emissions for this source of data, since its incomplete spatial coverage already precludes accurate spatial distribution at a global scale. Therefore, the main results and discussion on emissions per region of the world is focused on OAG and Flightradar24. If OpenSky coverage continues to increase over time, the need for such compromise between magnitude and spatial distribution will diminish.

Latitude and longitude coordinates and elevation for each airport given by either International Air Transport Association (IATA) or ICAO code are obtained from the OpenFlights database [260]. The number of runways and maximum runway lengths for each airport are obtained from OurAirports [261]. In the analysis of results, regional grouping of departing airports and of emissions is done according to the geoscheme used by the United Nations Statistics Division.

3.2.2 Airport, aircraft, and engine data

Aircraft performance is modeled with Base of Aircraft Data (BADA) 3.15 [262]. The mapping of IATA aircraft type codes present in schedule data to ICAO type codes used by the emissions model is given in Table A.1. To exclude military flights captured in ADS-B data, which is outside the scope of this study, a list of aircraft types considered to be military is removed from the input data (Appendix A.3).

Fuel mass flow rates, emission indices (defined as mass emitted per mass of fuel burned, EI) of NO_x, CO, HC, and nvPM, and additional engine information are taken primarily from certification data in the ICAO Engine Emission Databank [169]. Given that this

database covers only turbofans with a rated thrust greater than 26.7 kN, it is complemented with piston engine data from the Swiss Federal Office of Civil Aviation [263], and data for older engines and some turboprops as given by the U.S. Environmental Protection Agency [264] or used by Stettler et al. [265].

Because neither ADS-B nor the OAG data available in this study allow the identification of specific engine models used in each individual aircraft, reference engine models are assigned to each aircraft type [266]. This approach has been used by other global bottom-up emission inventories [41, 235, 258]. Additionally, to calculate emissions of narrowbody and widebody aircraft with multiple engine suppliers, one model is assigned for each engine family and emissions for all flights are calculated using each of those engines. The resulting emissions are then combined in a weighted sum using the aircraft type-specific market share of each engine manufacturer (Table A.4). Within an engine family for an aircraft, there are typically multiple versions due to variants with different rated thrusts and to different design revisions. In general, the newest engine versions available are used for modeling, on the assumption that the survival rate of newer versions of each aircraft type will be higher than older versions, and that old engines might be retired to comply with tightening emissions regulations. The uncertainty in global emission estimates due to the lack of knowledge of the prevalence of specific engine versions is discussed further in Section 3.3.3.

3.2.3 Flight model

The landing and takeoff portion of flights are modeled using a time-in-mode approach, in which engines are considered to run at a constant thrust for a given period of time for every phase of LTO. LTO cycles are separated into the phases of taxi-out, taxi-out acceleration, hold, takeoff, initial climb, climbout, approach, landing, reverse thrust, taxi-in acceleration, and taxi-in, according to the model proposed by Stettler et al. [265], which is based on studies conducted in the United Kingdom on airports of various sizes [267]. This model is used instead of the four-phase cycle adopted by ICAO's standard on engine emissions [7] with the goal of better capturing modern LTO conditions, considering that ICAO's cycle remains unchanged since the first edition of the standard in 1981.

Auxiliary Power Unit (APU) emissions are modeled with times-in-mode and emission indices by aircraft class according to the "advanced approach" defined in ICAO's Airport Air Quality Manual [21, 266]. Where data are available, the generic emission indices are substituted by known model specific values [173, 266].

The climb, cruise, and descent portion of flights are simulated using the BADA 3 model following a geodesic starting from 3000 ft above the origin airport and ending 3000 ft above the destination airport. BADA is formulated in terms of the total energy balance, considering the aircraft as a point of (varying) mass subjected to drag, lift, and thrust [262]. The model includes aircraft aerodynamic coefficients, operational parameters such as a climb speed schedule, and other properties necessary to obtain fuel mass flow rates for different flying conditions. Wind speed is applied through all non-LTO phases using year-specific monthly average vectors from the MERRA-2 reanalysis product in a $0.5° \times 0.625°$ grid with 72 hybrid-eta vertical levels [268]. Each flight is affected by the wind pushing the aircraft one direction or another, but the geodesic flight trajectory is maintained, with no optimization of the path due to wind being considered.

Climb is simulated in steps of 1000 ft until cruise altitude, simulated at constant altitude in ground track steps of 50 NM (nautical miles). Descent is simulated in steps of 1000 ft. For flights of at least 200 NM in length, cruise flight level is set for each aircraft type from the most common cruise altitude observed in the first 70 days of 2020 by Flightradar24. The company's proprietary system processes the ADS-B feeds to determine a flight path and identifies changes of flight mode, such as gate departure, takeoff, and start of cruise. For this study, data were provided containing the altitude for every flight at the point determined as the start of cruise. Flights with a great circle distance less than 300 NM (turbojets) or 200 NM (turboprops and piston) are excluded in the analysis since they might not adequately represent typical cruise altitudes for aircraft that have longer ranges. Altitudes are binned into flight levels at 500 ft intervals from FL100 to FL200 and at 1000 ft intervals above. The mode of cruise flight level across all flights is taken as the aircraft type's cruise flight level.

The resulting histogram for the most common aircraft type is presented in Figure 3.1. There is a tendency in the data for lower cruise levels for longer flight distances, more noticeable in long range aircraft, as illustrated by the plot in Figure 3.1. This is likely associated with the greater takeoff weight resulting in a lower flight level at the start of cruise. As an aircraft becomes lighter during a flight, the optimal cruise altitude in terms of fuel consumption increases, but eventual cruise flight level changes during long flights are not captured in the data used here.

For aircraft with less than 100 flights in the analysis, the cruise altitude is kept as 7000 ft below the maximum operating altitude defined in BADA. Figure 3.1 shows the histogram of cruise altitudes for the aircraft type with the fewest data points for which the ADS-B derivation is still adopted. For short flights, cruise altitude is further limited by values that apply for all aircraft types according to engine type (Table 3.2), based on aggregated U.S. Federal Aviation Administration (FAA) radar data from Ref. [269].

Table 3.2: Maximum cruise flight level adopted for short flights.

Flight length [NM]	Turboprop, piston	Turbojet
0–100	FL85	FL170
100–150	FL150	FL230
150–200	FL150	FL250

3.2.4 Fuel burn and emissions model

For each aircraft type-origin-destination combination, the LTO and non-LTO phases of flight are simulated, resulting in flight segments with an associated fuel flow rate and duration. During LTO, fuel flow rate at a given thrust is piecewise linearly interpolated from available engine data. In the non-LTO phases of flight, fuel flow is pre-calculated in BADA as a function of thrust and speed, such that the energy and mass balance are kept while the aircraft (with its specific aerodynamic and kinetic properties) keeps a modeled schedule of speed and climb or descent rates [262]. Emissions of NO_x, CO, and HC are calculated for each segment using the Boeing Fuel Flow Method 2 [246] with the same additional

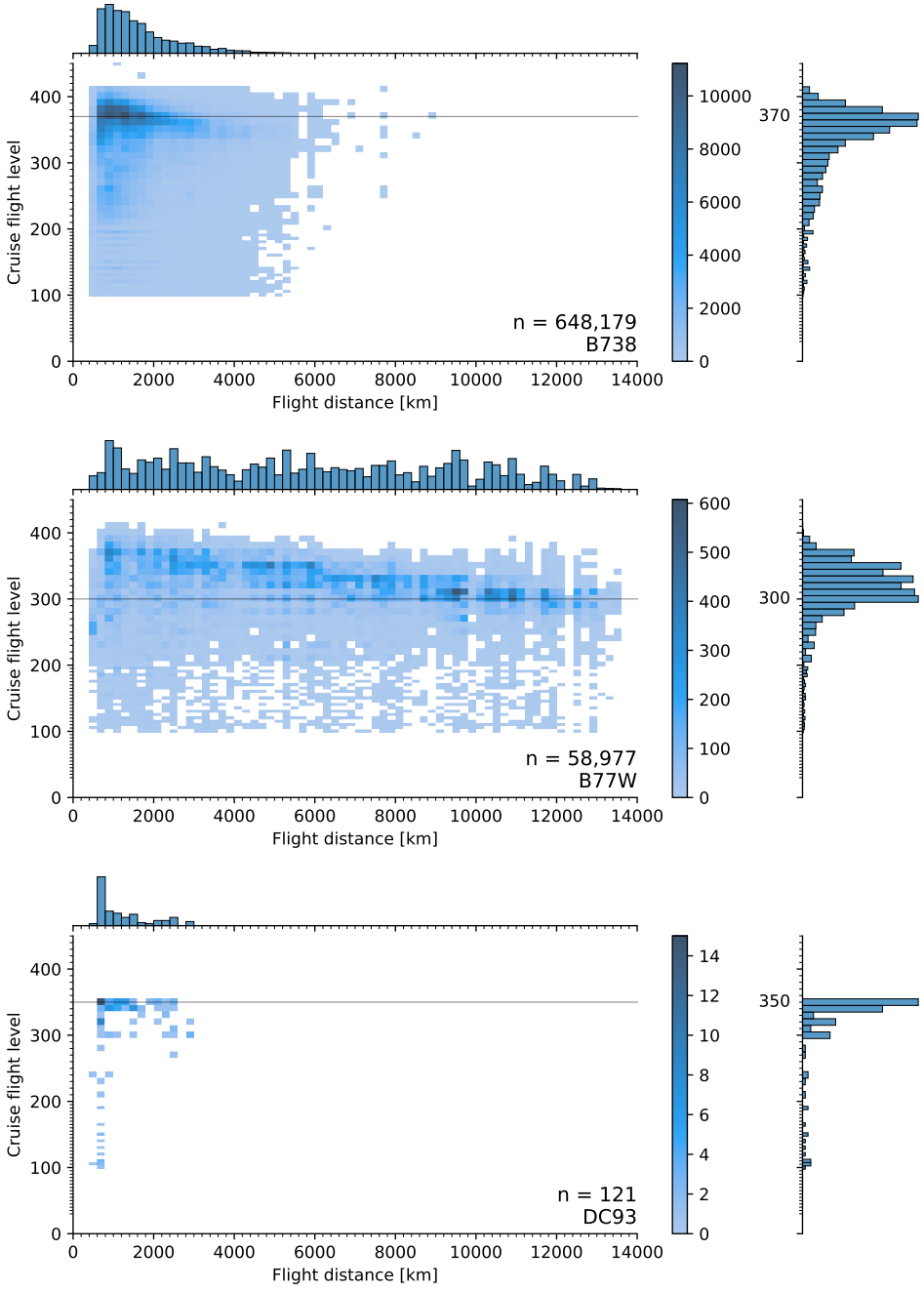

Figure 3.1: Number of flights for each combination of cruise flight level and total flight distance for the aircraft type codes B738 (Boeing 737-800), B77W (Boeing 777-300ER), and DC93 (DC-9-30). The mode of flight level, used as this aircraft types' cruise flight level in the openAVEM model is 370 (B738), 300 (B77W), 350 (DC93).

considerations for edge cases used by Kim et al. [269]. This method establishes how to interpolate the emission indices between the thrust levels used for emissions certification (the points at which emissions are measured), and adjusts it from sea level to atmospheric conditions at altitude. NO_x emissions are expressed as NO_2 equivalent, and HC emissions are expressed as CH_4 equivalent. Nonvolatile particulate matter mass ($nvPM_m$) and number ($nvPM_N$) emission indices at the engine certification thrust levels are taken from measured data (corrected for system losses) when available in the ICAO database, otherwise they are estimated from smoke number using the FOA 4.0 method [21, 270]. When smoke number data are also absent, such as for turboprop and piston engines, constant nvPM mass emission indices of 0 and 30 mg/kg are adopted for LTO and non-LTO, respectively, and nvPM particle numbers are disregarded, on the basis of the method used and values suggested by the U.S. Federal Aviation Administration's (FAA) emissions model, AEDT [271]. The lack of available data for those types of engines will therefore lead to an underestimate of nvPM emissions. For the non-LTO portion of flights, nvPM emissions are scaled using the same method adopted by AEDT [271], which is based on the work by Peck et al. [272]. Constant EIs of 3.155 kg/kg and 1.237 kg/kg are used for CO_2 and H_2O, respectively, the same values adopted by AEDT [271].

Initial aircraft mass for each flight is estimated following the method used by Eyers et al., which adds fuel for reserve, diversions, and time in a holding pattern according to a classification of short or long haul flight [235]. Takeoff mass is calculated as the sum of aircraft empty mass, estimated fuel to cruise the entire flight distance, fuel reserves, and payload. Payload mass is calculated as a fraction of maximum payload capacity on the basis of annual weight load factor statistics [273]. Since the significantly lower average factor for 2020 is due to pandemic impacts which started manifesting globally approximately in March, two different factors are applied for that year: the 2019 average value is carried over for January and February 2020, and a lower value is applied for the remaining months such that the yearly average weighted by the number of flights matches the value of 59.5% given by reference data [273]. The number of flights in each month recorded by Flightradar24 is used in the weighted average, and the resulting mass load factor of 55.2% is applied equally to all model runs for March through December of 2020 (Table 3.3).

Table 3.3: Mass load factors adopted for each month in the analysis, based on estimates from IATA [273].

Period	Factor
2017/01–2017/12	70.3%
2018/01–2018/12	70.5%
2019/01–2020/02	70.0%
2020/01–2020/02	70.0%
2020/03–2020/12	55.2%

To account for the larger actual flight distance relative to the geodesic simplification, emissions for the non-LTO portion of flights are multiplied by a lateral inefficiency factor based on a trajectory analysis by Seymour et al. of ADS-B telemetry data [258]. This scaling factor is equivalent to adding 3.87% plus 40.5 NM to the great circle distance. Con-

sidering that this correction is based solely on distance flown, it might overestimate fuel burn for cases in which longer trajectories are purposely flown to take advantage of favorable wind conditions, as longer paths could actually result in lower fuel consumption in that scenario [274]. While this factor adjusts the magnitude of emissions, it does not capture the true spread of their spatial distribution, with the added emissions being applied along the great circle line.

The sum of emissions calculated from the Flightradar24 flight movement data available for the second half of 2017 are scaled by a factor of 1.93 when estimating total emissions for that entire year. This is done on the basis of 51.6% of fuel burn calculated for 2018 occurring in the months of July through December, and the assumption that the month-by-month distribution of emissions is similar across both years.

3.2.5 Model sensitivity, uncertainty, and limitations

The accuracy of the emissions inventories produced is a function of the accuracy of the underlying models used in the calculations. The aircraft performance model used, BADA, derives each aircraft's properties from manufacturer supplied data and in-flight measurements, with comparison of the resulting model's fuel flow and vertical speed with flight data being reported [275]. Emission rates of NO_x, HC, CO, $nvPM_m$, and $nvPM_N$ are based on measured data used to certify engine models [169]. Engine and airframe degradation are not considered in this study.

Results are compared both to similarly produced emissions inventories and to top-down estimates of fuel consumption. Factors that contribute to uncertainty include: measurement errors and sample variability in determining engine emission indices, assumed specific engine model and version used by each individual aircraft, uncertainty in the models of estimating emissions at different thrust levels and atmospheric conditions relative to ground reference conditions, and estimation of takeoff mass for each flight.

The lateral inefficiency parameter corrects the amount of emissions for differences between the actual flown trajectory and the modeled trajectory, which adopts a constant cruise altitude for each aircraft type and horizontal trajectories that follow the shortest path between origin and destination. However, the actual spatial distribution of those emissions might be different than the geodesic trajectory used in the model. Potential effects of reduced air traffic in 2020 on cruise altitude and on lateral inefficiency are not evaluated in this study.

The sensitivity of emissions output to several variables in the model is quantified by performing simulations with alternative input parameters for: wind, LTO time-in-mode and thrust levels, aircraft-engine mapping, APU modeling, nvPM calculation methods, mass load factor, cruise flight level, flight simulation step size, and lateral inefficiency model. Sensitivity results are discussed throughout Section 3.3, with additional details presented in Appendix A.5.

Non-commercial or unscheduled flights that do not have their telemetry captured—because of lack of transmitter, being outside tracker coverage, or because anonymity was requested to the tracking platforms—are not captured in either OAG or ADS-B dataset, and thus do not have their emissions counted. Finally, note that emissions from tires, brakes, ground support equipment, road transport, and other airport activities are not considered in this study.

3.3 Results

3.3.1 Annual fuel and emission masses

Using OAG flight schedule data, 280 Tg of fuel burn is found globally for 2018 (Table 3.4), which is 1.9% lower and 9.1% higher than the estimates by Graver et al. [257] and Seymour et al. [258], respectively, who also used schedule data from OAG for the same year. Within the analyzed period of 2017–2020, the annual sum of emissions is highest for 2019, with 297 Tg of fuel burn resulting from flights appearing in the ADS-B data from Flightradar24. The estimates of aviation CO_2 emissions using this source of ADS-B data are equivalent to 2.4% to 2.6% of all anthropogenic CO_2 emissions—excluding land-use change—for 2017-2019; this reduces to 1.4% for 2020, indicating the increased effect of COVID-19 related restrictions on aviation emissions compared with other sectors [276]. Calculated fuel burn in 2018 is 12.9% (OAG), 10.4% (Flightradar24), and 53.8% (OpenSky) lower than the worldwide jet kerosene consumption reported by the International Energy Agency (IEA) which consists of the sum of fuel delivered by producers and is not necessarily restricted to civil aviation [277]. Few estimates are available of military aviation emissions, with previous studies estimating a military share of global aviation fuel burn of 18% in 1992 [247], 11% in 2002 [235], and a similar 10–15% range for the United States between 1990 and 2000 [278]. Note that the underestimate using OpenSky data is mainly driven by its more limited coverage, and will be discussed in the following sections. Fuel burn from international flights in 2018 is 14.7% (OAG) and 18.8% (Flightradar24) higher than the estimate for 2015 by Fleming and de Lépinay [221], with similar fractions of international to total (domestic plus international) fuel burn: 65.5% (OAG) and 65.9% (Flightradar24) versus 65% in Fleming and de Lépinay [221].

Table 3.4: Annual global fuel burn and emissions from civil aviation estimated from different sources of flight movement data.

	OAG	Flightradar24				OpenSky			
Species	2018	2017[a]	2018	2019	2020	2017	2018	2019	2020
Fuel, Tg	280	277	288	297	157	130	149	171	95
CO_2, Tg	885	873	910	937	496	410	469	538	298
H_2O, Tg	347	342	357	367	194	161	184	211	117
SO_x, Gg[b]	168	166	173	178	94	78	89	102	57
NO_x, Tg[c]	4.32	4.26	4.47	4.62	2.44	2.08	2.38	2.71	1.49
HC, Gg[d]	34.7	39.3	40.6	42.6	27.3	16.3	18.9	22.6	15.4
CO, Gg	624	721	753	814	569	168	312	370	234
$nvPM_m$, Gg	9.69	9.34	9.57	9.68	4.79	4.29	4.83	5.53	2.83
$nvPM_N$, 10^{26}	3.43	3.27	3.4	3.47	1.73	1.44	1.66	1.92	0.99

[a] Flightradar24 2017 values are scaled from results for the months of July–December.
[b] SO_x = oxides of sulfur, as mass of S, considering a fuel sulfur content of 600 ppm.
[c] NO_x = oxides of nitrogen, as mass of NO_2.
[d] HC = hydrocarbons, as mass of CH_4.

The horizontal and vertical distribution of average fuel burn rates in 2019 for the Flightradar24 dataset are shown in Figure 3.2, and maps of each pollutant and each flight

movement dataset are provided in Appendix A.6. It is found that 92% and 65% of fuel burn shown in Figure 3.2 occurs north of the equator and north of 30 °N, respectively. Additionally, 72% of fuel burn occurs at altitudes higher than 9 km, representing the cruise portion of jet-powered flights. The regions with the highest amount of fuel burn occurring over them in 2018 per area are Western Europe (12.2 $Mg \cdot km^{-2}$) and Southern Europe (5.3 $Mg \cdot km^{-2}$), with 23% of global fuel burn occurring over the oceans between all continental regions, for the region definitions described in Appendix A.6.

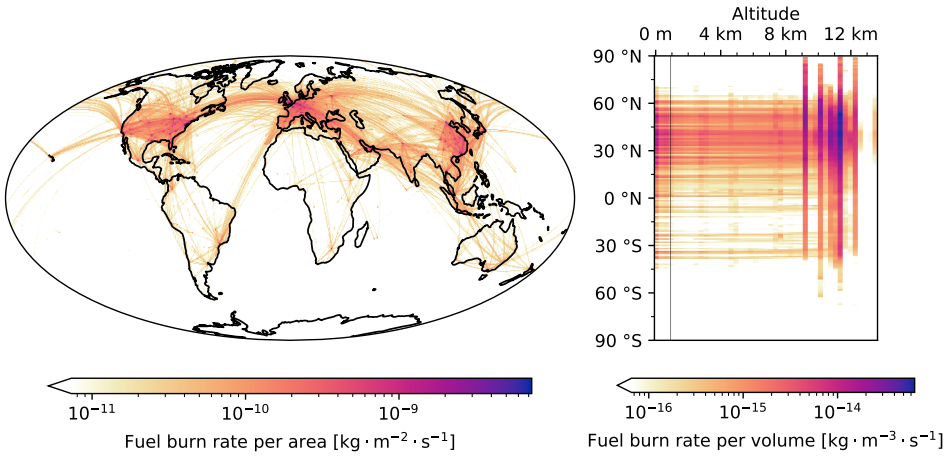

Figure 3.2: Average fuel burn rates in 2019 from Flightradar24 data summed vertically (left), and averaged longitudinally (right). The thin line indicates the 3000 ft altitude (LTO threshold).

Across all months, between 8.2%–10.0% of fuel burn and 7.8%–9.2% of NO_x are emitted during the LTO portion of flights, with the highest percentages occurring during 2020 (Appendix A.7). The fraction of fuel burn from LTO obtained here is similar to estimates from previous studies of 8.5% for the year 2015 [211] and 9.1% for 2005 [41]. By substituting the time-in-mode and thrust values applied here for the LTO cycle suggested by ICAO [7], the fraction of fuel burn occurring during LTO ranges from 10.8% to 13.5% (Appendix A.5.2), highlighting the uncertainty in the estimation of this portion of emissions. Considering that pushback control and reduced takeoff thrust are strategies to reduce LTO emissions that are currently being pursued [279, 280], an updated model of LTO cycles could in future work be valuable in representing their emissions at a global scale. Although only 6.9% of fuel burn and 3.2% of NO_x emissions during LTO are due to auxiliary power units (APU; 2019 estimate using Flightradar24), APUs are responsible for 34% of $nvPM_m$ and 25% of $nvPM_N$ LTO emissions. The three alternative APU time-in-mode models evaluated lead to fuel burn between 16% and 145% higher along with a 6% to 8% higher average $nvPM_m$ and $nvPM_N$ EIs, while adopting different sources for the emission indices lead to between −4% and +14% $nvPM_m$ and $nvPM_N$ EIs (Appendix A.5.3). Fewer resources are openly available to estimate accurate emission indices and running times of APUs compared with aircraft main engines, but these results suggest that they are a significant contributor to low altitude nvPM emissions.

3.3.2 Temporal trends

Average daily fuel burn in 2017–2020 is presented in Figure 3.3, reflecting both the ongoing decades-long growth and the reductions due to COVID-19 restrictions. Comparing the 2018 estimate using OAG with a 2005 inventory that also used data from that company [41], a globally averaged increase of 55% is found between the two years (Appendix A.6). This varies regionally: for example, there is a below-average increase in the fuel burned over Northern America (2%), Northern (25%) and Western (36%) Europe, whereas the opposite holds for Eastern Asia (131%), Southern Asia (137%), and Western Asia (177%). This spatial nonuniformity should be taken into account when assessing aviation's climate or air quality impacts, as the sensitivity of impacts can vary significantly depending on the location of emissions [12, 212, 217]. In addition, it further highlights the need for spatially resolved and up-to-date inventories. In terms of seasonal trends, lower and higher air traffic during boreal winter and summer, respectively, lead to fuel burn rates up to −5.7% (January) and +7.2% (August) relative to the annual averages in 2018 and 2019.

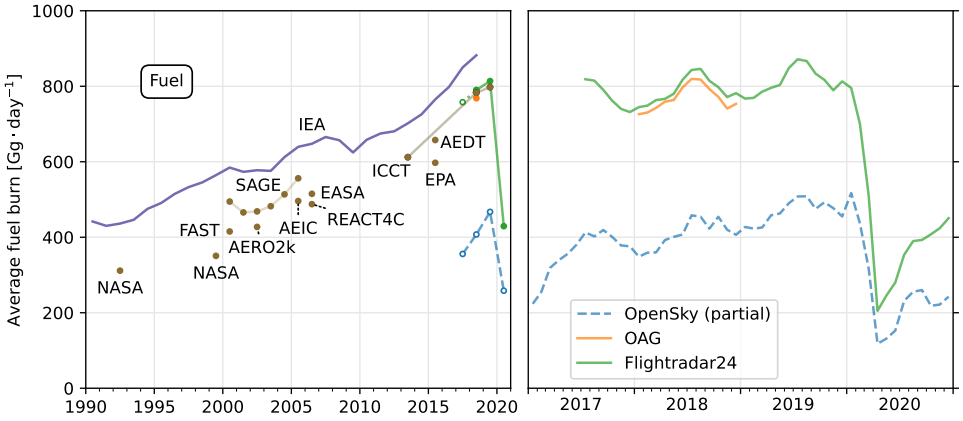

Figure 3.3: Global fuel burn in the period 2017–2020 calculated from: OpenSky (partial spatial coverage), OAG, and Flightradar24. Previous estimates from literature are shown next to the name of the institution that performed the study or name of the model used: NASA [247, 248], FAST [234], AERO2k [235], SAGE [250], AEIC [41], REACT4C [31], EASA [254], ICCT [257], EPA [256], and AEDT [211, 252]. The purple line represents jet kerosene consumption statistics from the IEA [277].

The 4.62 Tg of NO_x (base NO_2) released by aviation globally in 2019 (estimate using the dataset from Flightradar24) represents an increase of 222% and 59% relative to values reported for 1992 [246] and 2005 [250], respectively. This is driven both by more fuel being burned and by higher emission indices: the annual global average EI (NO_x) of 15.5 g/kg is 3.3% higher than the value of 15.0 g/kg used by Grobler et al. [211] for the year 2015 from the AEDT inventory (Figure 3.4). The observed decades-long trend of increasing EI (NO_x) is consistent with increases in engine overall pressure ratios and turbine inlet temperatures, which are pursued mainly with the goal of reducing fuel consumption [10, 281]. On the other hand, higher temperatures along with improved combustor designs, result in increased combustion efficiency and reduced emissions of HC and CO [4]. The average HC EIs in 2018 are estimated as 141 mg/kg (Flightradar24) and 124 mg/kg (OAG), which are 10% and 21% lower than the 2015 value for the AEDT inventory [211], and 73%

and 76% lower compared with the AEDT inventory for 2006 [252]. The average CO EIs in 2018 of 2.61 g/kg (Flightradar24) and 2.23 g/kg (OAG) are closer to AEDT values for previous years: +5% and −10% relative to 2015 [211], and −28% and −38% relative to 2006 [252], respectively. Monthly fleet average EIs of CO and HC calculated from Flightradar24 data increased up to a maximum in June 2020 of +68% and +46%, respectively, relative to the 2019 annual averages as a consequence of the changes in traffic due to the COVID-19 pandemic (Appendix A.8).

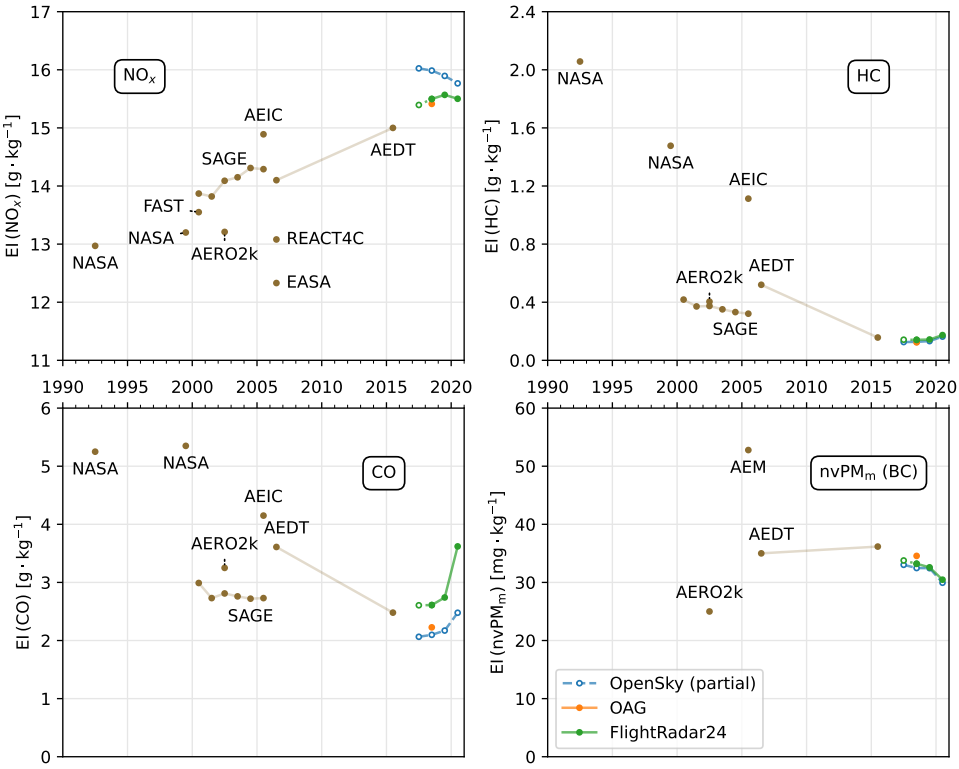

Figure 3.4: Average emission indices of NO_x, HC, CO, and $nvPM_m$ in the period 2017–2020 calculated: OpenSky (partial spatial coverage), OAG, and Flightradar24. Previous estimates are shown next to the name of the institution that performed the study or name of the model used: NASA [247, 248], FAST [234], AERO2k [235], SAGE [250], AEIC [41], REACT4C [31], EASA [254], AEDT [211, 252], and AEM [232].

Historically, adoption of a constant EI or the use of empirical correlations to the smoke number measurements made during engine certification have yielded a wide range of estimates of particulate matter emissions [232, 282]. A standard procedure to measure nvPM EIs during engine certification was adopted in 2017 [7], with the first batch of test results being added the ICAO Engine Emissions Databank in December 2020 [169], which is included in the present model. Considering all three sources of flight movement data, the global annual fleet averaged EIs for 2017–2019 for turbofan engines with certification nvPM measurements—which account for 69% to 75% of fuel burn given the engine aircraft

assignments used—are between 33.5–36.3 mg/kg and $1.26 \cdot 10^{15}$–$1.38 \cdot 10^{15}$ particles/kg. For turbofans with only smoke number data the average is between 35.1–37.3 mg/kg and $9.03 \cdot 10^{14}$–$1.04 \cdot 10^{15}$ particles/kg. This result, along with overall lower average EI ($nvPM_m$) than previous estimates shown in Figure 3.4, is consistent with the expected trend of reduced nvPM for newer engines. Note that, by assigning a single engine to each aircraft type, older, less common, engine versions are likely to be underrepresented, which is expected to result in an underestimate of nvPM emissions.

Overall, the resulting annual nvPM EIs for 2017–2019 averaged across all aircraft types are 32.5–34.6 mg/kg and $1.11 \cdot 10^{15}$–$1.22 \cdot 10^{15}$ particles/kg. Compared with a previous estimate of 2005 emissions [232], these results are 34–39% lower in mass and 83–102% higher in particle count, driven by changes both in engine characteristics and in the methods used to calculate emissions. Notably, the AEDT method employed here corrects $nvPM_m$ for altitude, but not $nvPM_N$, leading to higher particle counts in the non-LTO phases of flight [271]. Compared with estimates for 2015 from Ref. [270], the results here have average nvPM EIs during LTO, excluding APUs, between 41–52% higher in mass and 12–15% lower in number. Using the same SCOPE11 method as Ref. [270], these differences to their 2015 LTO estimate are between 48–58% higher in mass and 1–4% lower in number. The full-flight estimates here are also 30–38% higher (mass) and 317–361% higher (number) than the AERO2k inventory for the year 2002 [235].

The EI ($nvPM_N$) obtained here are within the range of $1 \cdot 10^{14}$–$1 \cdot 10^{16}$ particles/kg found for typical cruise conditions by both ground [160, 167, 270] and in-flight measurement campaigns [35–37, 39]. The large range of reported experimental values reflects the influence of different engine models, engine wear levels, thrust levels, atmospheric conditions, and measuring methods. Finally, the results are sensitive to the chosen nvPM estimation method. Not considering the new nvPM certification measurements and using only the FOA4 method with smoke numbers results in a 3% increase in LTO $nvPM_m$ and a 3% decrease in $nvPM_N$. The older FOA3 method leads to a 22% decrease in LTO $nvPM_m$, while the alternative FOX method results in $nvPM_m$ values that are 2.0 and 2.8 times the baseline for LTO and full-flight, respectively (Appendix A.5.4).

3.3.3 Impact of engine model assignments on emission totals

Although the flight movement data available for this research list the aircraft type per flight, each type might support multiple engine models. Besides the possibility of option for engines of different manufactures, it is common for engine models to have a series of versions with different rated thrusts, and an engine line might go through various revisions over time as new parts are introduced. As described in Section 3.2.2 and Appendix A.4, the emissions inventory is produced by assigning a representative model for each engine family available for each aircraft type. In this section, the impact of selecting different engine versions on the global sum of emissions is evaluated.

Global fuel burn and emissions summed over 2019, using the Flightradar24 dataset, are calculated for each aircraft type using every engine version available that has emissions data in the ICAO Engine Emissions Databank [169]. Figures 3.5 and 3.6 show the ratios relative to the values obtained by a specific engine model and version adopted as the reference, with each horizontal marker indicating the result of one engine version. For simplicity, only the 22 aircraft types with the most fuel burn (~95% of total) are shown.

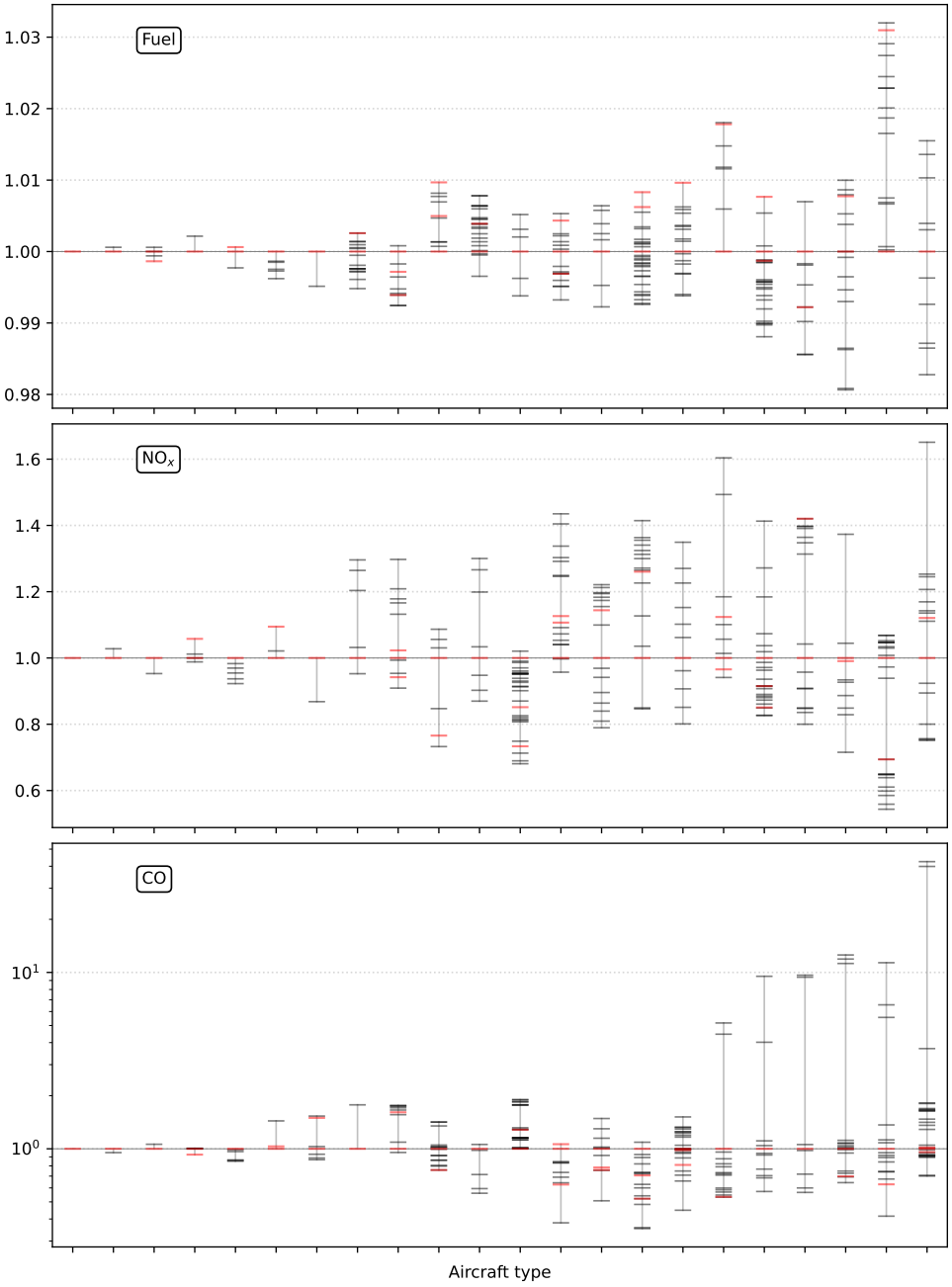

Figure 3.5: Ratio of global fuel burn and NO_x and CO emissions in 2019 (Flightradar24) between every engine version available for each of the 21 aircraft types with the most fuel burn and a reference version assigned to that type. Red markers indicate engine versions assigned as the reference of an engine family for the type. Aircraft types are ordered, for each species, by the range between maximum and minimum values across engine versions.

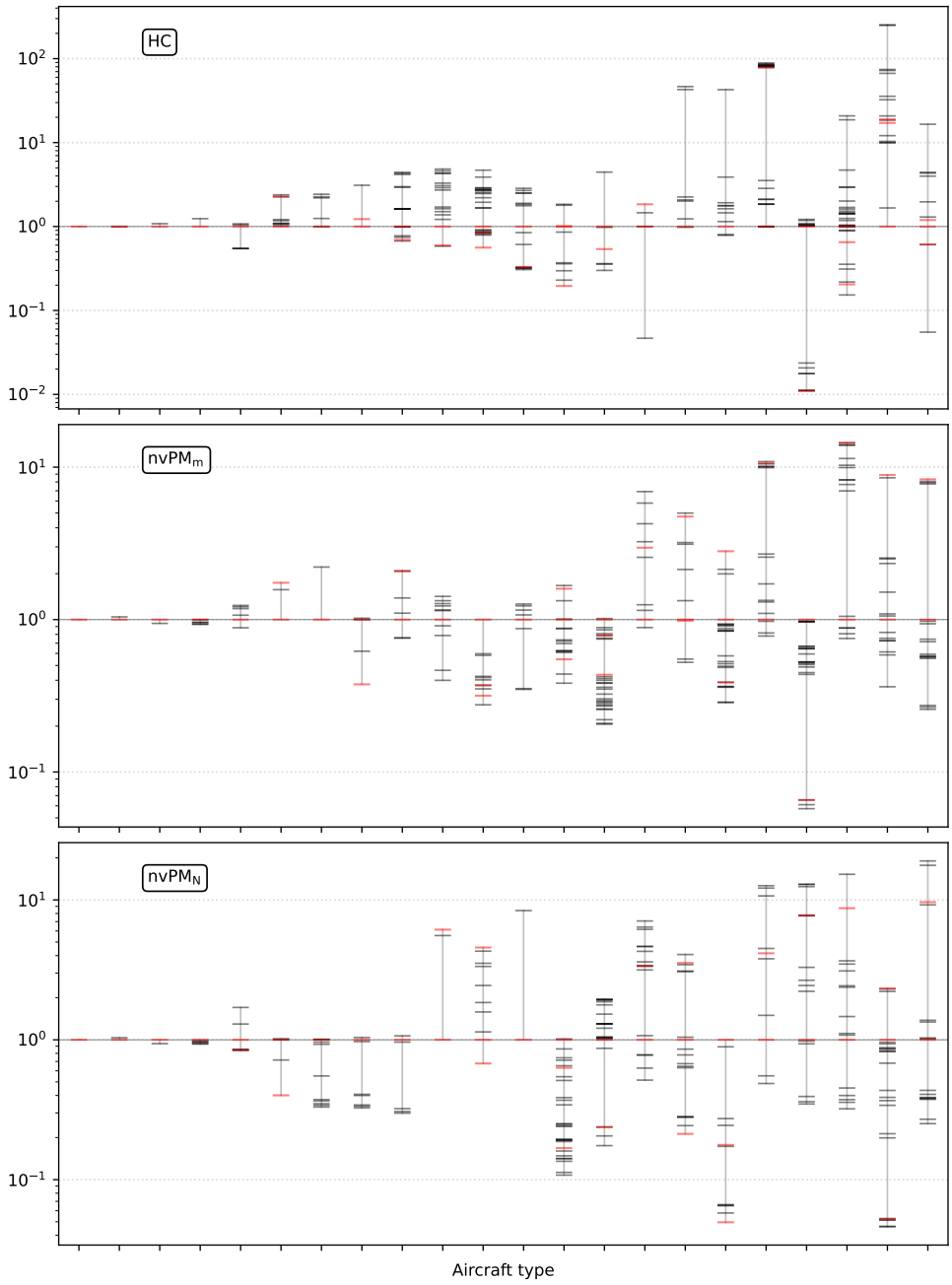

Figure 3.6: Ratio of global emissions of HC, nvPM$_m$, and nvPM$_N$ in 2019 (Flightradar24) between every engine version available for each of the 21 aircraft types with the most fuel burn and a reference version assigned to that type. Red markers indicate engine versions assigned as the reference of an engine family for the type. Aircraft types are ordered, for each species, by the range between its most and least emitting engine versions.

The amount of HC, CO, $nvPM_m$, $nvPM_N$, and to a lesser extent NO_x emissions is found to be very sensitive to the choice of specific engine model and version as the reference engine in the model of each aircraft type, with outlier engine versions leading to tens of times more emissions compared to other versions. Since fuel burn rates during non-LTO are given by the BADA model, only LTO fuel burn vary with engine assignment. Full-flight fuel burn changes at most 3.3% with engine selection for the analyzed aircraft. Emissions have a much wider range, with the maximum ratios between the most and least emitting engine versions across all aircraft considered being 2.2 (NO_x), 300 (HC), 61 (CO), 32 ($nvPM_m$), 76 ($nvPM_N$). This means that there are aircraft types for which different engine versions exist that have emission rates of tens or even hundreds of times larger or smaller than the other version. This makes the overall magnitude of emissions highly dependent of the selection of engine version to model each aircraft, especially for the types that burn the most fuel. The effect that outliers and the uncertainty in engine allocation have on global emissions is lessened due to the number of aircraft types contributing to the global sum of emissions, and the incorporation in the model of the contribution to emissions from each engine family in the case of aircraft that have multiple engine suppliers.

3.3.4 Reduction of emissions in 2020

Fuel burn in the month of January increased by 3.0% between 2018–2019 and 3.7% between 2019–2020, as calculated from Flightradar24 data. That growth abruptly stopped due to the COVID-19 pandemic, with fuel burn in the month of April changing by −74.2% between 2019 and 2020. As Figure 3.7 shows, the timing of the reduction in activity varied by aircraft segment. In 2019, widebodies, narrowbodies, regional jets and business jets were responsible for 51.4%, 41.9%, 4.3%, and 1.2% of fuel burn, respectively. During May 2020, the distribution was 67.0%, 26.2%, 3.4%, and 1.9%, indicating that larger aircraft and business jets were less affected by the reduction in activity during this specific period. One of the possible driving factors for this is the difficulty faced in 2020 by air cargo services to meet demand with reduced passenger hold capacity available, leading to increased utilization of cargo aircraft [283].

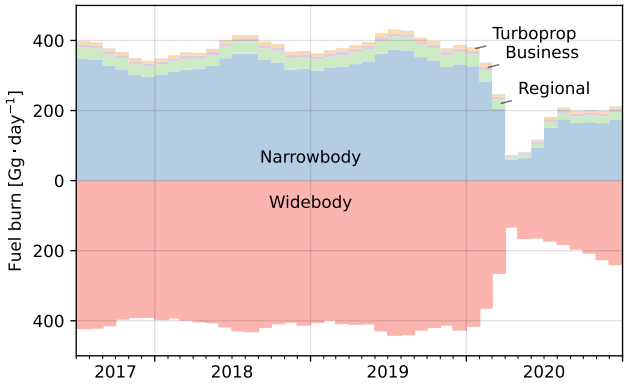

Figure 3.7: Changes in monthly global civil aviation fuel burn calculated from Flightradar24 flight movement data per class of aircraft in 2017–2020.

Significant reductions in aviation emissions due to the pandemic occurred in all regions of the world in March 2020, after a 64% fuel burn decrease in February 2020 from flights taking off from China relative to February 2019 (Figure 3.8). The proportional reduction and recovery in emissions per country varied in part due to different usual ratios of domestic and international flights, with countries that have proportionally more domestic flights, such as the United States, China, and Russia, reducing emissions less, because international routes were more impacted by pandemic related restrictions [284]. Domestic flights were responsible for 35% of global fuel burn in the second half of 2019 and for 49% in the second half of 2020 (Appendix A.9). Overall shorter flights led to a larger share of emissions occurring during LTO: 10.0% of fuel burn, compared with 8.7% in 2019 (Appendix A.7). The changes in active fleet composition and routes flown also caused higher average EIs of HC and CO and lower average EI of nvPM during this period (Appendix A.8). Comparing the calculated global emission totals for 2020 against 2019 values scaled by +2.3%, to match the expected annual fuel consumption growth forecast by IATA in December 2019 [285], it is found that actual fuel burn in 2020 was 48% lower, with 463 Tg less CO_2 and 2.29 Tg NO_2 less NO_x emitted.

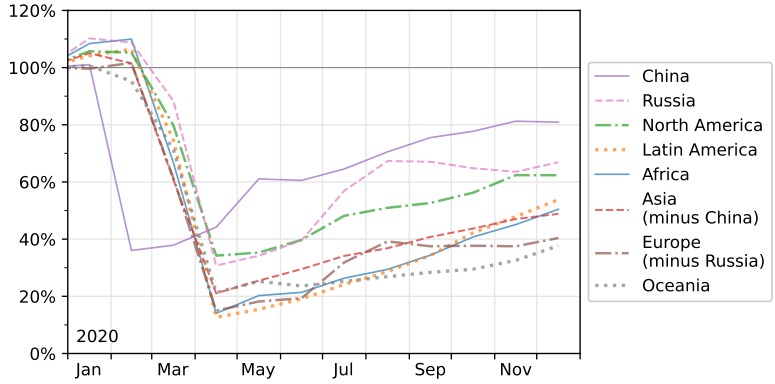

Figure 3.8: Changes in monthly fuel burn calculated from Flightradar24 flight movement data per region of departure in 2020 relative to the same month in 2019.

The changing conditions of the aviation industry in 2020 contribute to the uncertainty in estimating emissions, as the per flight deviations from the constant (annual, fleet-wide) payload mass fraction adopted are expected to be generally larger. In this period, load factors were particularly low for passenger services and particularly high for cargo services [273, 283], whereas the model emissions does not make distinctions between the two types of flight. Changing the mass load factor in the model by ±0.077 from a baseline of 0.628 leads to a change of ±1.1% in global fuel burn mass (Appendix A.5.5). Lower takeoff weights associated with lower load factors and the regionally nonuniform sharp reductions in air traffic in 2020 could also bring about changes in the pattern of flown trajectories, making the cruise altitudes and lateral inefficiency correction factors adopted here (based on pre-pandemic data) be less representative of actual flight paths. The lateral inefficiency correction applied results in a 6.5% increase of fuel burn relative to emissions from great circle trajectories (Appendix A.5.8). This latter limitation can in future studies

be overcome by using ADS-B position data to provide a more accurate estimate of lateral inefficiency during this period [286].

3.3.5 Viability of ADS-B and open data for global emission estimates

Despite not all civil aircraft possessing ADS-B transmitters and tracker coverage not being globally complete, fuel burn in 2018 calculated for flights recorded by Flightradar24 is 2.8% larger than that calculated for flights in the OAG schedules (Table 3.4). Several factors cause differences in the two estimates of emissions, with their geographical distribution shown in Figure 3.9. In regions where telemetry tracker coverage is higher—such as Europe, North America, Australia, and Japan in the case of Flightradar24—emissions estimates are higher due to unscheduled flights, including general aviation, charter, and private jet flights, which are not recorded in the data sources traditionally used to generate global emissions inventories, such as OAG. This ability to record unscheduled flights is exemplified by a previous study that demonstrated the use of an ADS-B receiver network to track a number of government and private operated flights [287]. The omission of the freight carriers FedEx, UPS, and DHL in the OAG data for 2018 is apparent by the large differences in fuel burn around their hubs in Memphis and Louisville. Excluding fuel from flights of these operators, the global fuel burn in 2018 calculated from Flightradar24 is still 0.5% larger than the value calculated from OAG schedules. Information from OAG on the type of service of each flight allows emissions from cargo flights to be calculated separately, and complementing those with data from Flightradar24 on the missing airlines it is possible to make a more complete estimate of emissions from cargo flights than using either source: 8.1% of fuel burn and 8.2% of NO_x from global aviation in 2018 came from cargo flights (Appendix A.10).

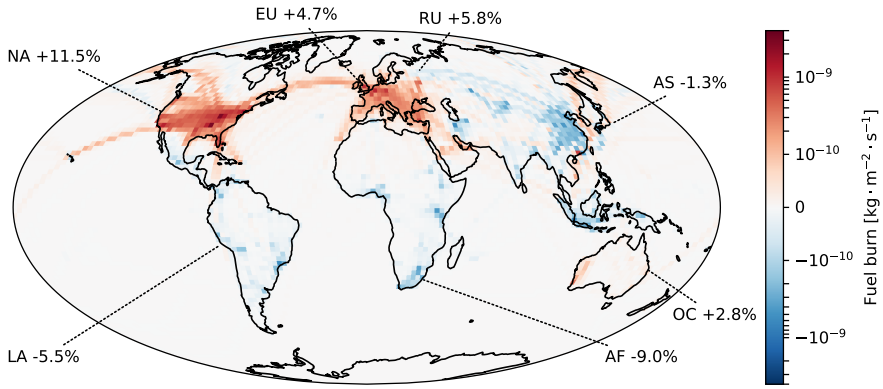

Figure 3.9: Difference between fuel burn rates in 2018 from Flightradar24 ADS-B and OAG schedule data, including the relative difference in fuel burn mass from flights originating in each region.

Estimates of emissions based on flight movement data from OpenSky were generally lower than those using Flightradar24, mainly driven by more limited geographical coverage and lack of multilateration, which is needed to track aircraft without ADS-B. Annual global fuel burn masses calculated using OpenSky were 52% (2018), 57% (2019), and 60%

(2020) of the values calculated using Flightradar24 (Table 3.4). But even in regions where coverage is nearly complete and ADS-B mandates are being implemented, such as Europe and North America, fuel burn estimated from OpenSky is still typically between 60% and 80% of the values estimated from Flightradar24 (Appendix A.11). This results from, in addition to ADS-B tracker coverage, lack of multilateration capabilities to track aircraft without ADS-B and from absent data associating an aircraft type to each transponder's unique identifier that is transmitted. In the period of February through December 2020, between 25% and 46% of monthly flights recorded by OpenSky did not have an aircraft type assigned (Appendix A.1).

Despite these limitations, OpenSky or its underlying network of volunteer trackers could be used to estimate local or regional aviation emissions, and the open nature of this source of data also facilitates research incorporating reported aircraft positions over time to accurately represent flight trajectories [241, 288]. Future research could use per flight trajectories as tracked by ADS-B directly in the flight simulation model, as opposed to considering great circle distances and assuming a lateral inefficiency factor, to improve accuracy of global emission estimates. Transparency, reproducibility, and ease of update of aviation emissions inventories could be further improved by additionally incorporating an openly available aircraft performance model derived from ADS-B [244].

3.4 Conclusions

Coverage of networks like Flightradar24 and OpenSky is expected to increase due to mandates of ADS-B transmitters in various airspaces and new availability of satellite receivers. It is shown that, already in 2018, globally more aviation emissions and 2.8% more fuel burn can be accounted for by using a network of ADS-B and multilateration trackers than by using schedule data from a market intelligence company. The different properties of flight schedule data and ADS-B data create the potential for them to be used complementarily, as exemplified by the estimate made of emissions from cargo flights. The ability to include non-scheduled flights, such as military or privately operated, in emission inventories contributes to their completeness. Using this new source of data, the first openly available spatially resolved 3-D inventory of global aviation emissions for the period of 2017–2020 is produced, in which 937 Tg of CO_2, 4.62 Tg NO_2 of NO_x, 42.6 Gg CH_4 of hydrocarbons, 814 Gg of CO, and $3.47 \cdot 10^{26}$ nvPM with a mass of 9.68 Gg are estimated to have been released in 2019 directly from the operation of civil aircraft. The inventory contains only nominal values, and future work could improve on it by providing a spread of estimates based on modeling the uncertainties present in the calculation of aviation emissions.

The trend of growth in aviation emissions, demonstrated by the finding that fuel burn increased by 55% between 2005 and 2018, is expected to continue in the coming decades. And as changes in emissions from other sectors continue to change the sensitivity of local and global environmental impacts to local aviation emissions, ADS-B data can be useful in enabling more up-to-date emissions estimates, with the added benefit of increasing transparency in the calculation process. The improved agility in this method makes it easier to quantify the effects of current events on emissions, such as the 48% reduction in fuel burn in observe in 2020 relative to the fuel that was expected to be used prior to the COVID-19 pandemic. Data being provided sooner and more openly can also be useful in keep track of sustainability goals, such as the various net-zero CO_2 aviation pathways to 2050 currently

proposed [49–54], facilitating earlier interventions or adjustments if needed.

For comprehensive aviation environmental impacts analyses, both CO_2 and non-CO_2 emissions are required, and more emissions reporting may be anticipated from the aviation industry in the coming years. For example, this is expected for CO_2 emissions with the adoption of market-based instruments such as ICAO's carbon offsetting scheme, called CORSIA. The European Union Emissions Trading System (ETS), which currently caps CO_2 from intra-European flights, will also require monitoring of non-CO_2 emissions from 2025, with the goal of supporting future mitigating measures [289]. Scientific understanding is improving concerning aviation's non-CO_2 impacts on the climate, in part driven by NO_x emissions, but as the results here indicate, the global average emission index of this pollutant is increasing over time, indicating that the growth of NO_x emissions could outpace CO_2 emissions. Because this trend is driven by engine design choices with the aim of reducing fuel consumption, inventories such as those produced here can be useful in investigating the atmospheric impacts of the tradeoff between CO_2 and NO_x emissions. This aspect of aviation's emissions will likely continue to be in focus even as the industry pledges carbon neutrality, since one of the main pathways currently being considered to achieve that goal is the adoption of sustainable aviation fuels, which is a measure that does not address NO_x emissions. In addition, the increasing awareness of the human health impacts associated with particulate matter of different sizes (including ultrafine particles, UFPs) is resulting in increased attention on these species emitted by aircraft. The combination of a spatially resolved emissions estimation tool with ADS-B data sources, such as that used in this study, can produce the required emissions data for complete and timely assessments of civil aviation's climate and air quality impacts, and contribute towards the transparent monitoring of aviation's progress towards its sustainability goals.

3.5 Data availability

The emissions inventory produced is available under the following data repository DOI: 10.4121/15015390 and the openAVEM code is available under DOI 10.4121/15062478.

3.6 Acknowledgments

The author would like to thank Flightradar24 AB and the OpenSky Network for providing flight movement data from ADS-B, and Paul Roling for the helpful discussion on the OAG schedule data. This work made use of the Dutch national e-infrastructure with the support of the SURF Cooperative using grant no. EINF-1694. The Modern-Era Retrospective Analysis for Research and Applications, Version 2 (MERRA-2) wind data used in this study have been provided by the Global Modeling and Assimilation Office at NASA Goddard Space Flight Center.

4

Future aircraft NO_x emissions

[...] Thus, the principal impact of aircraft emissions is local in nature and is expected to become more severe in future years. It is also likely that aircraft emissions will constitute a more significant portion of community-wide pollutant loadings as new aircraft are introduced and as emissions from other sources are reduced. It is further concluded that, whenever a reduction of aircraft emissions becomes desirable, a variety of practicable approaches exist to reducing both the quantities of pollutants emitted and their impact upon the community.

Nature and control of aircraft engine exhaust emissions[1]
Northen Research and Engineering Corporation,
1968

Aircraft emitted oxides of nitrogen (NO_x) contribute both to climate change and air quality degradation. The trend of higher gas temperatures, caused by engine design choices seeking lower fuel consumption and achieve more complete combustion, has the adverse effect of increasing NO_x formation, which might however be compensated by improved combustor designs. The tradeoff between lowering NO_x or CO_2 emissions is an important consideration in mitigating the environmental impacts of aviation, and, and in context of the industry's environmental targets and forecasts, quantifying the technological trend taking place can provide an indication of future emission totals. In this study, bottom-up estimates of global fleet average aviation fuel burn and NO_x emissions are produced for the years 2005 and 2018 and extrapolate their totals to 2030, 2040, and 2045 with current air traffic and engine performance forecasts. Average NO_x emission indices are evaluated for different aircraft classes at each year considered, and their changes over time are discussed together with a sensitivity analysis on the assumptions made.

This chapter is based on work presented at the AIAA SciTech 2022 conference, listed at the end of this thesis.
[1]Report No. 1134-1, prepared for the National Air Pollution Control Administration, Department of Health, Education, and Welfare. Cambridge, MA, USA.

4.1 Introduction

Emissions of oxides of nitrogen (NO_x) are the main contributors to the air quality impacts associated with aviation [1, 4, 32], as further discussed in Chapter 6, and play a significant role in the climate forcing by aviation [5], estimates of which are also still being refined by current research efforts [290, 291]. The social cost of air quality impacts have been found to be a significant component of the overall environmental damage from aviation [292], in particular having a comparable magnitude to the social costs associated with climate impacts if the effects of cruise emissions are considered [211]. Based on aviation activity in 2015, the marginal environmental cost of a metric ton of fuel burn has been estimated to be $560 [180-1,400, 90% CI] , with $140 [21-360, 90% CI] being attributable to the climate impacts of CO_2 and $330 [38-1,100, 90% CI] attributed to the aggregate air quality and climate impacts of NO_x. If the full environmental impacts of aviation are to be addressed, design and policy decisions have to consider the air quality degradation associated with non-CO_2 emissions in addition to their short-term and long-term climate forcing.

Despite technological improvements, it is expected that the growth of civil aviation will cause the amount of NO_x emissions to increase between the years 2005 and 2050 [6, 11]. Reducing these emissions and their associated environmental effects is complicated by the existence of tradeoffs in engine design, in which higher pressure ratios and turbine inlet temperatures are beneficial in terms of thermodynamic efficiency, specific thrust, and combustion completeness, but detrimental in terms of increasing NO_x formation [147, 293]. The trend in turbofan design of higher overall pressure ratios leads to decreased fuel consumption, which is both economically desirable and reduces CO_2 emissions along with their associated climate impacts [294]. Some studies have analyzed the tradeoff between CO_2 and NO_x emission reductions, suggesting that regulating aviation NO_x to more stringent values might have an overall detrimental effect on climate change due to the incurred loss of fuel efficiency [10, 11]. However, the inclusion of air quality social costs in the analysis can lead to the conclusion that limiting engine pressure ratio to favor reducing NO_x over CO_2 from current engine design points is a net benefit [295]. While opportunities for simultaneous reduction of both pollutants do occur, deciding on the future direction of emissions regulations involves political choices on how to weigh different environmental effects that can have significantly different timescales, in addition to significant uncertainties in their magnitude [291, 296].

NO_x emissions during landing and takeoff operations (LTO) are regulated for the turbofan engines used in airliners by the International Civil Aviation Organization (ICAO), with limits on emitted mass per thrust increasing according to the engine's overall pressure ratio [7]. After their adoption in 1981, these limits have been tightened in 1993, 1999, and 2005, with new requirements coming into effect some years after each new standard was accepted. Parallel to that, new combustor technologies have been implemented to meet emission requirements while seeking overall lower fuel consumption. ICAO's first standard setting minima for aircraft fuel efficiency took effect for new designs in 2020 and will be applied to all newly built aircraft from 2028 [297]. However, the fact that multiple currently sold aircraft already meet this standard has led to arguments that the standard's impact will be mild [298]. The combined effects of lower fuel consumption and higher NO_x emission indices (EI, defined as mass emitted per mass of fuel burned) caused by higher pressure ratios have led to relatively stable levels of NO_x per passenger seat-km in that

period [294]. With this trend not expected to change significantly, total NO_x emissions are forecast to increase in the next three decades, following the growth of civil aviation, according to ICAO's Committee on Aviation Environmental Protection (CAEP) [6].

In this study, further insight into these trends is provided by estimating the annual global fleet average fuel burn and NO_x emission indices for different aircraft classes in the years 2005 and 2018 using flight schedule data and a spatially resolved model simulating aircraft performance to estimate fuel burn and emissions, with a bottom-up approach. Emissions are then scaled up to the year 2050 using projections available in 2021 of technological advancements and aviation activity. These estimates show how aviation NO_x and CO_2 emissions changed over time for each aircraft class and how they are expected to change in the coming decades.

4.2 Methods

4.2.1 Estimating realized global aircraft emissions

An inventory of aircraft emissions is created for the years 2005 and 2018 by following the methodologies developed in Chapter 3. In summary, first a comprehensive list of any civil aviation flights that occurred is produced, then each flight's emissions are estimated, and finally those emissions are aggregated as needed for analysis.

Flight schedule data compiled by the company OAG are used to create a list of global flight movements for the entirety of the years 2005 and 2018. Additionally, the 2018 dataset is complemented with flight movement data compiled by the aircraft telemetry tracking company Flightradar24, specifically to obtain a list of flights for some cargo operators missing in the schedule dataset: FedEx, UPS, and some airlines owned by DHL. Due to limited data availability, only passenger flights were evaluated for 2005. The emissions for each combination of aircraft type, origin, and destination in each month are simulated with the openAVEM model, further described in Section 3.2 and Ref. [299] and summarized in this paragraph. LTO emissions are calculated with time-in-mode values proposed by Stettler et al. [265]. The non-LTO portion of each flight is simulated with the BADA 3.15 aircraft performance model, which uses a total energy formulation of aircraft kinetics [262]. Flights follow a geodesic trajectory with a constant aircraft type dependent cruise flight level. Wind speeds are applied using monthly average values of the MERRA-2 reanalysis product from the Global Modeling and Assimilation Office (GMAO) at NASA Goddard Space Flight Center. Non-LTO emissions are calculated using the Boeing Fuel Flow Method 2 [246, 269], and CO_2 emissions are calculated using the constant EI of 3155 g/kg as used in the U.S. Federal Aviation Administration's emissions model [271]. To account for the actual distance flown, the non-LTO emissions are multiplied by a lateral inefficiency factor equal to 1.0387 plus the equivalent of additional 40.5 NM to the great circle distance, based on Ref. [258]. Engine emission indices at certification operation points are taken from the ICAO Engine Emission Databank for turbofans [169], and the U.S. Environmental Protection Agency for turboprops and older turbofans [264]. Airport properties are sourced from the OpenFlights and OurAirports databases [260, 261].

Aircraft types are grouped into the classes of widebody (twin aisle), narrowbody (single aisle), regional jet, and turboprop based on form and engine type. Transport jet aircraft were also classified ad hoc as widebody or narrowbody for this analysis, according to their

size. Emissions from business jets and piston engine aircraft, which are estimated to contribute ~1–2% of global fuel burn [299], are not included in this analysis due to unscheduled flight movement data not being available. As simplifications due to unavailability of data, engine degradation is disregarded and a single specific engine model is assigned for each engine family for aircraft type instead of considering all engine options, as described in Section 3.2.2.

4.2.2 Projecting aircraft fuel burn towards 2050

For the four aircraft classes mentioned, projections are calculated in yearly steps up to 2050 by considering that new traffic demand, according to ICAO's long-term passenger and cargo traffic forecasts from 2021 [224, 300], is met by a representative aircraft. These generic representative aircraft start from the performance of (real) reference aircraft type in 2018 and each year the performance of newly introduced aircraft is progressively increased based on the engine fuel burn and NO_x emission goals identified by ICAO's 2017 independent expert integrated review panel [148] and those used in ICAO's environmental trends analysis in 2019 [221]. The emission goals defined by the expert panel relate to engines which enter into service by the target dates of 2027 and 2037. In this study, the use of conventional (fossil-based) jet fuel is assumed, and future engine performance is modeled with a continuous improvement, with piecewise linear interpolation between those goal points, extrapolating improvements from 2037 to 2050. Transformative engine or aircraft technologies, such as electric or hydrogen propulsion, beyond those considered relevant until 2037 by the ICAO panel, are not contemplated in the analysis.

An overview of how the emission projections are produced is given in Figure 4.1, with the relevant factors being described in more detail further in this section. This calculation pipeline is performed twice in parallel, once for passenger services, and another for cargo services. In this setup, "cargo" includes exclusively freight and mail services, while mixed services that carry both passenger and cargo are included in the "passenger" part of calculations. For cargo flights, only three classes of aircraft are considered, with the omission of a regional jet class.

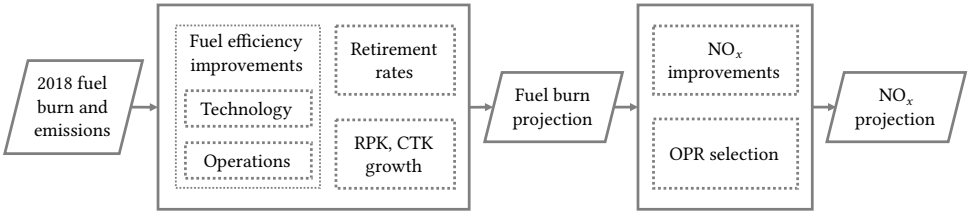

Figure 4.1: Overview of the process of projecting 2018 fuel burn and NO_x emissions.

Passenger air traffic is modeled by considering the revenue passenger-km (RPK) achieved by each aircraft type for each pair of origin and destination world regions. The definition of regions follows that used in the ICAO's long-term traffic forecast [300]. The OAG schedule data include available seats for each flight, allowing for the calculation of total available seat-km (ASK) for each aircraft type and regional pair. A global average passenger load factor of 81.7% is then estimated from the ratio of total ASK and the global

RPK value published by ICAO [301]. This load factor is applied equally to all aircraft type and region combinations to estimate specific RPK values for 2018. Note that the choice of load factors (also for cargo, described ahead) do not impact fuel burn and emissions values, as everything is relative to the base year of 2018 and the factors are applied uniformly to all flights.

Likewise, cargo air traffic is modeled according to the cargo ton-km (CTK) specific to each aircraft type and flight origin regions. The OAG dataset used lists "typical" available freight ton-km (AFTK) for some flights, and for missing values a constant payload mass for each aircraft type is applied. These listed "freight" values are considered in this analysis as "cargo", i.e. freight plus mail, so the available cargo ton-km (ACTK) is equal to the listed AFTK. A global average load factor of 49.3% is applied uniformly to calculate CTK, based on data from the International Air Transport Association (IATA) [285].

Calculations for passenger and cargo are done in parallel with the same approach, using RPK and CTK, respectively, as a metric of air traffic volume T (Eq. (4.1)). The 2018 values of traffic are projected forward to each year y by applying the regional-pair specific compound annual growth rates ($r_{y,rgn}$) from the ICAO's long-term forecast[2] (Eq. (4.2)). Four forecast scenarios are considered: the medium traffic projection made prior to the COVID-19 pandemic (Pre-COVID) [224], and three projections made in July 2021 with different levels of recovery and growth (High, Mid, Low) [300]. Constant growth rates are given for the periods from 2018 to 2028, 2038, and 2048 (or 2050 for the post-COVID scenarios). For the three post-COVID cases, the pre-COVID forecast is applied between 2018 and 2019, and zero RPK growth is applied between 2019 and 2023 (High), 2024 (Mid), or 2027 (Low), with growth resuming at a pace that matches the forecast traffic for 2028 in each scenario. Likewise, CTK growth is set to zero between 2019 and 2021 (High), 2022 (Mid), or 2023 (Low). This is done to reflect in the model that aircraft were not scrapped en-mass during the pandemic and then replaced with newer aircraft once traffic returned; the lower traffic is not modeled and that period is thus disregarded in the results. As a simplification, the extra length of leap years is not taken into account, effectively underestimating traffic in those years by 0.3%. Since ICAO's air-traffic forecasts concern only total passenger and cargo traffic and there is no consensus on how this new demand will be spread in the various segments of the aircraft market, the proportion of traffic met by each class of aircraft is kept constant from 2018 onwards (Eq. (4.3)). Although the present trend of growing market share by low-cost carriers, if continued, might drive a shift in these proportions [302].

$$T = \{RPK, CTK\} \tag{4.1}$$

$$T_{y,rgn} = r_{y-1,rgn} \cdot T_{y-1,rgn} \tag{4.2}$$

$$T_{y,class} = T_y \frac{T_{y=2018,class}}{T_{y=2018}} \tag{4.3}$$

[2] ICAO lists values for freight, but those values are used here with no distinction being made between FTK and CTK

At each year, the projected traffic demand is met by a combination of aircraft that were already operating, of various types i, and aircraft were introduced that year, of each generic $class$ (Eq. (4.4)). The traffic demand fulfilled by already existing aircraft is calculated as the same as the previous year scaled to the expected fraction of aircraft that remain in service (Eq. (4.5)). A generic aircraft of each class, with up-to-date performance, is introduced every year to make up the difference between the total traffic projected and the traffic achieved by the aircraft that remain operating (Eq. (4.6)).

$$T_y = \left(\sum T_{y,i}\right)_{old} + \left(\sum T_{y,class}\right)_{new} \tag{4.4}$$

$$T_{y,i,old} = T_{y-1,i,old} \cdot (1 - ret_i) \tag{4.5}$$

$$T_{y,class,new} = T_{y,class} - (T_{y,i,old})_{class} \tag{4.6}$$

Fleet renewal is modeled by applying, each year, a class-specific retirement rate to the current age distribution of each aircraft type. The fraction of a type's fleet that retires in a year (ret_i) is calculated according to Equation (4.7), where $N_{i,t}$ denotes the number of aircraft of age t at year i. Retirement rates are modeled as a logistic function (Eq. (4.8)), using the parameters (a_1, a_2) given by Ref. [303]. In these functions, the median retirement ages are 27.7, 28.9, 29.5, and 33.2 years for widebody, narrowbody, regional jet, and turboprop classes respectively. The initial aircraft age distribution (for 2018) is primarily estimated by applying the retirement model to historic annual delivery numbers from Boeing, Airbus, Embraer, and Bombardier. Additionally, the initial ages of some aircraft types are estimated based on the entries present in the national aircraft registries of the US, Brazil, and Spain. If age data for a type are still insufficient, online crowdsourced aircraft databases (such as planespotters.net) are used, or a constant delivery rate during the years of production is assumed.

$$ret_i = \sum_t \left(ret_{class,t} \frac{N_{i,t}}{N_i} \right) \tag{4.7}$$

$$ret_{class,t} = \exp\left(-a_{1,class} - t \cdot a_{2,class}\right) \tag{4.8}$$

To evaluate the impact of retirement rate on the results, four alternative not necessarily realistic scenarios are considered: faster retirement, slower retirement, full fleet annual replacement, and no retirement whatsoever. For the faster and slower cases, the a_1 parameters were adjusted so that the medians retirement ages were reduced or delayed by 10 years (Figure 4.2).

Specific fuel consumption (c) is quantified for 2018 for each aircraft type by the ratio between fuel burn (C) and the traffic metric. These values are calculated globally, as some aircraft types might fly only a low number of routes for a given pair of regions which might not be representative of the aircraft performance if the routes were to change within the same regional pair. The traffic-specific fuel consumption values calculated for 2018 are then scaled every year by the expected average reduction due to operational improvements, k_{op} (Eq. (4.9)).

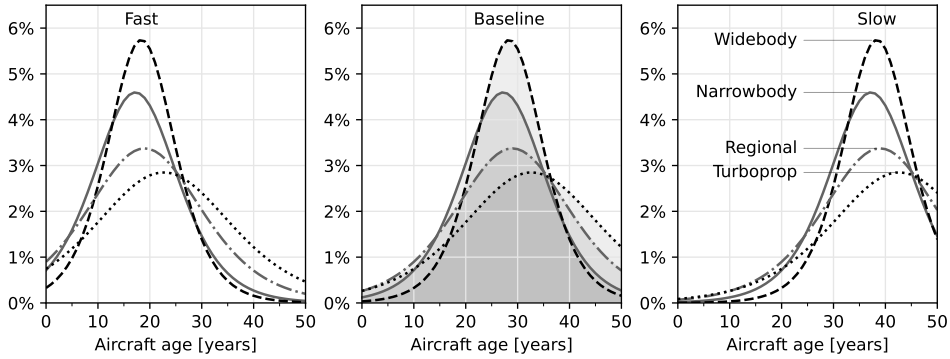

Figure 4.2: Probability mass function of retirement age at annual intervals (% per year), for the baseline [303] and a faster and slower alternative scenarios.

$$c_{y,i} = \begin{cases} \dfrac{C_{y,i}}{T_{y,i}} & y = 2018 \\ c_{y-1,i} \cdot (1 - k_{op,y-1}) & y > 2018 \end{cases} \tag{4.9}$$

k_{op} is calculated according to the two sets of goals set in 2014 by a panel of independent experts under the ICAO CAEP (Committee on Aviation Environmental Protection) [304]. The baseline goals are cumulative improvements relative to 2010 of 3.25% (2020), 6.75% (2030), and 9.00% (2040) as shown in Figure 4.3. The other set of goals established are referred by the panel as "lower limits of the confidence range", which are denominated here as the "low" scenario for operational fuel consumption improvements. For both scenarios, no further improvements are considered beyond the year 2040, which is an assumption that all possible efficiency improvements in operations will have been realised by then.

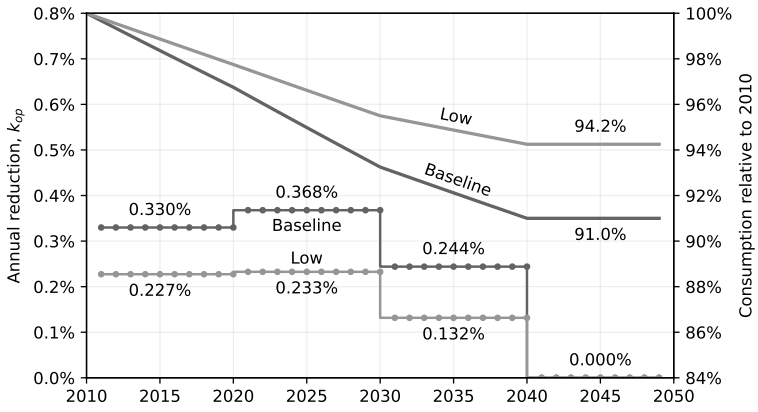

Figure 4.3: Scenarios of reduction in fuel consumption due to operational improvements, equivalent to goals from Ref. [304].

A set of reference aircraft are chosen to represent the present-day performance typical of new aircraft from each class, serving as the starting point for future projection (Table 4.1). These values are taken as the mean of two representative aircraft types, for which the average performance values are calculated across all passenger or cargo flights in 2018. As an exception, only one reference turboprop type is used for cargo, due to the small number of flights available. Specific fuel consumption of future aircraft, in addition to being adjusted by k_{op}, is also adjusted by a factor to account for technological improvements, k_{tec} (Eq. (4.10)).

Table 4.1: Reference aircraft types used to represent present technology level.

Class	Passenger	Cargo
Widebody	A359, B78X	A332, B77L
Narrowbody	A20N, B38M	A320, B737
Regional	E290, BCS3	n/a
Turboprop	AT72, DH8D	AT72

$$c_{y,class,new} = \begin{cases} \text{mean}\left(c_{y=2018,i}\right)_{i \in ref,class} & y = 2018 \\ c_{y-1,class,new} \cdot (1 - k_{op,y-1}) \cdot (1 - k_{tec,y-1}) & y > 2018 \end{cases} \tag{4.10}$$

For k_{tec}, the adopted values are the same as used by CAEP for the long-term trends analysis published in their Environmental Report 2019 [221]. Four scenarios are considered, with a constant annual fuel reduction applicable to all aircraft classes: 0.57% (low), 0.96% (moderate), 1.16% (advanced), and 1.50% (optimistic). Another scenario adopted here, labeled "IE", consists of the aircraft class-specific values found by a panel of independent experts under CAEP from 2017, which were also published in 2019 [148], shown in Figure 4.4. The source for this last scenario does not consider turboprop improvements, which is thus set to zero in this analysis. This is not expected to have a large effect, as the fraction of total fuel burn attributed to turboprops is very small (~1–2%), see Figure 3.7). A (unrealistic) scenario with no technology improvement is also included in this study.

Finally, the total amount of fuel burned in future years is determined by the combination of traffic and specific fuel consumption projections for each aircraft type, both existing and generic future types (Eq. (4.11)). Note that the fleet of generic aircraft introduced each year continues in the calculation for future years, being subjected to the retirement and operational improvement functions described previously.

$$C_y = \sum c_{y,i} \cdot T_{y,i} + \sum c_{y,class,new} \cdot T_{y,class,new} \tag{4.11}$$

4.2.3 Projecting aircraft NO_x emissions towards 2050

The starting point of NO_x emission projections is the average emission indices and engine certification emissions results of the reference aircraft (Table 4.1). These EI values are then projected forward according to technology improvements quantified as a ratio (k_{NO_x}) to the goal for the year 2027 proposed by CAEP's 2017 independent expert integrated review panel [148]. As the panel did not consider turboprops, emission indices for this class are

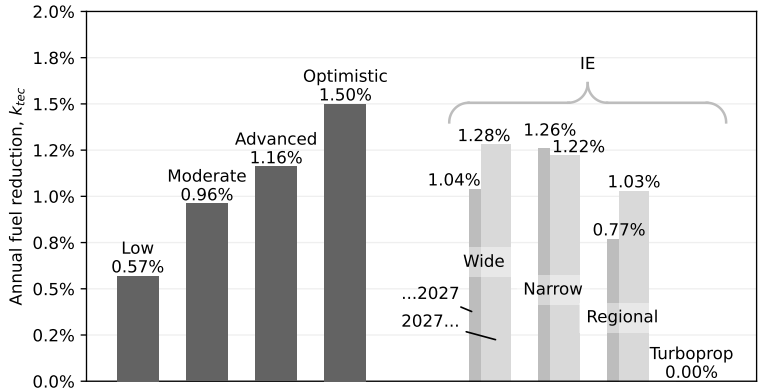

Figure 4.4: Scenarios of reduction in fuel consumption due to aircraft technological improvements, based on Ref. [221] (Low, Moderate, Advanced, Optimistic) and Ref. [148] (IE).

frozen at the values of the reference aircraft in 2018, assuming no change in technology or engine pressure ratio. In the same format as the ICAO emission standards [7], the goal gives the mass of emissions in the standard certification cycle (D_p) normalized by engine rated thrust (F_{00}) as a function of the engine's overall pressure ratio (OPR, π_{00}). Equations (4.12) and (4.13) show these calculation steps.

$$\left(\frac{D_p}{F_{00}}\right)_{y,class} = \left(5.75 + 0.577 \cdot (\pi_{00})_{y,class}\right) \cdot \left(k_{\mathrm{NO}_x}\right)_{y,class} \tag{4.12}$$

$$EI(\mathrm{NO}_x)_{y,class} = EI(\mathrm{NO}_x)_{ref,class} \frac{\left(D_p/F_{00}\right)_{y,class}}{\left(D_p/F_{00}\right)_{ref,class}} \tag{4.13}$$

k_{NO_x} varies per year, representing technological improvement, with the values for 2018 chosen to match how far the modeled reference aircraft are to the 2027 goal. k_{NO_x} then linearly goes to unity in 2027 for all classes of aircraft. Three scenarios are considered in terms of what happens beyond: no further improvement (baseline), emissions cut by another 10% by 2037 (continued-conservative), and emissions cut by another 50% by 2047 (conservative-optimistic). A fourth (unrealistic) scenario consists of no improvements from 2018 (Figure 4.5).

As the baseline estimate, π_{00} is considered to increase constantly up to the values of 60, 65, and 70 in 2027 for regional jets, narrowbodies, and widebodies, respectively, as shown in Figure 4.6. This scheme represents a new generation of turbofans with increased pressure ratios being introduced 10 years after the base year for the technology forecasts, with no further increases afterwards. Alternative scenarios considered include a delayed (to 2037) introduction of this new generation of engines (Low scenario), and a scenario in which OPR increases a second time from 2027 to 2037 (High), representing a second future generation of engines. While the OPR value affects the NO_x emissions, it also impacts the overall engine efficiency, and thus the resulting fuel burn. Note that this later effect is not

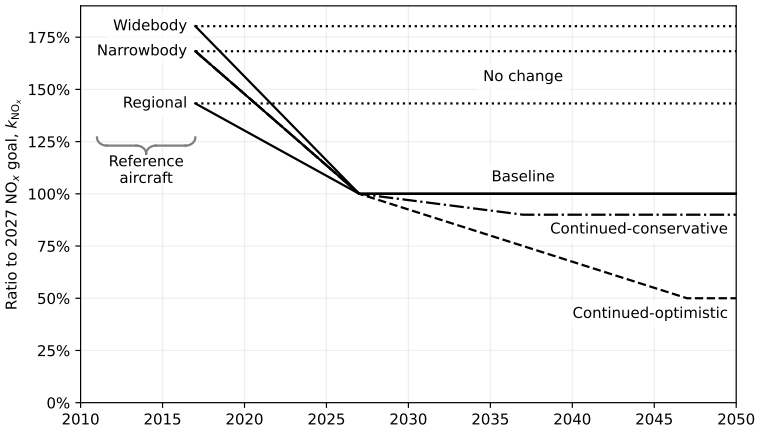

Figure 4.5: Scenarios of NO_x technology improvements, in terms of the ratio to the 2027 goal.

captured in this modeling chain, and that aircraft and engine technological improvements are solely represented in terms of the overall fuel efficiency technology targets as stated in ICAO's 2017 independent expert integrated review panel [148]. This mismatch is not expected to introduce significant uncertainty in the estimated EIs, but future work could focus on coupling projections of fuel efficiency improvements to OPR.

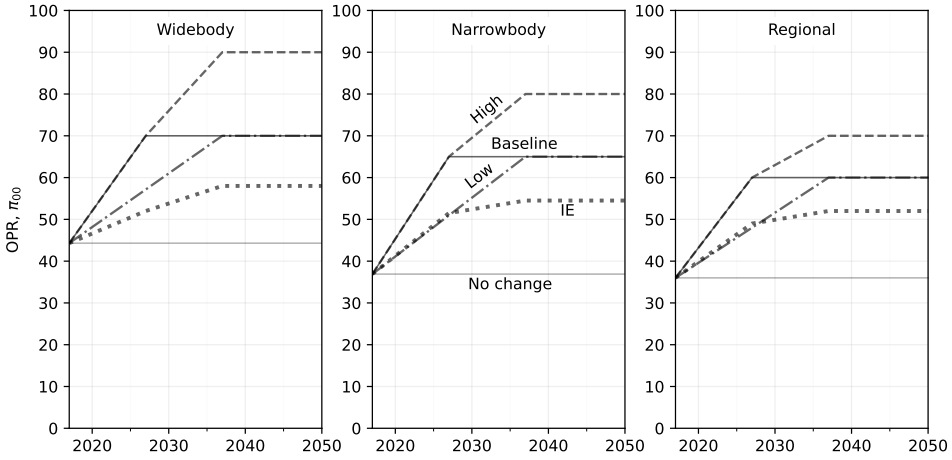

Figure 4.6: Scenarios of overall engine pressure ratio for future aircraft, "IE" scenario based on Ref. [148].

4.2.4 Overall projection scenarios

Throughout Sections 4.2.2 and 4.2.3, various scenarios for individual model parameters were described. From a baseline setting, each parameter is changed individually to evaluate the sensitivity of the results to the input changes. Additionally, two other overall

scenarios are evaluated, consisting of different selections of input parameters as listed in Table 4.2: Low and High (emissions). While subjective, these selections allow the production of some form of an overall realistic lower and upper boundary of future emissions.

Table 4.2: Parameter selection for the overall scenarios of emissions projections.

	Overall scenario			
Parameter	Low	Baseline	High	Other parameter options
T	Low	Mid	High	Pre-COVID
ret	Baseline	Baseline	Baseline	Fast, Slow, Annual replacement, No retirement
k_{op}	Baseline	Baseline	Low	No change
k_{tech}	Advanced	Moderate	Low	Optimistic, IE, No change
k_{NO_x}	Continued-conservative	Baseline	Baseline	Continued-optimistic, No change
π_{00}	Low	Baseline	High	IE, No change

4.3 Results

4.3.1 Aircraft fuel burn and NO_x emissions in 2005 and 2018

The resulting total (passenger and cargo) fuel burn for 2018 is 287 Tg (Table 4.3) which is comparable to other estimates: it is 12% higher than the 2018 fuel burn estimate by Seymour et al. [258] and 1% higher than the estimate by Graver et al. [257]. Passenger aircraft operations account for 92% of that amount, and the total RPK considered here matches (to < 0.1%) the annual statistic published by ICAO [301]. Total CTK is only 42% of the value published by ICAO, but such large difference is expected since the numbers presented here refer only to dedicated freight and mail services, not including cargo transported in the bellyhold of passenger aircraft. Of the 2018 fuel burn from cargo flights, 97.6% came from widebody aircraft, although this includes 3.5% from the B752 type which is structurally a narrowbody that was grouped with widebodies for cargo analysis due to its range and payload, in order to be more consistent with the class definitions used for transport aircraft.

For 2005, 177.7 Tg of fuel burn is estimated from passenger aircraft (Table 4.3), indicating a 48.7% increase between 2005 and 2018. In both years, this fuel burn is primarily used by widebody and narrowbody aircraft, with regional jets and turboprops responsible for 6.4-8.2% of fuel burn. The fuel burn per RPK is ~20% higher for widebodies compared to narrowbody aircraft, which is consistent with their typically longer range of operation.

NO_x emissions in 2018 totaled 4.43 Tg (base NO_2), yielding a global fleet average NO_x EI of 15.4 g/kg in that year. This EI for 2018 is 10% higher than the one for 2005 (14.0 g/kg), which is in agreement with the observed trend of increasing EI $\left(\mathrm{NO}_x\right)$ and improved fuel efficiency over time (Figure 3.4). Twin-aisle aircraft have a higher global fleet average EI $\left(\mathrm{NO}_x\right)$, which has increased twice as fast as the average for single-aisle aircraft, from

Table 4.3: Global fuel burn for passenger flights in 2005 and 2018, per aircraft class. For 2018 the RPK, CTK and the fuel burn including cargo operations is also presented.

	Fuel burn [Tg] (% of total)			RPK $[10^9]$	CTK[a] $[10^6]$
Aircraft class	2005	2018	2018 w/ cargo	2018	2018
Widebody	94.8 (53.4)	125.8 (47.6)	148.0 (51.5)	3634	98099
Narrowbody	68.3 (38.4)	121.7 (46.0)	122.4 (42.6)	4289	1481
Regional jet	11.3 (6.3)	13.3 (5.0)	13.3 (4.6)	280	n/a
Turboprop	3.3 (1.9)	3.6 (1.4)	3.6 (1.3)	74	28
Total	177.7	264.3	287.3	8278	99608

[a] Values for dedicated cargo services only, excluding cargo transported by passenger aircraft.

16.0 g/kg in 2005 to 18.5 g/kg in 2018. Assuming that the currently estimated environmental cost of NO_x is ~2.3 times that of CO_2 for every ton of fuel burn [211], this increasing trend in its EI is concerning with regard to the total atmospheric impacts of aircraft emissions, and contributes to the motivation for research into the tradeoff between mitigation of these pollutants [10, 11, 295].

Table 4.4: Global average NO_x emission indices in 2005 (passenger flights only) and 2018, per aircraft class.

	EI (NO_x)[g/kg]		
Aircraft class	2005	2018	2018 w/ cargo
Widebody	16.0	18.5	18.1
Narrowbody	11.9	12.8	12.8
Regional jet	10.5	11.3	11.3
Turboprop	9.3	9.3	9.3
Total	14.0	15.4	15.4

4.3.2 Future emissions under different traffic and overall scenarios

Projected fuel burn and NO_x emissions from 2018 to 2050 for the three different overall scenarios, and for the baseline settings but with different traffic forecasts are shown in Figure 4.7. In all cases, fuel burn and the resulting NO_x emissions grow continuously to 2050. Under the different overall scenarios, annual fuel burn grows by 45% (Low), 104% (Baseline), 155% (High), and the annual NO_x emissions by 36%, 113%, and 209%. When the only parameter changed is the traffic volume, the ranges of growth are 51%–128% (fuel) and 56%–138% (NO_x). As efficiency improves over time, these ranges are all lower than the forecast increases in global RPK to 2050: 148% (Low), 237% (Baseline/Mid), and 274% (High).

The projected variation of EI (NO_x) over time is shown in Figure 4.8 for the different overall and traffic scenarios, as well as how it varies between the aircraft classes for the Baseline scenario. In 2050, projected average EI (NO_x) is 14.4 g/kg (Low), 16.1 g/kg

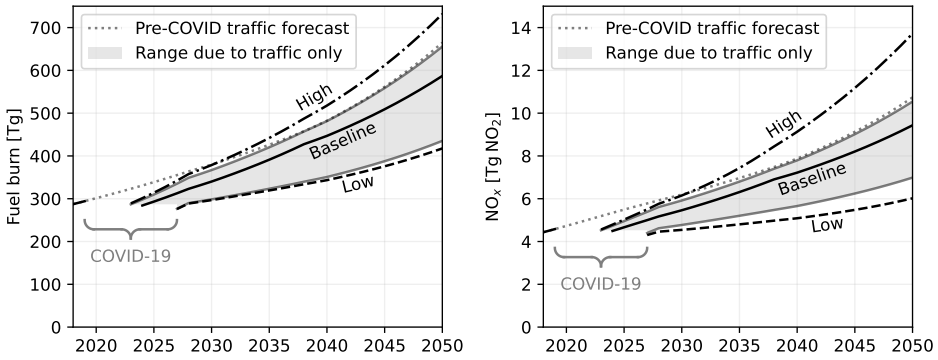

Figure 4.7: Annual fuel burn and NO_x emissions projections for the three overall scenarios considered (black lines), and under the Baseline scenario combined with different traffic forecast scenarios (solid gray lines closer to the Baseline, and dotted gray line for the Pre-COVID traffic forecast).

(Baseline), 18.7 g/kg (High), primarily driven by different projections of OPR (Figure 4.6). Driven by the underlying modeling assumptions, all air traffic growth scenarios result in a similar EI (NO_x) at 2050, ranging between 16.05–16.08 g/kg, i.e. a 4% further increase compared to 2018. However, there are slight differences within traffic scenarios as the rate at which new aircraft are introduced is different, with the higher traffic leading to higher fleet average EI (NO_x) in the first two decades. This is a result of the fact that the EIs of the reference aircraft are higher than the global fleet average in this period, before the combined effects of OPR and the NO_x technology goals push them below the existing average. For the baseline scenario considered, OPR and k_{NO_x} are constant from 2027 (Figures 4.5 and 4.6), so the fleet average for each class start converging to the EI of aircraft introduced since then. These forecast values are lower than the present reference widebody, but higher than the present reference narrowbody and regional jet, combining to a relatively stable average across all aircraft.

The spatial distribution of the projected NO_x emissions is heterogeneous, driven by the underlying varying air traffic growth rates between the different regions. Considering just passenger traffic in the baseline scenario, while NO_x emissions from flights departing Europe and North America are expected to grow by 76% and 67% between 2018 and 2050, respectively, NO_x emissions from flights departing from the remaining regions are expected to grow by 153% in total. With the definition of regions used, both in 2018 and 2050 the largest amount of NO_x emissions from passenger flights are attributed to air traffic departing from Europe (24.3%, 19.9%), North America (22.8%, 17.7%), and China and Mongolia (13.6%, 17.4%). Out of the six regions considered for cargo flights, most NO_x emissions came from Asia and the Pacific (33.7% in 2018, 32.3% in 2050) and North America (31.6%, 28.4%), with the Middle East's share doubling in the period (10.2%, 22.2%). Globally, the share of NO_x emissions due to cargo flights drop in the baseline scenario from 8.1% to 7.3%, even though the share of fuel burn stays at 8.0%, due to lower EI (NO_x) for widebodies.

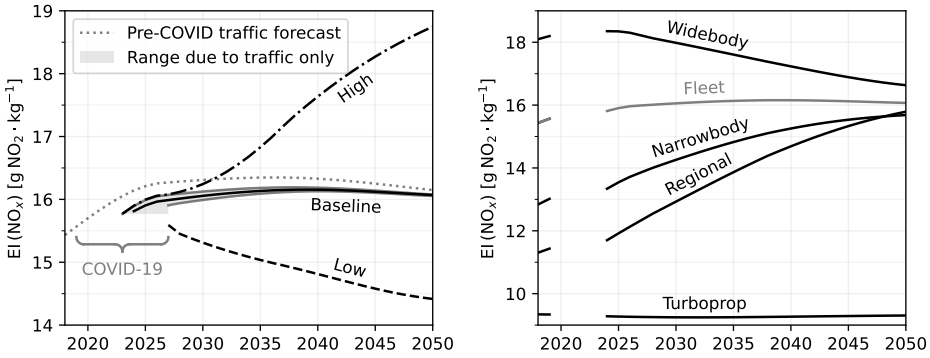

Figure 4.8: Left: fleet average EI (NO_x) for the three overall scenarios considered (black lines), and under the Baseline scenario combined with different traffic forecast scenarios (solid gray lines closer to the Baseline, and dotted gray line for the Pre-COVID traffic forecast). Right: average EI (NO_x) per aircraft class for the overall Baseline scenario.

4.3.3 Sensitivity of future fuel burn and NO_x emissions to different forecast parameters

Table 4.5 presents the relative changes in the aggregate fuel burn and NO_x emissions over the period of 2018 through 2050 as a result of different individual modeling choices, changing parameters one at a time form the overall baseline scenario (Table 4.2). Overall, individual scenario choices can result in total fuel burn variations of −20% to +12%, total NO_x emissions variations of −23% to +48%, and the time-averaged EI (NO_x) and the EI (NO_x) in 2050 varying by −23% to +48% and −32% to +67%, respectively. The two alternative traffic forecasts from ICAO result in −21% and +12% NO_x emissions by themselves.

While faster retirement rates would reduce emissions by accelerating the adoption of more efficient aircraft, the likely unrealistic reduction of median retirement age by 10 years lead only to a reduction of 5% of emissions over the 2027–2050 period. And the more extreme hypothetical of replacing all aircraft every year reduces NO_x by 14%. The baseline projected operational and technological improvements avoid 6% and 11% of fuel burn, respectively (compared to the "no change" scenarios). The optimistic technology forecast would reduce fuel burn by another 6% relative to the baseline.

The largest variations in NO_x emissions are introduced by the NO_x technology and OPR scenario selection, which directly affect EI (NO_x). The baseline scenario, considering OPRs of 70:1 (widebodies) and 65:1 (narrowbodies) in 2027, lead to a 47% higher EI (NO_x) in 2050 relative to not changing the OPR further from the present reference aircraft, which are in the 33:1 to 48:1 range. Higher pressure ratios are compensated by the NO_x technology improvement parameter, with the 2050 fleet average EI (NO_x) being 40% for the baseline case relative considering no change in k_{NO_x}. The "continued-optimistic" scenario, which projects another halving of NO_x emissions for a given OPR from 2027 to 2047, would reduce the fleet average EI (NO_x) in 2050 by 28% relative to the baseline.

Table 4.5: Effects of different modeling parameter choices on the total fuel burn and NO_x emissions between 2027 and 2050, as well as the estimated global fleet average EI (NO_x) averaged over the 2027–2050 and the estimated global fleet average EI (NO_x) for 2050. Values indicate relative differences resulting from changing one parameter at a time. Descriptions of the different scenarios are provided in Section 4.2.

Parameter (baseline)	Scenario	2027–2050 period [%]			2050 [%]
		Fuel	NO_x	EI (NO_x)	EI (NO_x)
Traffic (Mid)	Low	−20.5	−20.8	−0.5	−0.2
	High	+9.0	+9.4	+0.3	+0.1
	PreC	+10.3	+11.5	+1.1	+0.5
Retirement (Baseline)	No retirement	+10.7	+8.4	−2.1	−1.4
	Slow	+4.9	+4.0	−0.9	0.0
	Fast	−4.8	−4.2	+0.6	−0.2
	Annual replacement	−14.3	−14.8	−0.6	−0.4
Operations (Baseline)	No change	+6.2	+6.2	+0.0	+0.0
	Low	+2.4	+2.4	+0.0	0.0
Fuel burn technology (Moderate)	No change	+12.4	+12.4	0.0	0.0
	IE	−2.3	−2.4	−0.1	−0.1
	Low	+4.8	+4.8	0.0	0.0
	Advanced	−2.3	−2.3	+0.0	+0.0
	Optimistic	−6.1	−6.0	+0.0	+0.0
NO_x technology (Baseline)	No change	+0.0	+47.9	+47.9	+67.3
	Continued-conservative	+0.0	−3.8	−3.8	−7.3
	Continued-optimistic	+0.0	−12.2	−12.2	−27.7
OPR (Baseline)	No change	+0.0	−23.2	−23.2	−31.9
	IE	+0.0	−11.4	−11.4	−14.5
	Low	+0.0	−5.0	−5.0	−3.3
	High	+0.0	+8.6	+8.6	+16.4

4.4 Discussion and conclusions

In this work, the recent and projected trends in global aviation fuel burn and NO_x emissions were estimated. Between 2005 and 2018, it is found that aviation fuel burn (and thus CO_2 emissions) have increased by 49%, and that the growth in NO_x emissions has surpassed that of CO_2, resulting in a global fleet average EI (NO_x) increase of 10% between the two years. This is in agreement with the trends discussed in Chapter 3 (seen in Figure 3.4) driven by engine designs using higher pressure ratios in search of fuel efficiency improvements [295], which are allowed more NO_x emissions by the ICAO CAEP standards (Section 2.4.2).

With the increasing understanding of the atmospheric impacts of aircraft emissions, NO_x has gained attention as a key contributor to aviation's environmental impacts. Despite the higher uncertainty ranges and lower level of scientific understanding compared to the climate effects of CO_2 [5], aviation NO_x emissions are currently estimated to lead to

more damage from environmental externalities than CO_2 emissions, primarily driven by the air quality impacts associated with emissions [211]. With the multiple international, regional and national targets in the coming decades for addressing aviation's impact on the environment, forecasts of potential future emissions are essential. In contrast with CO_2 impacts, which scale linearly with fuel burn, NO_x emissions partake in multiple nonlinear chemistry processes, resulting in the same amount of emissions leading to different air quality and climate impacts depending on the location they are emitted and the background level of atmospheric composition (driven by other sectors' emissions, among other factors) [10, 11, 212, 231]. This spatial difference in potency of impacts is also seen with regard to air quality in Chapter 5. As a result, forecasts are needed not just in terms of emissions totals, but also in terms of their spatiotemporal distribution in the global domain over the years.

To aid such analyses and to provide insight on the potential future developments in the engineering tradeoffs between fuel efficiency and EI (NO_x), existing passenger traffic as well as technological and operational improvements targets were used in this chapter to forecast global aviation fuel burn and NO_x emissions through 2050. The scope of this study does not include all aspects of civil aviation, with business jets and piston aircraft not covered, and with turboprops modeled with additional simplifications; focus is put on widebody, narrowbody, and regional jets, which uses around 97–98% of fuel across all civil flights. While the short-term effects of COVID-19 restrictions are not captured, these are included in the traffic scenarios used, and are thus reflected in the longer-term estimates provided. In all scenarios considered, aviation fuel burn and the associated NO_x emissions continue to increase, including by 104% and 113% respectively for the baseline scenario, which are less than the 210% increase in RPK. Based on the considered projection of engine OPR and NO_x technology improvements, the global fleet average EI (NO_x) will further increase by an estimated 4% by 2050, after a 10% growth between 2005 and 2018. The "slowing down" of the EI (NO_x) growth trend is consistent with the assumptions in the model of changing OPR and k_{NO_x} only up to 2027. How these parameters will evolve afterwards remains uncertain, and the effects of unconventional propulsion configurations not considered here are likely to become more significant. Different combustor designs can have vastly different emissions characteristics, given the nonlinear nature of trace pollutant formation, such that newer models can have significantly different performance in this regard, although the existing requirements of ICAO's Annex 16 should ground EI values to some extent.

While there are strong incentives to reduce fuel consumption, the format of the present engine emissions standard does not incentivise further reductions in NO_x emissions, as extra margin to the NO_x regulatory limits obtained from improved technologies might enable further increases in pressure ratio [295]. A future lowering of EI (NO_x) could occur with shifting focus of the OEMs towards reducing NO_x emissions through the introduction of new technologies that do not substantially impact the fuel efficiency, but the opposite might occur if the non-binding technology improvement targets considered here are proven to be too optimistic. Future work could focus on coupling the modeling assumptions between the fuel efficiency estimates and NO_x improvements, and on uncertainty quantification of the modeling parameters which can complement these findings and can further increase the robustness of the sensitivity analysis presented here. Finally, as the

COVID-19 related effects on air traffic were still on-going when ICAO released the traffic forecasts used here (September 2021), the estimates presented also depend on how the aviation sector bounces back from that situation. Additionally, financial pressure and the temporarily lower aircraft usage due to the pandemic might lead to lower retirement rates. The slower rate of efficiency improvements, consistent with a hypothesis that technology is converging and with the observed increase in time between new model introductions, can also reduce over time the motivation to replace aircraft.

Another factor that might interfere with the projections shown here is an increase in geopolitical tensions, which might be seen as more likely after the 2022 Russian invasion of Ukraine. Political instability and military conflicts can pose a direct obstacle to operational improvements through additional restrictions of airspace, as conflict mentioned illustrates [305]. Increased economic sanctions and protectionism might, to some extent, drive aircraft and engine adoption independently of technological optimization. This might lead to the proliferation of aircraft in specific regions of the world that lag behind in performance relative to a global state of the art, which goes against one of the premises of the modeling approach adopted in this chapter. And finally, cross-border tensions caused by conflicts, pandemics, or otherwise, can lead to sharp impacts on air traffic, although aviation long-term trends have historically proven to be resilient to events such as the September 11 attacks in the United States and the 2008 global financial crisis [284].

Overall, based on the technological goals assumed here, both aviation fuel burn and NO_x emissions will continue to increase in the coming decades, unless actions beyond these targets are taken. More frequent aircraft replacement and more optimistic operational improvements do not substantially alter this result. However, this work does not account for innovations in the energy source, fuel used, or unconventional designs that could be introduced. Specifically, in the operations modeled here, the use of conventional jet fuel is assumed and thus the take-up of sustainable aviation fuels (SAF) is not explicitly taken into account. It should be noted that drop-in SAFs do not substantially impact the fuel consumption, and previous studies indicate that their NO_x emissions also do not substantially differ from those of conventional jet fuel [306]. Likewise, new technologies that deviate substantially from the current configurations, such as electric, hybrid or hydrogen-fueled aircraft are not considered here. This work further highlights the need for such technologies or other demand-based interventions in order to meet aviation's environmental goals. Future work could introduce these new technologies to the modeling chain described here.

4.5 Acknowledgments

The author would like to thank Flightradar24 AB for providing flight movement data from ADS-B, and Paul Roling for the helpful discussion on the OAG schedule data. This work made use of the Dutch national e-infrastructure with the support of the SURF Cooperative using grant no. EINF-1694.

5

Regional air quality sensitivities to aircraft emissions

Deus te leve á salvo, brioso e altivo barco, por entre as vagas revoltas, e te poje n'alguma enseada amiga. Soprem para ti as brandas auras; e para ti jaspêe a bonança mares de leite. Enquanto vogas assim á discrição do vento, airoso barco, volva ás brancas areias a saudade, que te acompanha, mas não se parte da terra onde revôa.

God keep thee safe, stout barque, amidst the boiling billows! God steer thee to some friendly blight! May softer breezes waft thee, and for thee may the calm jasper seas be like plains of milk! But whilst thou sailest thus at the mercy of the winds, graceful barque, waft back to that white beach some of the yearning that accompanies thee, but which may not leave the land to which it returns.

Iracema – A Lenda do Ceará, by José de Alencar. Translation by Isabel Burton.

Previous studies have indicated that aviation emissions in different regions have varying corresponding air quality and human health impacts. Given the global nature of aviation activity and its forecast regionally heterogeneous growth, this phenomenon poses challenges in aviation decision making regarding air quality. In this chapter, the differences in regional air quality responses to aviation emissions are quantified, and their drivers analyzed. Specifically, the GEOS-Chem atmospheric chemical transport model is used to quantify the regional fine particulate matter ($PM_{2.5}$) and ozone sensitivity to aviation emissions over Asia, Europe, and North America in 2005. Simulations with perturbed regional aviation emissions are used

This chapter was originally published in the journal Environmental Research Letters. Please cite as shown in the list of peer-reviewed journal articles, item 2.

to isolate health impacts of increases in aviation emissions originating from and occurring in different regions. Health impacts are evaluated as premature mortality attributed to both landing and takeoff (LTO) and cruise emissions. It is found that the sensitivity of $PM_{2.5}$ global population exposure to full-flight emissions over Europe is 57% and 65% higher than to emissions over Asia and North America, respectively. Additionally, the sensitivity of ozone global population exposure to aviation emissions over Europe is higher than to emissions over Asia (32%) and North America (36%). As a result, a unit of fuel burn mass over Europe results in 45% and 50% higher global health impacts than a unit of fuel burn mass over Asia and North America, respectively. Overall, 73% and 88% of estimated health impacts from aviation emissions over Europe and North America, respectively, occur outside the region of emission. These results suggest that inter-regional effects and differences in regional response to emissions should be taken into account when considering policies to mitigate air quality impacts from aviation, given the projected spatially heterogeneous growth in air transportation.

5.1 Introduction

As was seen in Chapter 2, emissions from the combustion associated with aircraft, in addition to impacting the climate [307], are also a known contributor to the degradation of air quality [4, 209]. Among other deleterious consequences such as worsened visibility [308], decreased crop yields [309], and damage to wildlife and vegetation [310], this additional air pollution in the form of fine particulate matter ($PM_{2.5}$) and ozone (O_3) is associated with adverse effects on human health [104, 114], as detailed further in Section 2.2. Yim et al. estimated that the civil aviation activity in the year 2005 was associated with 16 000 (90% CI: 8 300–24 000) premature deaths globally, with 87% of that amount due to increased surface concentrations of $PM_{2.5}$ and 13% due to increased ozone surface concentrations [1]. Societal costs associated with the air quality impacts of aviation have been found to be comparable to those related to climate and noise impacts [211, 307, 311].

Long-term forecasts estimate a compound annual growth rate of ~ 3–4% in global air traffic between 2018 and 2050 [300]. This expected growth is not spatially uniform, with the "mid" scenario forecast intra-regional 2018–50 annual rates ranging from 2.5% for North America, 2.7% for Europe, to 5.8% for Southwest Asia [300]. As was explored in Chapter 4, despite improvements in aircraft technology and air traffic management, emissions from international aviation are projected to continue to grow through 2050 [6].

Policywise, measures regarding air quality are often guided by regional, national or local standards defining acceptable levels of concentration of various pollutants, and these standards may drive planning decisions concerning aviation [21]. The International Civil Aviation Organization (ICAO) engine emission standards, applicable to turbojet and turbofan engines, determine maximum emission indices (defined as mass of emission species per mass of fuel burned) allowed for a standard landing and takeoff (LTO) cycle, as described in Section 2.4.2 [7]. LTO is defined as the operations within 3000 ft above ground. These engine standards were created in 1981 and through revisions over the years continue to tighten the limits on the emission of oxides of nitrogen (NO_x), unburned hydrocarbons (HC), carbon monoxide (CO), and nonvolatile particulate matter. This regulatory framework, focused on LTO and local air quality standards, is consistent with the framing of aviation's air quality impacts as a local air quality issue. This is exemplified in Europe by the exclusion of non-LTO emissions in the National Emission Ceilings Directive (NEC) for

the accounting related to the emission targets up to the year 2030 [20], and in the United States by non-LTO emissions being considered a Categorical Exclusion for the environmental impact assessment of airports within the context of the National Environmental Policy Act [18].

However, there is increasing scientific evidence highlighting the contribution of non-LTO emissions and cross-border pollution transport to the air quality impacts of aviation [33]. Tarrasón et al., using an atmospheric chemical transport model (CTM) focused on Europe, identified the LTO NO_x impact on surface air quality as an order of magnitude smaller than that of non-LTO [29]. They attributed this to the larger share of non-LTO emissions (95% of all aviation emissions), atmospheric vertical transport and the high efficiency of NO_x ozone production in the free troposphere. They also found that about half of the impacts of full-flight (i.e. LTO plus non-LTO) NO_x emissions on air quality in Europe were associated with emissions outside the region. Barrett et al., employing a global CTM, found that 99% of population-weighted aircraft-attributable $PM_{2.5}$ is secondary sulfate-ammonium-nitrate aerosol (SO_4^{2-} – NH_4^+ – NO_3^-) formed primarily from NO_x [30]. And as seen in Chapter 3, about 90% of NO_x is emitted during non-LTO phases of flight [41, 233, 299]. Søvde et al., using an ensemble of five atmospheric models, found consistent increase in tropospheric ozone from aviation NO_x cruise emissions [31]. Aerosol precursors emitted at cruise level impact the surface both through vertical transport and by accelerating the oxidation of the precursors at the surface as they form aerosol, establishing an intercontinental mechanism of $PM_{2.5}$ impact [312]. Yim et al. combined global, regional and local atmospheric models and found that 75% of the global premature deaths due to aviation-attributable $PM_{2.5}$ and ozone were attributed to non-LTO emissions [1]. Koo et al. used the adjoint of a CTM, finding that non-LTO emissions were responsible for 60–90% of full-flight impacts in different regions[12]. They also found a significant cross-regional component to impacts, with 95% of the resulting premature mortalities from full-flight emissions over the US occurring outside the country, and 64% of impacts from emissions over Europe occurring outside the region.

Besides being involved in the aerosol formation pathway, the ozone produced from NO_x is also harmful to human health by itself (Section 2.2), with Eastham and Barrett estimating 8 600 premature deaths yearly due to (full-flight) aviation-attributable ozone [32]. Ozone produced at cruise altitudes has longer atmospheric lifetimes than the NO_x directly emitted near the ground, further enabling global-scale effects [8].

Intercontinental air pollution effects is a subject that has also been researched outside the context of aviation. The Task Force Hemispheric Transport of Air Pollution (TF HTAP) collaboration produced studies based on an ensemble of models looking at various aspects of this issue including ozone and primary $PM_{2.5}$ [197, 199]. Zhang et al. estimated the transboundary $PM_{2.5}$ impacts occurring through atmospheric transport and dispersion as well as through shifts in emissions due to international trade [207]. These studies show that even when considering other (non-aviation) anthropogenic emissions, which unlike aviation emissions are not located at high altitude, the inter-regional effects can be significant — being associated with 20% to more than 50% of ozone-related premature mortalities and 2% to 5% of particulate matter mortalities [197].

Given the long-distance nature of aviation's air quality impacts and since there is nonuniformity globally in the background atmospheric composition, in population den-

sity, in baseline disease incidence rates, and air traffic intensity, the same amount of emissions can result in different levels of impact depending on their source location. Population density has a strong effect of adding weight to Eastern Asia in terms of total premature mortality [12, 32]. As discussed by Yim et al. [1] and Grobler et al. [211], when country-specific valuations of mortality based on economic metrics are used, more weight is put on the air quality in North America and Europe.

Local atmospheric conditions, largely driven by emissions from other sectors and meteorology, also play a role in how sensitive a region's air quality can be to aviation emissions. Woody et al. explain higher levels of $PM_{2.5}$ formation from NO_x in the US by considering the abundance of ammonia available to react with nitrates [313]. However this has not been assessed for regions besides the US, and pollutants beyond $PM_{2.5}$. In contrast to previous studies that looked at the magnitude of global health impacts of aviation emissions [1, 32], this chapter focuses on the sensitivity of impacts to aviation emissions perturbations, and their differences across regions. The regional air quality responses to aviation emissions are quantified, and, for the first time, the extent to which different factors drive these responses are isolated (i.e. emissions within and outside of the region, population density, epidemiological characteristics, and background atmospheric processes). This is done by performing multiple simulations to isolate the impacts of increases in aviation emissions over Asia, Europe and North America. The long-range air quality impacts of aviation emissions are quantified for each source-receptor regional pair. Differences in the regional sensitivity of health impacts are calculated in stages, allowing for decoupling of the effects of population density and human health impact functions. Spatial variations observed in these sensitivities are then discussed in regard to their implications for air quality decision making for aviation.

5.2 Methods

The regional sensitivities of air quality impacts to aviation emissions are estimated using the GEOS-Chem atmospheric chemical transport model. Specifically, a set of scenarios are simulated where aviation emissions are increased alternatively in one of three continental regions shown in Figure 5.1, and the corresponding pollutant concentrations, population exposure, and human health impacts are quantified.

5.2.1 Aviation emissions and test scenarios

As this study predates the work described in Chapter 3, full-flight aviation emissions are obtained from the AEIC model [41], which builds estimates from 2005 civil aviation flight schedule data from OAG Aviation. Full-flight emissions are defined here as LTO emissions and non-LTO emissions (the latter primarily consisting of cruise level emissions but also emissions during the climb and descent above 3000 ft). The aviation emissions inventory used is produced by running AEIC with the BADA 3.15 aircraft performance model [262], and considering the LTO cycle described by Stettler et al. [265]. Emissions for NO_x, CO and HC are calculated from ICAO engine certification data. Black carbon emissions are estimated using the SCOPE11 method for LTO [270], and using a constant emission index of 30 mg/kg fuel for the non-LTO phases of flight, consistent with the values of 25–35 mg/kg adopted in other studies [1, 235, 252]. The speciation of the emission variables is the same

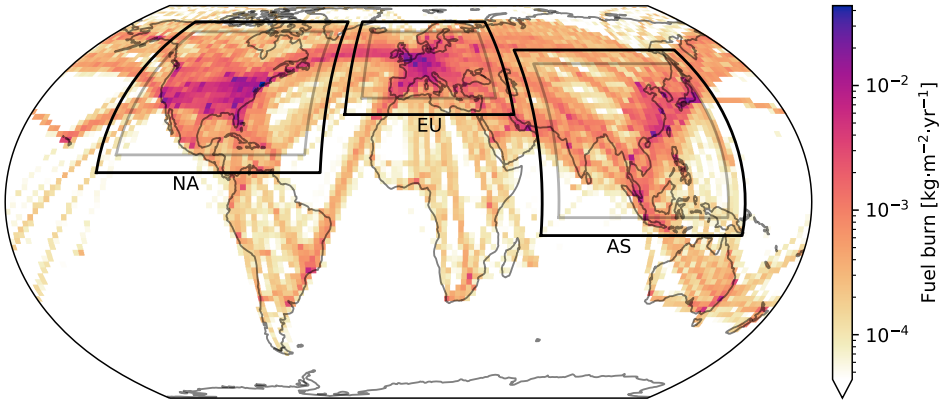

Figure 5.1: Baseline aviation fuel burn in 2005 summed over altitude, downscaled to 2° × 2.5° for visibility and the three nested domain regions. The frame area around each region is where perturbations are gradually reduced outwards to the edge of the domain.

used by default in GEOS-Chem, based on Barrett et al. [30].

The global sum of aviation fuel burn for the full year is 180 Tg, 16.4 Tg of which during LTO (9.1%). The inventory is built at the spatial resolutions of the simulation grids (Section 5.2.2) and with a monthly temporal resolution. Emissions are lower during winter, with individual months having a global average fuel burn between −4.5% (January) and +5.6% (July) the yearly average (Appendix B.1.1). Emission indices for each emitted species and a breakdown between domestic and international flight emissions are listed in Appendices B.1.2 and B.1.3. Considering flights between European Union countries as "domestic", international flights are responsible for 57% fuel burn mass.

Four different aviation scenarios are evaluated: the baseline case using the estimated 2005 aviation emissions, and three cases where all aviation emissions released within one of three regions are positively perturbed (multiplied by a constant). The regions, shown in Figure 5.1, represent Asia, Europe, and North America — denoted as AS, EU[1], and NA. The perturbations are tapered off towards the edges of the regions for a smooth transition to the unperturbed areas. A 1.1 multiplier is chosen for Europe as a compromise between having a strong enough model response above noise levels and having a low enough perturbation that corresponds to marginal increases representative of a few years worth of growth in emissions (3.6 years at 2.7% annual growth in the case of Europe). Different multipliers are applied for each region such that the increase of full-flight fuel burn mass per area is the same in all three cases, after accounting for differences in total areas and baseline aviation emissions between the regions (Table 5.1). Within each case, the same multiplier is applied to all emission species, at all altitude levels and constantly through time.

In order to observe the different effects of LTO and non-LTO emissions, a further three simulations are performed, where only the LTO emissions in each region are increased, using the same multipliers as before. These scenarios are simulated only on the perturbed

[1]In this chapter, EU refers to the geographical region shown in Figure 5.1, not to the European Union

Table 5.1: Annual global fuel burn and emissions from civil aviation estimated from different sources of flight movement data.

Region	Area [% of world]	Yearly fuel burn [% of world]	Perturbation multiplier
World	$5.11 \cdot 10^{14}$ m^2	180 Tg	n/a
AS	10.65%	21.6%	1.267
EU	3.81%	20.6%	1.100
NA	8.96%	34.3%	1.141

region instead of using the nested grid approach, since the inter-regional effects of LTO emissions are expected to be small [12].

5.2.2 Atmospheric modeling

The atmosphere is modeled using the GEOS-Chem model version 12.6.1 [314] with the Unified Tropospheric-Stratospheric Chemistry Extension (UCX) module [315], and meteorological data from the MERRA-2 reanalysis product from NASA/GMAO. The default aerosol simulation and $PM_{2.5}$ parametrization is used (Appendix B.2.3), including the secondary organic aerosols (SOA) simple parametrization model from Kim et al. [316]. The main emissions inventories used are the CEDS anthropogenic emissions as the global default [317], the U.S. Enrionmental Protection Agency's NEI2005, the APEI [318], the DICE-Africa [319], the MIX-Asia [320], and parts of EDGAR v4.3 [321]. Other emission modules used are listed in Appendix B.2.1.

Previous studies have indicated that higher resolutions are better able to capture local and regional scale aviation air quality effects [1, 322, 323]. Therefore, in order to capture both intercontinental transport of pollution and regional scale effects while conforming to a computational budget, the nested simulation approach is adopted. For each scenario analyzed, four model runs are performed: a global run at 4° × 5° resolution (latitude × longitude) and, using boundary conditions from the global run, three nested regional grids at 0.5° × 0.625° resolution, coinciding with the emissions perturbations Figure 5.1. Global impacts are calculated using the results of the nested simulations where available (the three regions of interest) and the results of the coarse global simulations elsewhere. The coarser global resolution is comparable to values used in global chemical transport models to study long range air pollution [33, 197], and is typical for the GEOS-Chem model, which is benchmarked with every update by running simulations at it. The finer nested regional resolution is the native resolution of the MERRA-2 meteorological fields. In all cases, GEOS-Chem is run with 72 vertical layers, using a terrain following hybrid sigma-pressure level definition with the top of the atmosphere being 0.01 hPa, and with timesteps of 10 minutes for transport and 20 minutes for chemistry and emissions. The effects of the grid resolution are discussed further in Appendix B.2.5.

The initial state for all runs is obtained by a 21 month spin-up of the global coarse resolution model. Then each individual run (global and regional) has 3 months of spin-up followed by 12 months. The latter is considered in the analysis. In total, 4 global simula-

tions and 5 nested simulations in each region are performed. The simulation period considered represents the year 2005 for meteorology, aviation and non-aviation emissions. An overview of the resulting background ground-level $PM_{2.5}$ concentrations and ozone mixing ratios in the simulations, as well as a comparison with air quality monitoring records, are presented in Appendix B.3.1. To evaluate the effect of background atmospheric composition on air quality sensitivity to aviation, an additional set of coarse global simulations is also performed using the 2005 aviation emissions inventory with meteorology and other emissions representing 2013.

The concept of "gas ratio" defined by Ansari and Pandis as the ratio between free ammonia and total nitrates, according to Equation (2.14), is used in the analysis of model outputs to identify atmospheric conditions favorable to $PM_{2.5}$ formation [188]. Gas ratios less than 1 indicate that competition between sulfates and nitrates for limited ammonia restrict $PM_{2.5}$ formation as NO_x is increased. Another metric used in the analysis is ground-level formaldehyde to reactive nitrogen (NO_y) ratio (FNR, alternatively defined as the ratio to NO_x or NO_2). This metric uses formaldehyde as a proxy for volatile organic compounds (VOC) to identify regions where ozone production is limited by VOC and where it is limited by NO_x [324]. Lower values of FNR are expected where ozone formation is NO_x saturated, and increases in NO_x might result in a net decrease of ozone concentration, due to competing chemical reactions.

The linearity of the model's response to the perturbation was evaluated by performing additional simulations with EU emissions multiplied by 1.3 instead of 1.1. This larger perturbation resulted in $PM_{2.5}$ and ozone sensitivities to emissions that were 0.3% and 1.1% lower, respectively, than those obtained with the smaller perturbation (Appendix B.2.4).

5.2.3 Health impact assessment

Health impacts are quantified as the increase in premature mortality in people over 30 years of age due to additional exposure to $PM_{2.5}$ and ozone. Population exposure to increases in ground-level concentration of pollutants is calculated by applying the LandScan 2005 global population distribution data, which sums to 6.44 billion people [325]. Area-averaged concentration increases are calculated considering either all grid cells or only those with a greater than zero population, which represents predominantly the changes over land (Appendix B.2.2). Country-specific age distribution (fraction of population over 30 years old) and baseline mortality rates for the relevant disease classes are taken from the 2005 estimates of causes of death from the Global Health Estimates 2015 (GHE) [326].

$PM_{2.5}$ health impacts are estimated as the increased mortality from noncommunicable diseases (GHE code 600) and lower respiratory infections (GHE code 390) according to the concentration-response function (CRF) defined by Burnett et al. [114]. This CRF is chosen as it was derived from an ensemble of studies covering a wide range of population characteristics and concentration levels. This model, called GEMM, is used to obtain mortality hazard ratios from the yearly average $PM_{2.5}$ concentrations output by the simulations, and the hazard ratios are then applied to the baseline incidence rate of cause-specific mortality to give a total number of excess deaths from concentrations above a counterfactual value. The excess premature mortality attributable to additional aviation emissions is taken as the difference to the baseline emissions scenario. Alternative estimations performed using different CRFs and different mortality endpoints are given in Appendix B.4. Consistent

with other aviation air quality studies [1, 211], different toxicities for specific $PM_{2.5}$ constituents are not considered, nor the effect of particle number.

Ozone health impacts are estimated as the increased mortality from all respiratory diseases (GHE codes 390, 400, and 1170) according to the CRF established by Turner et al. [104], which represents a 1.12 hazard ratio for a 10 ppbv increase in the yearly maximum daily 8-hour average (MDA8) ozone mixing ratio. This CRF is the result of an analysis of long-term ozone effects in a large cohort study in the United States, involving over 12.6 million person-years of follow-up. Alternative estimations with different CRFs and mortality endpoints are given in Appendix B.4.

5.2.4 Uncertainty estimation

Uncertainty is quantified using independent variables associated with atmospheric modelling in terms of $PM_{2.5}$ concentration and ozone mixing ratio changes and with the CRFs used. A multiplicative triangular error distribution T(0.36, 1, 2) is applied to $PM_{2.5}$ and T(0.5, 1, 1.5) to ozone changes, following the same methodology applied to GEOS-Chem results by Grobler et al. [211], based on an inter-model comparison study [33]. For the $PM_{2.5}$ CRF, a normal distribution in the theta parameter of the GEMM model is considered, as reported by Burnett et al. [114]. For the ozone CRF, a triangular distribution for the hazard ratio is adopted, defined by the central value and the 95% confidence intervals reported by Turner et al. [104]. The uncertainties are combined using a Monte Carlo approach with 10^5 samples, with 2.5th and 97.5th percentiles reported along with the results from nominal input values. Other sources of error, such as in the baseline disease incidence rates and population distribution are not considered.

5.3 Results and discussion

The effects of full-flight and LTO-only emissions perturbations on air quality are presented in Sections 5.3.1 and 5.3.2, respectively. Estimates of the resulting health impacts associated with the air quality degradation are presented in Section 5.3.3. How these sensitivities differ between two years is presented in Section 5.3.4 and the limitations of this analysis are discussed in Section 5.3.5.

5.3.1 Full-flight air quality impacts

The global average baseline $PM_{2.5}$ concentrations and ozone mixing ratios through 2005 are shown in Figure 5.2 considering only populated areas, which excludes most of the oceans. The seasonal patterns follow the Northern hemisphere, where 71% of the area considered is and where average concentrations are higher. $PM_{2.5}$ background levels are higher during the northern winter, driven by longer atmospheric lifetimes of nitrate precursors, while ozone levels are higher during summer when solar activity is highest.

Figure 5.2 also shows the marginal increase in global concentrations for each (full-flight) perturbation scenario, normalized by additional fuel burn mass. The largest increases happen during boreal winter. The aviation-induced increase in $PM_{2.5}$ is composed mainly by ammonium and nitrate (Appendix B.3.5). The sensitivity of concentrations to aviation emissions over Europe is consistently higher than those to emissions over the other regions throughout the year. The timing difference in aviation-attributable surface

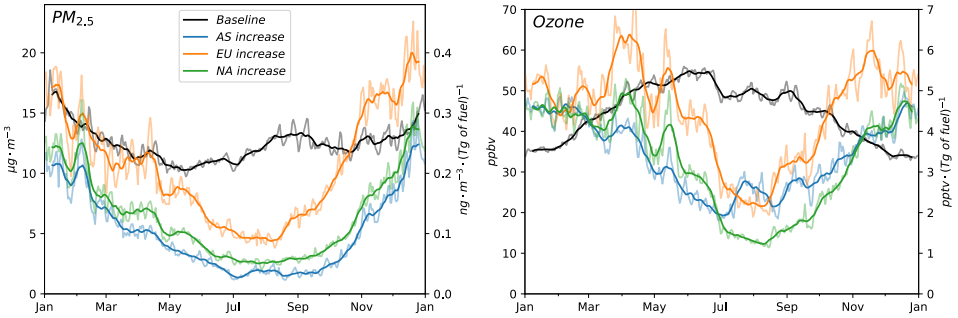

Figure 5.2: Daily and 14-day moving averages of global ground-level $PM_{2.5}$ concentration and ozone (MDA8) mixing ratio in populated areas for the baseline simulation and the global increases per additional mass of fuel burned due to increased full-flight emissions in each specific region.

ozone with background levels can be attributed to longer lifetimes in the mid-troposphere during winter while the surface background mixing ratios are governed by the steady-state photochemical seasonal cycles [32].

On average, the sensitivity of global ground-level $PM_{2.5}$ in populated areas to the EU perturbation is 107% and 64% greater than the sensitivities to the AS and NA perturbations, respectively (Figure 5.3). When changes over unpopulated areas are included, the sensitivity to the perturbation in EU is 33% and 40% greater than those in AS and NA, respectively. The population-weighted averages are 4.4 (AS), 3.3 (EU) and 3.3 (NA) times the non-weighted averages over populated areas. These results reflect both the proximity of aviation emissions near densely populated regions and the air quality sensitivity in these areas. When accounting for differences in the population spatial distribution by using the population-weighted metric, the sensitivity of global $PM_{2.5}$ to aviation emissions over AS is similar to that of emissions over NA (+5%), while the sensitivity to emissions over EU is higher (+57% than AS, +65% than NA). The fact that the air quality sensitivity to aviation emissions over EU is higher than to emissions elsewhere before population density data or CRFs are applied means that atmospheric conditions for emissions in that region are more favorable to $PM_{2.5}$ formation.

Westerly prevailing winds transport cruise emissions from EU to AS, while cruise emissions over AS and NA get advected first to the Pacific and Atlantic oceans respectively. Additionally, this higher impact of emissions in Europe is associated with higher availability of ammonia to react with NO_x, particularly during winter, compared to the United States coasts, East China and Japan (Appendix B.3.3). A lower percentage of population in NA (39%) is over areas where the average gas ratio over January is above 1.3, than in AS (82%) and EU (62%). The southeast of AS, where gas ratio is largely above 1.3 in both winter and summer, lies at lower latitudes than the majority of cruise emissions in the Northern Hemisphere. The mean atmospheric circulation patterns have been found to be associated with higher global impacts of aviation emissions above the northern tropic [12, 30]. Although these factors are identified as leading to differences in sensitivity, the results do not decouple which mechanism contributes the most.

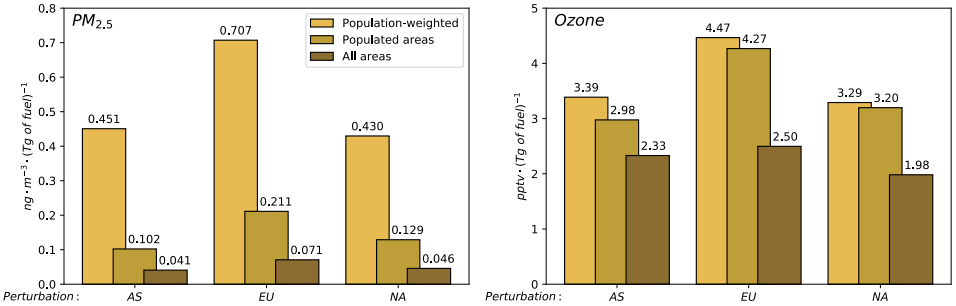

Figure 5.3: Global increase in ground-level $PM_{2.5}$ concentration and (MDA8) ozone mixing ratio per additional mass of (full-flight) fuel burned in a specific region.

Compared to existing literature, the $PM_{2.5}$ sensitivities to regional aviation emissions perturbations reported here are higher than the sensitivity to global aviation emissions estimated by values presented in Eastham and Barrett (0.282 population-weighted $\mu g \cdot m^{-3} \cdot (Tg\,fuel)^{-1}$ [32] and Yim et al. (0.033 area-weighted $\mu g \cdot m^{-3} \cdot (Tg\,fuel)^{-1}$ [1]. Differences in the models used, grid resolution, $PM_{2.5}$ parametrization, emission inventories, and the nonlinearity of the response to perturbation can all contribute to the observed differences.

Impacts on ground-level ozone are more spatially diffuse, with the population-weighted averages being 1.13 (AS), 1.05 (EU) and 1.03 (NA) times the averages over populated areas (Figure 5.3). Aviation emissions in Europe also lead to higher population-weighted ozone impacts (+32% than AS, +36% than NA). All cases have higher population-weighted increases than the 2.87 $pptv \cdot (Tg\,fuel)^{-1}$ estimated for global full-flight emissions by Eastham and Barrett [32], although they considered the maximum daily 1-h average over the ozone season, when aviation contribution is smaller.

While there is stronger association between impacts and the perturbation in the same region, there are still significant cross-regional effects, as shown in Figure 5.4. An increase in emissions over Europe impacts Asia more (+32% for $PM_{2.5}$ and +16% for ozone) than a local increase of the same amount. In terms of total population exposure, Asia receives most of the impacts in all cases. Additionally, most exposure from North American emissions happen outside the region (92% for $PM_{2.5}$ and 88% for ozone).

These significant cross-regional impacts pose regulatory challenges when accounting for aviation's environmental impact on a regional scale. For example, the projected long-term growth in air traffic is spatially heterogeneous, estimated at ~3% annually for EU and NA and ~6% annually for AS [327]. Considering the 2005 fuel burn over the EU and AS regions (Table 1) and the different air quality sensitivities over fuel burn increases (Figure 5.3), a twice as large rate of increase in emissions over AS compared to EU would result in proportionately lower impacts (34% and 59% higher increases in $PM_{2.5}$ and ozone global exposure, respectively). In the same scenario, the resulting AS population exposure attributable to emissions over EU would be 64% ($PM_{2.5}$) and 55% (ozone) of those due to the more rapidly increasing emissions over AS.

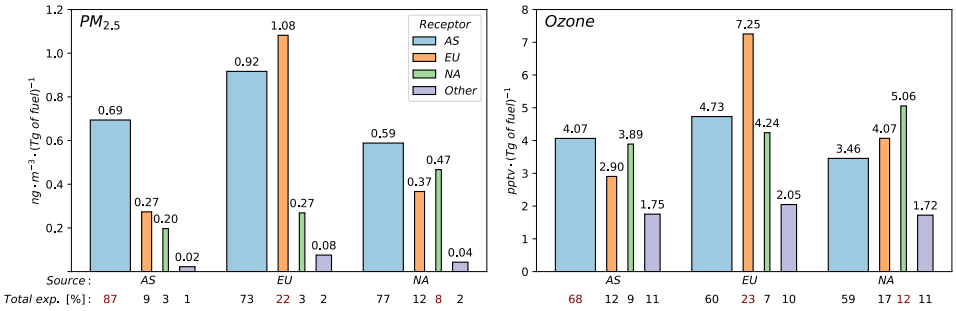

Figure 5.4: Populated-weighted average increase in yearly $PM_{2.5}$ concentration and ozone MDA8 mixing ratio at each (receptor) region for increased full-flight emissions in each (source) region. The widths of the bars are scaled to population count, such that the area represents total population exposure. For each scenario, the percentage of total population exposure in each area is indicated below, with self-regional values in red.

5.3.2 LTO air quality impacts

Air quality impacts observed in simulations in which only LTO emissions over a region were increased are compared to those in simulations with full-flight perturbations over the same region, in order to differentiate between the LTO and non-LTO contributions to full-flight impacts. For all three regions, the LTO contribution to full-flight population-weighted $PM_{2.5}$ increases varies from 10–20% during winter to 40–50% during summer (Figure 5.5a). This is in line with the shorter mid-tropospheric lifetime of nitrate precursors during summer which may reduce the impacts of cruise emissions. Over the full year, LTO-only perturbations result in 17% (AS), 26% (EU) and 29% (NA) of the population-weighted $PM_{2.5}$ within the same region attributed to full-flight emissions over that region. This is higher than the LTO 9–11% share of fuel burn, demonstrated by the higher impacts per fuel burn in Figure 5.5b.

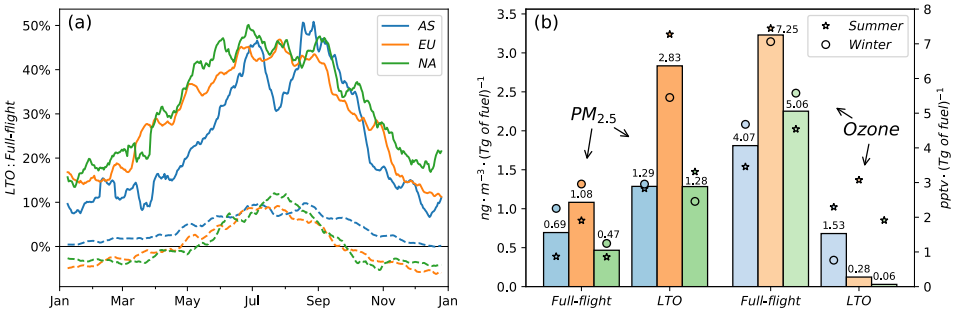

Figure 5.5: Population-weighted regional $PM_{2.5}$ and ozone increases with LTO and full-flight perturbations in the same region. (a) ratio between LTO and full-flight (14-day averages). (b) yearly averages per additional mass of fuel burn for each case, with summer (April through September) and winter (rest of the year) averages indicated with marks.

Sensitivity of $PM_{2.5}$ to LTO emissions in EU is higher compared to other regions (Figure 5.5b), which is consistent with higher ammonia availability. The percentage of LTO

NO_x released over areas with a monthly average GR > 1.3 for each region is 57% (AS), 74% (EU), 14% (NA) during January, and 68% (AS), 76% (EU), 21% (NA) during July (Appendix B.3.3).

LTO emissions cause close to zero net increase in ground-level ozone over the year: 3.5% (AS), 0.4% (EU) and 0.1% (NA) of the impacts on the same region from full-flight emissions over the region. Airports are often situated in areas with high NO_x ground-level concentrations, where ozone production becomes limited by VOC and additional NO_x emissions can cause a decrease in ozone. Decreases in ozone are associated with the formaldehyde to NO_y ratio, particularly during winter when most of the decreases are observed (Appendix B.3.4).

Operational strategies such as pushback control and de-rated takeoffs are a possible way of reducing LTO emissions [279]. The seasonal sensitivity trends reported here make the use of such strategies have a stronger air quality effect during summer at regional levels (Figure 5.5b). Similarly, alternative technological mitigation options targeting short-haul flights (which have higher percentage of LTO emissions/impact), such as electric or hybrid flying, would also have stronger effects during the summer, and in addition would result in approximately twice the air quality improvement (in terms of $PM_{2.5}$ concentration from LTO emissions) if they were to be introduced in EU compared to AS and NA.

5

5.3.3 Health impacts

Figure 5.6 presents the sensitivity of regional human health impacts to full-flight emissions per region of perturbation. Most of the increase in premature mortalities from additional aviation emissions from any of the three regions happens in Asia, both due to ozone and $PM_{2.5}$. The fact that Asia receives the largest share of health impacts despite not necessarily being the most affected region in terms of air quality from aviation emissions over other regions (Figure 5.4) is due to a larger population count, which leads to more total population exposure.

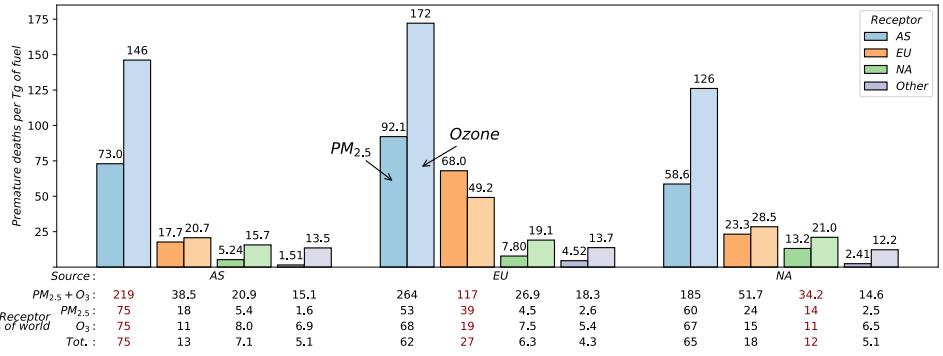

Figure 5.6: Premature mortality from aviation-attributable $PM_{2.5}$ and ozone at each (receptor) region for increased full-flight emissions in each (source) region.

The application of country-specific baseline disease mortality rates decreases the share of $PM_{2.5}$ impacts in Asia: in the case of perturbation in AS, for example, AS receives 87% of added global exposure (Figure 5.4) but has 75% of global excess deaths (Figure 5.6). For

ozone impacts the opposite occurs, with AS having 68%, 60%, and 59% of global exposure and 75%, 68%, and 67% of deaths resulting from perturbations over AS, EU, and NA, respectively. Country-specific baseline disease mortalities have a net effect from both $PM_{2.5}$ and ozone of higher global health impacts in all three full-flight perturbation cases. Estimates using different baseline disease mortality rates and different CRFs are given in Appendix B.4.

The sensitivity of total global health impacts to aviation emissions over EU is 45% and 50% higher than the sensitivity to emissions over AS and NA, respectively (Table 5.2). Extrapolating for the total 2005 aviation emissions – estimating the global sensitivity to emissions from other regions (23% of total) from an additional global coarse resolution simulation (Appendix B.5) – gives a total of 20 300 (95% CI: 9 800–40 300) premature deaths due to $PM_{2.5}$ and 38 300 (21 600–57 800) due to ozone. Both these numbers are highly sensitive to the choice of CRF used, however the ratio of impacts from different source regions is mostly independent from the CRF chosen (Appendix B.4).

Table 5.2: Aviation-attributable premature mortality by region of emission per mass of fuel burned [deaths·(Tg fuel)$^{-1}$] (95% confidence interval), the fraction of mortality by each pollutant and the fraction of mortality in the same region of perturbation.

Perturbation region	Mortality increase	$PM_{2.5}$:ozone impacts	Inside:outside
AS	294 (195–433)	33:67	75:25
EU	427 (284–641)	40:60	27:73
NA	285 (190–422)	34:66	12:88

For comparison, the number of yearly aviation-attributable premature deaths just from $PM_{2.5}$ was estimated by Yim et al. [1] as 13 900, considering the CRF of cardiopulmonary diseases and lung cancer from Ostro [328]. Eastham and Barrett estimated a 9 200 increase in cardiovascular mortality due to $PM_{2.5}$ [32] using a CRF from Hoek et al. [329]. Applying the same CRFs to this study results in 9 500 (Ostro) and 13 800 (Hoek et al.) premature deaths from $PM_{2.5}$.

Using a more conservative CRF for ozone [330] yields 12 800 premature deaths, and further restricting the mortality endpoints to just chronic obstructive pulmonary disease and asthma (excluding respiratory infections) would lead to 8 400 deaths, compared to the 6 800 deaths estimated by Eastham and Barrett [32] using this CRF.

Total ($PM_{2.5}$ and ozone) premature deaths from the LTO-only perturbations are 10.8% (AS), 16.7% (EU), 14.5% (NA) of mortality within the same region caused by local full-flight perturbation. For each region, the local deaths from LTO emissions are 7.8% (AS), 5.1% (EU), and 1.7% (NA) of the global mortality attributed to full-flight emissions over the region. The low contribution of LTO to health impacts results from the large portion of overall impacts caused by ozone and the near zero ozone increase in the LTO-only scenarios, which might not happen to the same extent for the 23% remaining emissions outside the three regions focused on here.

5.3.4 Effects of changing non-aviation emissions

The regional sensitivities presented in the previous sections are calculated for 2005, including a 2005 "baseline" atmosphere in terms of other (non-aviation) athropogenic and biogenic emissions, as well as meteorology. Background (non-aviation) emissions, a key component to different air quality sensitivities, as observed in this study and elsewhere [313], are also changing over the years [331, 332]. To quantify the effect of the background emissions and meteorology have on the sensitivity to aviation emissions, the coarse regional sensitivities are also calculated using non-aviation emissions and meteorology fields representative of the year 2013.

The sensitivities of global population $PM_{2.5}$ exposure to full-flight emissions are higher in the 2013 scenarios for perturbations in aviation emissions over AS (+8.2%), EU (+6.6%), and NA (+12.3%). The sensitivity of global $PM_{2.5}$ to aviation emissions over EU is still 57–60% higher than to aviation emissions in the other regions. While intra-regional $PM_{2.5}$ sensitivities changed by ~10%, the cross-regional sensitivity changes ranged from −29% to +16%. The sensitivities of global population ozone exposure to full-flight emissions change less: +1.5%, −1.4%, and +1.4% for perturbations over AS, EU, and NA, respectively.

Overall, increases of both $PM_{2.5}$ and ozone sensitivities are larger for intra-regional source-receptor pairs, suggesting that the relative importance of LTO emissions increases. This is consistent with the higher GR and FNR observed, however differences in meteorology may also be driving these sensitivity changes, and these are not directly decoupled here. An LTO-only perturbation simulated for the EU domain results in higher air quality impacts for the same amount of added emissions compared to the 2005 scenario (25% more perturbation-induced $PM_{2.5}$ exposure and 6.4% more ozone exposure). The ratio of population $PM_{2.5}$ exposure associated with LTO and full-flight emissions over EU is 8.8% for 2013 versus 7.5% for 2005.

These results underscore the importance of considering aviation emissions in the context of those from other sectors when estimating aviation's future air quality impacts, as well as the effects of aviation-related mitigation measures in the future, particularly for $PM_{2.5}$ impacts.

5.3.5 Limitations

While the most recent global aviation emissions inventory available for this study was of the year 2005, air traffic has approximately doubled since then [224], and the world population has increased by over 15%. While this may not necessarily affect the sensitivity values presented here, it is possible that second order air quality sensitivities to aviation emissions become significant for emission increases beyond the ranges evaluated here Appendix B.2.4. In addition to the effects of changing non-aviation emissions on the sensitivities presented in Section 5.3.4, air quality impacts from aviation could also be magnified by climate change effects on the atmosphere [230]. The effects of long-term evolutions in atmospheric composition and meteorology to air quality sensitivity to aviation were not investigated in this study.

Water and aerosol from aviation emissions influence cloud formation and radiative properties, with these effects being a significant part of aviation's climate impacts [3]. Aerosol interaction with clouds affect aerosol microphysical evolution (condensation, agglomeration, reactivity, photolysis rates, etc.) and wet deposition. Since the simulations

performed use prescribed meteorology with these interactions being simulated in a parameterized manner, this secondary effect of changes in clouds affecting particulate matter back is not captured. This can be considered an acceptable compromise given that the analysis concerns the impacts of marginal changes of aviation emissions. In addition, the near-surface aerosol impacts of aviation induced cloudiness could also be considered in future research.

Toxicity of $PM_{2.5}$ constituents was considered to be uniform, i.e. not being specific to their individual chemical composition or particle morphology. There is, however, growing evidence that particulate matter toxicity to humans is dependant on factors besides total $PM_{2.5}$ mass which are not accounted for here [61, 62]. Considering uniform $PM_{2.5}$ toxicity could underestimate the relative importance of LTO emissions, which have higher (ultrafine) black carbon components.

5.4 Conclusion

In this chapter, by using multiple simulations of a global and regional atmospheric CTM, the air quality and human health impacts of aviation emissions from different regions are isolated. Significant intercontinental effects are found, with 73% and 88% of premature mortality caused by aviation emissions over Europe and North America, respectively, occurring outside those regions. The largest receptor of health impacts from aviation emissions over any of the three regions is Asia, due principally a larger population. While total health impacts are driven largely by population densities, the air quality impacts of emissions are also driven by atmospheric conditions. Higher $PM_{2.5}$ sensitivities are associated with ammonia availability (GR) and ozone sensitivity to LTO emissions is associated with the formaldehyde to NO_y ratio. The same amount of emissions leads to higher $PM_{2.5}$ and ozone increases, and ultimately cause an average of 45–50% more health impacts if it is emitted over Europe instead of North America or Asia.

The cross-boundary nature of air quality impacts from aviation means that regional full-flight regulations alone in Europe and North America will yield the majority of corresponding air quality benefits outside those regions, while the opposite holds for Asia. The results obtained highlight the need to take non-LTO emissions into account when evaluating air quality, as they are associated with 83–89% of health impacts considering the same region as source-receptor, and 92.2–98.3% of global health impacts caused by emissions in each region.

The regional differences in the human health impact sensitivities to aviation emissions observed here underscore the importance of considering aviation emissions in the context of those from other sectors, particularly since background atmospheric composition remains a driver of aviation's regional impacts, when population distribution is decoupled. Overall, the findings that the same amount of aviation emissions can have impacts of significantly different magnitudes depending on the emission location suggest that this nonuniformity could be taken into account in policies aiming to minimize total health impacts from aviation more efficiently, considering the projected globally heterogeneous growth of aviation emissions. Finally, the results indicate that when optimizing aircraft design, operations and/or regulatory decisions for minimizing aviation's environmental footprint (air quality, climate, noise), full-flight (LTO and non-LTO) emissions need to be taken into account, as well as their regional distribution.

5.5 Data availability

The data that support the findings of this study (atmospheric model output used in the calculations and the baseline mortality rates considered) are openly available at the following DOI: 10.4121/uuid:842594f5-6ebc-4150-afbd-7fcaa407aadb.

5.6 Acknowledgments

This work made use of the Dutch national e-infrastructure with the support of the SURF Cooperative using grant no. EINF-396. The MERRA-2 data used in this study have been provided by the Global Modeling and Assimilation Office (GMAO) at NASA Goddard Space Flight Center. Grid cell country definitions were based on geocoding data from OpenStreetMap accessed via the Nominatim search tool.

6

Present and future air quality impacts from aircraft emissions

Por esse pão pra comer, por esse chão pra dormir
A certidão pra nascer, a concessão pra sorrir
Por me deixar respirar, por me deixar existir
Deus lhe pague
Pela cachaça de graça que a gente tem que engolir
Pela fumaça, desgraça, que a gente tem que tossir
Pelos andaimes, pingentes, que a gente tem que cair
Deus lhe pague
Pela mulher carpideira pra nos louvar e cuspir
E pelas moscas-bicheiras a nos beijar e cobrir
E pela paz derradeira que enfim vai nos redimir
Deus lhe pague

For this bread to eat, for this floor to sleep on
The certificate to be born, the concession to smile
For letting me breathe, for letting me exist
May God pay you back
For the free booze that we have to swallow
For the smoke, disgrace, that we have to cough
For the scaffolding, swinging, that we have to fall from
May God pay you back
For the mourner woman to praise us and spit upon us
And for the flies kissing and covering us
And for the final peace that will at last redeem us
May God pay you back

Construção (Construction), by Chico Buarque

Chapter 3 described the development of an up-to-date global inventory of aircraft emissions for the years 2017–2020, discussing how emissions increased from 2005. In Chapter 4, that inventory was projected forward to estimate how aircraft emissions might further increase up to the year 2050. Lastly, Chapter 5 explored how aircraft emissions released in different regions can impact air quality and human health. In this chapter, those previously produced

This chapter is based on a manuscript that is being prepared for a scientific journal. Please cite as shown in the list of peer-reviewed journal articles, item 6.

inventories are used in atmospheric simulations to quantify the global air quality and human health impacts due to aircraft emissions in 2019, and for multiple scenarios for the year 2040. It is estimated that a total of 33 900, 79 500, and 2700 deaths in 2019 are attributable to $PM_{2.5}$, ozone, and NO_2 increases caused by aircraft emissions. In the baseline 2040 scenario, the health impact from all three pollutants increases by 28%, 76%, and 135% relative to 2019 for low, baseline, and high scenarios of future aircraft emissions. Comparison of simulations with different scenarios of non-aviation emissions, aircraft emissions, and meteorology fields give further insight into how aviation's air quality impacts might change over the next decades.

6.1 Introduction

Aircraft emissions contribute to multiple environmental problems including climate change [5], excessive nitrogen deposition (Chapter 7), and air quality (as already discussed in Chapter 5). Degradation of air quality attributed to aircraft, in the form of higher ground-level concentrations of fine particulate matter ($PM_{2.5}$) and ozone, has been estimated to lead from hundreds to tens of thousands of additional human deaths annually [1, 30, 32, 158, 212]. The fast pace of aviation's growth, resulting in 3–4% average yearly increases in global jet fuel use over the past two decades (Chapters 3 and 4), poses a significant challenge to its environmental sustainability. Currently, pledges of carbon neutrality, generally aiming for the year 2050 as the target, take a prominent position in the sector's outlook for the upcoming decades, with the intent of addressing some of the climate forcing attributed to aviation [49–54]. In these plans, carbon neutral flights are to be achieved largely by the use of sustainable aviation fuels [144], which do not substantially change with regard to NO_x emissions [306], that are thus expected to continue to increase taking into account both traffic growth and technology improvements (Chapter 4). As aircraft impact air quality mainly through their NO_x emissions (Section 2.5 and Chapter 5), these impacts will increase significantly over time if their sensitivity to emissions remain similar or increase. Given that aviation is a particularly difficult sector to reduce emissions during the 21st century [143, 333], its environmental impacts, such as air quality degradation, might also increase in relative importance compared to other human activities.

Aircraft emissions are released mostly in the upper troposphere and lower stratosphere, impacting air quality at up to intercontinental distances, largely through secondary pollutants formed by photochemistry reactions and transport to the surface (Chapter 5). Because of this, the sensitivity of air quality and human health impacts to aircraft emissions are spatially nonuniform, and vary with background concentrations that depend on emissions from other sectors, in addition to being dependent on meteorological conditions. This makes assessing these impacts particularly challenging considering the spatial nonuniformity in temporal changes of air traffic (Chapter 3), population distribution [334, 335], anthropogenic emissions [336], and climate [337].

Previous studies have quantified the air quality impacts of aircraft emissions within local [338, 339], regional [212, 340–342], and global scopes [1, 30, 32, 33, 158, 323, 343–345]. The magnitude of results has showed significant variation across different atmospheric models, including both those with online and offline meteorology, and with different methods of modeling chemistry, aerosol microphysics, among other parameters [33]. Some of these studies also quantify the human health impacts associated with this degradation of air quality, with results also varying according to what is considered with regard to pol-

lutants (most commonly $PM_{2.5}$, and often ozone), mortality endpoints and concentration-response functions (CRF). Yim et al. found that aircraft emissions in 2005 led to 16 000 (90% CI: 8 300–24 000) additional deaths globally due to $PM_{2.5}$ and ozone, with the latter pollutant accounting for 2100 (90% CI: 1 000–3 300) of the total [1]. For the same year, the study described in Chapter 5, using different atmospheric modeling and CRFs, found 20 300 (95% CI: 9 800–40 300) premature deaths due to $PM_{2.5}$ and 38 300 (95% CI: 21 600–57 800) due to ozone. Analyzing the year of 2006, Eastham and Barrett found aviation-attributable premature mortality of 9 200 (95% CI: 5 200–13 000) for $PM_{2.5}$, and 6 800 (95% CI: 3 000–10 000) for ozone, as well as 400 (95% CI: 190–610) mortalities prevented due to reduced UV-B exposure from higher ozone column concentrations [32].

Comparing aviation's impacts on air quality between 2006 and 2050, one study found that non-LTO impacts increase over the northern hemisphere by ~150% ($PM_{2.5}$) and ~50% (ozone) [346], and another found that annual global mortality associated with $PM_{2.5}$ increases from 405 (95% CI: 182–648) to 2287 (1114–2889) [345]. Presently, there are some efforts to evaluate future atmospheric impacts of aviation with a focus on climate [34, 347], but those largely disregard the associated air quality impacts, which have been shown to result in the majority of marginal societal damages related to aircraft emissions [211].

In this chapter, the GEOS-Chem chemical transport model is used to quantify the past (year 2005), present (2019) and future (2040) global air quality impacts of aviation. Future impacts are evaluated by combining forecasts of aircraft emissions under different market and technology development scenarios with atmospheric simulations using non-aviation emissions consistent with seven different Shared Socioeconomic Pathways (SSP) [348]. Impacts in 2040 are also evaluated using meteorological inputs from a global climate model under different SSPs.

6.2 Methods

The GEOS-Chem model version 13.3.3 is used to quantify the impacts of aircraft emissions in the atmosphere at a global scale. Simulations are performed with and without aircraft emissions, and the difference in air quality across the simulation runs is taken as aviation's contribution to ground-level air pollution. The scope of this study includes only emissions from fixed-wing civil aircraft, so the terms "aviation" and "aircraft" are used interchangeably to refer to them. In some scenarios, aircraft emissions from landing and takeoff operations (LTO), defined as those up to 3000 ft above ground, are evaluated separately to isolate their contribution to impacts from full-flight emissions (LTO plus non-LTO). Human health impacts are quantified as the expected increase in mortality associated with long-term exposure due to changes in the surface level concentrations of $PM_{2.5}$, ozone, and NO_2.

Three sets of multiple scenarios are considered, with different aviation emissions, non-aviation emissions, and meteorological fields. Firstly, "present day" impacts on air quality and human health from aircraft emissions are investigated by performing simulations of the year 2019, as the last representative year of aviation activity before the COVID-19 pandemic (Section 6.3.1). Secondly, the effects of the evolution of both aviation and non-aviation emissions are evaluated by comparing results from simulations for the years 2005, 2019, and 2040 (Section 6.3.2). And thirdly, simulations using different meteorological fields for the year 2040 are compared in order to evaluate the sensitivity of aviation's

impacts on air quality to a range of atmospheric conditions representative of possible future SSP scenarios (Section 6.3.3). Table 6.1 summarizes the experiments performed.

Table 6.1: List of scenarios simulated. The three 2019 scenarios marked with an asterisk (*) are also simulated at higher resolution using nested domains.

Meteorology	Non-aviation emissions	Aviation emissions
2005	2005	2005, off
2019	2019	2019*, 2019 NO_x-only, 2019 LTO-only*, 2005, off*
2019	2040 SSP1-1.9, SSP2-4.5, SSP3-7.0, SSP4-3.4, SSP4-6.0, SSP5-8.5	2040 baseline, off
2019	2040 SSP2-4.5	2040 high, 2040 low, 2040 baseline NO_x-only
2019	2040 SSP1-1.9, SSP2-4.5, SSP3-7.0	2040 baseline LTO-only
2040 SSP1-2.6, SSP2-4.5, SSP5-8.5	2040 matching meteorology SSP	2040 baseline, off
2040 SSP2-4.5	2040 SSP1-2.6, SSP5-8.5	2040 baseline, off
2040 SSP1-2.6, SSP5-8.5	2040 SSP2-4.5	2040 baseline, off

6.2.1 Aircraft emissions

Civil aircraft emissions for all simulated years are modeled as three-dimensional fields of monthly-averaged emission rates of NO_x (as NO_2), CO, hydrocarbons (HC, speciated according to the U.S. EPA's profile #5565 [349]), SO_x (based on a constant 600 ppm fuel sulfur content), nonvolatile particulate matter mass ($nvPM_m$, as hydrophilic black carbon aerosol). Emission rates for 2019 are calculated from the bottom-up inventory described in Chapter 3, totaling 4.62 Tg of NO_x (in base NO_2) over the year. Fuel burn estimates are based on average time-in-mode values for LTO [265], and on the BADA aircraft performance model [262] for the non-LTO portions of flights. Emission indices (EI, mass ratio of emission and fuel burned) are calculated using data from the ICAO (International Civil Aviation Organization) Engine Emission Databank [169], according to the Boeing Fuel Flow Method 2 [246] and FOA 4 methods [21, 270]. Emission rates for 2005 are calculated in the same manner, using data published by Simone et al. [41]. For both years, only emissions from aircraft's main engines and APU are considered, without taking into account emissions from ground support equipment, tire and brake dust, and emissions from airport operations.

Aircraft NO_x emissions for the year 2040 are calculated as described in Chapter 4. Fuel burn for the year 2018 (Chapter 3) is used as a starting point for the projection, which con-

siders region-specific traffic growth rates forecast by ICAO for both passenger and cargo services [224, 300], reduction in fuel consumption rates due to technological [148, 221] and operational [304] improvements according to targets from ICAO, aircraft retirement rates [303]. NO_x emission indices of newly introduced aircraft in each future each until 2040 are modeled starting with a set of reference "state-of-the-art" aircraft types, and improved based on the technology goal for the year 2027 proposed by a 2017 independent expert integrated review panel from ICAO [148] and based on a continuing trend of overall engine pressure ratio increasing up to the year 2027 to values of 70 (widebodies), 65 (narrowbodies), and 60 (regional jets). Future aircraft emissions of CO, hydrocarbons, and nonvolatile particulate matter are estimated by multiplying projected fuel burn with the emission indices found for 2018, using values specific to each region and class of aircraft. Simulations including only NO_x emissions from aircraft provide an indication of the limit on the impact of a potential overestimation of non-NO_x emissions due to this assumption of constant EI.

6.2.2 Atmospheric modeling

The atmosphere is modeled with the GEOS-Chem classic v13.3 model [350], driven by MERRA-2 reanalysis meteorological fields for the years 2005 and 2019 [268] in Sections 6.3.1 and 6.3.2, and driven by meteorological fields for the year 2040 from GCAP 2.0 [351] in Section 6.3.3, which are generated for CMIP6 (Coupled Model Intercomparison Project, phase 6) scenarios [352] using the global climate model E2.1 from the NASA Goddard Institute for Space Studies (GISS) [353, 354]. GEOS-Chem simulates tropospheric and stratospheric photochemistry as described by Eastham et al. [315]. Sulfate-nitrate-ammonium aerosol thermodynamics modeling is described by Park et al. [355] and uses the ISORROPIA thermodynamic module [191]. Non-aviation anthropogenic emissions are from the CEDS v2 inventory for the years 2005 and 2019 [356], and from CMIP6 [348] processed by GCAP 2.0 for the year 2040 [351].

$PM_{2.5}$ concentration is calculated from model tracers according to Equation (6.1). In addition to ammonium, sulfate, and nitrate, the $PM_{2.5}$ definition also includes hydroxymethanesulfonate (HMS), hydrophilic and hydrophobic black carbon (BCPI, BCPO), hydrophilic and hydrophobic organic carbon aerosol (OCPI, OCPO), simplified secondary organic aerosol (SOAS), accumulation mode sea salt aerosol (SALA), and mineral dust with reference effective radii of 0.7 µm and 1.4 µm (DST1, DST2). Hygroscopic growth factors of GF_{SIA} = 1.10, GF_{org} = 1.08, and GF_{SSA} = 1.86 are used. The resulting $PM_{2.5}$ concentrations are corrected for standard temperature and pressure conditions, as is customary in air quality data used in epidemiological studies.

$$\begin{aligned} \mathrm{PM}_{2.5} = &\left(\mathrm{NH}_4^+ + \mathrm{SO}_4^{2-} + \mathrm{NO}_3^- + \mathrm{HMS}\right) \cdot GF_{SIA} \\ &+ \mathrm{BCPI} + \mathrm{BCPO} + \mathrm{OCPO} + (\mathrm{OCPI} + \mathrm{SOAS}) \cdot GF_{org} \\ &+ (\mathrm{SALA}) \cdot GF_{SSA} + \mathrm{DST1} + (\mathrm{DST2}) \cdot 0.3 \end{aligned} \tag{6.1}$$

Simulations are performed at 2° latitude and 2.5° longitude resolution globally, with either 72 (MERRA-2 meteorology) or 40 (GCAP 2.0 meteorology) vertical levels up the surface to 0.01 hPa. Results for the three scenarios quantifying impacts of aircraft emissions in 2019 — full-flight, LTO-only, and no aviation emissions, as indicated in Table 6.1 — are

further refined by nested simulations using 0.5° × 0.625° grids over Asia (60 °E – 150 °E, 11 °S – 55 °N), Europe (30 °W – 50 °E, 30 °N – 70 °N), and North America (140 °W – 40 °W, 10 °N – 70 °N). The nested simulations use the global coarse resolution runs for boundary conditions. At all spatial resolutions, timestep for transport and convection is 10 min and for chemistry and emissions it is 20 min.

6.2.3 Human health impacts

Exposure to pollutants is calculated using population maps for 2005 and 2019 from LandScan, totaling 6.44 and 7.56 billion people, respectively [325, 357]. Population distributions for the year 2040 from Jones and O'Neil are used [334], which take into account different national population and urbanization projections consistent for each SSP [335], totaling 8.35 (SSP1), 8.81 (SSP2), 9.28 (SSP3), 8.76 (SSP4), 8.41 (SSP5) billion people. Health impacts are quantified as the increase in yearly mortality of persons older than 30 years due to long-term exposure to $PM_{2.5}$, ozone, and NO_2. The fraction of population that is aged 30 or above is taken as country-specific values according to the Global Health Estimates (GHE) from the World Health Organization for the years 2005 (46.0% globally) and 2019 (50.1%) [326, 358]; the country-specific fractions for the year 2040 are given by the SSP definitions [335], ranging between 48.6% (SSP3) and 50.1% (SSP5). Cause-specific baseline mortality rates are also taken from the GHE for 2005 and 2019; estimates for 2040 adopt the same rates from 2019. Exposure and health impact are calculated with a global 0.5° × 0.625° grid (edge-aligned with the atmospheric model's 2° × 2.5°) in which a country is assigned to each cell based on geocoding data from OpenStreetMaps, accessed via the Nominatim search tool.

Mortality due to noncommunicable diseases and lower respiratory infections associated with annual average exposure to $PM_{2.5}$ is quantified by the GEMM nonlinear CRF, which was derived from a meta-analysis including a wide range of concentration values [114]. All-cause nonaccidental mortality associated with peak-season average daily maximum 8-hour average (MDA8) ozone is quantified by the relative risk of 1.01 (CI: 1.00–1.02) per 10 $\mu g \cdot m^{-3}$ suggested by the meta-analysis from Huangfu and Atkinson [117]. Peak-season ozone is taken as the grid-cell local highest 6-month rolling average MDA8 concentration, looping over December and January. All-cause nonaccidental mortality associated with annual average NO_2 is quantified by the relative risk of 1.02 (CI: 1.01–1.04) per 10 $\mu g \cdot m^{-3}$, based on a meta-analysis also from Ref. [117]. The same constant factors of 1.96 (ozone) and 1.96 (NO_2) used by Ref. [117] are adopted to convert mixing ratios in ppb to mass concentrations in $\mu g \cdot m^{-3}$.

Uncertainty in mortality estimates is calculated considering only the uncertainty associated with the CRFs. For $PM_{2.5}$, a normal distribution of the theta parameter in the GEMM model is considered, using the standard deviation provided with the CRF [114]. For the ozone and NO_2, triangular distributions are used for the hazard ratios, defined by the central values and the 95% confidence intervals reported with the CRFs [117]. The uncertainties are calculated using a Monte Carlo approach with $1 \cdot 10^4$ samples, with 2.5th and 97.5th percentiles reported along with the results from nominal input values. For clarity, the lower bound of ozone mortality estimates based on the reported hazard ratio of 1.00 are truncated to zero.

6.3 Results

6.3.1 Present-day impacts of aircraft emissions

In the simulations for the year 2019, full-flight emissions led to overall annual increases in $PM_{2.5}$ and ozone ground-level concentrations, and both increases near large airports and decreases elsewhere in NO_2 concentrations (Figure 6.1). Whereas low-altitude NO_x emissions increase NO_2 concentrations locally near airports, it is suggested that high-altitude NO_x largely affects the surface by way of producing ozone [32], which then drives additional conversion of ground-level NO_2 into HNO_3 [346]. Most of the global air quality impacts occur in the northern hemisphere, where 92% of fuel burn takes place: 93% ($PM_{2.5}$), 87% (ozone), and 97% (NO_2) of area-weighted concentration increases and 99% ($PM_{2.5}$), 97% (ozone), and 95% (NO_2) of population exposure increases due to full-flight emissions occur north of the equator. On average within that hemisphere, full-flight emissions increased the $PM_{2.5}$ concentration over populated areas by $0.051\,\mu g \cdot m^{-3}$, peak-season ozone MDA8 by 1.3 ppbv, and decreased NO_2 by 8.6 pptv. In the same area, these aircraft-attributable changes represent 0.2% ($PM_{2.5}$), 2.6% (peak-season ozone), and −0.7% (NO_2) of (all-source) background pollutant levels, i.e. both due to natural and anthropogenic emissions. The share of pollutant levels attributable to aircraft vary regionally; for example, aircraft emissions are responsible for more than 2% of $PM_{2.5}$ concentrations over large areas in Europe and North America (Figure C.2).

The comparison of northern hemisphere area-weighted air quality impacts to the population-weighted averages over select regions listed in Table 6.2 highlight differences in how pollutants are affected by aviation. While ozone impacts are more spatially uniform, $PM_{2.5}$ impacts from aviation are greater in more populated regions, affecting people in Asia more than in the other regions considered, with over 1.5 billion people in Asia experiencing an increase of more than $0.2\,\mu g \cdot m^{-3}$ in annual $PM_{2.5}$ (Figure 6.2). Globally, 95% of area and 71% of population see a decrease in NO_2 due to full-flight emissions (driven by non-LTO), but large concentration increases in populated regions cause the average exposure change to be positive (Figures 6.1 and 6.2). NO_2 average exposure increased significantly more in North America than in the other regions, which is consistent with the greater relative importance of LTO emissions to overall air quality impacts in that region (as discussed in Section 5.3.2), in addition to a higher ratio of LTO to full-flight emissions over the region. As Figure 6.2 shows, compared to other regions, North America has a lower proportion of population in areas with negative annual NO_2 changes. Globally, aviation represents 0.3% ($PM_{2.5}$), 1.8% (peak-season ozone), and 0.3% (NO_2) of all-source population exposure.

Landing and takeoff emissions are responsible for 10.9% ($PM_{2.5}$), 3.5% (peak-season ozone MDA8), and 159% (NO_2) of global exposure attributed to full-flight emissions, with the latter driven by non-LTO emissions having a net negative change on global NO_2 exposure. The share of full-flight impacts due to LTO emissions is not uniform spatially, for example in some areas close to large airports half of aircraft-attributable $PM_{2.5}$ is caused by LTO emissions (Figure C.3). The seasonality of LTO and non-LTO impacts is also different. Due to lower temperatures and solar radiation, the atmospheric lifetimes of NO_x released at cruise altitude and its products are longer during winter, which allows them to cause effects ultimately affecting the surface before they are removed by wet deposition [32]. This causes the average global concentration changes of both $PM_{2.5}$ and ozone due to full-

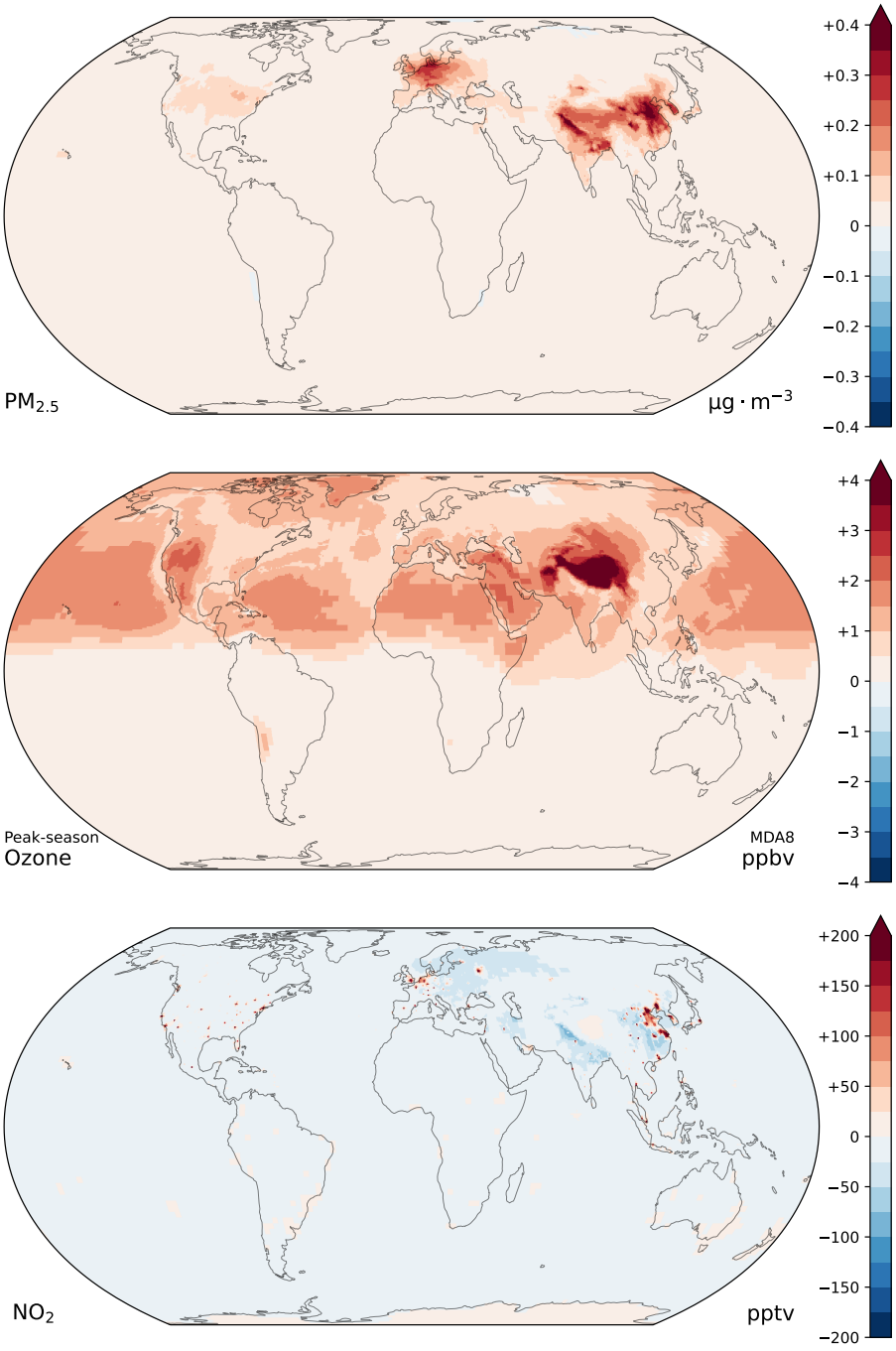

Figure 6.1: Ground-level $PM_{2.5}$ mass concentration, and ozone and NO_2 mixing ratio changes attributed to 2019 full-flight emissions.

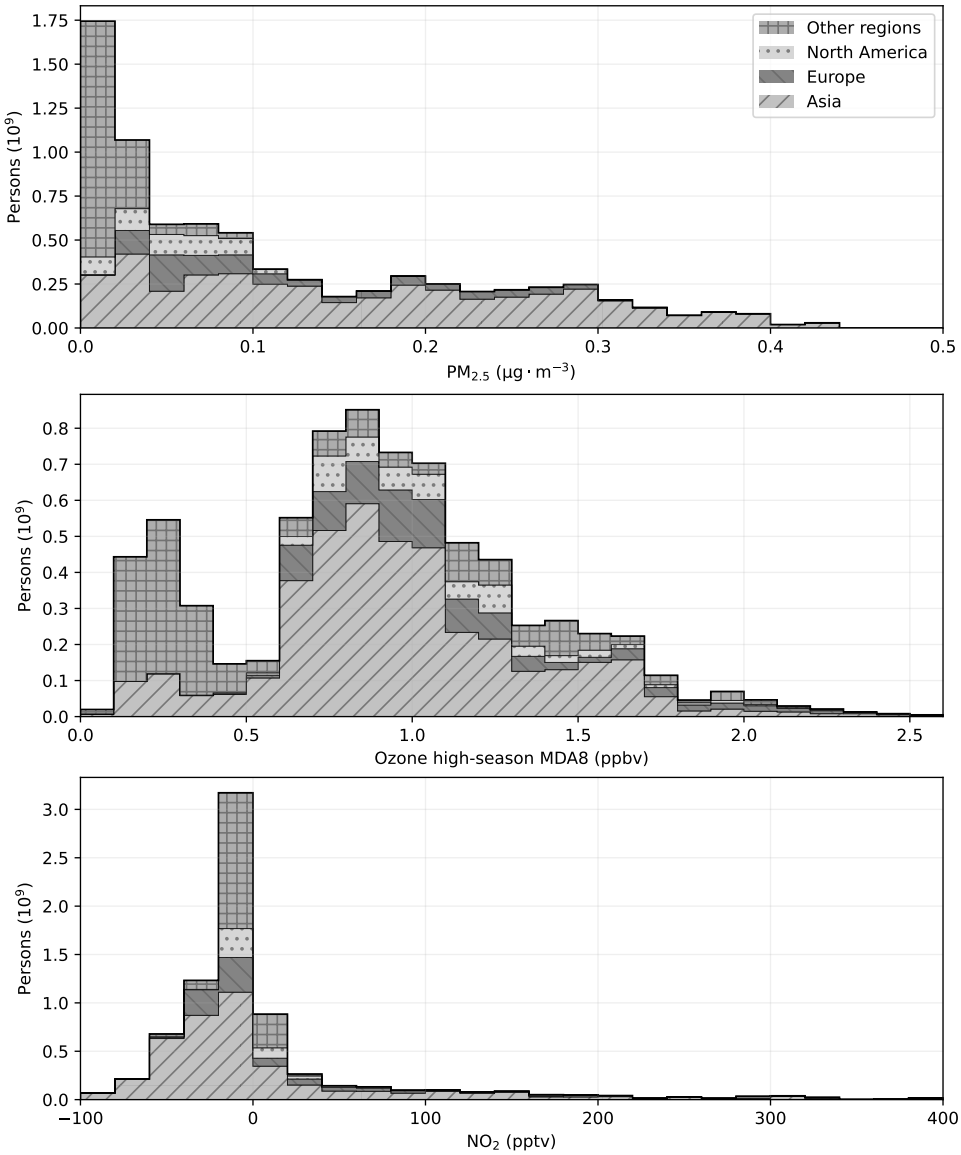

Figure 6.2: Histogram of population exposure attributed to 2019 full-flight emissions, per region.

Table 6.2: Modeled background and aircraft-attributable population-weighted concentrations in 2019 for Asia (AS), Europe (EU), North America (NA), and the whole world.

		AS	EU	NA	World
$PM_{2.5}$, annual mean, $\mu g \cdot m^{-3}$	Full-flight	0.165	0.122	0.054	0.121
	LTO-only	0.014	0.022	0.011	0.013
	Background	50.9	17.3	8.9	37.3
Ozone, peak-season mean MDA8, ppbv	Full-flight	0.954	1.065	1.074	0.920
	LTO-only	0.022	0.064	0.096	0.035
	Background	62.9	49.1	49.9	56.4
NO_2, annual mean, ppbv	Full-flight	0.017	0.023	0.052	0.017
	LTO-only	0.018	0.032	0.056	0.021
	Background	6.68	3.32	3.23	4.85

flight emissions to be twice as high during boreal winter compared to summer (Figure C.1), while the global net NO_2 reduction goes from ~0.4 pptv in June-July-August to ~5.4 pptv in December-January-February. Impacts from LTO emissions are less dependent on seasonal differences in tropospheric lifetime, and ozone changes are higher during summer due to higher solar radiation, in phase with impacts from other ground-level pollution sources.

The scenario where only NO_x emissions from aircraft are included in the simulation resulted in 70% (area-weighted) and 87% (population-weighted) of the global annual $PM_{2.5}$ changes observed when also including aircraft emissions of other species (Figure C.4). In the NO_x-only perturbation scenario, 97% of ground-level $PM_{2.5}$ increase (global annual area-weighted average) is in the form of ammonium and nitrate aerosol and 2.9% is sulfate aerosol (Table 6.3), which is formed due to the increased oxidizing capacity of the atmosphere promoting its formation from SO_2 [187]. When including emissions of other species from full-flight activities (SO_x, hydrocarbons, CO, and black carbon), global $PM_{2.5}$ changes consist of: ammonium and nitrate (71.5%), sulfate (23.5%), black carbon (0.6%), organic aerosol (4.5%). NO_x is responsible for almost all of ozone and NO_2 impacts, with the difference between the scenarios being less than 1%.

Table 6.3: Share of individual components (per mass) of modeled ground-level $PM_{2.5}$ attributed to aircraft emissions in 2019, for different perturbation scenarios. The values represent annual global area-weighted averages.

	Full-flight All-species	Full-flight NO_x-only	LTO-only All-species
Ammonium aerosol	52.1%	77.9%	13.0%
Sulfate aerosol	23.5%	2.9%	56.9%
Nitrate aerosol	19.4%	19.2%	20.8%
Organic aerosol	4.0%	0.0%	7.8%
Black carbon	0.6%	0.0%	1.1%

Globally, aircraft emissions in the year 2019 are associated with a total excess mortality of 116 100 (Table 6.4) due to $PM_{2.5}$ (29%), ozone (68%), and NO_2 (2%). 59% of aircraft-attributable mortality occurs in Asia, where 57% of the global population over age 30 is located. Emissions from LTO are responsible for 9.5% of total mortality attributed to full-flight emissions, having a greater health impact associated with $PM_{2.5}$ and NO_2 per mass of fuel burned than non-LTO emissions, and lower with ozone. LTO emissions lead to a decrease in ozone during winter near regions of large aircraft emissions, which is associated with conditions changing into an ozone production regime limited by volatile organic aerosols, as was observed in the study described in Chapter 5. If ozone health impacts are estimated using a CRF considering annual concentration averages instead of peak-season averages, such as the relative risk of death by respiratory diseases of 1.12 per 10 ppbv found by Turner et al. [104], the ratio of global mortality due to ozone between LTO and full-flight emissions is 2.2% instead of 4.1% as in Table 6.4. Mortality associated with NO_2, which has not been evaluated in previous studies of global aviation impacts, is only 2.4% of full-flight impacts, but 32% of LTO impacts, highlighting its importance at local scales. Using different models, Arter et al. found NO_2 to account for 91% of LTO-attributable mortality in the contiguous United States [359], compared to 43% found here for North America.

Table 6.4: Premature mortality in 2019 attributed to aircraft emissions, in thousands of deaths. LTO-only impacts in parenthesis.

	Asia	Europe	North America	World
$PM_{2.5}$	22.5 (2.0)	8.1 (1.5)	2.4 (0.5)	33.9 (4.2)
Ozone	45.2 (1.1)	16.6 (1.0)	8.4 (0.8)	79.5 (3.2)
NO_2	1.4 (1.6)	0.7 (1.0)	0.8 (0.9)	2.7 (3.5)
Total	69.0 (4.7)	25.4 (3.5)	11.7 (2.2)	116.1 (11.0)

6.3.2 Future emissions scenarios

Global aircraft NO_x emissions are estimated to increase between 2019 and 2040 by 10%, 56%, and 97% in the low, baseline, and high projection models, respectively. This follows the realized increase of 72% between 2005 and 2019. On the global average, surface aircraft-attributable $PM_{2.5}$ and ozone concentrations increase approximately in proportion to the mass of emissions in the perturbation (Figure 6.3). Across different future non-aviation emissions scenarios, mean concentration changes due to full-flight emissions vary relative to SSP2-4.5 from −4% to +13% for $PM_{2.5}$, and from −9% to +3% for ozone. NO_2 net decreases, on the other hand, have lower sensitivity to full-flight aircraft emissions in the future than in 2019, which in turn have decreased sensitivity compared to 2005. Relative to the other pollutants, there is also more spread in NO_2 mean concentration changes depending on future scenarios: from −62% to +15% relative to SSP2-4.5. For the same future non-aviation emissions (SSP2-4.5), the magnitude of impacts on concentration is close to linearly proportional to the amount of aircraft NO_x; with sensitivity decreasing as aircraft NO_x emissions go from the “low” to “high” scenario by 8% ($PM_{2.5}$ and ozone) and 15%

(NO_2).

As can be seen in the plots on the right of Figure 6.3, mean population exposure also increase with the amount of full-flight NO_x emissions. From 2005 to 2019, exposure sensitivity to the amount of aircraft NO_x increased for $PM_{2.5}$ (20%) and NO_2 (137%), and decreased for ozone (4%). From 2019 to 2040 SSP2-4.5, exposure sensitivity changes by +9% ($PM_{2.5}$), −1% (ozone), and −34% (NO_2). Normalized exposure for all three pollutants increases when changing just aircraft emissions to those of a previous year ("05a" vs. "2019", and "19a" vs. "(SSP)2-4.5" in Figure 6.3). These changes in sensitivity might not only be caused by nonlinearity in the atmospheric response, but also due to the fact that the scenarios with more aircraft emissions have a higher percentage of those emissions over Asia and lower over Europe, the latter having a stronger impact on pollutant exposure (Chapter 5). Across different future non-aviation emissions scenarios, the change in exposure sensitivity to aircraft NO_x relative 2019 ranges from −14% to +52% ($PM_{2.5}$), and from −7% to 4% (ozone). Due to countering effects of NO_2 increases near airports and decreases far from them, the average exposure associated with full-flight emissions can be either positive or negative, while the global (area-weighted) average concentration changes are negative in all scenarios. Notably, while net exposure to NO_2 in 2019 is positive when including the higher resolution simulations over the nested domains (Table 6.2), it is negative when only considering the coarser resolution global simulations.

The sensitivities of aircraft-attributable global exposure to aircraft LTO-only emissions (Figure 6.4) change from 2019 to SSP2-4.5 2040 by −58% ($PM_{2.5}$), +36% (ozone), and +8% (NO_2). Opposite to full-flight impacts, different non-aviation emission scenarios affect more the LTO impacts on $PM_{2.5}$ and ozone, and less NO_2. Relative to the baseline 2040 scenario (SSP2-4.5), global sensitivity of ozone and NO_2 exposure to LTO emissions increase in the less polluted scenario (SSP1-1.9) by 43% and 9%, respectively, and decrease in the more polluted scenario (SSP3-7.0) by 28% and 6%, in the same order. Both alternative future non-aviation emissions scenarios have more $PM_{2.5}$ exposure attributed to LTO (25% in SSP1-1.9, and 127% in SSP3-7.0). These net global changes are not uniform spatially, particularly for $PM_{2.5}$, with different regions experiencing either higher or lower sensitivity to aircraft emissions across the three scenarios (Figure C.5).

There is also spatial variability on the ground-level concentration impacts of full-flight emissions across different 2040 non-aviation emissions scenarios (Figure 6.5). For example, in the less polluted scenario (SSP1-1.9), $PM_{2.5}$ sensitivity to aircraft emissions is lower in India but higher in China compared to SSP2-4.5. Also compared to this baseline scenario, in the more polluted scenario (SSP3-7.0), ozone sensitivity is higher by less than 5% in most populated areas in the northern hemisphere, but lower by more than 20% or 30% in areas in eastern Asia.

Aircraft-attributable mortality in the year 2040, considering the baseline emissions scenario with SSP2-4.5 population and non-aviation emissions, add to a total of 177 200 deaths (Table 6.5). This represents a 76% global increase relative to 2019 when simulated at the same resolution (i.e. without incorporating the higher resolution simulations available only for 2019). This is the result of the combined effects of a 56% increase in aircraft NO_x emissions, a 13% increase in global population over age 30, and a similar sensitivity of ground-level pollution to aircraft emissions. For same future population and non-aviation emissions, and only changing aircraft emissions from 2019 to 2040 (baseline), global mor-

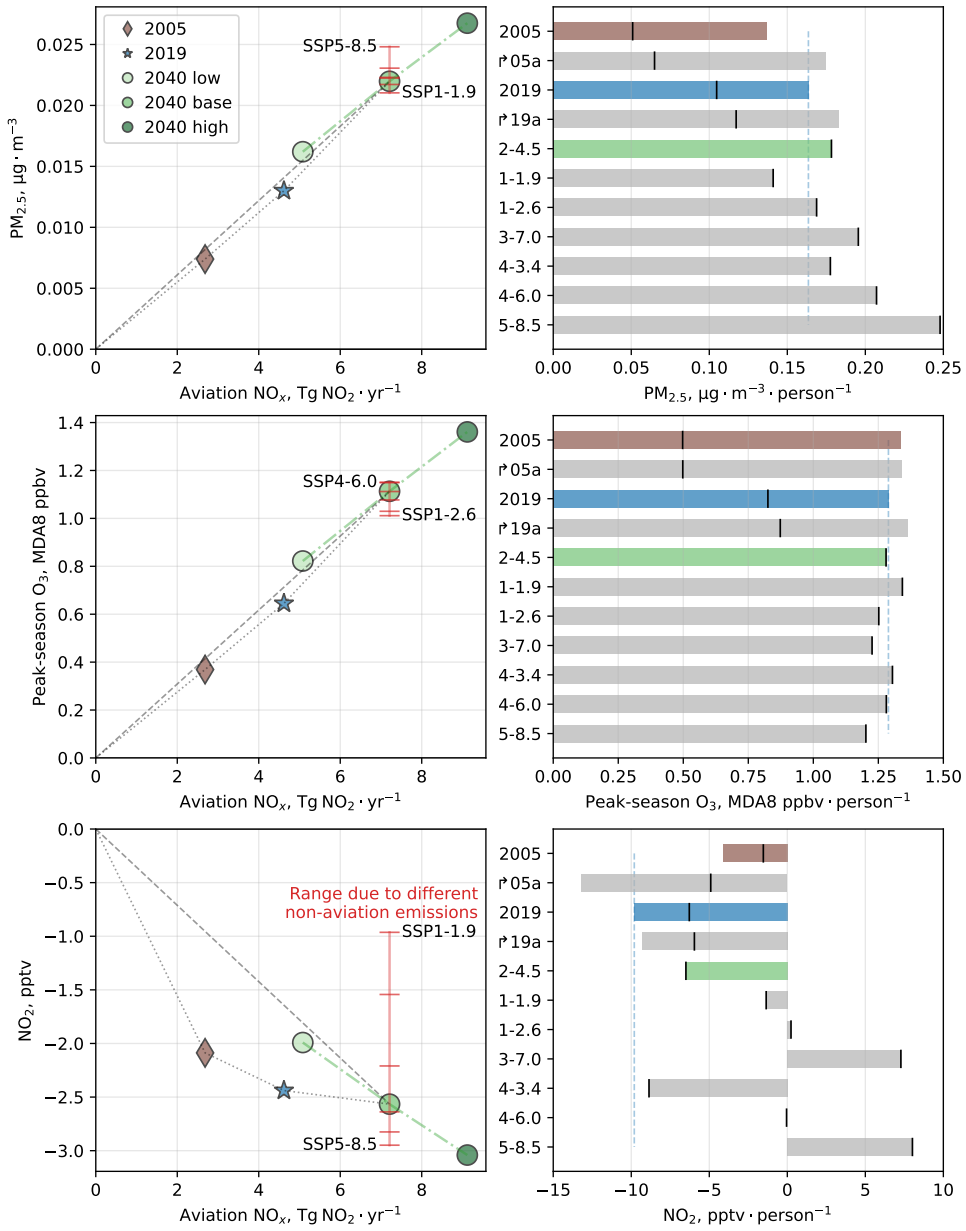

Figure 6.3: Left: global annual mean full-flight attributable pollutant levels versus NO_x emitted. Future estimates indicated by green circles are simulated with SSP2-4.5 non-aviation emissions. Gray and green lines connecting the markers are shown to highlight changes in sensitivity. Right: global annual mean population exposure attributable to full-flight emissions for different scenarios. Future scenarios all utilize the baseline 2040 aircraft emissions. Filled horizontal bars indicate values normalized according to the amount of aviation NO_x to 2040 levels; unnormalized values are indicated by black vertical dashes. "05a" and "19a" combine 2019 non-aviation with 2005 aircraft emissions and 2040 (SSP2-4.5) non-aviation with 2019 aircraft emissions, respectively.

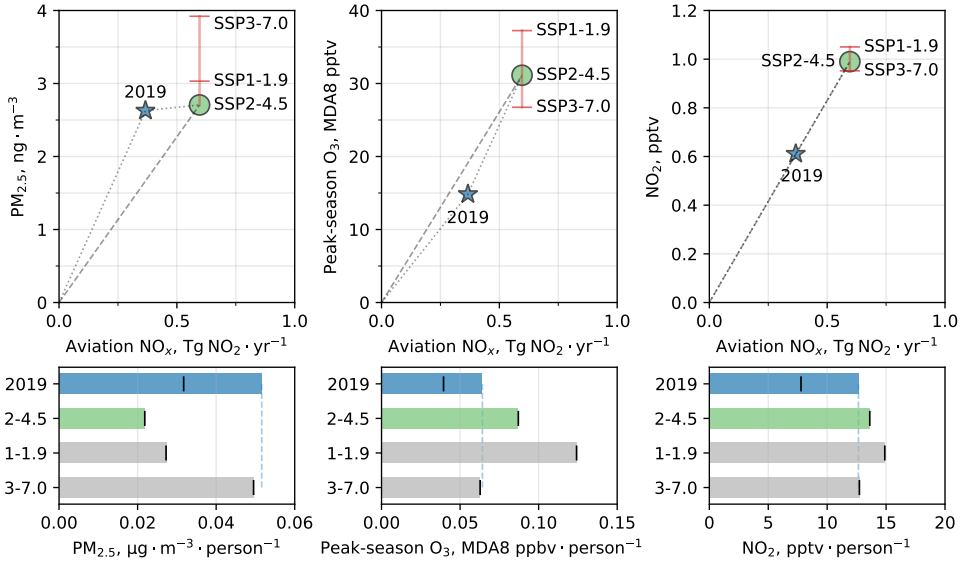

Figure 6.4: Top: global annual mean LTO-attributable pollutant levels versus NO_x emitted. The gray lines connecting the points are shown to highlight changes in sensitivity. Bottom: global annual average population exposure attributable to LTO emissions for different scenarios. Filled horizontal bars indicate values normalized according to the amount of LTO NO_x to 2040 levels; unnormalized values are indicated by black vertical dashes. Note the different $PM_{2.5}$ and ozone units across top and bottom plots.

tality increases by 47%. For the same non-aviation emissions scenario, the "low" and "high" aircraft emissions projections result in 129 500 and 217 800 annual deaths, respectively, representing increases of 28% and 115% relative to 2019. The simulation with only NO_x emissions from aircraft has similar effects in 2040 as it has in 2019: the absence of non-NO_x emissions reduces $PM_{2.5}$ health impacts by 14% in both years, and does not significantly affect ozone or NO_2. Changing population and non-aviation emissions from the baseline SSP2-4.5 scenario, results in −1% to +5% aircraft-attributable mortality, with the standout difference being a 32% increase in $PM_{2.5}$ mortality in SSP5-8.5 relative to the baseline. Of the two alternative LTO-only perturbation future scenarios, SSP1-1.9 resulted in the largest change in impacts relative to the baseline, with mortality increasing for all three pollutants, yielding a total that is higher by 37%.

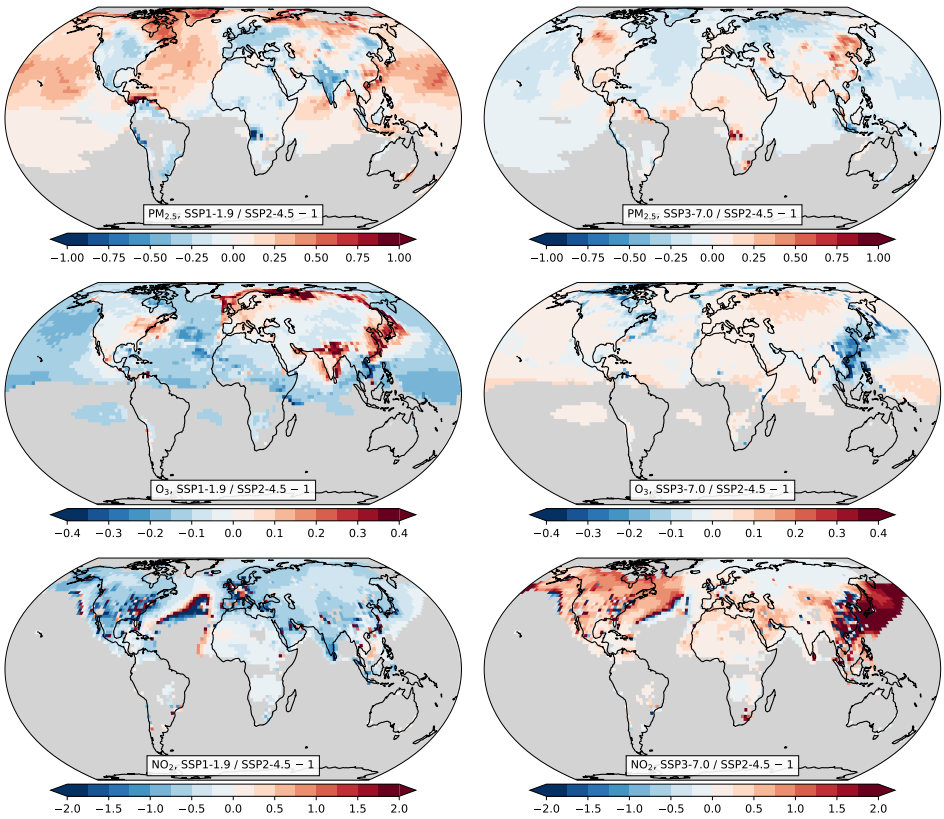

Figure 6.5: Relative difference in ground-level concentrations attributable to full-flight aircraft emissions in 2040 between a less polluted scenario (SSP1-1.9) or more polluted scenario (SSP3-7.0) and a more likely scenario (SSP2-4.5).

Table 6.5: Annual global premature mortality attributed to aircraft emissions for different scenarios. Negative values indicate an expected decrease in mortality. To allow for comparison, for the two 2019 scenarios also simulated at higher resolution with nested domains, marked with an asterisk (*), the values shown come only from the coarser global simulations.

Population and non-aviation emissions	Aircraft emissions	Early deaths $(\times 10^3)$			
		$PM_{2.5}$	Ozone	NO_2	Total
2005	2005	14.0	34.9	−0.1	48.8
2019	2005	19.5	42.6	−0.6	61.5
2019*	2019*	31.1	70.6	−0.8	100.9
2019	2019 NO_x-only	26.8	71.2	−0.8	97.2
SSP2-4.5	2019	36.0	85.6	−0.9	120.7
SSP2-4.5	2040	53.6	124.5	−0.9	177.2
SSP2-4.5	2040 NO_x-only	46.2	124.7	−0.9	169.9
SSP2-4.5	2040 low	38.7	91.6	−0.8	129.5
SSP2-4.5	2040 high	66.1	152.8	−1.1	217.8
SSP1-1.9	2040	52.3	126.1	0.2	178.6
SSP1-2.6	2040	58.4	117.9	0.6	176.9
SSP3-7.0	2040	50.4	123.2	1.3	174.9
SSP4-3.4	2040	52.1	124.5	−1.3	175.3
SSP4-6.0	2040	53.6	121.9	0.3	175.8
SSP5-8.5	2040	70.8	113.4	1.9	186.1
2019*	2019 LTO-only*	9.7	4.0	1.6	15.3
SSP2-4.5	2040 LTO-only	8.6	9.5	2.8	20.8
SSP1-1.9	2040 LTO-only	12.2	13.3	3.0	28.4
SSP3-7.0	2040 LTO-only	12.8	6.9	2.5	22.3

6.3.3 Different meteorological scenarios

Changes in mean aircraft-attributable exposure are evaluated for three alternative meteorological fields generated from a global climate model and prepared as the GCAP 2.0 model [351], representing three SSP scenarios. The results of these simulations are not directly comparable to those discussed in Sections 6.3.1 and 6.3.2, obtained by using GEOS-Chem driven by MERRA-2 fields, as each set of fields lead to significantly different vertical profiles of the concentration of species relevant to how aircraft emissions affect the atmosphere (such as OH, NH_3, NH_4^+, NO_3^-, as shown in Figure C.6). Additionally, the vertical grid definitions are different, with 72 levels for MERRA-2 and 40 levels for GCAP 2.0. In the GCAP 2.0 simulations, cruise-level NO_x forms aerosol more readily while at high-altitude, where more of it is removed by wet deposition processes before affecting air quality at ground-level. The resulting global $PM_{2.5}$ exposure attributable to full-flight emissions (Figure 6.6) are lower relative to the scenarios using 2019 meteorology: −49% for SSP1-2.6, −51% for SSP2-4.5, and −61% for SSP5-8.5. Aircraft-attributable global peak-season ozone exposures differ between the two models by −2% to +2%, and NO_2 exposures are more towards net global decrease in GCAP 2.0. This suggests that in this latter model full-flight aircraft emissions affect ground-level air relatively more in the form of ozone, which also tends to lead to a decrease NO_2 concentration.

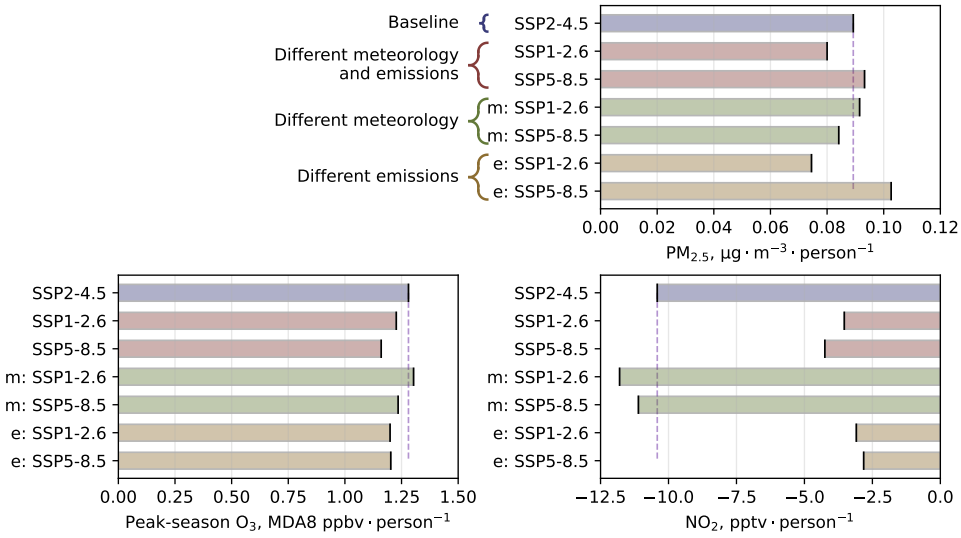

Figure 6.6: Global annual mean exposure attributed to full-flight emissions in 2040 for different scenarios of non-aviation emissions and meteorological fields from GCAP 2.0. For all cases, SSP2 population for the year 2040 is used.

As shown in Figure 6.6, the effect on global full-flight attributable exposure by changing only meteorology fields (up to 6%, 4%, 13% for $PM_{2.5}$, ozone, and NO_2, respectively) is smaller than by changing only non-aviation emissions (up to 17%, 6%, and 73%, in the same order). Different meteorology scenarios change (all-source) background exposure to the three pollutants by up to 3% relative to SSP2-4.5, which means that the effect of

weather is greater on the impacts from aircraft emissions, as is expected from their higher release altitude. It can be noted that the combined impacts of non-aviation emissions and meteorology (again using global exposure due to full-flight emissions as the metric) are in the expected direction of the combination of their impacts evaluated separately: when changing just meteorology increases impacts relative to the baseline, then the combined effects are larger than just changing emissions, and vice-versa.

6.4 Discussion

Air quality and human health impacts from aircraft emissions are estimated here for the years 2005, 2019, and 2040 using a consistent model framework. Total annual premature mortality due to these aviation emissions in 2019 is estimated as 116 100. This is further evidence that the increase of NO_x emissions in this sector, of 72% between 2005 and 2019, is accompanied by a corresponding increase in human health impacts. In fact, the combined effects of spatially nonuniform changing population counts, non-aviation emissions, and aircraft emissions can lead to increases in the sensitivity of global exposure to aircraft emissions, such that health impacts from aviation increase faster than emissions.

The aircraft-attributable mortality figures are significantly higher than those reported in previous work [1, 30, 32]. A part of this difference is due to a more recent inventory of aircraft emissions being used here, with a correspondingly larger amount of mass released. But the largest difference is due to significantly higher estimates of mortality due to ozone, which accounts for 68% of the total for 2019 here, compared to 13% in Yim et al. [1], and 40% in Eastham and Barrett [32]. This is both due to the chemical transport model used here estimating a larger ground-level ozone impact from cruise NO_x emissions, and due to different concentration-response functions (CRF) used to quantify mortality. The association of long-term exposure to $PM_{2.5}$ with higher mortality rates is clear and evidence continues to suggest this association even for exposure at levels below WHO air quality guidelines [116], but the evidence for the association of long-term ozone exposure and mortality is still limited, with high levels of heterogeneity in results from individual cohort studies [117]. Uncertainty in the CRF propagates to the health impacts of aviation, so care must be taken to consider the absolute magnitude of impacts in light of this context. By investigating various scenarios of aircraft emissions using a consistent methodology, the study presented in this chapter is able to provide insights into the evolution of their health impacts over time, which would not be affected by a systematic bias in the CRF. The magnitude of mortalities due to air quality degradation is essential, however, in the monetary valuation of these impacts, which is a necessary analysis when comparing them to the noise and climate impacts of aviation in order to guide environmental mitigation efforts [211, 295]. Eastham and Barrett have estimated that the aviation-attributable increase in column ozone can offset ~6% of ozone exposure mortalities, through a reduction in the incidence of melanoma due to lower surface UV-B [32], which is an effect not accounted for here.

The increased relative contribution of ozone to aircraft-attributed mortality leads to a corresponding increase in the share of impacts from non-LTO emissions: 9.5% for 2019 here, compared to 25% in Ref. [1], and 20% in Ref. [30]. However, three factors should be noted that may contribute to an underestimation of LTO impacts in this study. Firstly, only aircraft emissions were considered (main engine and APU), so the impacts of emis-

sions from ground operations, airport facilities, land-use changes, and airport-associated road traffic — all of which may be accounted for together with aircraft LTO emissions in national emissions inventories — are not included in this analysis. Secondly, differential toxicity based on chemical composition and particle size of $PM_{2.5}$ is not considered here. An increasing amount of evidence suggests that black carbon and ultrafine particles, which are affected proportionately more by LTO phases of flight, have a stronger impact per mass on human health relative to other $PM_{2.5}$ constituents [57, 59, 60, 360]. And thirdly, a global atmospheric model such as the one used here may not be able to resolve individual urban areas, not capturing co-location effects of aircraft emissions, non-aviation emissions, and population. Due to the nonlinear chemical processes affecting atmospheric pollution, the inability to resolve variations in concentration above emitting regions can lead to both under- and overestimates of the sensitivity of air quality to aviation emissions. Within the results presented here, the incorporation of higher resolution simulations over nested regional domains reduces LTO-attributable mortality due to $PM_{2.5}$, although Yim et al. found that incorporating higher resolution nested models increased LTO-attributable mortality due to $PM_{2.5}$ and ozone more than full-flight [1]. This study quantifies for the first time the global impacts associated with long-term NO_2 exposure, and while non-LTO impacts are negative (emissions lead to reduction in mortality), within LTO impacts, NO_2 leads to a similar amount of mortality compared to $PM_{2.5}$ and ozone. Arter et al. evaluated health impacts of LTO emissions within the United States, using different atmospheric models and CRFs than used here, and found that NO_2 was responsible for 91% of mortality from those emissions [359]. In the results presented here, NO_2 impacts are very sensitive to model resolution, increasing when the nested simulations are included. The sensitivity of health impacts from NO_2 to model resolution has been noted by Mehegh et al., in the context of impacts in the United States and India due to emissions from all-sources, suggesting that a 1 km would be adequate for such analysis [361].

Assuming that air traffic and the overall pressure ratio of new aircraft engines increase as projected, it is likely that global aircraft NO_x emissions will be significantly higher in 2040 than in 2019, such as by 56% in the baseline estimate presented here. Even in the "low" future aircraft emissions estimate, NO_x increases by 10%. This is consistent with an analysis published in 2022 by the International Civil Aviation Organization, which concludes that air traffic growth will lead to more total noise and CO_2 and NO_x emissions [144]. Current proposals for achieving carbon neutrality in aviation rely primarily on extensive use of biomass-derived or synthetic kerosene, which do not significantly impact NO_x emissions, but may lead to a reduction in SO_x, and primary particulate matter emissions, depending on the specific technologies employed [306]. For both 2019 and 2040, it is found here that NO_x alone is responsible for 86% of $PM_{2.5}$ and 96% of total mortality attributed to full-flight emissions, which is in line with the finding by Kapadia et al. that ultra-low sulfur jet fuel could reduce up to 17% of global aviation-attributed $PM_{2.5}$ mortality [158]. However, if higher toxicity of black carbon or ultrafine particles is considered instead of a single CRF for $PM_{2.5}$, and jet fuel is replaced with an alternative that lowers emissions of those pollutants, then further reductions in health burden could be achieved. In our baseline scenario for the year 2040, which does not consider potential mitigating effects of expanded biofuel usage or aircraft not powered by hydrocarbon fuel, aircraft emissions are responsible for 177 200 annual deaths, a 76% increase over the estimate for

2019 using the same model resolution. And while aviation's global impacts on air quality are expected to increase over the next few decades, other transportation sectors have more viable solutions to reduce emissions [143], such that those impacts from aviation are likely to also increase in relative terms [361]. The dependence of future air quality impacts from aircraft emissions on future population changes and emissions from other sectors is apparent in the results presented, as exemplified by global $PM_{2.5}$ mortality being 32% higher for the same aircraft full-flight emissions when released in an SSP5-8.5 scenario instead of the baseline SSP2-4.5, and by the LTO-attributable mortality being 42% ($PM_{2.5}$) and 40% (ozone) higher in the SSP1-1.9 scenario compared to SSP2-4.5.

Results from simulations using different meteorological fields suggest that their impact on the sensitivity of global pollutant exposure due to aircraft emissions — changes from the baseline of up to 6% ($PM_{2.5}$), 4% (ozone), and 13% (NO_2) — is lower than those due to changes in non-aviation emissions, but aircraft-attributable population exposure is more affected by meteorology changes than exposure to background pollution, of up to 3% across the three pollutants. Changes in atmospheric climate are also expected to continue to increase beyond 2040 [337], so these effects might become more significant in a longer timescale. Additionally, the atmospheric model used here simulates aerosol microphysics in a simplified manner and is driven by prescribed meteorology, such that the interaction between clouds and aircraft exhaust (and the secondary pollutants formed from it) is not considered, and the feedback mechanisms between meteorology and aerosol formation are not captured.

6.5 Data availability

The data that support the findings of this study, such as atmospheric model output used in the calculations, will become openly available accompanying the publication of the manuscript in preparation on which this chapter is based (item 6 in the list of peer-reviewed journal articles at the end of this thesis).

6.6 Acknowledgments

This work made use of the Dutch national e-infrastructure with the support of the SURF Cooperative using grant no. EINF-5454.

7

Nitrogen deposition from aircraft emissions

Canada, the most affluent of countries, operates on a depletion economy which leaves destruction in its wake. Your people are driven by a terrible sense of deficiency. When the last tree is cut, the last fish is caught, and the last river is polluted; when to breathe the air is sickening, you will realize, too late, that wealth is not in bank accounts and that you can't eat money.

Alanis Obomsawin[1]

Excess nitrogen deposition from anthropogenic sources of atmospheric emissions has negative effects on natural environments, and designing effective conservation efforts requires knowledge of the contribution of individual sectors. In this chapter, a global atmospheric chemical transport model is used to quantify, for the first time, the contribution of global aviation NO_x emissions to nitrogen deposition for 2005 and 2019. It is found that aviation led to an additional 1.39 Tg of nitrogen deposited globally in 2019, up 72% from 2005, with 67% of each year's total occurring through wet deposition. In 2019, aviation was responsible for an average of 0.66%, 1.13%, and 1.61% of modeled nitrogen deposition from all sources over Asia, Europe, and North America, respectively. These impacts are spatially widespread, with 56% of deposition occurring over water. Emissions during the landing, taxi and takeoff (LTO) phases of flight are responsible for 8% of aviation's nitrogen deposition globally, and between 16–32% over most land in regions with high aviation activity. Despite currently representing less than 1.2% of global nitrogen deposition, the anticipated growth of aviation emissions will result in an increase in aviation's contribution and the associated exceedance of critical loads.

This chapter was originally published in the journal Science of The Total Environment. Please cite as shown in the list of peer-reviewed journal articles, item 4.

[1]Quoted in *Conversations with North American Indians* by Ted Poole, in *Who is the Chairman of this Meeting? A Collection of Essays* by Ralph Osborne.

7.1 Introduction

Multiple sectors of human activity affect the Earth's nitrogen cycle due to atmospheric release of reactive nitrogen (N_r) [13]. The increase in the use of fertilizers and dense livestock farming since the early 1900s has been essential in supporting food supply for a growing world population, but these activities also lead to the emission of reduced N_r compounds, mainly NH_3 [123]. At the same time, burning fuel for transportation, energy generation, heating, and industrial processes leads to the emission of oxidized N_r compounds, such as NO_x ($NO + NO_2$). In addition to impacting the climate and air quality while in the atmosphere [362], the deposition of these species leads to degradation of water quality, causing higher toxicity to humans and animals, loss of biodiversity, and soil acidification [13].

Conservation objectives for nitrogen-sensitive natural assets in nature reserves (e.g. Natura 2000 in Europe) have set thresholds for the nitrogen load in such areas, but these are frequently exceeded. In 2017, ~64% of ecosystem areas in Europe exceeded the critical loads for eutrophication [363]. In hotspots such as the Netherlands, where in 2019 the specified critical loads were exceeded in 118 out of the 162 Natura 2000 sites [15], the resulting nitrogen problem is having increasing socioeconomic and political ramifications [16].

Current aircraft emissions, as calculated in Chapter 3, account for ~4.1% of anthropogenic NO_x [356]. However, due to the growth rate of aviation forecast at ~3–4% annually and to the lack of presently available NO_x reducing technologies for aircraft, aviation NO_x emissions are estimated to continue increasing in the coming decades, as discussed in Chapter 4. Part of the difficulty in reducing NO_x emissions are the decades-long trend in aircraft engine design of increasing gas temperature and pressure, which are beneficial for lowering fuel consumption but that promote NO_x formation, leading to tradeoffs that involve both climate and air quality impacts [11, 295]. Aviation is also unique in terms of the altitude at which the emissions are released; the average cruise altitude of present-day civil aircraft is around 11 km. Out of the total of ~1.4 Tg N that was emitted by aircraft in 2019, ~1.3 Tg N were emitted at an altitude higher than 3000 ft above ground, and primarily in the northern midlatitudes (Figure 3.2). The other N_r source at high altitudes is lightning, which has been estimated to release 2–8 Tg N per year [364], with more recent estimates at ~9 Tg N per year [365]. The portion of flights below 3000 ft is defined as the landing and takeoff (LTO) phases. While only approximately a tenth of all aircraft's NO_x is emitted in LTO, these emissions are largely within the Earth's planetary boundary layer, having a more localized effect and a larger air quality impact per mass than cruise emissions, as discussed in Chapter 6 and by Ref. [1]. These LTO emissions also constitute the focus of present environmental regulations for the aviation sector (Section 2.2.4).

Recent research efforts have aimed to improve estimates of the climate and air quality impacts associated from these aviation emissions [1, 5, 11, 295]. However, as society moves towards setting sectoral budgets for controlling nitrogen emissions and associated loads in areas of ecological interest, there is also a need to extend this body of research by quantifying aviation emissions' contribution to nitrogen deposition. This chapter presents the first comprehensive quantification of aviation's global nitrogen deposition impacts. A 3-D atmospheric chemical transport model and up-to-date aircraft emissions inventories are used to quantify the aviation-attributable nitrogen deposition globally and over different land cover classes, both for LTO emissions and high altitude (cruise) emissions.

7.2 Materials and methods

7.2.1 Methods overview

The GEOS-Chem chemical transport model is used to estimate the amount and location of wet and dry nitrogen deposition due to aircraft emissions. The model is run with and without aircraft emissions, with the difference in output being attributed to them. Aircraft emissions in this study consist of a nominal estimate of main engine and auxiliary power unit emissions of NO_x, SO_x ($SO_2 + SO_4^{2-}$), CO, hydrocarbons, and black carbon. The analysis is performed for the years 2005 and 2019, with simulations using meteorology and both aviation and non-aviation emissions estimates specific to each year. Two additional scenarios are also simulated: 2019 with only the LTO portion of aircraft emissions, and 2019 but with aircraft emissions as they were in 2005, as listed in Table 7.1.

Table 7.1: Summary of scenarios tested.

Year of non-aviation emissions and meteorology	Aviation emissions	Model grid resolution	
		Global 2° × 2.5°	Nested 0.5° × 0.625°
2005	2005 full-flight	✓	✘
2019	2005 full-flight	✓	✘
2019	2019 LTO	✓	✓
2019	2019 full-flight	✓	✓

7.2.2 Aviation emissions

Monthly-average civil aircraft emission rates in 2005 and 2019 are prepared from inventories produced using the methods and data published by Simone et al. [41], and in Chapter 3, respectively. Only emissions from aircraft main engine and auxiliary power unit are considered in this study, so the terms "aviation emissions" and "aircraft emissions" are used interchangeably. The emissions are allocated into a 3-D grid at the resolution of the atmospheric simulation. The 2005 inventory is created from a worldwide database of flight schedules produced by the company OAG, and the 2019 inventory uses a dataset provided by the company Flightradar24 listing all flights recorded by their network of telemetry receivers. Within those models, NO_x, CO, and hydrocarbon emissions throughout each flight are calculated from fuel burn and engine thrust setting using the Boeing Fuel Flow Method 2 [246], and engine data from the ICAO Engine Emissions Databank [169]. Black carbon emissions use the same engine data source and the FOA 4.0 method [21]. SO_x emissions are calculated with a constant emission index equivalent to a sulfur fuel content of 600 ppm. The annual sums of nitrogen in aircraft NO_x emissions is 0.82 Tg N (2005) and 1.41 Tg N (2019).

7.2.3 Atmospheric modeling

Global atmospheric photochemistry and transport are simulated with the GEOS-Chem 13.3.3 model [350], using the stratospheric chemistry model developed by Eastham et al.

[315], and driven by meteorology from the MERRA-2 reanalysis product [268]. Transport and convection are simulated at 10-min time steps, and chemistry and emissions at 20-min steps. Global simulations are performed at 2° latitude and 2.5° longitude resolution. For the 2019 scenarios, simulations are also performed using three 0.5° × 0.625° nested grids over Asia, Europe, and North America. Results from the nested grids are overlaid over the output from the coarser global simulation which provides boundary conditions for the regional simulations, improving the allocation of deposition into the different land cover types in the regions with highest airport activity. The boundaries of these nested domains are the same as those used in Chapters 5 and 6, shown again in Figure 7.1 along with the aircraft NO_x emissions used for 2019. The model is initialized by a 21-month spin-up run at 4° × 5° resolution followed by 3 months of spin-up at the final global resolution of 2° × 2.5°.

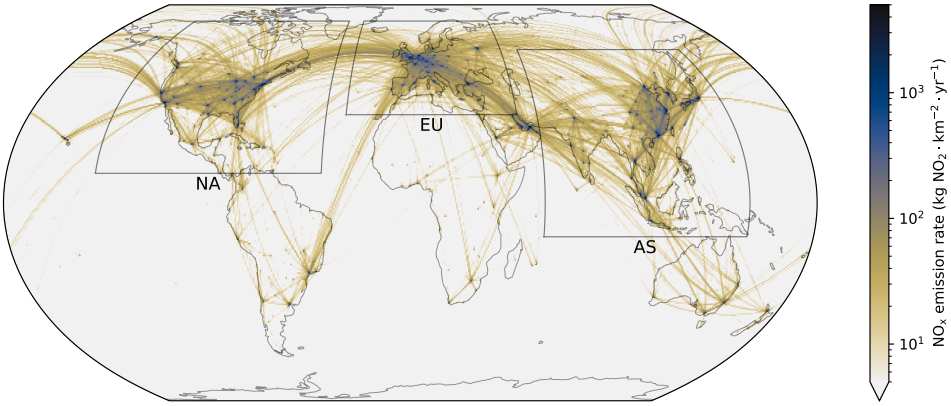

Figure 7.1: Vertically summed full-flight aircraft NO_x emission rates in 2019, and the boundaries of the three nested domains that are simulated in GEOS-Chem at higher resolution.

GEOS-Chem models sulfate-nitrate-ammonium aerosol coupled with gaseous chemistry as described by Park et al. [355], using the ISORROPIA thermodynamic module [191]. Heterogeneous chemistry of reactive nitrogen is modeled as described by Holmes et al. [366], and uses coefficients from McDuffie et al. [367, 368]. Aerosol hygroscopicity is based on Latimer and Martin [369], and cloud acidity on Shah et al. [370]. In-cloud aqueous-phase chemistry is modeled as described by Chin et al. [371], with wet deposition through rainout and washout of water-soluble aerosol [372] and gases [373]. The constants used for Henry's law are from Sander [374]. Modeling of aerosol scavenging by snow and cold clouds is described by Wang et al. [375, 376]. Dry deposition is modeled as a resistance-in-series scheme [377, 378], with parametrizations for aerosol deposition [379–381]. Low temperature dry deposition of HNO_3 is modeled according to Jaeglé et al. [382].

Nitrogen deposition is considered in the form of the following simulated species: NO_x, HNO_3, inorganic nitrates (NO_3^-), inorganic nitrates on sea salt aerosol, NH_4^+, NH_3, N_2O_5, and peroxyacetyl nitrate. Non-aviation anthropogenic emissions are from the CEDS v2 inventory, which includes the agriculture, energy, industry, surface transportation, residen-

tial, shipping, and waste sectors [356]. Soil NO_x, sea salt aerosols, and biogenic volatile organic compounds are calculated according to meteorological conditions [383]. Lightning emissions are parametrized from modeled convection and corrected using satellite flash rate data [384].

Because the results obtained are inherently limited by GEOS-Chem's ability to reproduce observed nitrogen deposition values, an evaluation is performed of GEOS-Chem against available wet and dry deposition measurements for 2005 and 2019 from North America, Europe, and Asia. Modeled annual nitrogen deposition rates, resulting from emissions from all sources, are compared to observations from the networks of ground-level measurement stations listed ahead.

- Wet deposition:

– National Trends Network by the National Atmospheric Deposition Program (NADP) covering the United States plus a few stations in Canada [385].
– European Monitoring and Evaluation Program (EMEP) covering Europe [386, 387].
– Acid Deposition Monitoring Network in East Asia (EANET) covering (mostly East) Asia [388, 389].

- Dry and total deposition:

– Clean Air Status and Trends Network (CASTNET) covering the United States [390].
– Acid Deposition Monitoring Network in East Asia (EANET) covering Japan, only for 2019 [389].

The location of the stations is shown in Appendix D.3. EMEP stations reporting less than 80% data availability are discarded from analysis (6 out of 85 stations in 2019, and none in 2005), and all stations from the other datasets that report annual average deposition rates are included. Each station is compared to the simulation values of the grid vertical column on which the station is located, with no interpolation of neighboring cells.

7.2.4 Land cover and conservation areas

Average deposition fluxes are calculated for different land cover classes, according to the Copernicus global land cover product for 2019 [391]. Areas not covered by the Copernicus dataset are disregarded in the analysis; this consists mainly of all the areas north of 80 °N and south of 60 °S. From this 100 m resolution land cover data, the fraction of each grid cell that contains each class of land cover is calculated. Likewise, the percentage of each grid's area that lies in Natura 2000 sites, protected either through the Birds Directive or the Habitats Directive, is calculated from the 2019 definitions of the protected areas, as shown in Figure 7.2 [392]. The analysis considering Natura 2000 sites is only performed for the scenarios that include the 0.5° × 0.625° resolution simulation over Europe.

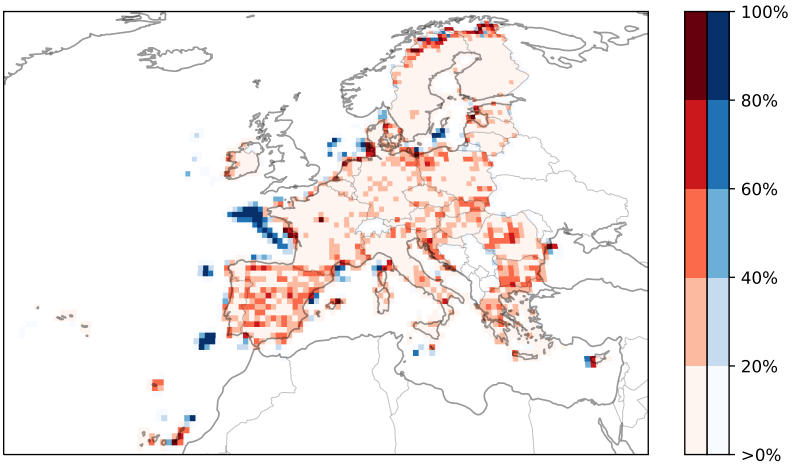

Figure 7.2: Fraction of grid cell area that lies within protected Natura 2000 sites [392]. Red grid cells are counted as (populated) land within EU countries.

7.3 Results and discussion

7.3.1 Comparison to nitrogen deposition measurement networks

Individual station results for wet deposition are shown in Figure 7.3 (2005) and Figure 7.4 (2019), and for dry deposition in Figure 7.5. Statistical summaries of comparisons of each measurement dataset with modeled results are given in Appendix D.3, and Table 7.2 gives comparisons combining all stations from different regions.

For most species and regions, the simulations show a bias toward more central values, which is expected to some extent when comparing a point measurement with a grid cell that serves as an average over a large area. The GEOS-Chem results match the observations more closely in North America, which is consistent with findings from previous studies [46, 393, 394]. The correlation between modeled and observed dry deposition rates is lower than for wet deposition, consistent with previous results [393]. There are additional challenges associated with the measurement and modeling of dry deposition which might lead to worse model performance [140]. The "observed" dry deposition values in this analysis are actually obtained by an inferential method, that considers deposition as the product of measured concentrations in the air with dry deposition velocities modeled using parametrizations based on the station's surroundings and measured local meteorological conditions. There are also fewer measured data points for the comparisons of dry deposition in this study, with only 8 stations in Japan reporting data outside of the United States.

The resulting model biases are between −20% and +29% for wet deposition (Table 7.2). For the three datasets that also included dry deposition estimates, dry deposition has biases of +7%, 0%, and +104%, and total (wet + dry) deposition biases of +4%, 0%, and +51%. Combining all measurements for 2019, the model shows a +2.5% bias in total deposition. The inclusion of higher resolution nested simulations did not reduce this bias compared

to measurements (the bias of just the coarse resolution global simulation is +2.2%). While it is chosen not to incorporate these biases in the results presented in this chapter, in line with other work [46], note that there might nitrogen deposition might be overestimated or underestimated in different regions. These biases could be carried over in the aviation-attributable nitrogen deposition estimates, for which there are no measurements to validate against. However, this is not expected to influence the relative results on the contribution of high-altitude emissions to nitrogen deposition.

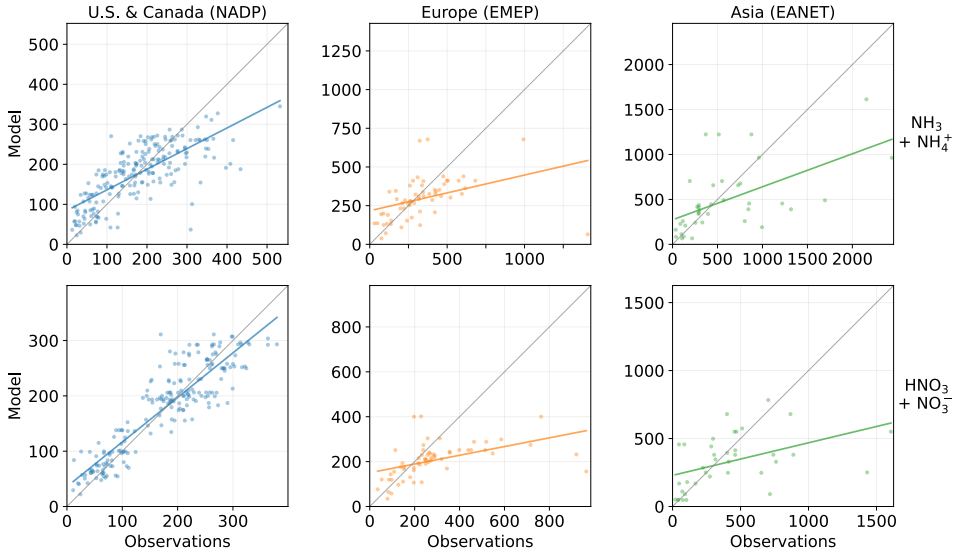

Figure 7.3: Modeled and observed average wet nitrogen deposition rates in 2005, in $kg N \cdot km^{-2} \cdot yr^{-1}$, per region (columns) and species (rows).

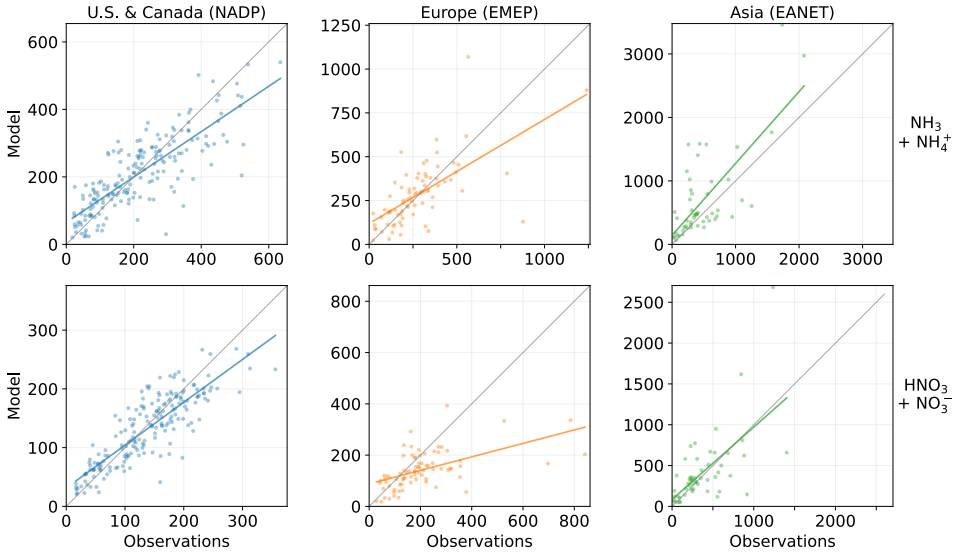

Figure 7.4: Modeled and observed average wet nitrogen deposition rates in 2019, in kg N·km^{-2}·yr^{-1}, per region (columns) and species (rows).

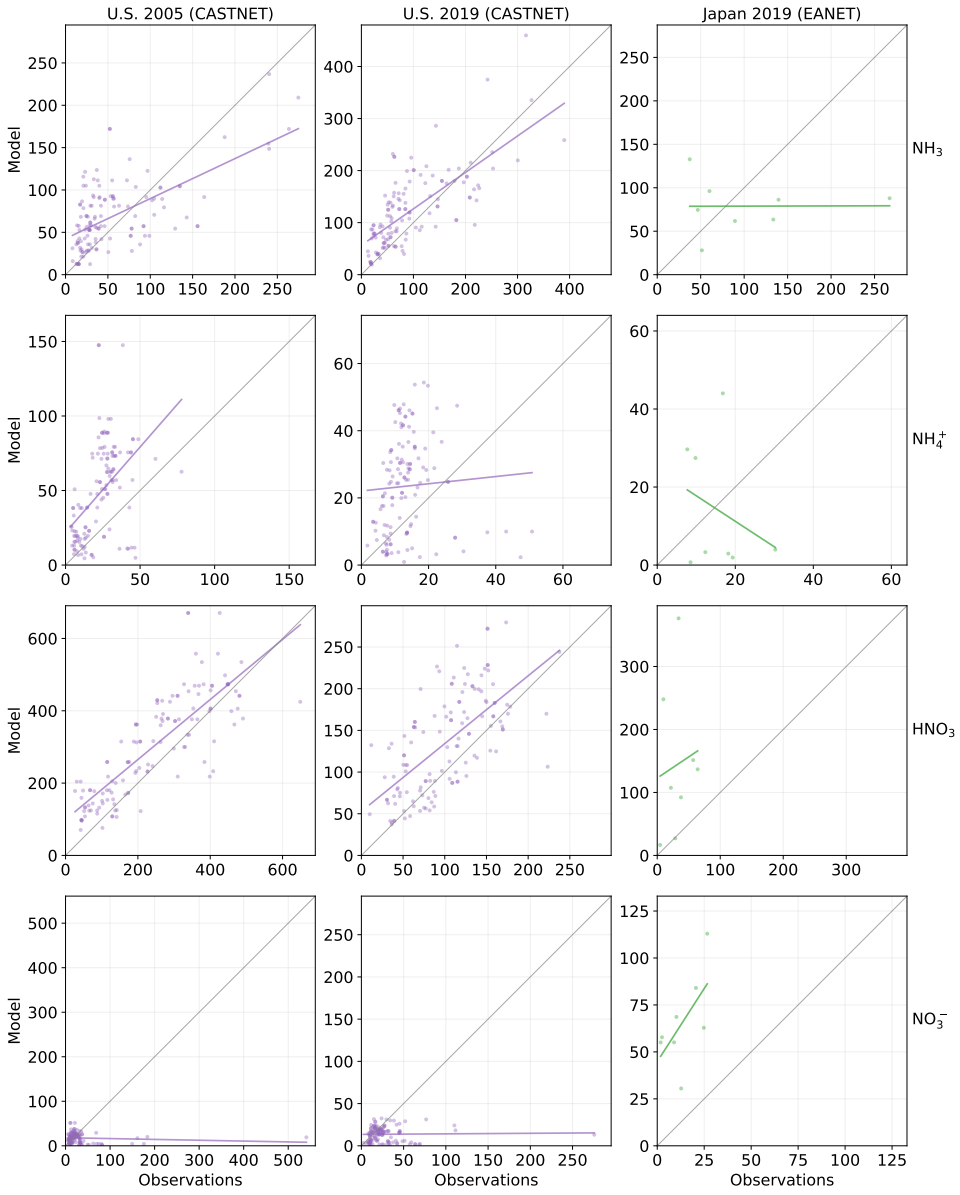

Figure 7.5: Modeled and observed average dry nitrogen deposition rates, in $kg\,N{\cdot}km^{-2}{\cdot}yr^{-1}$, per region and year (columns) and species (rows).

Table 7.2: Comparison of modeled (M) against observed (O) [385–390] annual average dry and wet + dry nitrogen deposition rates from all species ($kgN \cdot km^{-2} \cdot yr^{-1}$), per year, combining all measurement stations from different regions.

	Wet			Dry			Wet + Dry N		
	2005	2019		2005	2019		2005	2019	
Measurement coverage	U.S. Canada Europe Asia	U.S. Canada Europe Asia		U.S.	U.S. Japan		U.S.	U.S. Japan	
Number of stations	301	318		132	140		132	140	
Mean (O)	488	469		494	337		860	689	
Standard deviation (O)	418	388		267	175		399	321	
Nested model results	✘	✘	✓	✘	✘	✓	✘	✘	✓
Mean (M)	441	425	489	528	357	346	897	704	706
Standard deviation (M)	285	342	538	221	134	139	353	270	292
Mean bias	−47.2	−44.0	19.6	34.6	19.4	8.84	37.2	14.9	17.2
Mean error	150	145	162	127	92.5	91.9	168	143	138
RMS error	292	250	325	170	128	133	216	189	207
Normalized mean bias	−9.7%	−9.4%	4.2%	7.0%	5.8%	2.6%	4.3%	2.2%	2.5%
Normalized mean error	30.7%	30.9%	34.6%	25.7%	27.4%	27.2%	19.6%	20.7%	20.0%
Correlation coefficient	0.72	0.78	0.8	0.78	0.69	0.66	0.85	0.81	0.78
Index of agreement	0.67	0.69	0.68	0.70	0.65	0.65	0.75	0.72	0.73

7.3.2 Quantification of aviation-attributable nitrogen deposition

Throughout 2019, aircraft emissions led to additional 1.39 Tg N of nitrogen wet + dry deposition globally, which is 1.13% of total modeled deposition. While certain areas might be net importers or exporters of N_r due to transport [43, 395, 396], the increase in global deposition is equal to 99.0% of the amount of N_r mass released by aviation that year. In both 2005 and 2019, wet deposition accounts for approximately 67% of total nitrogen deposition from aviation. Total aviation-attributable nitrogen deposition in 2019 is 72% larger than in 2005 (0.81 Tg N), in the same proportion as aircraft emissions, which increased an average of 4% per year in this period. By contrast, global anthropogenic NO_x emissions in 2019, other than aviation, were only 7.5% higher than in 2005. Given the long useful life remaining in the present fleet of conventionally powered aircraft, aviation emissions will likely continue to increase for decades if air traffic grows as projected in Chapter 4, with the sector being responsible for a growing share of anthropogenic nitrogen deposition worldwide. The potential adoption of sustainable aviation fuels, currently being pursued to reduce net carbon emissions, is unlikely to lead to changes in aviation NO_x emissions [306].

This deposition, however, does not occur uniformly over the globe's surface, nor does it match the spatial or speciated distribution of emissions. The highest fluxes of aviation-attributable nitrogen deposition are close to the regions of highest aviation activity (the coasts of North America, Europe, and Eastern Asia), but the high values extend out following the prevailing winds and in regions of heavy precipitation, as seen in the Atlantic off the coast of North America, and in waters west of China and Japan (Figure 7.6a). Although the absolute amount of aviation-attributable deposition is lower over the oceans than in the continents, the share of modeled nitrogen deposition that is due to aviation is higher there, where there are fewer other sources of emission besides aircraft (Figure 7.6b). It is expected that the further away from continents, the larger is the percentage of nitrogen deposition that is due to non-land emissions, which also include oceanic NH_3 and shipping NO_x [397, 398]. Considering only populated grid cells (i.e. including only land, Figure D.1) [357], aviation is responsible for 0.66%, 1.13%, and 1.61% of all modeled nitrogen deposition averaged over Asia, Europe, and North America, respectively. Locally, this contribution can be up to 10%, in Greenland, where other sources of nitrogen are less significant.

Over land with high aviation activity, LTO emissions account for more than 16% of total nitrogen deposition from aviation, even though globally LTO contributes to 7.8% of aviation's nitrogen deposition impacts (Figure 7.6c). Compared to full-flight emissions, a larger fraction of deposition due to LTO emissions occurs as dry deposition, 50% (Figure 7.7). This is expected due to the closer proximity of emissions to the ground, leading to more of the nitrogen to deposit through dry processes before water precipitation takes place.

The three simulations with full-flight emissions (2005, 2019, and 2005 aviation with 2019 background), in addition to having similar ratios of wet and dry deposition, also show similar distributions of (aviation-attributable) species deposited, once normalized by the extra amount of N_r emitted (Figure 2). The proportionality of aviation-attributable total N_r mass deposited to NO_x emissions is a consequence of this species being the main responsible for the deposition and the linearity of their relationship, with the response to non-N_r emissions expected to be more nonlinear [397]. In all scenarios, most of the ni-

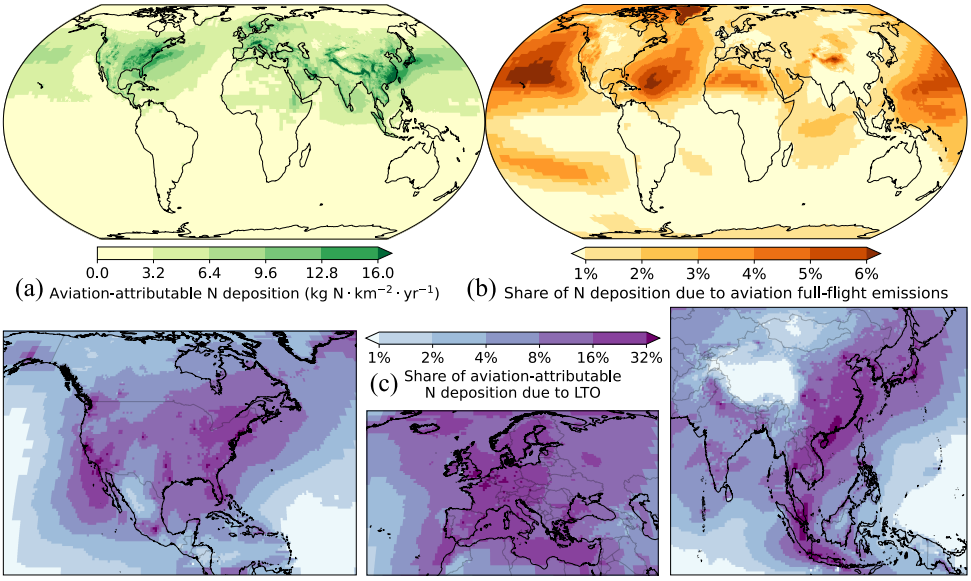

Figure 7.6: Aviation-attributable total (wet + dry) nitrogen deposition in 2019: flux (a), relative to deposition from all sources (b), LTO-attributable relative to deposition from full-flight emissions (c).

trogen is deposited as HNO_3. A smaller fraction is deposited as inorganic nitrates, either aggregated on sea salt or dissolved in water precipitation. The aviation-induced increase in NH_4^+ + deposition is matched by a decrease in NH_3 deposition, as the HNO_3 formed from NO_x released by aircraft reacts with NH_3 already present in the atmosphere, released by other sources, to form ammonium nitrate. This also drives the difference in the speciated distribution of the nitrogen deposition of 2005 full-flight emissions in a 2005 and a 2019 atmosphere (two bottom rows in Figure 2). Primarily driven by non-aviation emissions changes, the "potential" of NO_x emissions to form fine particulate matter ($PM_{2.5}$) increases from 2005 to 2019, as discussed in Chapters 3 and 5 and by Refs. [231, 332]. Increases in the background concentration of NH_3 and lower emissions of NO_x from other sources can increase the sensitivity of ground-level particulate matter to aviation emissions, affecting the form in which reactive nitrogen from aviation will deposit [313]. Attribution to specific aircraft emissions species was not evaluated in this study, but the speciation of nitrogen deposition obtained is consistent with NO_x being the main driver of these impacts, as is also suggested by previous findings that most of aviation-attributable ground-level particulate matter is due to its NO_x emissions [187, 211].

7.3.3 Aviation-attributable nitrogen deposition per land cover type and on Natura 2000 areas

Environmental policies aim to reduce excessive nitrogen deposition over areas with ecosystems sensitive to it, such as Natura 2000 sites, and therefore a quantification of aviation's impacts also requires an estimate of how much nitrogen is deposited on vulnerable areas. Due to the extensive area covered by flights and their altitude, with most

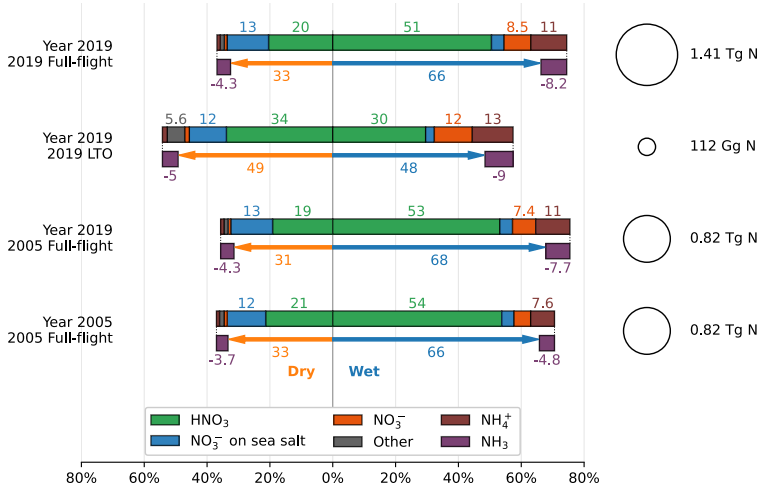

Figure 7.7: Mass of aviation-attributable nitrogen deposited globally, per species, relative to the nitrogen mass emitted by aviation as NO_x, which is indicated by the quantities on the right.

emissions released above the planetary boundary layer, NO_x emitted by aircraft tends to have more widespread impacts than that emitted by sources closer to the ground. In the 2019 simulation, 38% of nitrogen from all sources is deposited over water, while 43% and 56% of nitrogen attributable to LTO and full-flight emissions, respectively, do so (Table 7.3). Within land areas, LTO impacts are more concentrated on urban areas (2.1% of global deposition due to LTO emissions) than impacts from full-flight emissions (0.8%) and from all sources (1.4%). The global average of aviation-attributable nitrogen deposition flux over land are 0.46% (2005) and 0.80% (2019) of the fluxes from all sources in those areas. These global values are lower than the averages for regions with higher aviation activity, such as 1.61% over populated grid cells in North America in 2019. Despite the global sum of aviation-attributable nitrogen deposition increasing by 72% between 2005 and 2019, and despite different growth rates of aircraft emissions per region, the fraction of deposition over each land cover class remained similar. The use of nested simulations to increase resolution over North America, Europe, and Asia had some effect on the distribution of aviation-attributable nitrogen deposition per land cover class, most notably increasing deposition on urban areas due to LTO emissions by 13% (Appendix D.5), as the concentrated effects around airports from those emissions are better resolved.

Throughout 2019, aviation led to an average increase of 7.40 kg N·km^2 in nitrogen deposition on Natura 2000 conservation sites, with 1.38 kg N·km^2 being due to LTO emissions (Table 7.4). Aviation is responsible for an average of 1.0% of nitrogen deposition from all sources in those areas. The ratios between the average aviation-attributable nitrogen deposition fluxes over Natura 2000 sites on land with the averages over all European land of members of the European Union are 0.977 for full-flight emissions and 0.946 for LTO emissions[2], meaning that the impacts are only marginally smaller in Natura 2000 regions

[2]Correction of values published in the paper (0.973 and 0.941)

than in other areas of the EU. Besides the spatially widespread nature of nitrogen deposition caused by aviation, this may also be partially attributed to the spatial coarseness of the model used (with grid cells in the region having sides of roughly between 25–55 km), which does not resolve small features such as the borders of these conservation areas. This analysis is made considering global aircraft emissions, but future work could highlight emissions from specific sources or locations that have the highest impact on ecologically vulnerable areas [397].

7.3.4 Limitations

This study focuses on the impacts associated with inorganic nitrogen deposition, as this has been shown to be responsible for over 85% of anthropogenic nitrogen deposition impacts [45], although organic nitrogen deposition may be growing [399]. Only impacts associated with aircraft activity are evaluated, including the use of the auxiliary power units at the airports, and the use of ground support equipment and other airport-related operations are not accounted for. As the amount of aviation-attributable nitrogen deposition is directly proportional to NO_x emissions, the magnitude of this impact depends on the accuracy of emission estimation. The 12% higher top-down estimate of global fuel burn based on jet fuel sale data, which also include military uses, compared to the bottom-up estimate used here is indicative of the combined uncertainty in fuel burn estimation (Section 3.3). The accuracy in the fleet-average NO_x emission index is dependent on the uncertainty in assigning the correct engine model to each aircraft, and in the uncertainty in the emission measurements for each engine and the difference between them and performance in operation, including inaccuracies in the correction for atmospheric conditions. Finally, future work could address the ecosystem implications of the aviation-attributable nitrogen deposition, given that the different nitrogen forms deposited will be affecting ecosystems in different ways and magnitudes [46, 400, 401].

Table 7.3: Proportion of nitrogen mass of each emissions scenario deposited on each land cover class from all sources in 2019 and from aircraft emissions for the four scenarios considered.

Land cover class	Percentage of total area considered	Percentage of total nitrogen mass deposited				
		All sources in 2019	LTO emissions in 2019	Full-flight emissions in 2019	2005 full-flight emissions in 2019	Full-flight emissions in 2005
Urban / built up	0.3	1.4	2.1	0.8	0.8	0.8
Cultivated and managed vegetation	3.2	14.3	11.5	7.0	6.9	7.2
Closed forest	7.7	21.0	20.5	13.2	12.4	12.8
Open forest	2.8	7.6	6.8	4.5	4.3	4.5
Shrubs	2.4	3.4	2.5	2.6	2.7	2.7
Herbaceous vegetation	6.0	9.3	6.8	7.8	7.7	7.4
Herbaceous wetland	0.5	0.8	0.7	0.6	0.6	0.6
Moss and lichen	0.3	0.1	0.1	0.1	0.1	0.1
Bare / sparse vegetation	4.3	3.9	5.6	6.8	6.7	6.2
Snow and ice	0.4	0.2	0.2	0.3	0.3	0.3
Permanent water bodies	0.7	1.2	1.4	1.0	1.1	1.1
Open sea	71.6	37.1	41.7	55.3	56.4	56.3
All land classes	27.8	61.7	56.9	43.7	42.5	42.6
All water classes	72.2	38.3	43.1	56.3	57.5	57.4
Natura 2000	0.2	0.70	1.54	0.65	n/a[a]	n/a[a]

[a] Deposition over Natura 2000 sites is only evaluated for the finer resolution simulations.

Table 7.4: Average nitrogen deposition flux over different land cover classes from all sources in 2019 and from aircraft emissions for the four scenarios considered.

Land cover class	Area ($10 \cdot 10^6$ km^2)	Average nitrogen deposition flux ($\mathrm{kg\,N \cdot km^{-2} \cdot yr^{-1}}$)				
		All sources in 2019	LTO emissions in 2019	Full-flight emissions in 2019	2005 full-flight emissions in 2019	Full-flight emissions in 2005
Urban / built up	1.2	1397	1.95	9.15	5.14	5.54
Cultivated and managed vegetation	14.9	1169	0.84	6.52	3.77	3.93
Closed forest	36.4	703	0.61	5.04	2.76	2.84
Open forest	13.2	703	0.56	4.69	2.66	2.75
Shrubs	11.2	365	0.24	3.22	1.95	1.95
Herbaceous vegetation	28.4	400	0.26	3.81	2.18	2.10
Herbaceous wetland	2.3	422	0.34	3.35	1.97	1.96
Moss and lichen	1.4	48	0.06	1.36	0.76	0.69
Bare / sparse vegetation	20.3	232	0.30	4.60	2.68	2.48
Snow and ice	2.0	98	0.11	2.43	1.28	1.15
Permanent water bodies	3.2	457	0.49	4.45	2.72	2.88
Open sea	338.5	134	0.13	2.26	1.35	1.34
All land classes	131.2	574	0.47	4.61	2.62	2.62
All water classes	341.7	137	0.14	2.28	1.36	1.36
Natura 2000	1.2	705	1.38	7.40	n/a[a]	n/a[a]

[a] Deposition over Natura 2000 sites is only evaluated for the finer resolution simulations.

7.3.5 Conclusions

Overall, it is found that aviation NO_x emissions contribute 1.39 Tg N (or 1.13%) of global nitrogen deposition. LTO emissions are responsible for 8.0% of those global impacts, but regionally this can be up to 30% for areas with dense air traffic (specifically landing and takeoff operations), such as Europe and North America. The majority (73–75%) of deposited nitrogen mass associated with aircraft emissions is in the form of HNO_3, with aircraft emissions resulting in a reduction in the mass of NH_3 deposition, and an increase in the mass of deposited NH_4^+. A larger portion of deposition from full-flight (55%) and LTO (42%) occur over open seas, which are largely not targeted by current environmental protection policies, then the all-source average in the model (37%), suggesting a relatively lower impact intensity of emissions from aviation due to their spatial distribution. The non-local reach of aviation's nitrogen deposition impacts observed in the results, exemplified by similar deposition rates in Natura 2000 sites compared to adjacent areas, as well as the transnational nature of air travel, pose challenges in the implementation of local policies aiming to protect vulnerable areas. Present aviation NO_x emissions controls, such as those by ICAO CAEP, focus on the LTO phase and are primarily motivated by controlling local air quality around airports. Multiple modeling studies indicate that high altitude emissions, relative to LTO emissions, contribute to 3–9 times more to aviation's impacts on global air quality and human health, much in line with what is also found for nitrogen deposition in this work. Efforts to control nitrogen deposition on a global scale would benefit from addressing full-flight aviation emissions. However, it should be noted that similarly with air quality impacts, the nitrogen deposition improvements will not necessarily be close to airports. Even surface level emissions result in impacts far from their emission location [201, 332]. This is already acknowledged in a policy context, as significant nitrogen is imported from country to country.

7.4 Data availability

The nitrogen deposition rate data resulting from the simulations are available under the following data repository DOI: 10.4121/20359683.

7.5 Acknowledgments

This work made use of the Dutch national e-infrastructure with the support of the SURF Cooperative using grant no. EINF-3690.

8

Conclusions and outlook

Whereas there are growing concerns about the impact of aviation on the atmosphere with respect to local air quality and the associated human health and welfare impacts;

Whereas the evidence of this impact from emissions of NO_x and particulate matter (PM) from aircraft engines on local surface and regional air quality is now more compelling;

ICAO Assembly[1]

8.1 Conclusions

Conclusions obtained from the studies described in Chapters 3 to 7 are summarized here, organized by the research objectives of the thesis, which are also listed in Section 1.2.

Quantify present-day global civil aircraft emissions, with three-dimensional spatial resolution.

Commercial aircraft telemetry receiver networks, such as Flightradar24, are already widespread enough that global bottom-up emissions inventories produced from this data source can be more comprehensive than inventories produced from (commercially acquired) flight schedule data, as was done previously. This allowed a more up-to-date quantification of civil aircraft emissions (Chapter 3), including the first quantification of then recent impacts on emissions due to the COVID-19 pandemic, in the year 2020. This improved readiness of data can be useful in future efforts to continuously monitor the aviation sector's progress in limiting its emissions. The non-commercial OpenSky network yielded adequate results in specific regions, but its use for comprehensive global inventories is precluded by limited coverage in some areas of the world, although coverage has

[1]Resolution A41-20: Consolidated statement of continuing ICAO policies and practices related to environmental protection — General provisions, noise and local air quality. Appendix H: Aviation impact on local air quality. 41st Session of the ICAO Assembly, (2022).

increased over the years, and limited by an incomplete database listing aircraft type for each unique transponder identification code.

Results showed that aircraft fuel burn increased globally by 55% between 2005 and 2018, and that the average emission index of NO_x increased over time, by 3.3% from 2015 to 2019. Relative fuel burn increases across the years varied significantly between different regions, with rapid growth in Asia compared to slower growth in Europe and North America. This scenario changed abruptly in February of 2020, when restrictions associated with the COVID-19 pandemic reduced fuel burn from flights departing China to less than 40% of what they were a year prior. Reductions down to less than 20% in other regions followed towards April 2020, with recovery through the rest of the year also varying on a regional basis. Emissions quantification showed that reductions in emissions associated with the pandemic were not uniform not only spatially, with relatively higher usage of widebody aircraft and a larger percentage of fuel burn occurring during landing and take-off operations (LTO). Overall, it was estimated that global aircraft fuel consumption over the year of 2020 was 48% lower than what would be expected had growth trends not been affected by the pandemic.

Sensitivity analysis revealed that there is a large uncertainty in emissions quantification associated with the specific engine model used for each aircraft, as different models available for the same aircraft type can have emission rates of different orders of magnitude, and this uncertainty has not been discussed in previous studies. An additional conclusion is that although aircraft auxiliary power units (APU) burn 7% of fuel from LTO, they were estimated to account for 34% (mass) and 25% (number) of nonvolatile particulate matter in those phases of flight, being potentially attractive targets for measures to improve air quality within and surrounding airports. However, data availability on APU running times and emission indices is worse than for aircraft main engines.

Project global civil aircraft emissions to the year 2040, maintaining spatial resolution.

By modeling multiple parameters affecting the evolution of global aircraft NO_x emissions up to the year 2050, it was found that even in a "low" aircraft emissions scenario global fuel burn and NO_x emissions are expected to continue to increase (Chapter 4). The combination of air traffic growth and increasing engine overall pressure ratio of new aircraft dominate over reductions expected due to technological and operational improvements, with a net effect of NO_x emissions more than doubling between 2018 and 2050 in the baseline scenario. Besides the large traffic growth expected, the total amount of NO_x emitted during the 2027–2050 period was also found to be sensitive to the expected reductions in EI (NO_x) due to technological improvements, with the emissions amount being 48% higher if no such reductions were considered. Additionally, NO_x emitted over the 2027–2050 period was sensitive to the projection of engine pressure ratio, being 23% lower if no increases relative to present ratios were considered.

These results highlight the importance of the role of engine design in the evolution of global aircraft NO_x emissions over the next three decades. The current format of regulatory emissions requirements, in which limits increase with overall engine pressure ratio, allows for emissions per aircraft to increase while still meeting the standard. This, com-

bined with the tradeoff between NO_x and CO_2 emissions, poses a challenge to goals of reduction in aircraft NO_x emissions.

Estimate the differences in the sensitivity of air quality to aircraft emissions according to the source and receptor world regions.

Atmospheric simulations were performed with perturbations in aircraft emissions separately over Asia, Europe, and North America, allowing for air quality and human health impacts to be isolated per regional source-receptor pairs (Chapter 5). According to the results of these global simulations, most air quality and human health impacts from aircraft operation are due to non-LTO emissions, which account for 83–89% of health impacts for the same region as source-receptor, and 92–98% of global health impacts caused by emissions over each region. 73% and 88% of premature mortality caused by aircraft emissions over Europe and North America, respectively, occurs outside the region of emission, such that most of the benefits from reductions in emissions in those regions would be felt elsewhere. For all perturbation scenarios, the majority of health impacts took place in Asia, primarily driven by its larger population count.

Higher sensitivity of $PM_{2.5}$ to full-flight emissions was associated with availability of ammonia to react with NO_x, as evaluated by the gas ratio metric. Higher ozone sensitivity to LTO emissions was associated with higher ratios of formaldehyde to NO_y. The sensitivity of global health impacts to full-flight emissions was found to be 45–50% higher for emissions released over Europe compared to over Asia and North America, highlighting that the same amount of emissions can have impacts of significantly different magnitudes depending on where they are released. The higher sensitivity of impacts to emissions over Europe is consistent with the "favorable" conditions of westerly prevailing winds transporting cruise emissions from Europe to Asia, and higher ammonia availability in Europe compared to the other regions. The overall conclusion from this study is that the spatial distribution of aircraft emissions and population, emissions from other sectors, and atmospheric transport patterns need to be carefully considered in order to evaluate the environmental cost of aviation activities, or the benefits of potential mitigating actions, particularly in the context of spatially heterogeneous scenarios.

Quantify the present-day global air quality and associated human health impact of aircraft emissions.

Previous studies in the literature had made estimates of the global air quality and human health impacts from aviation in the past, when both aviation and non-aviation emissions were significantly different. Combining an atmospheric chemical transport model with the up-to-date aircraft emissions inventory developed in Chapter 3, those impacts were quantified for the year 2019 in Chapter 6. Aircraft emissions were found to be responsible for 0.3%, 1.8%, and 0.3% of global population exposure to $PM_{2.5}$, (peak-season) ozone, and NO_2 from all sources. For the concentration-response functions (CRF) adopted, this exposure to pollution is estimated to lead to 116 100 additional annual deaths. The magnitude of health impacts are sensitive to the choice of CRF, such that the relative importance of the three pollutants to the total health impacts is also sensitive to that choice, with this

study finding that two thirds of impacts come from ozone exposure, compared to previous studies that estimated that most aviation-attributable health impacts are due to $PM_{2.5}$. This uncertainty also carries over to the relative importance of phases of flight to health impacts, as LTO disproportionately impacts $PM_{2.5}$ more, while non-LTO impacts ozone more. Health impacts of aircraft-attributable NO_2, which were not considered in previous global studies, was estimated to be of similar magnitude to impacts from the other two pollutants when considering only LTO emissions. While low-altitude emissions near airports increase NO_2 locally, high-altitude emissions cause a spatially widespread decrease in ground-level NO_2 concentrations. The higher resolution simulations suggest that the effect of full-flight emissions is a net global increase in NO_2 exposure, in contrary to the coarser resolution results, but further work could provide a more robust conclusion in that regard.

Regardless of systematic biases in health impact estimation, air quality impacts attributed to air travel have increased over time (compared to 2005), consistent with the increase in the amount of aircraft emissions. Between the two years, it was also found that sensitivity of ground-level $PM_{2.5}$ and NO_2 to aircraft emissions increased, while sensitivity of ground-level ozone decreased. The changing (2005 to 2019) spatial distribution of aircraft emissions has a net negative impact on the sensitivity of exposure to the amount of NO_x emitted, as proportionately less emissions are released over Europe, where their global effects would have higher intensity. The results obtained suggest that a potential large scale worldwide deployment of sustainable aviation fuels would have only limited effect on global health impacts from full-flight emissions, as 86% of mortalities due to $PM_{2.5}$ and 98–100% due to ozone and NO_2 are attributed to NO_x emissions, which are not expected to change significantly with this change of fuel.

Compare how different future atmospheric scenarios can be expected to change the global air quality impacts from aircraft emissions.

Atmospheric simulations were performed to evaluate air quality impacts from aviation under different scenarios for the year 2040 (Chapter 6). The sensitivity of air quality to aircraft full-flight emissions changes across different future scenarios of non-aviation atmospheric emissions, with larger changes occurring in impacts on $PM_{2.5}$ and NO_2 compared to ozone. Depending on the future scenario and pollutant considered, global population exposure sensitivity to aircraft emissions may either increase or decrease relative to the present day. Changes in air quality sensitivity between different future scenarios are also not uniform spatially, without a consistent pattern of less/more polluted scenarios being more/less sensitive. Changing non-aviation emissions was found to affect LTO-attributable global exposure to $PM_{2.5}$ and ozone more than exposure to NO_2. These results are consistent with the hypothesis that impacts that depend more on nonlinear chemistry in the near-surface atmosphere are more affected by changes in non-aviation emissions, which are almost exclusively released at ground-level.

Overall, different non-aviation emissions led to total global health impacts due to $PM_{2.5}$, ozone, and NO_2 attributed to full-flight emissions varying from −1% to +5% relative to a baseline case. These values would be higher if a different choice of CRF reduced the share of mortality attributed to ozone exposure. Across the various scenarios evaluated, impacts increased with the amount of aircraft NO_x released. Compared to changing

scenarios of non-aviation emissions, a larger range of total aircraft-attributable mortality was observed across the different future aircraft emissions scenarios considered: −27% to +23% relative to the baseline. The effect on aviation's global air quality impacts of different meteorological fields, generated under different climate change scenarios, was found to be smaller than the effect of different non-aviation emissions. Although aircraft-attributable exposure was affected more than exposure to background pollution, which is consistent with the hypothesis that air quality impacts from aviation are more sensitive to weather conditions due to their higher altitude.

Estimate the spatial distribution of present-day global nitrogen deposition attributable to aircraft emissions.

From the atmospheric simulations performed, it was estimated that aircraft NO_x emissions are responsible for 1.1% of global nitrogen deposition, including both natural and anthropogenic sources of emission (Chapter 7). The inclusion of aircraft emissions in the model results in an additional amount of deposition of reactive nitrogen that is 99% of the mass of emissions, as the only significant atmospheric sinks for it (as modeled) are through deposition. Therefore, non-LTO phases of flight account for the majority of aircraft-attributable nitrogen deposition, estimated here at ~92%, matching the percentage of full-flight NO_x emissions in non-LTO. Because of the high altitude and wide geographical span of release, these emissions cause spatially widespread deposition, making aviation a more significant contributor to deposition in remote regions such as over the oceans and over large deserts. This is exemplified by the finding that 55% of deposition attributed to full-flight emissions occur on open seas, which, even if not targeted by environmental protection policies, are still affected by eutrophication, acidification, and deoxygenation; all of which are problems driven in part by nitrogen deposition from combustion emissions. Most benefits (with regard to nitrogen deposition) from potential reductions in aviation emissions are not going to occur close to airports, and not even necessarily within the countries of flight origin and destination. Accurate evaluation of aviation-attributable over vulnerable natural areas requires higher resolution (more local) atmospheric and emissions modeling, such that for example the contribution of LTO emissions to nitrogen deposition within specific Natura 2000 areas in Europe cannot be accurately quantified with the global modeling performed. Because the amount of deposition is proportional to NO_x emissions, aviation is contribution to this issue is expected to continue to increase for at least the next few decades.

8.2 Outlook

The civil aviation industry has grown continuously since the beginning of the jet age, and this is reflected on the amount of atmospheric emissions it releases. At the same time, scientific knowledge on the various environmental impacts these emissions have has expanded. In addition to climate forcing, these impacts also include air quality degradation and excessive nitrogen deposition, as studied in this thesis. Especially as air traffic and its associated emissions are expected to continue to increase in the foreseeable future, motivation for research on the environmental footprint of aviation should increase accordingly. This thesis contributed to this by both providing an up-to-date picture of air quality and

nitrogen deposition impacts from aviation and by modeling a wide range of future scenarios using consistent methods, which enables the estimation of the uncertainty associated with different factors involved in projecting aviation's impacts.

Historically, air quality has been treated as a local issue. Despite the global nature of air transport, the sector still treats air quality as local, as evidenced by the stated three cores areas of the International Civil Aviation Organization (ICAO) Committee on Aviation Environmental Protection (CAEP): climate change and aviation emissions, aircraft noise, *local* air quality (emphasis added). It should also be noted that ICAO is a specialized agency of the United Nations that, under the Chicago Convention, is responsible for regulating international flights. The principle that emissions above the mixing height can be excluded from air quality analysis has been challenged by a growing body of evidence suggesting that high-altitude aircraft emissions cause higher concentrations of ground-level $PM_{2.5}$ and ozone. A major contribution of this thesis is providing further evidence that aircraft emissions affect air quality at a global scale, and that while impacts at a specific area might not be large, the global sum of these widespread impacts is significant.

A crucial limitation of the work presented here is that the estimates of air quality degradation and related health impacts are completely dependent on the ability of the atmospheric model in accurately simulating the processes involved in the pathways between emissions and ground-level pollution. The model used, GEOS-Chem, is itself a collection of multiple sub-models and input datasets. These undergo continuous development by the approximately 150 research groups worldwide that use GEOS-Chem, so as to reflect the latest field measurements and the scientific state of the art as best as possible. Still, this is only one of multiple atmospheric chemical transport models available, in addition to other kinds of modeling tools that can be used to study air quality. More research on aviation's air quality impacts with other models is needed, allowing for model intercomparisons to increase the confidence that modeled results are not merely artifacts of a specific modeling approach. There is also a lack of results on how online modeling of aerosol microphysics and dynamic interactions with clouds and solar radiation incidence might affect impacts from aircraft emissions. It has been shown, by this and earlier studies, that model resolution can have a significant effect on its sensitivity to aircraft emissions; so it would be interesting to extend this and evaluate the effects of modeling the atmosphere at grid resolutions on the order of tens of kilometers versus a higher resolution grid that can allow for the dispersion of individual jet plumes to be modeled. More clarity is needed on the implications of treating aircraft emissions as instantly mixed into a much larger box of air, instead of modeling chemical reactions (and aerosol microphysics) within the plume as it leaves the engine and is gradually mixed with the surrounding atmosphere.

Validation of modeled air quality impacts of non-LTO emissions by measurements remains challenging. The output of atmospheric models are routinely compared to ground-based, sonde, and space-based measurements, but isolating the contributions from different emission sources to the observed concentrations is difficult. Aircraft emissions affect air quality mostly by increased formation of secondary pollutants, often involving intermediate species and long-range transport, for which case connections cannot be directly observed between pollution levels and emissions. Nevertheless, increased availability of aircraft tracking data and satellite measurements of the atmosphere might provide more opportunities for the identification of large scale patterns relating non-LTO emissions with

air quality.

The scientific understanding of the association between with air pollution and human health is constantly improving, and this should be reflected when evaluating impacts from aviation. In particular, there is a growing concern about the deleterious health effects of ultrafine particles, such that the number of particles in the air is increasing being used as an air quality metric. Aviation is already known to be a significant contributor to this type of pollution, at least within airports, but the extent of the impacts associated with these emissions is yet to be determined in detail. Additionally, higher certainty of evidence in the association between premature mortality and long-term exposure to ozone would be beneficial in assessing impacts from non-LTO emissions, especially in light of the results presented here.

Like air quality, excessive nitrogen deposition is often treated as a local problem, as the magnitude of impacts can vary significantly by location. But impacts at a specific point are the combined effect of emissions from local and faraway sources, and from all sorts of emitters. Until now, barely any research has focused on the contribution of aviation to this problem. In addition to more modeling efforts, including global scale ones like presented here, ground measurement campaigns could attempt to trace deposition of nitrogen species from aircraft in the scope of vulnerable areas near large aviation sources. More detailed analyses in such areas could provide new insights that would be useful in mitigating impacts from aviation.

The quantification of aircraft emissions, in turn, is usually limited by data availability. This was partially overcome by the use of ADS-B telemetry, which provides a faster, more comprehensive, and more open source of flight movements. Greater privacy consciousness, particularly by private aircraft operators, and security concerns might eventually limit this data stream however. Additionally, instead of simulating flights as great-circle trajectories and scaling to account for lateral inefficiency, telemetry data can be leveraged further by incorporating actually recorded trajectories in the emissions modeling, which is an improvement that has been pursued by other researchers since the publication of the work described in Chapter 3.

However, several limitations regarding data availability still remain, including some that were identified in this thesis. Data transmitted by aircraft do not include identification of the aircraft type, which is required to model emissions, so databases linking unique identifier code of transponders to aircraft types are required, which typically rely on a combination of official government aircraft registries, crowdsourced data, and commercially aggregated data. A more critical limitation for emissions estimation is that the specific engine model used in each aircraft is unknown, and this can contribute to a large degree of uncertainty as different versions of the same engine can have vastly different emissions performance. Beyond the findings presented, there is currently no publicly available study that has quantified the errors in emissions inventories due to the simplification of adopting only one specific engine version for each aircraft type. Inventories are also wholly dependent on public emissions data from engine certification, which are only available for turbofans with a nominal thrust >26.7 kN, and therefore missing for piston, turboprop, and small jet aircraft. Acquisition of more emissions data during actual operations would be beneficial in increasing confidence on estimates based on certification data, and it could also enable further studies on the effect of engine wear on emissions, which

has not been investigated publicly for modern aircraft. Data on usage and emissions performance of auxiliary power units are even more lacking, and the results obtained here suggest that APUs can be significant contributors to nonvolatile particulate matter near airports. Lastly, engine emissions performance measured in the ground must be adjusted for operating conditions at altitude, which carries additional uncertainty. This last point is being addressed by flight measurement campaigns, although data are still limited by the cost of such measurements.

Looking towards the future, as a particularly difficult sector in which to reduce emissions, aviation should have its environmental impacts monitored more closely. As seen in this thesis, their nonlinear dependency on weather and non-aviation emissions, as well as the nonuniform growth in aircraft emissions, calls for continuous reevaluation of impacts. Given the long timescales of aircraft development and the inertia to changes by the industry and its regulators, timely assessments of aviation's multiple environmental impacts can provide valuable guidance to policy and technology decisions.

A

Additional details on the estimation of aircraft emissions

This appendix contains additional details relevant to Chapters 3 and 4. It includes OpenSky origin-destination-typecode assignments (A.1), ICAO-IATA typecode conversion table (A.2), list of military typecodes excluded from analysis (A.3), aircraft engine and APU allocation (A.4), sensitivity analysis of emissions model (A.5), spatial distribution of aircraft emissions (A.6), proportion of LTO to full-flight emissions (A.7), changes in emission indices between 2017–2020 (A.8), ratio between emissions of domestic and international flights (A.9), emissions from cargo flights (A.10), and ratio between emissions calculated from OpenSky and Flightradar24 (A.11).

This appendix was originally published as Supplemental Materials to an article in the Journal of Aircraft. Please cite as shown in the list of peer-reviewed journal articles, item 3.

A

A.1 OpenSky origin, destination, and type code assignment

Automatic Dependent Surveillance-Broadcast (ADS-B) messages do not include aircraft type, origin or intended destination of a flight, therefore this information needs to be somehow inferred. Individual aircraft can still be identified by a unique number ("ICAO 24-bit code") assigned to its transponder. The availability of these fields in the OpenSky dataset, extended to include the year 2016 is shown in Figure A.1.

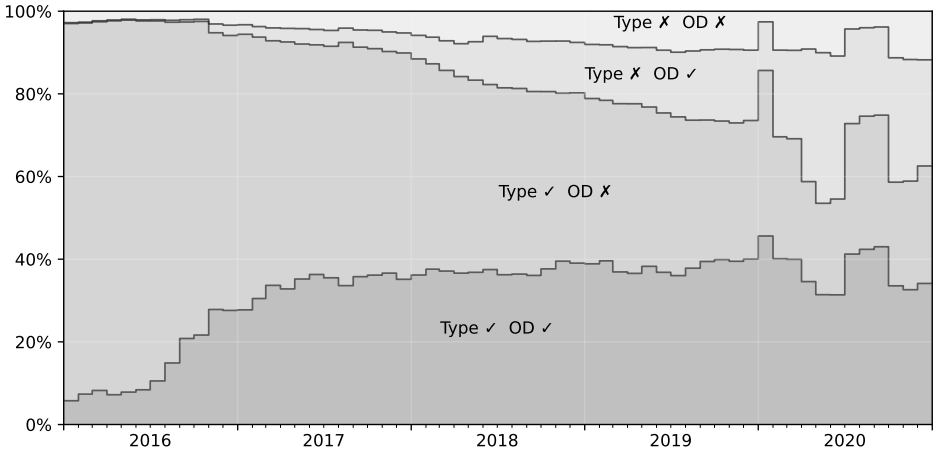

Figure A.1: Percentage of monthly flights in the OpenSky dataset that contain information on aircraft type (Type) and both origin and destination (OD).

OpenSky assigns aircraft types to ICAO 24-bit codes using a database that relies on the aircraft registries of a handful of countries (United States, United Kingdom, Ireland, and Switzerland) as well as crowd-sourced data. The fraction of flights in the dataset that contain type codes is 83% (2018), 75% (2019), 68% (2020).

Route identification can be achieved by observing the initial and final ends of trajectories or by correlating a specific aircraft ICAO 24-bit code and callsign with known routes. The original processing of the dataset by Strohmeier et al. used in this study consisted of extrapolating both ends of a flight trajectory and selecting the nearest airports [259]. However, airports are only assigned if the last position tracked is at or below 2500 m in altitude and if an airport is found within a 10 km radius of the extrapolated landing (or takeoff) position. These limits provide a certain degree of confidence in the airport estimation but, given the incomplete coverage of the OpenSky monitoring network, a significant portion of flights do not have their beginning or end recorded in the data: 48% (2018), 54% (2019), and 62% (2020) of total annual flights in the dataset have either origin or destination airport not assigned.

Since this study aims to estimate global sums of emissions, flights partially captured in the data are included by estimating the closest airport even when the first seen or last seen position is above 2500 m. For each flight, the following method is applied to assign

airports:

- Draw a geodesic from the first to the last recorded position and extrapolate it by the distance required to descend from current altitude to ground level at a constant angle of 3°.
- Consider all airports within 500 km of the extrapolated ground position and make new extrapolations by descending only to the elevation of each of those airports.
- Calculate the distance between each extrapolated landing (or takeoff) point and the corresponding airport at that elevation.
- Select the airport with the shortest distance or do not make an assignment if no airport is within 500 km.

Figure A.2 shows the ratio between the monthly global fuel burn calculated from the list of flights with airports assigned in the original dataset and with the expanded list of flights. Data for 2016 are also included, showing that the smaller network coverage in the past leads to a larger effect of considering partially recorded flights.

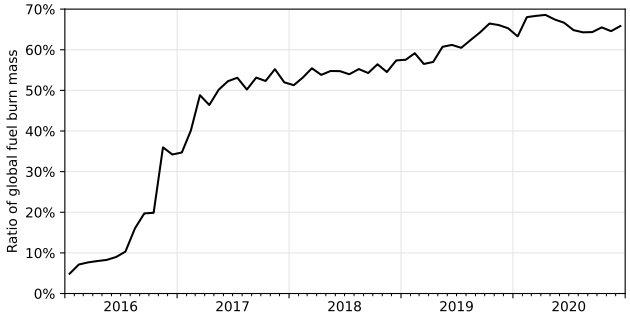

Figure A.2: Ratio of monthly global fuel burn calculated with only flights with airports identified by Strohmeier et al. [259] to that calculated with the extended list of flights with additional airport assignments.

A

A.2 Aircraft type code conversion

Table A.1: Map of IATA to ICAO aircraft type codes.

IATA	ICAO	IATA	ICAO	IATA	ICAO	IATA	ICAO
100	F100	722	B722	757	B752	ABX	A30B
141	B461	727	B722	75F	B752	ABY	A306
142	B462	72F	B722	75T	B753	AGH	A109
143	B463	72Y	B722	75V	B752	AN4	AN24
146	B462	731	B731	75W	B752	AN6	AN26
14F	B462	732	B732	762	B762	ANF	AN12
14Y	B462	733	B733	763	B763	AR1	RJ1H
290	E290	734	B734	764	B764	AR8	RJ85
310	A310	735	B735	767	B763	ARJ	RJ85
313	A310	736	B736	76F	B763	AT4	AT43
318	A318	737	B737	76V	B763	AT7	AT72
319	A319	738	B738	76W	B763	ATF	AT75
31B	A319	739	B739	76X	B762	ATP	ATP
31F	A310	73C	B733	76Y	B763	ATR	AT76
31Y	A310	73E	B735	772	B772	ATZ	AT43
320	A320	73F	B737	773	B773	AWH	A109
321	A321	73G	B737	777	B773	BE1	B190
32A	A320	73H	B738	77F	B77L	BE2	BE65
32B	A321	73J	B739	77L	B77L	BE4	BE40
32N	A20N	73L	B738	77W	B77W	BE9	BE20
32Q	A21N	73M	B732	77X	B77L	BEC	BE20
32S	A320	73N	B738	781	B78X	BEH	B190
330	A332	73P	B737	787	B788	BES	B190
332	A332	73Q	B738	788	B788	BET	B190
333	A333	73R	B738	789	B789	BH2	HELI
339	A339	73S	B732	7M8	B38M	BNI	BN2P
33F	A332	73W	B737	7M9	B39M	BNT	TRIS
33X	A332	73X	B732	7S8	B738	BUS	GRND
340	A343	73Y	B733	A26	AN26	C27	AJ27
342	A342	744	B744	A32	AN32	CJ8	C68A
343	A343	747	B744	A38	AN38	CN1	C182
345	A345	74E	B744	A40	A140	CN2	C402
346	A346	74F	B744	A4F	A124	CNA	C172
350	A359	74H	B748	A58	A158	CNC	C208
351	A35K	74N	B748	A81	A148	CNF	C208
359	A359	74X	B742	AB3	A30B	CNJ	C56X
380	A388	74Y	B744	AB4	A30B	CNT	F406
388	A388	752	B752	AB6	A306	CR1	CRJ1
717	B712	753	B753	ABF	A30B	CR2	CRJ2

Table A.1 continued from previous page

IATA	ICAO	IATA	ICAO	IATA	ICAO	IATA	ICAO
CR7	CRJ7	DHD	DOVE	FRJ	J328	PA1	P28R
CR9	CRJ9	DHL	DHC3	GJ5	GLF5	PA2	PA31
CRA	CRJ7	DHP	DHC2	GRJ	GLF4	PAG	PA46
CRF	CRJ2	DHS	C208	I14	SB20	PL2	PC12
CRJ	CRJ7	DHT	DHC6	IL7	IL76	RFS	GRND
CRK	CRJX	E70	E170	IL9	IL96	S20	SB20
CS1	BCS1	E75	E75S	J31	JS31	S76	S76
CS2	C212	E7W	E75L	J32	JS32	SF3	SF34
CS3	BCS3	E90	E190	J41	JS41	SFB	SF34
CV5	CVLT	E95	E195	L4T	L410	SH3	SH33
CVF	DC3	EC3	EC30	LCH	GRND	SH6	SH36
CVY	CVLT	EM2	E120	LMO	GRND	SU9	SU95
D28	D228	EMB	E110	LOH	C130	SWM	SW4
D38	D328	EMJ	E190	M11	MD11	T20	T204
D6F	DC3	EP1	E50P	M1F	MD11	TGV	GRND
D9F	DC94	EP3	E55P	M80	MD82	TRN	GRND
DC9	DC94	EQV	HELI	M81	MD81	TRS	GRND
DH1	DH8A	ER3	E135	M82	MD82	TU3	T134
DH2	DH8B	ER4	E145	M83	MD83	TU5	T154
DH3	DH8C	ERD	E135	M87	MD87	YK2	YK42
DH4	DH8D	ERJ	E135	M88	MD88	YK4	YK40
DH7	DHC7	F28	F28	M90	MD90	YN2	Y12
DH8	DH8D	F50	F50	MA6	MA60	YN7	AN24
DHC	DHC4	F70	F70	NDE	HELI		

A

A.3 Military aircraft

Military aviation emissions are outside the scope of this study, but both the ADS-B datasets from OpenSky and Flightradar24 contained some military flights. Military aircraft have the ability to turn ADS-B transmitters off, and their operators can request online ADS-B trackers that these flights be unlisted, but that does not necessarily occur. For this study, ICAO type codes of military aircraft are filtered out of the flight movement data. The filter includes some aircraft partially retired from service and aircraft that are judged as being mostly used in military activities despite some smaller amount of civilian service (Table A.2), as well as types identified as military aircraft still in service (Table A.3). Figure A.3 shows the monthly fuel burn that is added if military aircraft types are not excluded.

Table A.2: Aircraft type codes of partially military aircraft excluded from ADS-B datasets.

A178	C160	ETAR	F260	HAR	M55	S208	SB7
A748	CJ6	F1	F8	IL86	MIR4	S211	SB91
AN22	DHC4	F106	G115	JAGR	PC7	SB32	SSAB
AN26	DHC5	F111	G120	KC39	S05F	SB35	WB57
AN32	E121	F14	G12T	M17	S05R	SB37	YK52

Table A.3: Active military aircraft type codes excluded from ADS-B datasets.

A10	BE12	E6	FLCO	L39	P1	SB05	TEX2
A3	BTX1	E737	G222	L59	P1HH	SB39	TOR
A37	C1	E767	G4SG	L70	P2	SBR2	TS11
A4	C101	EUFI	HAWK	L90	P3	SR71	TU22
A400	C135	F104	HURK	LH10	P38	STRK	TU95
A50	C141	F117	IA63	M339	P8	SU17	TUCA
A6	C17	F15	IL38	M345	PC21	SU24	U2
A7	C2	F16	IR99	M346	PC9	SU25	UT75
AJET	C27J	F16X	J10	MF17	PZ3T	SU27	V22
AMX	C295	F18H	J20	MG15	Q01	SU7	V280
AN30	C30J	F18S	K35A	MG21	Q1	T160	VF35
AN70	C5	F2	K35E	MG23	Q2	T2	X47B
ANKA	C5M	F22	K35R	MG25	Q4	T22M	Y130
ARVA	CL41	F26T	KC2	MG29	Q9	T37	YAK3
AT3	DHC1	F35	KE3	MG31	R135	T38	YAK9
ATLA	E2	F4	KFIR	MIR2	RFAL	T4	YK11
B1	E314	F5	KT1	MIRA	S15U	T50S	YK18
B17	E3CF	F5SA	L159	MRF1	S2P	TB30	YK28
B2	E3TF	FGTH	L29	MS30	S2T	TB31	YURO
B52	E530	FGTL	L37	NIM			

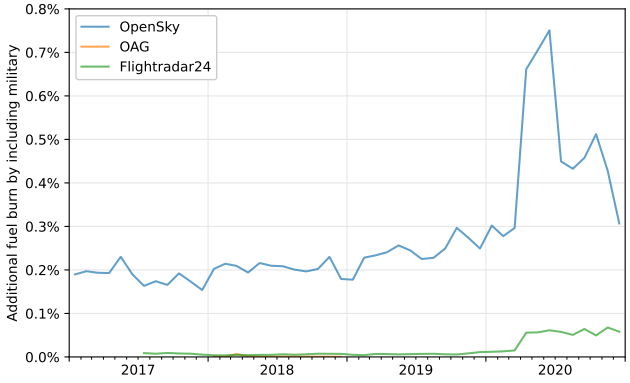

Figure A.3: Increase in monthly fuel burn estimate resulting from including military aircraft types in each flight movement data source relative to fuel burn calculated for that source excluding military aircraft.

A

A.4 Aircraft engine and APU allocations

Each aircraft type is assigned representative engine models and at most one auxiliary power unit (APU) to be used for all its flights, based on data from Jane's All the World's Aircraft and Jane's Aero Engines[1]. Airliners that have engines available from multiple manufacturers are assigned a specific engine version for each manufacturer, and emissions taken as the weighted average according to each engine family's market share (Table A.4). This distribution for each type's fleet is estimated by the reported number of units delivered [402–404], crowdsourced fleet databases [405], and a market analysis report [406]. Emissions data are not available for some turboprop, piston, and low thrust turbojets (< 27 kN), requiring substitution to similar engines. Substitutions are selected based on engine power or thrust, family, and date of development. Every type with an APU is assigned a generic "APU fuel group" determining which averaged EIs would be applicable according to the "Advanced approach" of APU emission estimation described in ICAO's Airport Air Quality Manual [21]. All engine and APU allocations other than those in Table A.4 are listed in the file `engines/eng_allocations.csv` of the model [266].

Table A.4: Engine name and ICAO's EEDB unique identifier (UID) assigned to aircraft with engine options from multiple manufacturers, and aircraft class definition used (W = widebody, N = narrowbody).

Type code	EEDB's unique identifier (UID)	Engine	Market share	Share source	Class
A19N	01P20CM127 01P22PW160	CFM LEAP-1A24 PW1124G-JM (Block D)	53% 47%	[403, 404]	N
A20N	01P20CM128 01P22PW163	CFM LEAP-1A26 PW1127G-JM (Block D)	53% 47%	[403, 404]	N
A21N	01P20CM132 01P22PW167	CFM LEAP-1A30/32/33 PW1133G-JM (Block D)	53% 47%	[403, 404]	N
A306	3GE056 1PW048	CF6-80C2A5F PW4158	56% 44%	[405]	W
A310	2GE037 1PW047	CF6-80C2-A2 (1862M39) PW4156A (reduced smoke)	90% 10%	[405]	W
A318	01P08CM109 7PW083	CFM56-5B8/3 PW6122A	58% 42%	[403, 404]	N
A319	01P08CM106 01P10IA020	CFM56-5B5/3 V2524-A5 (SelectOne)	58% 42%	[403, 404]	N
A320	01P08CM105 01P10IA021	CFM56-5B4/3 V2527-A5 (SelectOne)	58% 42%	[403, 404]	N
A321	01P08CM104 01P10IA025	CFM56-5B3/3 V2533-A5 (SelectOne)	58% 42%	[403, 404]	N

[1] https://www.janes.com, accessed between 2020-08-28 and 2021-02-01.

Table A.4 continued from previous page

Type code	EEDB's unique identifier (UID)	Engine	Market share	Share source	Class
A332	01P14RR102 4GE081 9PW094	Trent 772 (Phase 5) CF6-80E1A4 (low emissions) PW4168A-1D	68% 17% 15%	[406]	W
A333	01P14RR102 4GE081 7PW082	Trent 772 (Phase 5) CF6-80E1A4 (low emissions) PW4168A (Talon II)	58% 28% 14%	[406]	W
A388	9EA001 01P18RR105	GP7270 Trent 972E-84	52% 48%	[405]	W
B744	1GE024 4RR037 12PW102	CF6-80C2B1F RB211-524H-T PW4062A	48% 34% 18%	[402]	W
B752	5RR039 4PW072	RB211-535-E4-B-37 (Phase 5) PW2037	58% 42%	[402]	N
B753	5RR039 4PW073	RB211-535-E4-B-37 (Phase 5) PW2040	71% 29%	[402]	N
B762	1GE012 12PW101	CF6-80A2 PW4060 (Phase III)	50% 50%	[402]	W
B763	2GE055 1PW043 4RR037	CF6-80C2-B7F (1862M39) PW4060 RB211-524H-T	72% 25% 3%	[402]	W
B772	5RR040 6GE090 10PW099	Trent 895 GE90-90B (DAC III) PW4090	36% 33% 31%	[402]	W
B773	2RR027 5PW076	Trent 892 PW4098	70% 30%	[402]	W
B788	01P17GE209 02P23RR130	GEnx-1B70/75/P2 Trent 1000-H3	65% 35%	[402]	W
B789	01P17GE211 02P23RR132	GEnx-1B74/75/P2 Trent 1000-K3	63% 37%	[402]	W
B78X	01P17GE214 02P23RR132	GEnx-1B76A/P2 Trent 1000-K3	69% 31%	[402]	W
DC10	3GE074 1PW033	CF6-50C1/2 (low emissions) JT9D-59A	91% 9%	[402]	W
MD11	2GE049 1PW052	CF6-80C2D1F (1862M39) PW4460	59% 41%	[402]	W

A

A.5 Sensitivity of total emissions to model parameters

The sensitivity of the global sum of emissions to various model parameters is evaluated by a series of tests varying one parameter at a time. Some of these tests are performed only for a sample of 10 combinations of month and flight movement source (Table A.5) representative of the full dataset, while others are performed on the entire 102 months of flight movement data (across OpenSky, OAG, and Flightradar24). Each sensitivity test, listed in Table A.6, is discussed in this section.

Table A.5: Sample of 10 test months of flight movement data (across multiple sources) used in the evaluation of sensitivity of model results to various parameters.

Year/Month	Source(s)
2018/01	OpenSky, OAG, Flightradar24
2018/07	OAG
2019/07	OpenSky, Flightradar24
2020/01	OpenSky, Flightradar24
2020/04	OpenSky, Flightradar24

Table A.6: Parameters tested in the sensitivity analysis.

Section	Parameter altered	Months tested
A.5.1	Wind	All 102 months available
A.5.2	LTO cycle	
A.5.3	APU methods	
A.5.4	nvPM LTO method	
A.5.4	nvPM non-LTO method	10 test months
A.5.5	Mass load factor	
A.5.6	Cruise altitude	
A.5.7	Simulation step size	
A.5.8	Lateral inefficiency	

A.5.1 Wind

The simulations in the main study apply monthly average wind speed vectors to flying aircraft, with wind values taken from the nearest grid cell in the MERRA-2 native resolution of 0.5° × 0.625° (latitude × longitude) with 72 hybrid-eta vertical levels [268]. Compared to simulating flights without wind, monthly global fuel burn is between 0.23% to 1.35% higher (Table A.7), with differences being larger during northern winter (Figure A.4). Simulated trajectories are geodesics, while actual flights take weather conditions in planning and execution, which may reduce actual fuel consumption, and which is not accounted for here.

Table A.7: Changes in emissions resulting from including wind in the simulation. The average of 102 monthly differences is given, with minimum and maximum in parentheses.

Fuel burn	+0.68% (+0.23%, +1.35%)
EI (NO_x)	−0.07% (−0.15%, +0.00%)
EI (HC)	−0.38% (−0.76%, −0.12%)
EI (CO)	−0.27% (−0.56%, −0.06%)
EI ($nvPM_m$)	−0.20% (−0.38%, −0.07%)
EI ($nvPM_N$)	+0.04% (−0.04%, +0.17%)

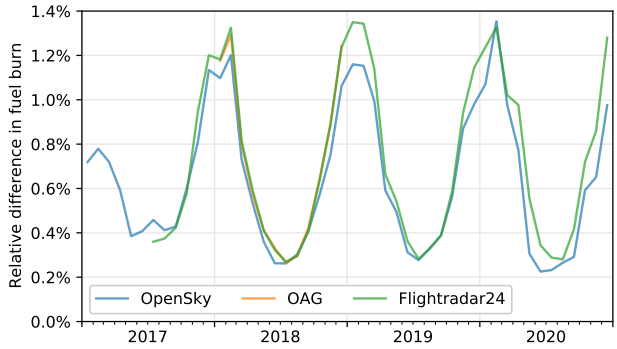

Figure A.4: Relative increase in fuel burn resulting from including wind in the simulations.

A.5.2 LTO cycle

Airport size and traffic volume are influential to taxiing times. Because airports of a wide range of sizes are considered in this study, the LTO cycle is modeled according to the time-in-mode values suggested by Stettler et al. [265], since it assigns taxiing times as a function of runway length and hold time as a function of yearly airport movements per number of runways. The use of such model instead of adopting the LTO cycle defined in ICAO's Annex 16 [7], leads to a decrease of monthly LTO fuel burn between 27–30% (Table A.8).

Table A.8: Changes in LTO emissions resulting from modeling the cycle according to Stettler et al. [265] instead of using the ICAO standard cycle [7]. The average of 102 monthly differences is given, with minimum and maximum in parentheses.

Fuel burn	−29% (−30%, −27%)
EI (NO_x)	+14% (+12%, +16%)
EI (HC)	−36% (−41%, −33%)
EI (CO)	−28% (−34%, −20%)
EI ($nvPM_m$)	+17% (+16%, +18%)
EI ($nvPM_N$)	+3% (+1%, +4%)

A

A.5.3 APU emissions estimation method

Auxiliary power unit (APU) emissions are modeled by assigning a specific model or a generic class of unit to each aircraft type and by considering a fixed amount of time spent at each given power mode for every flight cycle. For the main study, the time-in-mode and generic class emission indices are taken from the "advanced approach" in ICAO's Airport Air Quality Manual [21], with specific APU model data from a study by the Airport Authority Hong Kong used where available [173]. There is a large difference in APU operating times depending on whether the airport has ground equipment providing power, cooling, and heating, and this is reflected in the wide range of time-in-mode models. Adopting different times presented by the same ICAO manual (the values suggested by ATA) leads to APU fuel burn increases of 143% to 152% (Table A.9).

Table A.9: Changes in global monthly APU emissions resulting from adopting alternative time-in-modes. The average of 102 monthly differences is given, with minimum and maximum in parentheses.

	APU time-in-mode (baseline = ICAO Advanced [21])		
	AEDT [407]	AEIC [265]	ATA [21]
Fuel burn	+16% (+15%, +17%)	+113% (+111%, +113%)	+145% (+143%, +152%)
EI (NO_x)	+0% (+0%, +0%)	+0% (+0%, +0%)	+1% (+1%, +2%)
EI (HC)	−1% (−2%, −1%)	−1% (−2%, −1%)	+0% (−1%, +1%)
EI (CO)	−1% (−2%, −1%)	−1% (−2%, −1%)	0% (−1%, +1%)
EI $(nvPM_m)$	+8% (+6%, +10%)	+8% (+6%, +10%)	+8% (+6%, +11%)
EI $(nvPM_N)$	+8% (+7%, +10%)	+8% (+7%, +10%)	+6% (+5%, +6%)

Using a different scheme of generic APU classes and their emission indices, as well as not using specific model EIs where available, leads to changes in monthly global APU fuel burn between −13% and +3% (Table A.10). The prevalence of APUs in business jets is not readily known, and the main study considers all such aircraft have a class average APU. Disregarding all APU emissions from business jets leads to a decrease in APU fuel burn between 0% (in the case of OAG data, where business jets are not included) to 13% (Table A.11).

A.5.4 nvPM estimation methods

LTO nonvolatile particulate matter (nvPM) emission indices at certification thrust levels are preferentially taken from directly measured values or estimated from smoke number measurements using the FOA 4.0 method, when measured values are not available. If the measured emission indices are disregarded and only smoke number measurements are used with the FOA 4.0 method, monthly LTO mass emissions are 2% to 5% higher and particle number emissions are 1% to 5% lower. Disregarding direct measurements and using the older correlation method FOA 3, described by Wayson et al. [409], gives monthly LTO mass emissions between 20% and 23% lower than the main study results, with no provision in FOA 3 to estimate number of particles. The alternative FOX method, which estimates particulate matter mass emissions from a thermodynamic model independent of the smoke number data [251], results in 94% to 163% higher monthly LTO emissions relative to our main study. Adopting the SCOPE11 method to estimate nvPM number

Table A.10: Changes in global monthly APU emissions resulting from adopting alternative emission indices for generic classes and from considering emission indices of specific APU models. The average of 102 monthly differences is given, with minimum and maximum in parentheses.

	APU emission indices (baseline = ICAO Advanced [21] with specific APUs [173])				
Generic APU	ACRP [408]	ACRP [408]	ICAO Simple [21]	ICAO Simple [21]	ICAO Advanced [21]
Specific APU	No	Yes	No	Yes	No
Fuel burn	−13% (−13%, −11%)	−3% (−6%, −2%)	−3% (−5%, +3%)	1% (+1%, +2%)	−6% (−8%, −4%)
EI (NO_x)	9% (+7%, +11%)	−2% (−3%, −1%)	28% (+20%, +33%)	4% (+2%, +6%)	2% (+1%, +5%)
EI (HC)	32% (−15%, +48%)	−20% (−28%, −12%)	−29% (−42%, −19%)	−23% (−33%, −14%)	15% (−3%, +24%)
EI (CO)	4% (−26%, +8%)	−6% (−10%, −4%)	−50% (−63%, −48%)	−11% (−17%, −6%)	21% (−6%, +26%)
EI $(nvPM_m)$	14% (+13%, +16%)	4% (+2%, +6%)	5% (−4%, +9%)	1% (−4%, +6%)	6% (+4%, +9%)
EI $(nvPM_N)$	14% (+13%, +16%)	4% (+2%, +6%)	−0% (−11%, +13%)	−4% (−16%, +11%)	6% (+4%, +9%)

Table A.11: Changes in global monthly APU emissions resulting from considering business jets without APUs. The average of 102 monthly differences is given, with minimum and maximum in parentheses. Note that the 0% are driven by the OAG simulations which do not capture business jets.

Fuel burn	−5% (−13%, −0%)
EI (NO_x)	+0% (−0%, +1%)
EI (HC)	−9% (−19%, −0%)
EI (CO)	−3% (−6%, −0%)
EI $(nvPM_m)$	−0% (−0%, +0%)
EI $(nvPM_N)$	+3% (+0%, +9%)

emissions, which is only different to FOA 4.0 by considering engine specific geometric mean diameters [21, 270], yields between 9% to 21% higher monthly emissions. The resulting changes from these alternative methods of estimating nvPM LTO emissions are summarized in Table A.12.

Non-LTO nonvolatile particulate matter (nvPM) emissions are estimated using the method adopted by the FAA's emissions model, AEDT [271], which is based on the pro-

A

Table A.12: Changes in LTO nvPM mass and number emissions resulting from adopting different calculation methods relative to the method used in the main study. The average of 102 monthly differences is given, with minimum and maximum in parentheses.

	LTO $nvPM_m$	LTO $nvPM_N$
FOA 3 [409]	−22% (−23%, −20%)	n/a
No direct measurements	+3% (+2%, +5%)	−3% (−5%, −1%)
FOX [251]	+105% (+94%, +163%)	n/a
SCOPE11 [270]	n/a	+10% (+9%, +21%)

cedure described by Peck et al. [272]. This method makes thermodynamic adjustments to emission indices at ground-level reference conditions, obtained by interpolation of directly measured values at engine certification thrust levels or of values calculated from smoke number measurements using FOA 4.0. When neither kind of ground level measurements is available, a constant emission index of 30 mg/kg is used, and particle number ($nvPM_N$) is not counted. If this default constant EI is instead used for all engines, monthly global non-LTO nvPM mass emissions ($nvPM_m$) are 75% to 112% higher than in the main study results (Table A.13). If nvPM emissions are instead disregarded for engines without measurement data, global (fleet) emissions are between 0.8% and 2.6% lower (Table A.13).

An alternative method proposed for estimating in-flight nvPM, named FOX, consists of also calculating both reference ground and cruise level emissions directly from a thermodynamic model of a (generic) engine [251]. Using the FOX method results in monthly nvPM masses that are between 4.5 and 6.4 times the results in the main study (Table A.13). The tendency of the FOX method towards higher values and the overall wide range of results has been observed in previous studies [232, 282], however there is a lack of high-altitude measurements to assess the accuracy of all the available methods.

Table A.13: Changes in non-LTO nvPMm emissions resulting from adopting different calculation methods relative to the method used in the main study. The average of 10 monthly differences is given, with minimum and maximum in parentheses.

Method	Non-LTO $nvPM_m$ (baseline = AEDT [271])
Constant EI = 30 mg/kg	+11 % (−1%, +36%)
No constant EI backup	−1.1% (−1.6%, −0.5%)
FOX [251]	+184 % (+145%, +279%)

A.5.5 Mass load factor

Different mass load factors, ranging from 55.2% to 70.5%, are used for different years in the takeoff mass estimation, as described in Section 3.2.4. The sensitivity of global aviation emission totals to the mass load factor is evaluated by running 10 test months (Table A.5) in the model using three different values for the factor: 55.2%, 62.8%, and 70.5%. An increase

or decrease relative to the intermediate value leads to changes of less than 1.1% in fuel burn (Table A.14).

Table A.14: Changes in global fuel burn and emissions resulting from adopting different mass load factors relative to emissions calculated using an intermediate baseline value for the factor. The average of 10 monthly differences is given, with minimum and maximum in parentheses.

	Mass load factor (baseline = 62.8%)	
	55.2%	70.5%
Fuel burn	−1.07% (−1.08%, −1.04%)	+1.08% (+1.05%, +1.09%)
EI (NO_x)	−0.69% (−0.73%, −0.67%)	+0.69% (+0.67%, +0.73%)
EI (HC)	+0.84% (+0.78%, +0.88%)	−0.81% (−0.85%, −0.76%)
EI (CO)	+1.51% (+1.34%, +1.59%)	−1.48% (−1.56%, −1.30%)
EI ($nvPM_m$)	−0.32% (−0.36%, −0.29%)	+0.34% (+0.31%, +0.37%)
EI ($nvPM_N$)	+0.20% (+0.16%, +0.31%)	−0.22% (−0.31%, −0.19%)

A.5.6 Cruise altitude

Adopting aircraft type specific cruise flight levels determined from ADS-B data and limiting cruise levels for short flights results in a −1.44% to +1.02% difference in global monthly fuel burn relative to using the default type specific values from the BADA model (Table A.15).

Table A.15: Changes in global fuel burn and emissions resulting from adopting different aircraft type specific cruise flight levels relative to using default BADA values. The average of 10 monthly differences is given, with minimum and maximum in parentheses.

	Cruise flight level determination (baseline = BADA)	
	BADA + short flight limits	ADS-B + short flight limits
Fuel burn	+0.02% (+0.01%, +0.02%)	−0.76% (−1.44%, +1.02%)
EI (NO_x)	−0.09% (−0.13%, −0.07%)	+0.53% (+0.26%, +1.25%)
EI (HC)	−0.45% (−0.68%, −0.32%)	+0.28% (−1.90%, +1.26%)
EI (CO)	−0.51% (−1.38%, −0.09%)	+0.53% (−2.11%, +2.10%)
EI ($nvPM_m$)	−0.05% (−0.11%, −0.03%)	−1.08% (−2.61%, +2.80%)
EI ($nvPM_N$)	−0.00% (−0.03%, +0.02%)	−1.44% (−4.31%, −0.48%)

A.5.7 Simulation step size

The non-LTO portion of flights is simulated by calculating aircraft state and emission rates at discrete points along the flight trajectory. Point separation is determined by a vertical distance during climb and descent and by a horizontal distance during cruise. Increasing horizontal frequency (i.e. decreasing step size) by a factor of 2.5 (to 20 NM) leads to a

A

decrease of 0.05% to 0.04% in monthly global fuel burn (Table A.16). Increasing vertical frequency by a factor of 2.0 (to 500 ft step size) leads to a decrease of 0.04% to 0.03% in monthly global fuel burn (Table A.17). The resolution of gridded emissions is independent of the simulation step sizes and emissions are spread uniformly across grid cells along the trajectory between simulated points, according to the length of trajectory that falls within each cell.

Table A.16: Changes in emissions resulting from adopting different cruise simulation steps relative to the value used in the main study. The average of 10 monthly differences is given, with minimum and maximum in parentheses.

	Horizontal cruise simulation step (baseline = 50 NM)	
	125 NM	20 NM
Fuel burn	+0.10% (+0.09%, +0.11%)	−0.04% (−0.05%, −0.04%)
EI (NO_x)	+0.06% (+0.06%, +0.06%)	−0.02% (−0.02%, −0.02%)
EI (HC)	−0.08% (−0.10%, −0.07%)	+0.03% (+0.03%, +0.04%)
EI (CO)	−0.15% (−0.16%, −0.14%)	+0.06% (+0.06%, +0.06%)
EI ($nvPM_m$)	−0.01% (−0.02%, +0.00%)	+0.01% (−0.00%, +0.01%)
EI ($nvPM_N$)	−0.02% (−0.03%, −0.02%)	+0.01% (+0.01%, +0.01%)

Table A.17: Changes in emissions resulting from adopting different climb and descent simulation steps relative to the value used in the main study. The average of 10 monthly differences is given, with minimum and maximum in parentheses.

	Vertical climb and descent simulation step (baseline = 1000 ft)	
	2000 ft	500 ft
Fuel burn	+0.09% (+0.08%, +0.10%)	−0.04% (−0.04%, −0.03%)
EI (NO_x)	+0.25% (+0.24%, +0.26%)	−0.22% (−0.23%, −0.20%)
EI (HC)	−0.96% (−1.05%, −0.73%)	+0.51% (+0.41%, +0.56%)
EI (CO)	−0.70% (−0.85%, −0.39%)	+0.36% (+0.21%, +0.43%)
EI ($nvPM_m$)	+0.47% (+0.44%, +0.51%)	−0.24% (−0.25%, −0.22%)
EI ($nvPM_N$)	−0.05% (−0.06%, −0.02%)	+0.02% (+0.01%, +0.03%)

A.5.8 Lateral inefficiency

Emissions are scaled up to account for the longer distances actually flown relative to the great circle distances in the simulated trajectories. In this study, the lateral inefficiency factor is adopted as a function of great circle distance, as described by Seymour et al. [258] for their emissions model named FEAT. Not applying this correction leads to monthly fuel burn totals between 6.36% and 6.72% lower (Table A.18). Modeling lateral inefficiency with the same method used by the model AEIC described by Simone et al. [41], which

uses different factors for emissions inside the terminal control area and emissions en-route based on results from Reynolds [410], yield monthly fuel burn totals between 0.12% lower and 0.14% higher than obtained in our main study (using the method from FEAT).

Table A.18: Changes in global emissions resulting from adopting different methods of correcting for lateral inefficiency. The average of 10 monthly differences is given, with minimum and maximum in parentheses.

	Lateral inefficiency (baseline = FEAT) [258]	
	No correction applied	AEIC [41, 410]
Fuel burn	−6.53% (−6.72%, −6.36%)	+0.02% (−0.12%, +0.14%)
EI (NO_x)	+0.18% (+0.09%, +0.22%)	+0.04% (−0.01%, +0.08%)
EI (HC)	+0.64% (−0.22%, +1.12%)	+5.89% (+4.87%, +6.56%)
EI (CO)	−0.99% (−4.19%, +0.22%)	+4.22% (+1.62%, +5.41%)
EI ($nvPM_m$)	−0.15% (−0.36%, +0.03%)	+0.37% (+0.13%, +0.48%)
EI ($nvPM_N$)	−0.19% (−0.32%, −0.10%)	−0.13% (−0.15%, −0.09%)

A.6 Spatial distribution of emissions

The aviation emissions calculated are gridded at a resolution of 0.5° × 0.625° (lat × lon), and each grid cell (except for unpopulated islands, water, and the Antarctica) is assigned to a region according to the "Standard Country or Area Codes for Statistical Use (M49)" scheme from the United Nations' Statistics Division [411] (Figure A.5). These assignments are made based largely on geocoding data from OpenStreetMap accessed via the Nominatim search tool. The horizontal distributions of fuel burn in 2018 as calculated from OpenSky, OAG, and Flightradar24 are presented in Figure A.6. Table A.19 lists the amount of fuel burned over each region, regardless of origin and destination of the flights, for the year 2018 (OAG and Flightradar24 estimates) as well as for 2005 based on results from Simone et al. [41].

Fuel burn rates and emission rates of NO_x, HC, CO, $nvPM_m$, and $nvPM_N$ for 2019, calculated from Flightradar24 data, are presented in Figure A.7. For this same scenario, the distribution of fuel burn per longitude, latitude, and altitude are given in Figure A.8, along the distribution from the 2005 inventory from Simone et al. [41] for comparison. The fuel burn in this scenario per region of departure and arrival is given in Figure A.9.

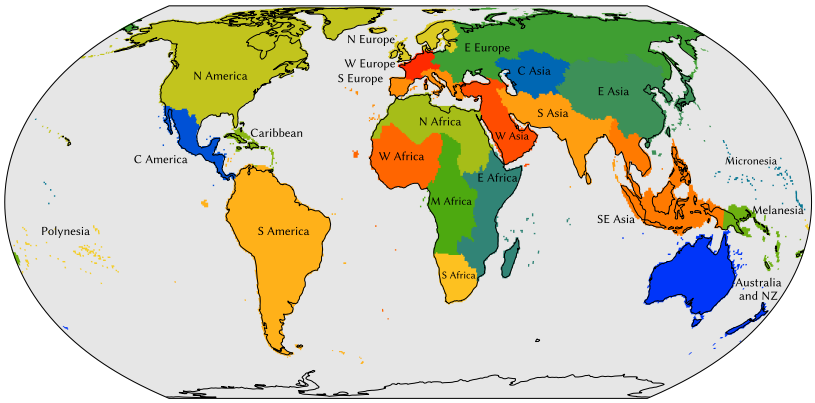

Figure A.5: Region definitions applied to gridded emissions, based on the United Nations' M49 standard [411].

Table A.19: Fuel burn mass over different regions in 2005, based on the AEIC inventory [41], and 2018, calculated from OAG and Flightradar24 data. The relative difference to 2005 is shown in parentheses.

Region	AEIC 2005 [Tg]	OAG 2018 [Tg]	FR24 2018 [Tg]	FR24 2018 [kg·km^{-2}]
Northern Africa	1.71	2.85 (+67%)	2.88 (+69%)	359
Eastern Africa	0.98	2.13 (+118%)	1.76 (+80%)	235
Middle Africa	0.77	0.98 (+28%)	0.92 (+20%)	138
Southern Africa	0.84	1.09 (+30%)	0.80 (−5%)	283
Western Africa	0.81	1.23 (+52%)	1.11 (+37%)	178
Caribbean	0.92	1.03 (+12%)	1.06 (+14%)	1 328
Central America	2.42	3.27 (+35%)	3.11 (+29%)	1 056
South America	5.45	9.37 (+72%)	8.61 (+58%)	452
Northern America	52.15	53.13 (+2%)	59.89 (+15%)	2 353
Central Asia	1.84	2.93 (+59%)	2.88 (+56%)	712
Eastern Asia	18.18	42.02 (+131%)	40.48 (+123%)	3 227
South-eastern Asia	6.81	13.98 (+105%)	13.25 (+95%)	1 483
Southern Asia	5.76	13.64 (+137%)	13.32 (+131%)	1 894
Western Asia	4.59	12.71 (+177%)	13.37 (+191%)	2 704
Eastern Europe	10.74	19.46 (+81%)	20.15 (+88%)	1 011
Northern Europe	6.32	7.91 (+25%)	8.25 (+30%)	3 246
Southern Europe	6.04	9.46 (+57%)	10.03 (+66%)	5 275
Western Europe	10.26	13.93 (+36%)	14.71 (+43%)	12 168
Australia and NZ	3.66	5.43 (+49%)	5.67 (+55%)	624
Melanesia	0.17	0.22 (+30%)	0.19 (+14%)	105
Micronesia	0.04	0.04 (−19%)	0.04 (−19%)	108
Polynesia	0.03	0.03 (+12%)	0.03 (+2%)	73
Other (oceans)	39.99	63.53 (+59%)	65.81 (+65%)	185
World	180	280 (+55%)	288 (+60%)	565

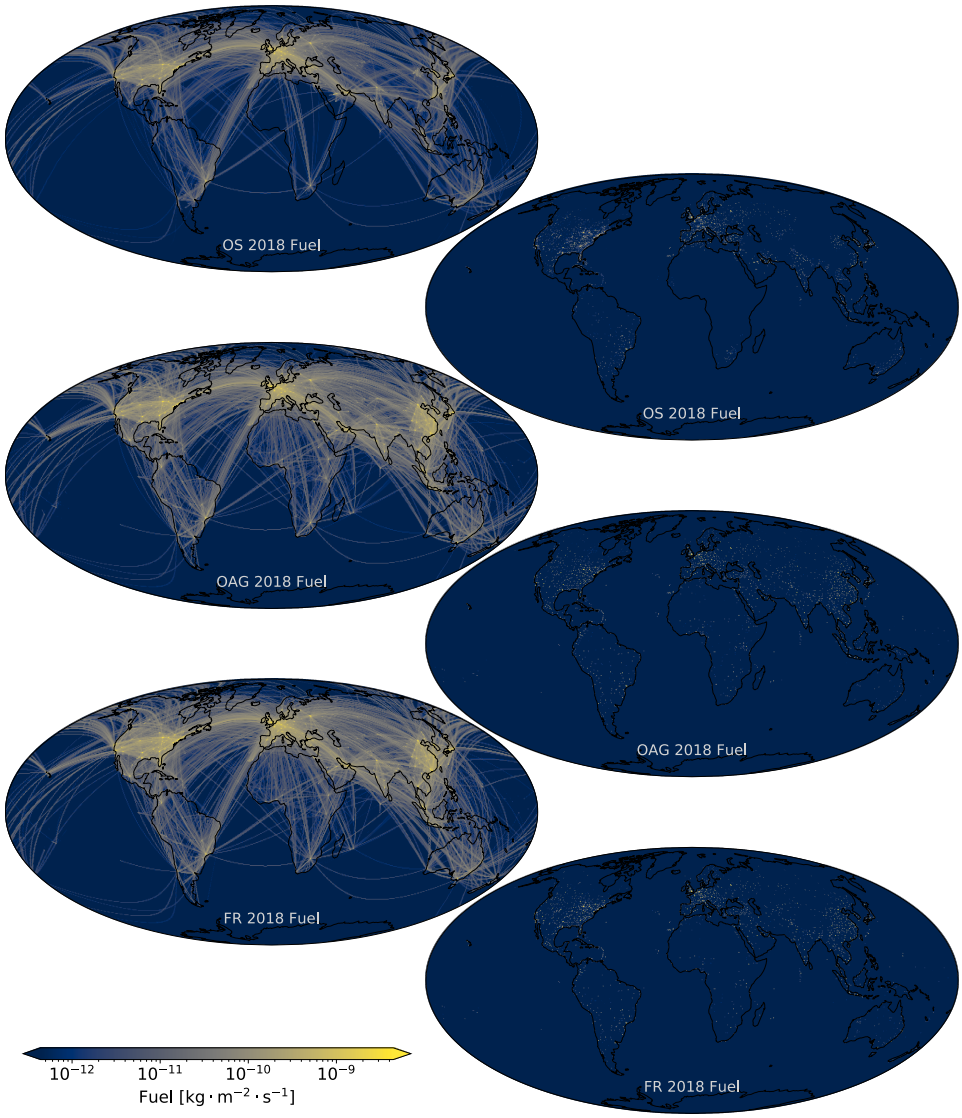

Figure A.6: Horizontal maps of full-flight (left) and LTO (right) average fuel burn rates in the year 2018 for OpenSky, OAG, and Flightradar24.

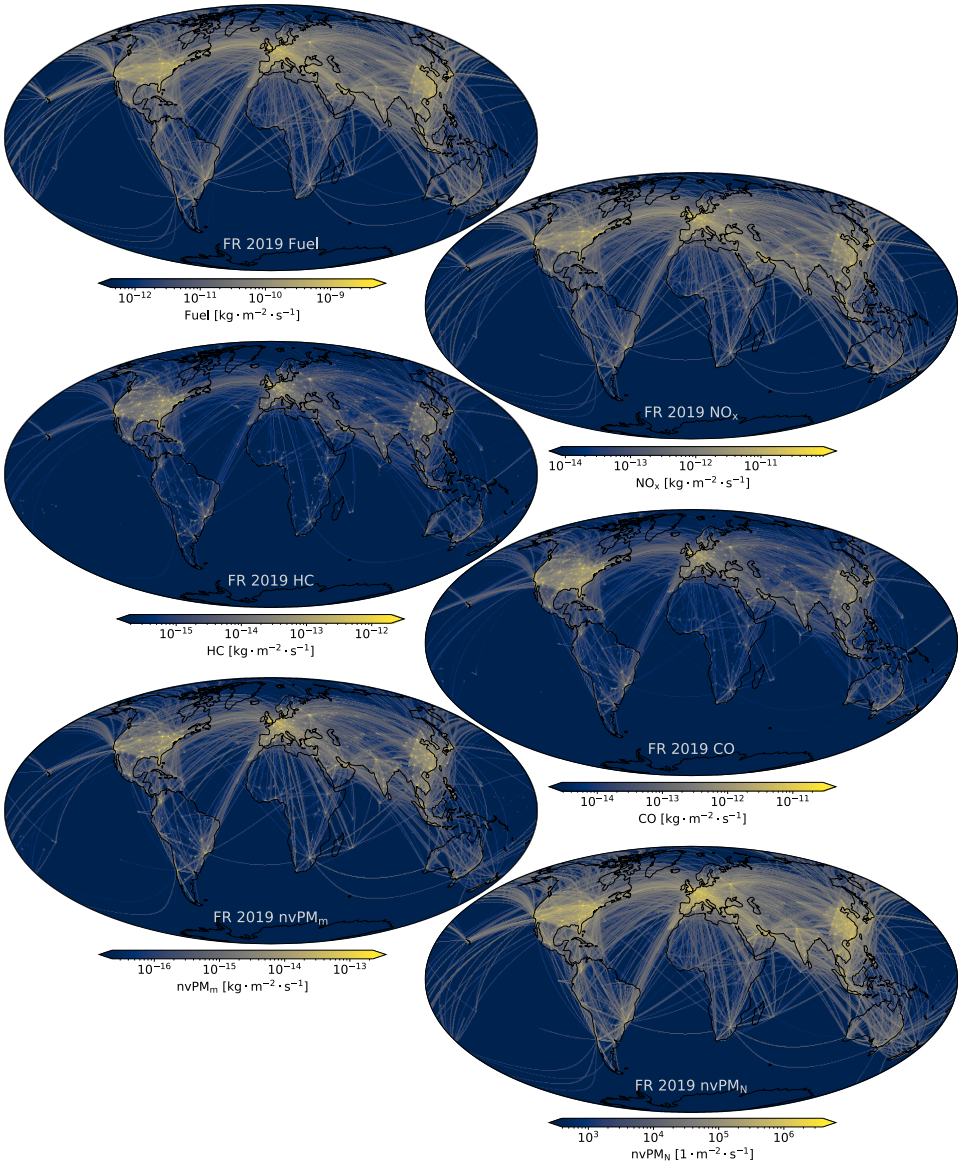

Figure A.7: Horizontal maps of average fuel burn rate and mass emission rates of different species in the year 2019 for Flightradar24.

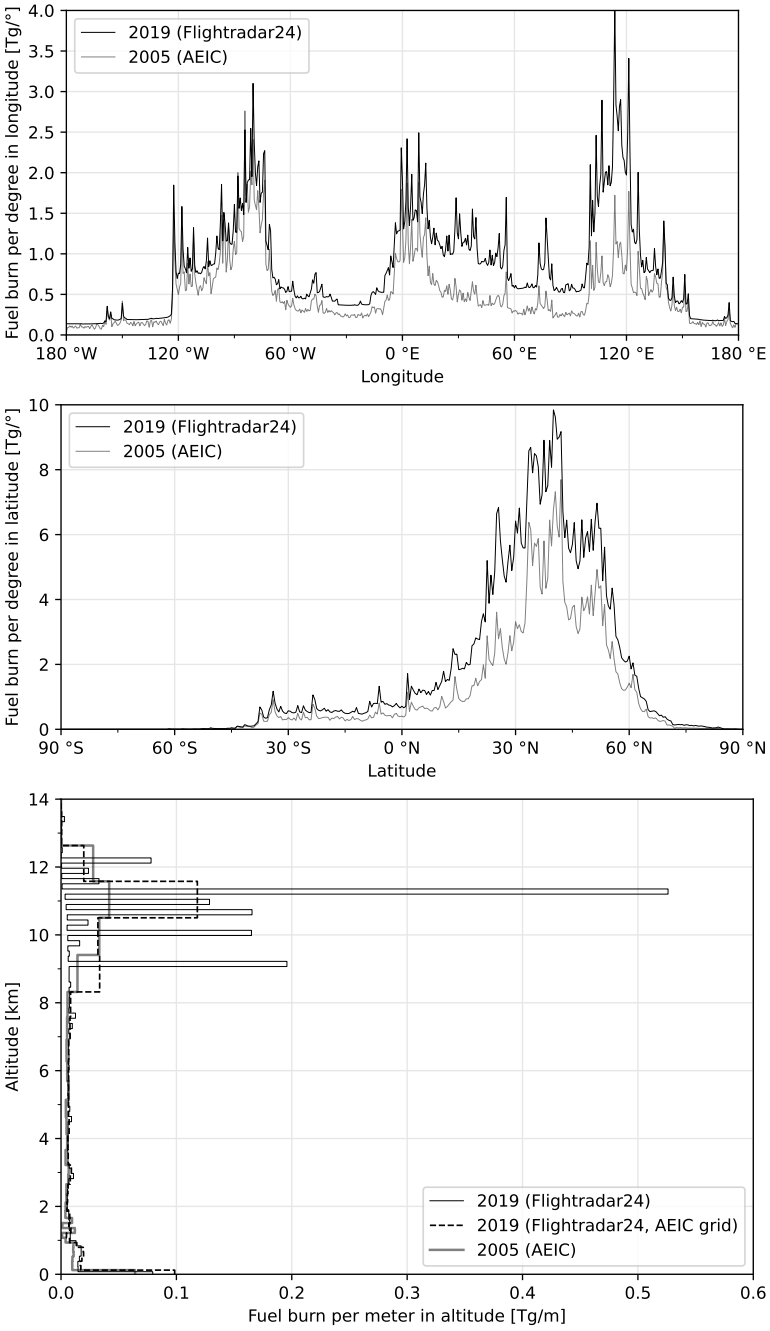

Figure A.8: Fuel burn mass in 2019 by longitude, latitude, and altitude for Flightradar24 and in 2005 from the AEIC inventory [41].

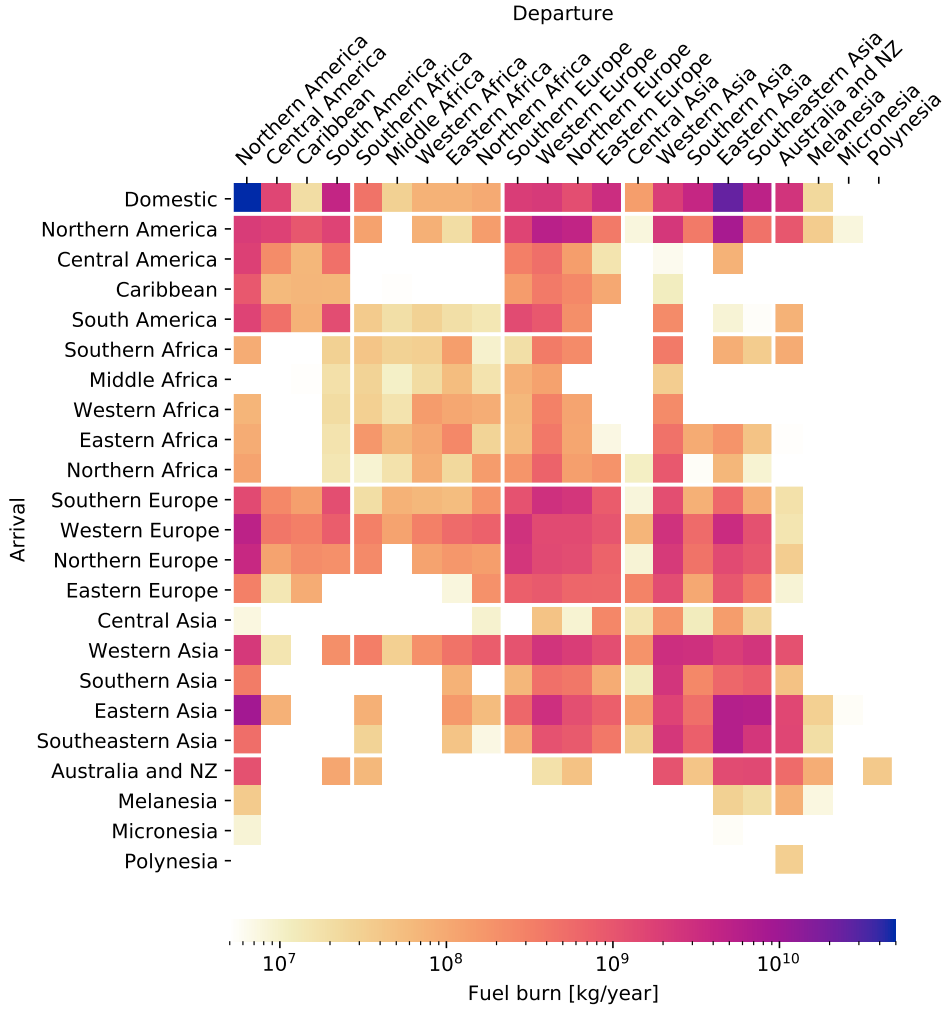

Figure A.9: Fuel burn mass in 2019 calculated with data from Flightradar24 for domestic flights (first row) and international flights per pair of regions of departure and arrival.

A.7 Proportion of LTO emissions

The proportion over time of monthly fuel burn and NO_x emissions that occur during landing and takeoff (LTO) phases of flight is shown in Figure A.10. In 2018, the simulation of OAG flights had a higher proportion of fuel burn in LTO (8.73%) compared to Flightradar24 (8.58%), which could suggest better capture of short flights by OAG. In 2020, the changes in air traffic due to the COVID-19 pandemic caused a swing in the proportion of fuel burn in LTO between 8.15% and 9.97% in the Flightradar24 results.

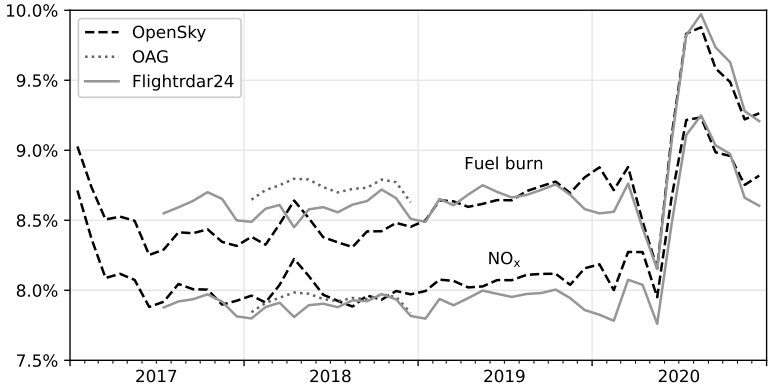

Figure A.10: Fraction of full-flight fuel burn and NO_x emissions that occur during LTO phases. The fraction for fuel is always higher than for NO_x.

A.8 Emission indices changes during 2017–2020

Changes in civil aviation activity in 2020 caused both an overall decrease in fuel burn and changes in the average emission indices (EI). Appendix A.9 shows the monthly average EIs in the period of 2017–2020 calculated using Flightradar24 flight movement data. The increase in global fleet average EIs for HC and CO is consistent with a decrease in flight length associated with relatively fewer international flights (discussed in Appendix A.9), as the emission of these species is less intense during cruise than during the LTO phase of flights. In June 2020, the average EIs for HC and CO were 46% and 68% higher than the 2019 annual averages, respectively.

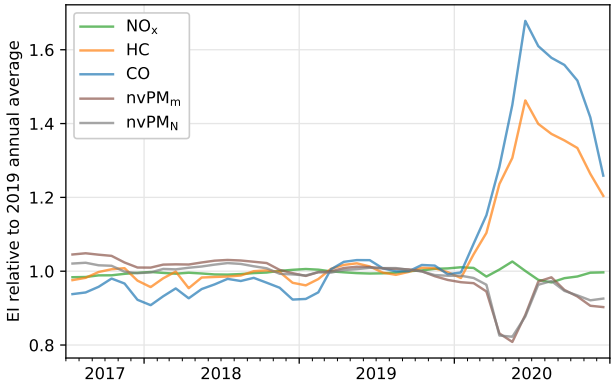

Figure A.11: Monthly global average emission indices normalized by 2019 annual average values.

A.9 Domestic and international flights

Flights are classified as domestic or international based on the ISO 3166-1 alpha-2 country code assigned to each airport. For this purpose, each signatory of the Convention on International Civil Aviation (Chicago Convention) is treated as a separate country[2]. Aruba (AQ), Bonaire, Sint Eustatius and Saba (BQ), Curacao (CW), Sint Maarten (SX), and the Netherlands (NL) are each counted separately. The following states not at least directly listed in the Chicago Convention are considered as individual countries in the analysis: Western Sahara (EH), Liechtenstein (LI), Niue (NU), Palestine (PS), Taiwan (TW), and Kosovo (XK). Certain countries are considered to consist of multiple ISO two-letter codes, according to Table A.20.

Table A.20: Groups of ISO 3166-1 alpha-2 codes defining regions of domestic flights.

Country	Codes
Australia	AU, CC, CX, NF, HM
China	CN, HK, MO
Denmark	DK, FO, GL
Finland	FI, AX
France	FR, BL, GF, MF, MQ, NC, PF, PM, RE, WF, YT, TF, GP
United Kingdom	GB, AI, BM, FK, GG, GI, IM, IO, JE, KY, MS, SH, TC, VG, GS, PN
Norway	NO, BV, SJ
New Zealand	NZ, TK
United States	US, AS, GU, MP, PR, UM, VI

The ratio of fuel burn from domestic to total flights is presented in Figure A.12 for emissions calculated using data from OpenSky, OAG, and Flightradar24. While prior to

[2]ICAO, https://www.icao.int/secretariat/legal/List%20of%20Parties/Chicago_EN.pdf, accessed on 2021-04-15.

2020 domestic flights were on average responsible for ~4% of fuel burn, this grew up to ~49% in 2020 due to the COVID-19 related restrictions.

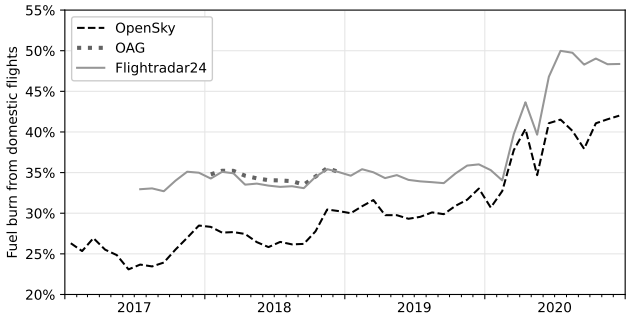

Figure A.12: Percentage of fuel burn attributed to domestic flights.

A.10 Cargo flights

An estimate of global emissions from cargo flights in 2018 is made by combining flights marked as cargo or mail services in the OAG data with flights from FedEx, UPS, and DHL in the Flightradar24, which are absent in OAG. Total mass emitted and their spatial distribution are shown in Figure A.13 and Table A.21, respectively.

Table A.21: Fuel burn and emissions from cargo flights in 2018 from a combination of OAG and Flightradar24 data. Their share of all flights that year (including non-cargo flights) is shown in parentheses.

Fuel burn, Tg	22.6 (8.1%)
NO_x, Gg	355 (8.2%)
HC, Gg	3.91 (11.3%)
CO, Gg	40.9 (6.5%)
$nvPM_m$, Mg	565 (5.8%)
$nvPM_N$, 10^{25}	1.54 (4.5%)

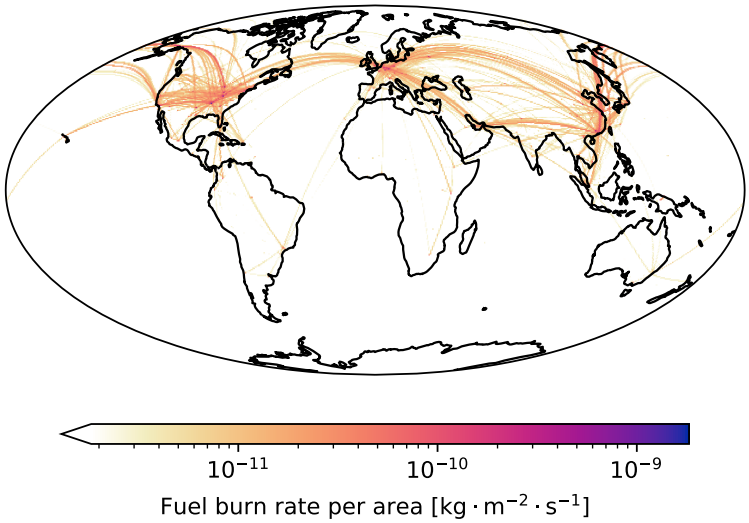

Figure A.13: Average vertically summed fuel burn rates of cargo flights in 2018 from a combination of OAG and Flightradar24 data.

A.11 OpenSky fuel burn relative to Flightradar24

Flight coverage during the 2017–2020 period is different between OpenSky and Flightradar24 in several ways: a significant fraction of OpenSky flights have missing aircraft type data (Appendix A.1), military aircraft appear more often in the OpenSky records (Appendix A.3), OpenSky lacks tracking in certain regions (Appendix A.6), and the OpenSky network does not include data obtained by multilateration of non-ADS-B telemetry signals. The lack of trackers in certain regions is illustrated by the ratio of fuel burn in 2019 between OpenSky and Flightradar24 for flights departing China being 24%, while the ratio for flights departing Europe (minus Russia) is 70% and the ratio for all flights is 57% (Figure A.14).

The ratio of emissions between OpenSky and Flightradar24 per aircraft type (Table A.22), besides being affected by changing spatial differences in ADS-B coverage, is also affected by the lack of multilateration in OpenSky (leading to underrepresentation of older aircraft) and by missing data associating the unique identifiers of ADS-B transmitters to aircraft type codes (leading to underrepresentation of newer aircraft).

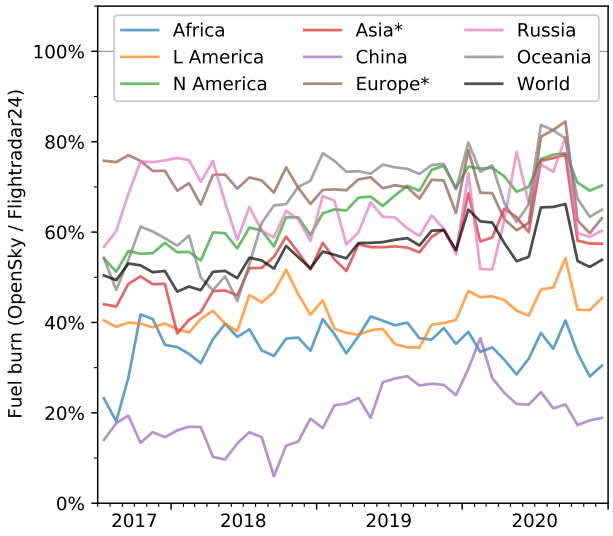

Figure A.14: Ratio of fuel burn from flights departing in specific regions estimated using flight movement data from OpenSky and from Flightradar24. "L America" represents Latin America and the Caribbean. Asia does not include China and Europe does not include Russia.

Table A.22: Ratio of global fuel burn in 2019 per aircraft type calculated using OpenSky (OS) and Flightradar24 (FR24) for the 30 types with the most fuel burn in the Flightradar24 results.

Type code	$\frac{\text{OS}}{\text{FR24}}$	Share of total FR24	Type code	$\frac{\text{OS}}{\text{FR24}}$	Share of total FR24
B738	53%	13.4%	B788	58%	2.2%
B77W	67%	10.7%	B748	74%	2.0%
A320	51%	10.7%	B739	63%	1.8%
A321	55%	5.5%	A20N	20%	1.7%
A333	61%	5.2%	B752	74%	1.4%
A388	80%	4.3%	E190	30%	0.7%
A332	53%	4.0%	A343	55%	0.7%
B744	71%	3.7%	E75L	68%	0.7%
B789	40%	3.7%	MD11	84%	0.7%
B772	70%	3.5%	CRJ9	56%	0.6%
B763	62%	3.0%	A346	68%	0.6%
A319	63%	2.7%	A21N	9%	0.5%
A359	41%	2.5%	A306	76%	0.5%
B77L	61%	2.5%	DH8D	22%	0.4%
B737	62%	2.4%	CRJ7	53%	0.3%

B

Additional details on health impact regional sensitivity to aircraft emissions

This appendix contains additional information relevant to Chapter 5, as listed below along with section numbers:

- B.1 provides details on regional differences in aircraft emissions.
- B.2 provides details on the methods for atmospheric modeling.
- B.3 gives additional results from atmospheric modeling.
- B.4 gives health impacts estimated with alternative concentration-response functions.
- B.5 describes how results from the separate regional perturbations were combined to estimate global health impacts.

This appendix was originally published as Supporting Information to an article in the Environmental Research Letters. Please cite as shown in the list of peer-reviewed journal articles, item 2.

B.1 Regional differences in aircraft emissions

B.1.1 Temporal variation

The AEIC aviation emissions inventory is based on a list of scheduled flights with departure times with a resolution of 1 hour [41]. The emissions corresponding to each flight are allocated to a month, and all emissions during a month are averaged over time and applied as a constant rate for the month. This captures a seasonal variation, with higher emissions during summer, as shown in Figure B.1.

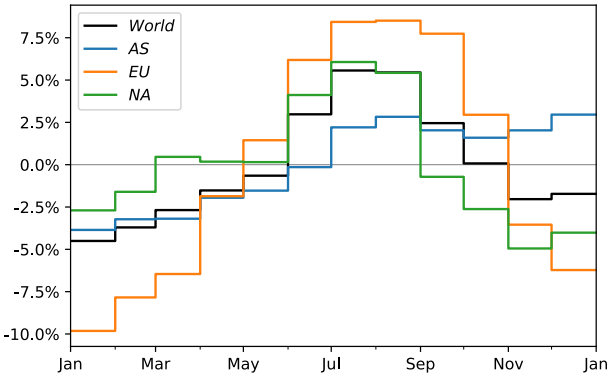

Figure B.1: Aviation fuel burn rate over time relative to the annual average; globally and within each region.

B.1.2 Spatial variation

For each scenario evaluated (one of the three regions perturbed), all emissions were multiplied by a constant number, with the multiplier being set at 1.10 for Europe and the others calculated so that the increase in fuel burn per area was the same. This approach preserves the spatial and temporal distribution of each emission species. The breakdown of emission mass summed over the year by species, region, and altitude is given in Table B.1. Landing and takeoff (LTO) emissions are defined as those up to 3000 ft above ground level. Since SO_x emissions are calculated using constant emission indices of $1.176\,\mathrm{g\,SO_2 \cdot kg^{-1}}$ and $0.036\,\mathrm{g\,SO_4^{2-} \cdot kg^{-1}}$, their temporal and spatial distribution is equal to that of fuel burn.

Table B.1: Percentage of fuel and emissions mass during LTO (when compared to full flight). HC = hydrocarbons, BC = black carbon.

Region	Fuel, SO_x	NO_x	HC	CO	BC
World	9.1%	7.7%	28.8%	35.0%	16.7%
AS	9.4%	9.0%	34.2%	31.1%	15.5%
EU	9.8%	8.3%	21.6%	31.4%	20.1%
NA	10.6%	8.1%	50.1%	46.0%	17.4%

Table B.2: Averaged regional and global emission indices over LTO and full-flight. HC = hydrocarbons, BC = black carbon.

	Full-flight [g/kg]			
Region	NO_x	HC	CO	BC
World	14.9	1.04	4.13	0.0328
AS	16.5	0.60	3.68	0.0322
EU	15.0	2.18	4.91	0.0339
NA	13.7	0.53	4.35	0.0325
	LTO [g/kg]			
World	12.7	3.29	16.0	0.0606
AS	15.9	2.20	12.2	0.0532
EU	12.7	4.79	15.7	0.0693
NA	10.5	2.48	18.9	0.0533

B.1.3 Share of international flights

Atmospheric chemistry is indifferent to our legal definitions of statehood, but in the context of discussing the transboundary nature of aviation's air quality impacts, it is worthwhile to note the relative amount of emissions that come from international versus domestic flights (Figure B.2), as they are regulated differently. In addition to that, the length of flights are a significant driver of regional differences in emission indices and vertical distribution of emissions. International flights tend to be longer, spending more time cruising (higher EI (NO_x)), while emissions for shorter domestic flights are weighted more towards LTO (higher HC, CO, and BC), as shown in Table B.3.

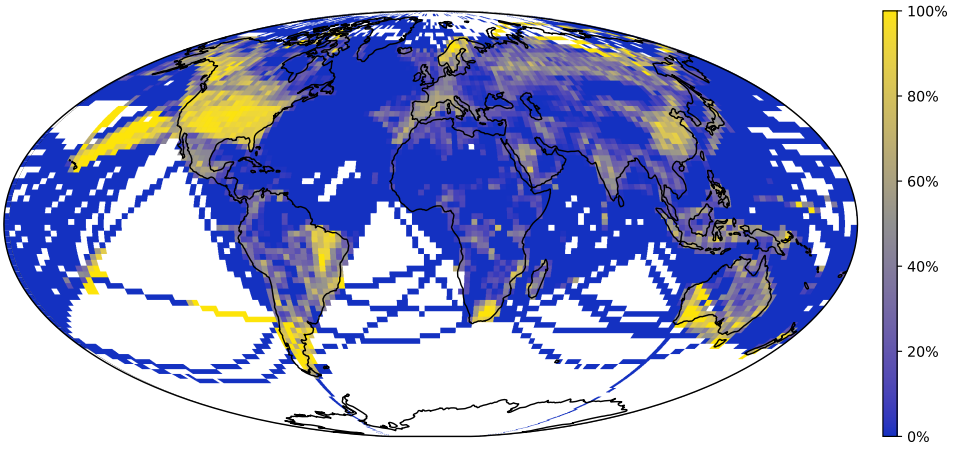

Figure B.2: Percentage of annual full-flight fuel burn by domestic flights at every grid cell, downscaled to 2° × 2.5° to improve visibility.

Table B.3: Averaged global full-flight emission indices and fraction of total emissions from domestic and international flights. HC = hydrocarbons, BC = black carbon.

	Fuel burn [Tg]	Full-flight EI [g/kg]			
		NO_x	HC	CO	BC
Domestic	n/a	13.6	1.63	5.88	0.0341
International	n/a	15.8	0.59	2.84	0.0318
Dom:Int mass	43:57	39:61	67:33	61:39	44:56

B.2 Atmospheric modeling

B.2.1 Non-aviation emissions

The default non-aviation emissions inventories of GEOS-Chem v12.6.1 are used in the simulations of Chapter 5. Inventories of anthropogenic emissions and the regions they are applied:

- CEDS: global.
- NEI2005: U.S. (2005 only).
- NEI2011: U.S. (2013 only).
- APEI: Canada.
- DICE-Africa: Africa.
- MIX-Asia: Asia.
- EDGAR v4.3: sectors not included in DICE-Africa.

Other inventories or modules, and the type of emissions:

- GFED4: biomass burning.
- PARANOX: ship plume model.
- Lightning NO_x (nameless).
- DEAD: mineral dust.
- Sea salt (nameless).
- MEGAN: biogenic.
- AeroCom: volcanic.

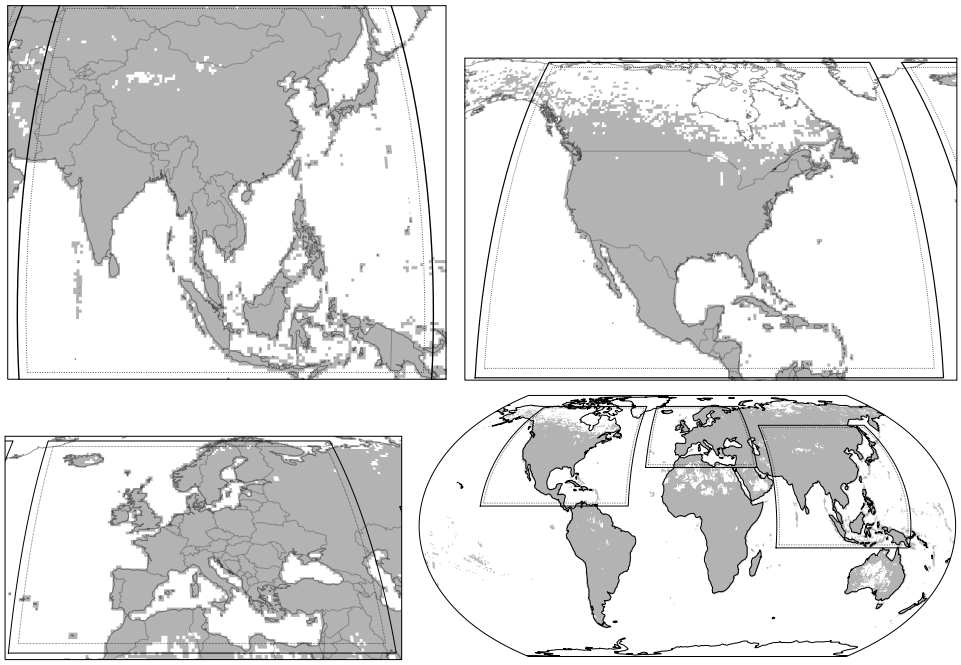

Figure B.3: Region definitions and grid cells with a population greater than zero.

B.2.2 Grid definitions and populated areas

The perturbations to aircraft emissions are applied with a 12-cell linear taper to zero at the edges of each region. To avoid numerical noise effects of the interface between grids, a border 3 grid cells wide (shown in Figure B.3) is discarded from each regional grid for analysis, with the global coarser resolution data used elsewhere.

The areas where the global LandScan 2005 population count, after being re-gridded to $0.5^\circ \times 0.625^\circ$, are greater than zero are presented in Figure B.3. Only these grid cells are used when calculating "populated area" averages. Global coarse grid results are upsampled to $0.5^\circ \times 0.625^\circ$ before applying population maps or the mapping of countries for health impact calculations.

B.2.3 Aerosol modeling

GEOS-Chem simulates not just aerosol dispersion, but also its photochemistry. Photolysis in the troposphere and stratosphere is calculated using the Fast-JX algorithm [315, 412, 413]. Aerosol effects on photolysis by radiative scattering are calculated at each grid cell, using the parametrization (of aerosol optical and physical properties, size distribution, hygroscopic growth factors, etc.) described by Latimer and Martin [369].

Sulfate-nitrate-ammonium thermodynamic equilibrium is calculated with the ISORROPIA II model [191] and is coupled to the gas-phase chemistry simulation [355]. Aerosol water content used in heterogeneous chemistry is from the ISORROPIA II thermodynamics. Surface and multiphase chemistry of nitrates in clouds is simulated by the model

described by Holmes et al. [366]. The cloud properties are taken from the meteorological data driving GEOS-Chem, i.e. the MERRA-2 reanalysis product in this case. This means that the effect of aerosol on cloud formation is not fed back to the photochemistry calculations, therefore not capturing this second order effect. NO_x emissions from lightning are calculated from the meteorological data, so effects of induced (or altered) cloudiness from perturbation of aircraft emissions on lightning occurrence and subsequent effects on natural NO_x emissions are also part of this second order impact mechanism that this setup does not capture. Finally, black carbon and organic aerosol models in GEOS-Chem, described by Wang et al. [376] and Pai et al. [414], also interact with local conditions and with background emissions.

There are other configurations of GEOS-Chem that treat aerosol microphysics more explicitly, using either the TOMAS [415] or APM [416] modules. However, since the adopted concentration-response functions relate health impacts to aerosol mass instead of particle number, the atmospheric model used is considered appropriate.

The GEOS-Chem model uses a number of tracers to represent the various species that form fine particulate matter ($PM_{2.5}$). All $PM_{2.5}$ concentrations used in Chapter 5 are calculated from these tracers according to the default diagnostic output of GEOS-Chem [314], according to Equation (B.1). This definition is slightly different than that in a newer version of GEOS-Chem used in Chapters 6 and 7, described in Equation (6.1). Note that mineral dust and sea salt aerosol are not significantly affected by aircraft emissions.

$$\begin{aligned} \mathrm{PM}_{2.5} = &\left(\mathrm{NH}_4^+ + \mathrm{SO}_4^{2-} + \mathrm{NO}_3^-\right) \cdot GF_{SIA} \\ &+ \mathrm{BCPI} + \mathrm{BCPO} + \mathrm{OCPO} + (\mathrm{OCPI} + \mathrm{SOAS}) \cdot GF_{org} \\ &+ (\mathrm{SALA}) \cdot GF_{SSA} + \mathrm{DST1} + (\mathrm{DST2}) \cdot 0.38 \end{aligned} \tag{B.1}$$

where:

- BCPI = hydrophilic black carbon aerosol
- BCPo = hydrophobic black carbon aerosol
- OCPI = hydrophilic (primary) organic aerosol
- OCPO = hydrophobic (primary) organic aerosol
- SALA = accumulation mode (fine) sea salt aerosol
- DST1 = mineral dust with radius between 0.1 µm–1.0 µm
- DST2 = mineral dust with radius between 1.0 µm–1.8 µm
- SOAS = simple parametrization of secondary organic aerosol
- GF_{SIA} = 1.0 = particle size growth factor for secondary inorganic aerosols (NH_4^+, SO_4^{2-}, and NO_3^-)
- GF_{org} = 1.0 = particle size growth factor for OCPI and SOAS (organic aerosols)
- GF_{SSA} = 1.0 = particle size growth factor for SALA

Growth factors are applied in Equation (B.1) in order to consider the water content of aerosol particles. They represent the ratio between the size of wet and dry particles:

$$GF_k = 1 + \left(\left(\frac{r_{wet}}{r_{dry}} \right)^3 - 1 \right) \cdot \frac{\rho_{water}}{\rho_k} \tag{B.2}$$

where:

- GF_k = grwoth factor for species k
- r_{wet} = radius of wet particle
- r_{dry} = radius of dry particle
- ρ_k = specific mass of species k

Constant growth factors representing a relative humidity of 35% are applied globally. When individual $PM_{2.5}$ components are discussed in Appendix B.3.5, the same growth factors are also applied. The parameters used by GEOS-Chem to estimate the growth factors are discussed by Latimer and Martin [369], and result in GF_{SIA} = 1.233, GF_{org} = 1.049, and GF_{SSA} = 1.856.

B.2.4 Linearity of atmospheric model response

Throughout Chapter 5, air quality and health impacts are discussed for each scenario normalized by additional fuel burn mass. The nonlinear nature of the processes involved means that large perturbations will deviate from a constant proportional response. The sensitivities calculated are representative of marginal changes in emissions comparable to the magnitude of perturbation in the experiment. These marginal changes in aircraft emissions are on top of the baseline scenario, which includes global aircraft emissions along with emission sources from all other sectors. Since the perturbation multipliers are chosen to achieve the same average additional fuel burn mass per area, and the area of each region is different, the total amount of additional fuel burn is different for each case. A 10% increase in aircraft emissions is achieved in 3.6 years at 2.7% annual growth (representative of Europe, according to Ref. [224]), while a 26.7% increase takes 3.6 years at 6.7% growth (representative of Central Southwest Asia) and a 14.1% increase takes 5.1 years at 2.6% growth (representative of North America).

To evaluate how much the model response deviates from linearity with a threefold increase in perturbation, an additional set of simulations are performed for the global coarse grid and the EU nested grid, in which EU aircraft emissions are multiplied by 1.3 instead of 1.1. This leads to a total additional fuel burn mass of 11.2 Tg, compared to the amounts for the perturbations in the main study of 3.7 Tg (EU), 8.8 Tg (NA), and 10.4 Tg (AS). In this section, the increase in fine particulate matter ($PM_{2.5}$) concentration and ozone mixing ratio resulting from this 30% increase in EU emissions are compared relative to the changes caused by the 10% increase in emissions.

The ratios between ground-level changes (from the baseline simulations) resulting from the two levels of EU perturbation (30% and 10%) are listed in Table B.4 for three different spatial averaging methods and for the global coarse grid and the EU nested fine

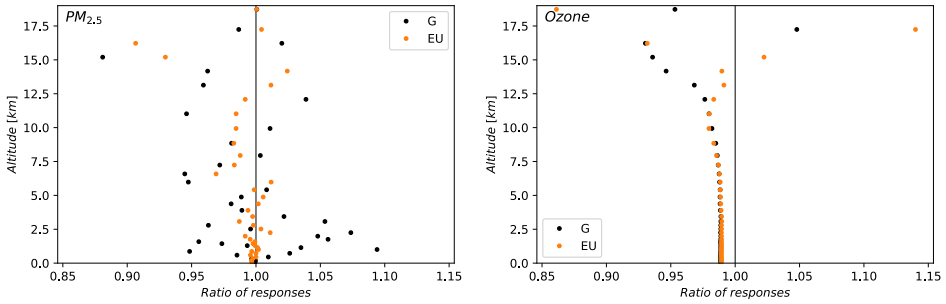

Figure B.4: Ratio between results of 30% and 10% EU perturbation: increases in $PM_{2.5}$ concentration and (MDA8) ozone mixing ratio per additional mass of fuel burned, averaged horizontally over all areas over the year for each vertical level, for the global (G) and EU simulations.

grid. The (three times) stronger perturbation resulted in 0.1% and 0.3% less $PM_{2.5}$ increases per additional fuel burn mass averaged over all areas in the global and regional simulations, respectively. Ozone (maximum daily 8-hour averages, MDA8) changes per additional fuel burn averaged over all areas were 1.1% smaller for the stronger perturbation, indicating a negative second order sensitivity to the added emissions. While the effect of a 3-fold perturbation to have a ~1% difference in the sensitivity, implying a relatively linear response (for full-flight impacts), nonlinearity may be present in larger perturbation sizes or around different baseline values (e.g. a more recent aircraft emissions scenario).

Table B.4: Ratio between results of 30% and 10% EU perturbation: increases in ground level $PM_{2.5}$ concentration and (MDA8) ozone mixing ratio per additional mass of fuel burned, averaged over the year.

Variable	Simulation	All areas	Populated areas	Population-weighted
$PM_{2.5}$	Global (coarse)	0.999	1.001	1.017
	EU (nested grid)	0.997	0.997	0.996
Ozone	Global (coarse)	0.989	0.989	0.987
	EU (nested grid)	0.989	0.990	0.989

The ratios in terms of concentration and mixing ratio changes averaged over all areas for each vertical level are shown in Figure B.4. The $PM_{2.5}$ ratios range from 0.94 to 1.10 up to 13 km in altitude, while ozone ratios are consistently less than 1.00.

The horizontal distribution of the absolute differences between ground level $PM_{2.5}$ and ozone changes per additional fuel burn mass are shown in Figure B.5. Ozone (normalized) response from the larger perturbation is lower than from the smaller perturbation throughout the Northern hemisphere, while $PM_{2.5}$ has grid cells with higher and lower responses. The largest $PM_{2.5}$ and ozone differences occur in East China and the Tibetan Plateau, respectively, which are also areas with high background concentrations (Figure S-9 and Figure S-10 in section S3.1) and large perturbation induced increases (Figure S-15 in section S3.2).

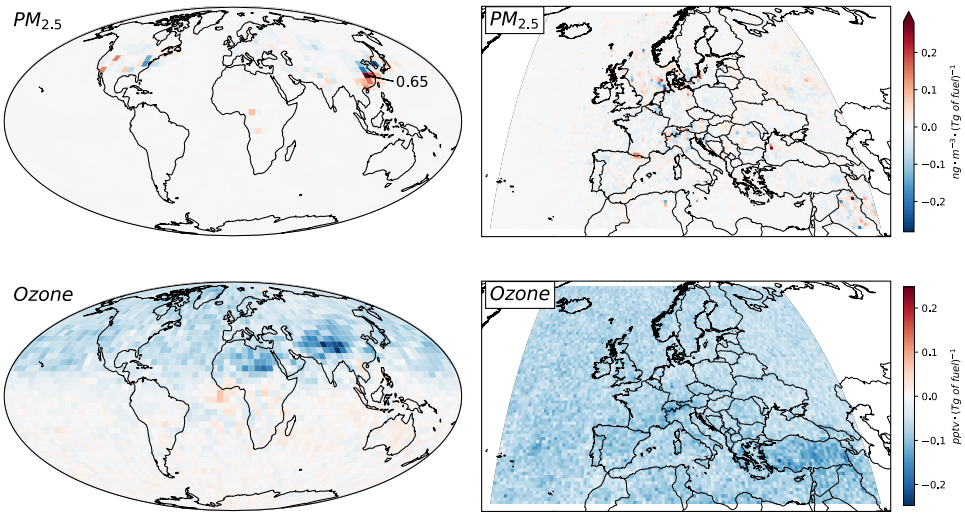

Figure B.5: Ground level $PM_{2.5}$ concentration and (MDA8) ozone mixing ratio changes per amount of additional fuel burn mass caused by 30% increase of EU aircraft emissions minus those caused by a 10% increase, averaged over the year.

B.2.5 Effects of grid resolution

Previous studies have shown that estimates of air quality sensitivity to aircraft emissions can vary with the horizontal resolution of the atmospheric model [322, 341]. Also, near airport effects are only captured at higher resolutions compared to global effects [1]. This section presents the difference between using only the global coarse resolution simulations and using the coarse simulation combined with the fine resolution regional nested simulations for the study in Chapter 5. Table B.5 compares $PM_{2.5}$ concentration and ozone mixing ratio changes, Table B.6 compares population-weighted changes, and Table B.7 compares health impacts. By all measures listed here, the aviation-attributable response of the combined nested simulations is larger than the response from just the coarse simulation across all three perturbation scenarios: 9–12% higher (area-weighted) global concentration (and mixing ratio) increases, 37–42% higher $PM_{2.5}$ population-weighted concentration increases, 19–22% higher ozone population-weighted mixing ratio increase, and 25–28% higher increase in mortalities. The coarser resolution may not be able to properly represent pollution gradients close to large cities, and since there is a correlation between spots of high population density and aircraft emissions, the coarser grid can underrepresent the exposure in those areas. This is consistent with larger differences observed in $PM_{2.5}$ compared to ozone, since its impacts are more localized.

The observed results with different resolutions indicate that, for the range of resolutions considered, resolution choice affects the calculated air quality impacts, by around 10%. Since health impacts also depend on population spatial distribution, it is influenced by resolution further: 19–40% higher impacts when incorporating the higher resolution simulations. It should be noted that for the estimation of the magnitude of aviation's

Table B.5: Comparison of results between coarse resolution and nested simulations: sensitivity of global yearly average ground level $PM_{2.5}$ concentration and ozone mixing ratio to aircraft emissions per region of emission.

	$PM_{2.5}$ $[ng \cdot m^{-3} \cdot (Tg\,fuel)^{-1}]$			Ozone $[pptv \cdot (Tg\,fuel)^{-1}]$		
Perturbation:	AS	EU	NA	AS	EU	NA
Coarse	0.037	0.064	0.042	2.13	2.23	1.79
Nested	0.041	0.071	0.046	2.33	2.50	1.98
Difference	+11%	+11%	+9%	+9%	+12%	+11%

Table B.6: Comparison of results between coarse resolution and nested simulations: sensitivity of population-weighted regional yearly average ground level $PM_{2.5}$ concentration and ozone mixing ratio to aircraft emissions; average of the three perturbation cases.

	$PM_{2.5}$ $[ng \cdot m^{-3} \cdot (Tg\,fuel)^{-1}]$			Ozone $[pptv \cdot (Tg\,fuel)^{-1}]$		
Perturbation:	AS	EU	NA	AS	EU	NA
Coarse	0.318	0.516	0.313	2.84	3.66	2.78
Nested	0.451	0.707	0.430	3.39	4.47	3.29
Difference	+42%	+37%	+37%	+19%	+22%	+19%

Table B.7: Comparison of results between coarse resolution and nested simulations: sensitivity of yearly excess mortality to aircraft emissions per region of perturbation.

	$PM_{2.5}$ $[deaths \cdot (Tg\,Fuel)^{-1}]$			Ozone $[deaths \cdot (Tg\,Fuel)^{-1}]$			Total $[deaths \cdot (Tg\,Fuel)^{-1}]$		
Perturbation:	AS	EU	NA	AS	EU	NA	AS	EU	NA
Coarse	69	130	73	164	203	156	234	333	229
Nested	97	172	97	196	254	188	294	427	285
Difference	+40%	+32%	+34%	+19%	+25%	+20%	+26%	+28%	+25%

health impacts — as opposed to the goal of comparing regional sensitivities — even higher resolution models could be incorporated close to airports to capture local air quality impacts, like the approach taken by Yim et al. [1]. As a result, an estimate of total health impacts from the sensitivities calculated here would likely be an underestimate due to the model's resolution.

B.3 Atmospheric modeling results

B.3.1 Baseline fine particulate matter and ozone

The yearly averages of ground-level fine particulate matter ($PM_{2.5}$) concentrations and ozone mixing ratios for the baseline simulation (those in which aircraft emissions are unperturbed) are presented in Figures B.6 and B.7. Increases attributable to the perturbation in aircraft emissions are defined as the difference in the concentrations or mixing ratios between the perturbed and baseline simulations.

Validation of the ability of GEOS-Chem to accurately represent the atmosphere is continuously performed by several studies, as improvements and new features are developed and incorporated into the model. Every significant update to the model is accompanied by a benchmark simulation to avoid regressions. Stratospheric chemistry results from the unified chemistry extension (UCX) module were compared by Eastham et al. with multiple weather balloon and satellite measurements [315]. Aerosol measurements over the United States from various surface, aircraft, and satellite observations were compared with GEOS-Chem results by Kim et al. [316]. Modeled organic aerosol chemistry was compared by Pai et al. with 15 globally distributed airborne measurement campaigns [414]. Latimer and Martin compared modeled aerosol mass scattering with ground air quality station measurements over the United States [369].

In this section, modeled surface concentrations of ozone and $PM_{2.5}$ from the EU and NA regional nested simulations are compared to ground station measurements for the year 2005. For Europe, data from the European Environment Agency's (EEA) AirBase version 8 are used for both $PM_{2.5}$ and ozone (Figures B.8 and B.9). Only "background" type stations were considered. For North America, data from the US EPA (Environmental Protection Agency) are used: NCore for $PM_{2.5}$ measurements (Figure B.10), and CASTNET (Clean Air Status and Trends Network) measurements of ozone (Figure B.11). For both regions, only stations with sufficient data representative of the whole year are used. Grid cells with more than one ground station are compared with the average of the values reported there. The results of the comparison are presented in Table B.8.

The ability of the model to accurately represent the sensitivity of air quality to aviation emissions is harder to verify as there is no direct measurement that can be used for comparison. This is why the uncertainty estimates described in Section 5.2.4 are based on an inter-model comparison study looking specifically at impacts from aviation emissions [33].

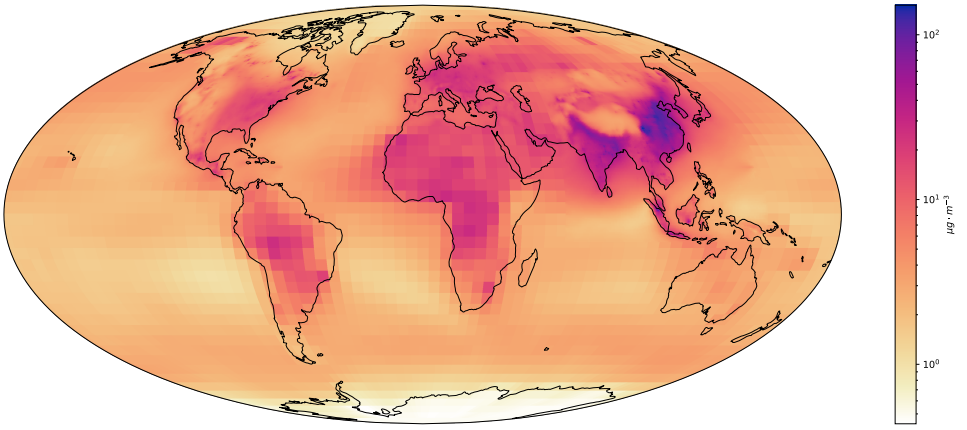

Figure B.6: Yearly average background surface level concentration of $PM_{2.5}$ for the baseline scenario, log-scale.

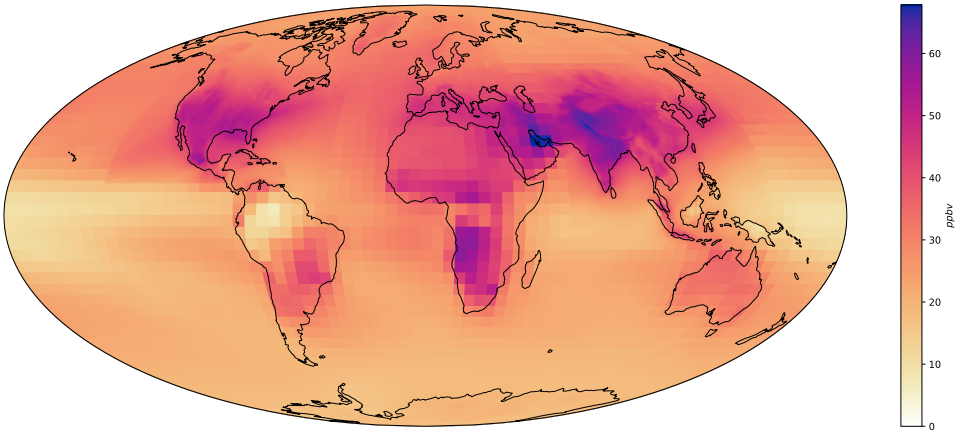

Figure B.7: Yearly average background surface level maximum daily 8-hour average (MDA8) mixing ratio of ozone for the baseline scenario, linear scale.

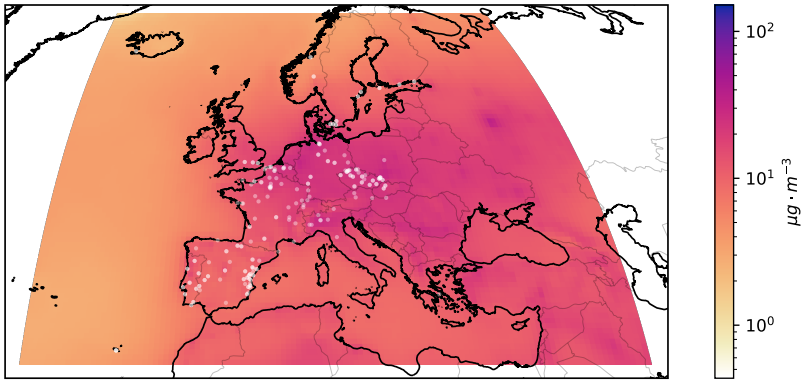

Figure B.8: Yearly average background surface level concentration of $PM_{2.5}$ over the EU domain for the baseline scenario, with EEA AirBase air quality monitors used for comparison marked by semi-transparent white dots.

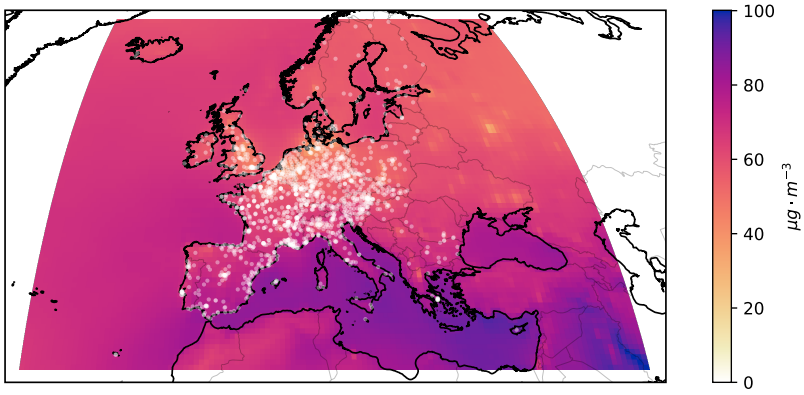

Figure B.9: Yearly average background surface level concentration of ozone over the EU domain for the baseline scenario, with EEA AirBase air quality monitors used for comparison marked by semi-transparent white dots.

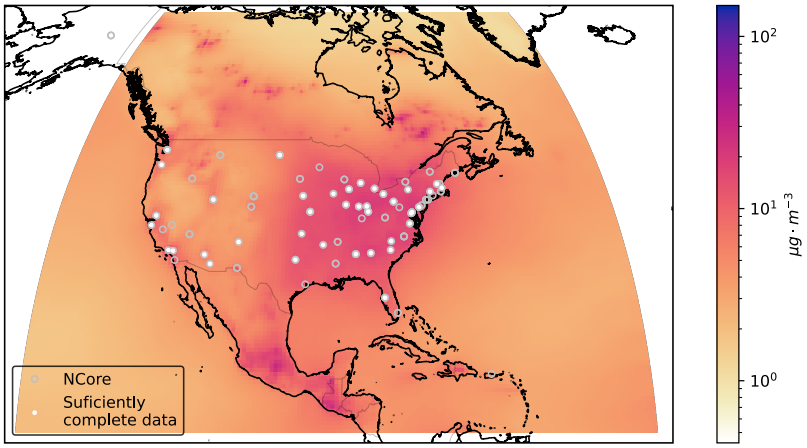

Figure B.10: Yearly average background surface level concentration of $PM_{2.5}$ over the NA domain for the baseline scenario and the location of CASTNET air quality monitors used for comparison.

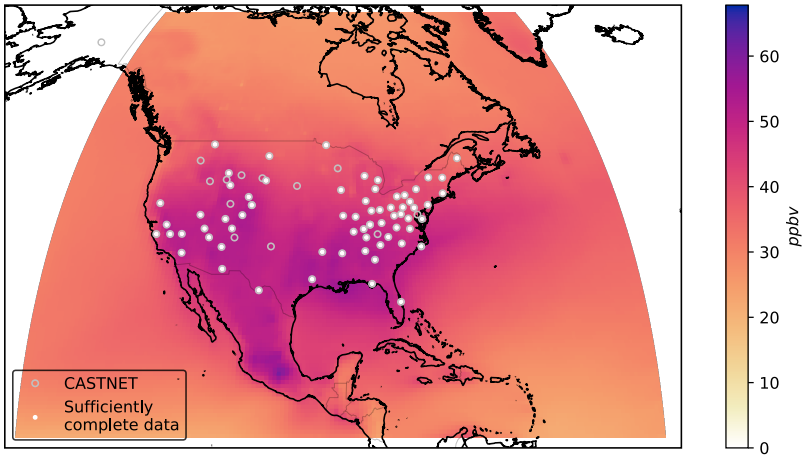

Figure B.11: Yearly average background surface level maximum daily 8-hour average (MDA8) mixing ratio of ozone over the NA domain for the baseline scenario and the location of NCore air quality monitors used for comparison.

Table B.8: Comparison of modeled (M) background surface level $PM_{2.5}$ and ozone values against observed (O) values at air quality monitoring stations in Europe and North America.

	$PM_{2.5}$		Ozone	
	EU [$\mu g \cdot m^{-3}$]	NA [$\mu g \cdot m^{-3}$]	EU [$\mu g \cdot m^{-3}$]	NA [MDA8 ppbv]
Measurement source	AirBase	NCore	AirBase	CASTNET
Number of stations	130	39	715	67
Mean (model)	16.2	14.2	60	46.3
Mean (observed)	15.2	13.2	54.1	48.5
Standard deviation (M)	6.5	4.6	10.2	5.25
Standard deviation (O)	7	3.7	12.4	5.38
Mean bias	1.03	1.07	5.9	-2.25
Mean error	4.84	2.76	10.8	4.66
Root mean square error	6.38	3.35	14	5.52
Normalized mean bias	6.8%	8.1%	10.9%	-4.6%
Normalized mean error	31.9%	21.0%	20.0%	9.6%
Correlation coefficient	0.577	0.742	0.38	0.56
Index of agreement	0.755	0.819	0.602	0.718

B.3.2 Perturbation-induced fine particulate matter and ozone changes

The yearly average changes in surface $PM_{2.5}$ and ozone are shown for all three perturbation cases in Figure B.12, with the nested simulation results overlaid on those from the global (coarser resolution) simulation. These changes are averaged spatially (weighted by area or population) to calculate the overall air quality impacts.

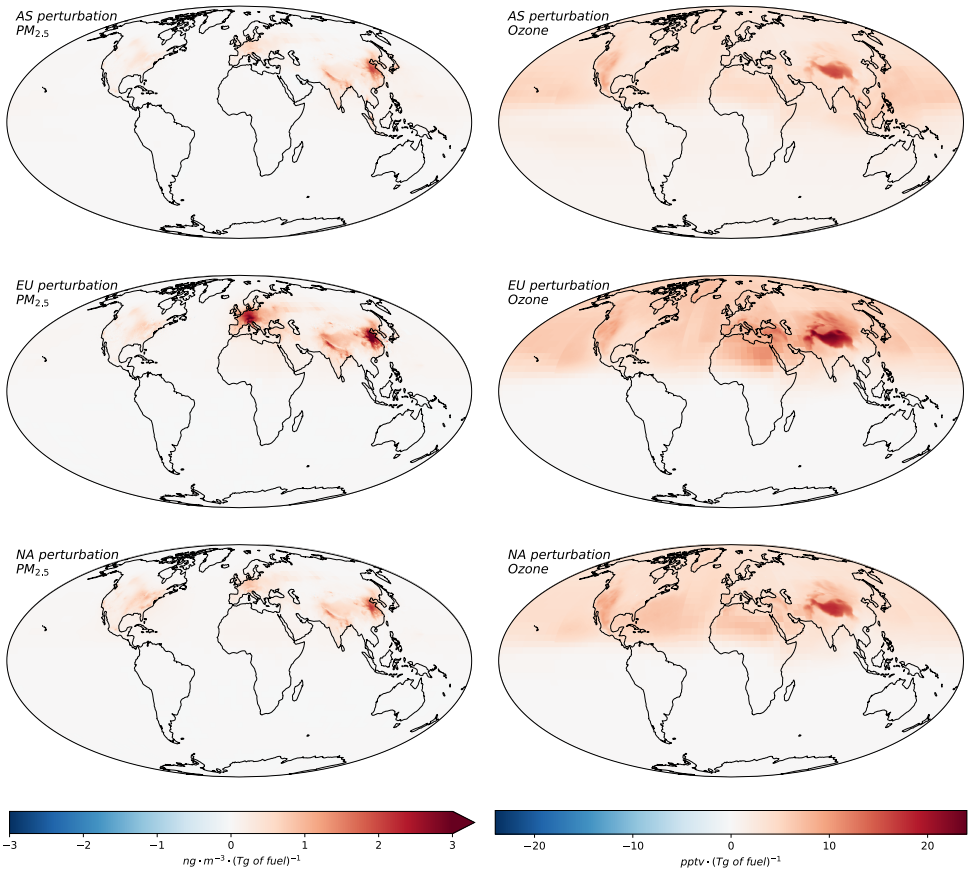

Figure B.12: Yearly average increase of ground level $PM_{2.5}$ (left) and ozone MDA8 (right) for perturbed (increased) full-flight emissions.

B.3.3 Background gas ratio

The (background) gas ratios were calculated using Equation (2.14) with ground level concentrations from the baseline simulation. The average GR values for each grid cell in the AS, EU and NA regions during the months of January and July are shown in Figure B.13. GR values of less than one are found during winter (represented by January in Figure B.13) in some of the areas of high aviation LTO emissions in AS and NA: part of East China, South Korea, Japan, and the coasts of the United States. At the same time, average GR values greater than one occur in most of Western Europe in January. In July, GR is higher across the three regions, but a significant portion of NA remain with GR values less than one. The lower GR values in NA compared to EU are in line with the maps presented in the Supplementary Material of Ref. [417], and the low GR values along the coasts of the Unites States are also in line with the results obtained by Woody et al. [313].

Table B.9 lists the percentage of aviation emissions and population within each region that are over areas with high GR (greater than 1.0, 1.3, and 1.5). Compared to the other regions the lower fraction of LTO emissions in NA over areas with high GR is reflected in the lower $PM_{2.5}$ sensitivity to aviation emissions and in the speciation of $PM_{2.5}$ changes: lower nitrate formation and a net increase in sulfates (Appendix B.3.5).

Table B.9: Percentage of regional NO_x aircraft emissions and population over grid cells with a monthly average GR greater than 1.0, 1.3, and 1.5.

		January			July		
Variable	GR > than	AS	EU	NA	AS	EU	NA
Full-flight NO_x	1.0	53	68	29	63	71	37
	1.3	44	58	15	56	65	28
	1.5	40	51	12	51	61	22
LTO NO_x	1.0	76	87	33	86	84	35
	1.3	57	78	15	68	77	21
	1.5	50	76	14	60	75	15
Population	1.0	87	78	55	94	83	58
	1.3	82	62	39	90	76	45
	1.5	79	52	36	87	71	37

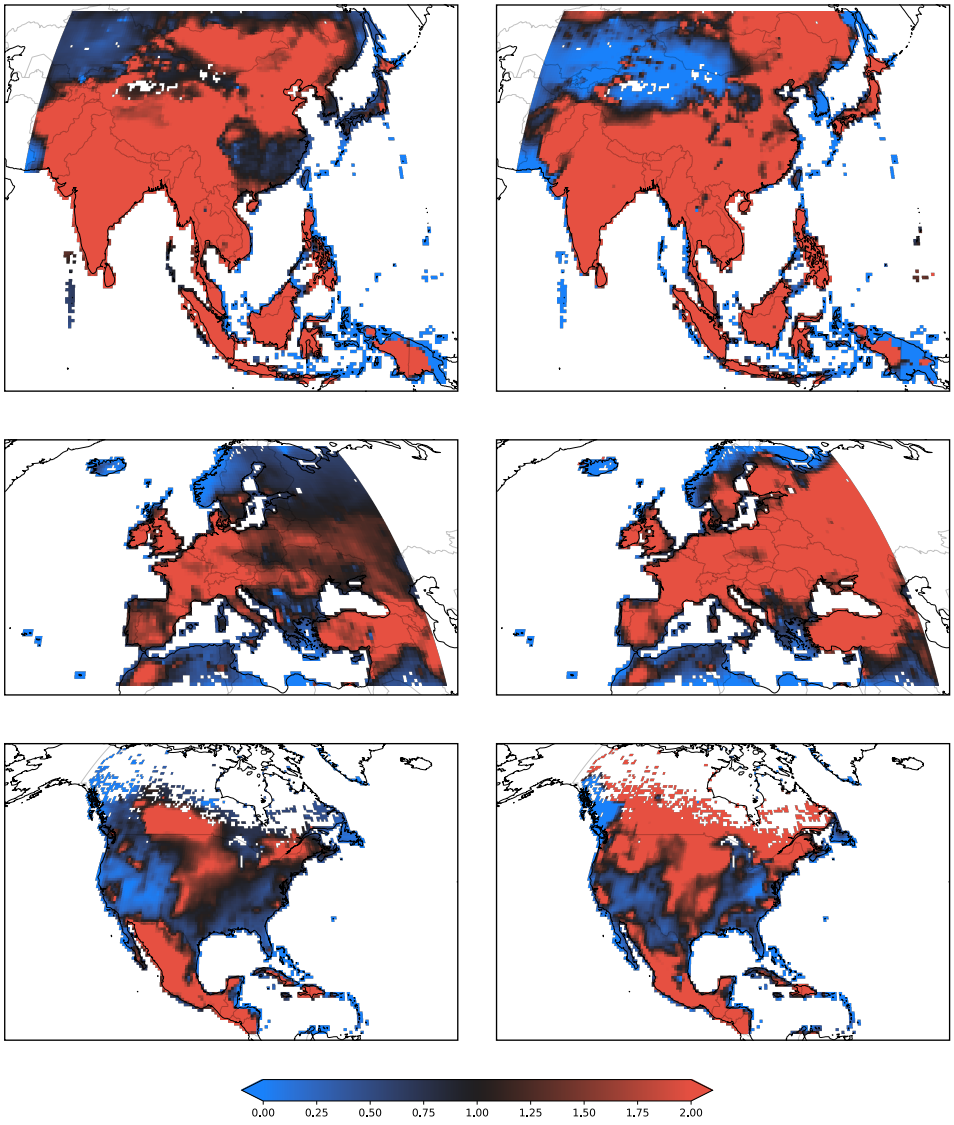

Figure B.13: Average ground level gas ratio (free ammonia to total nitrates) during January (left) and July (right). Only populated grid cells are shown.

B.3.4 Formaldehyde to NO_y ratio and ozone sensitivity to LTO emissions

In all full-flight perturbation cases simulated, cruise emissions cause widespread increases in ozone mixing ratio, from cruise levels down to the surface (Figure B.12). However, landing and takeoff (LTO)-only perturbations cause both local increases and decreases in ground-level ozone. This is expected from the photochemistry of ozone formation, with its sensitivity to additional NO_x depending on the ratio of volatile organic compounds (VOC) and NO_x, the main precursors of lower tropospheric ozone formation [324]. The formaldehyde (CHOH) to NO_y or NO_2 ratio (FNR) can be used as an indicator of the relative levels of these ozone precursors, identifying whether ozone production in a given area is NO_x-limited or NO_x-saturated [418].

FNR is calculated here using Equation (B.3) with average ground-level concentrations during January and July from the baseline simulation. NO_y is calculated as the sum of the following GEOS-Chem tracers: NO, NO_2, NO_3, HNO_2, HNO_3, HNO_4, N_2O_5, PAN (peroxyacetyl nitrate), MONITS and MONITU (saturated/unsaturated first generation monoterpene organic nitrates), HOMIT (second generation monoterpene organic nitrates).

$$FNR = \frac{[\mathrm{CHOH}]}{[NO_y]} \tag{B.3}$$

The ozone changes from increased LTO emissions are plotted in Figure B.14 along with two FNR contour lines (0.25 and 0.3). Ozone decreases associated with LTO emissions occur mostly in areas with FNR less than 0.25, consistent with the NO_x-VOC regime change point of 0.28 observed in the study by Sillman [324]. Higher FNR values in July are accompanied by larger ozone increases.

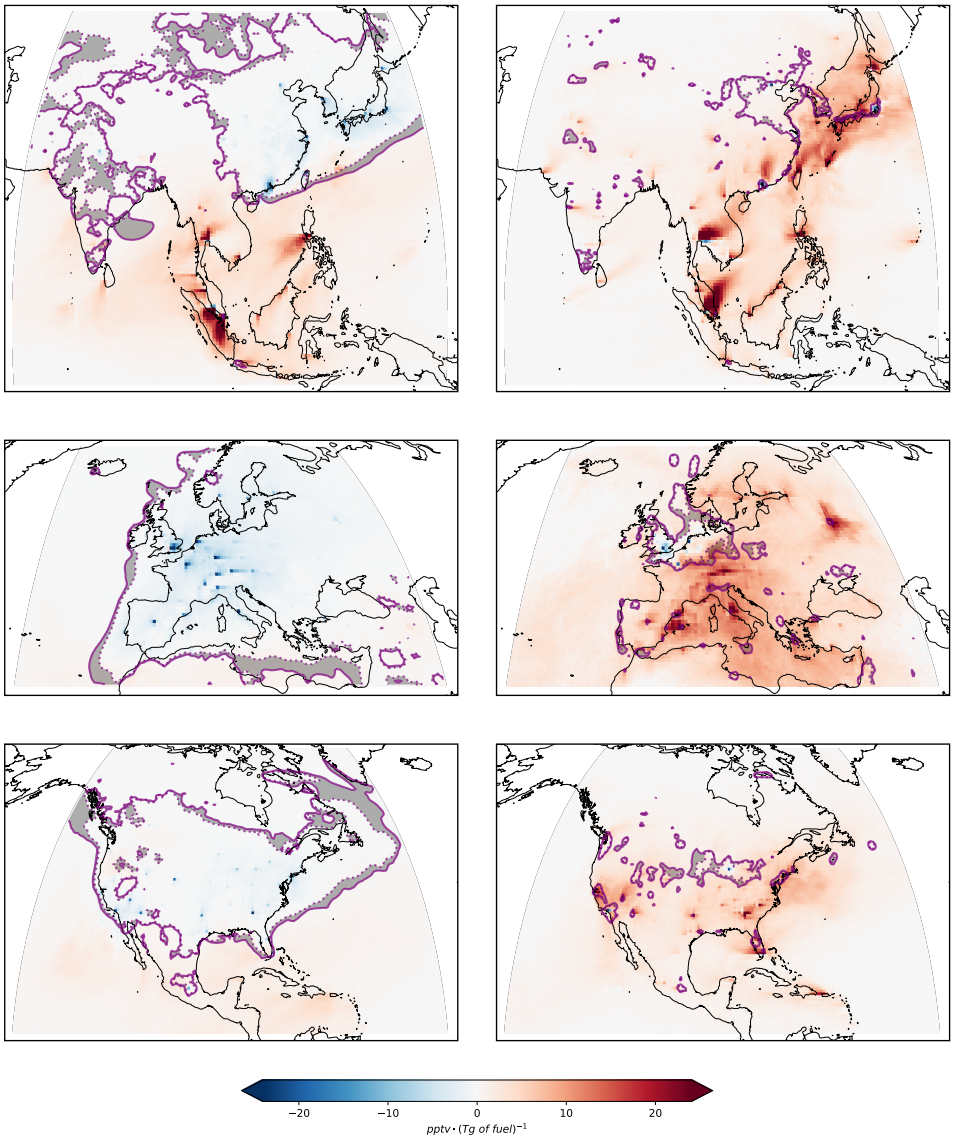

Figure B.14: Average change of ground-level ozone MDA8 for increased LTO emissions during January and July. The dashed and solid purple contour lines mark FNR values of 0.25 and 0.30, respectively. Areas with FNR between 0.25–0.30 are darkened.

B.3.5 $PM_{2.5}$ speciation

In all three regions, almost all of the population-weighted increase in $PM_{2.5}$ concentrations comes in the form of additional nitrates and ammonium, which is partially offset by decreases in sulfates (Figure S-18). In the LTO scenarios, organic aerosols become more relevant, which is expected from their higher emission indices at taxing conditions. Their percentage of total $PM_{2.5}$ is particularly higher in North America, due to the lower amount of nitrate formed.

Source:	AS						EU						NA					
Receptor	SO_4^{2-}	NO_3^-	NH_4^+	BC	POA	SOA	SO_4^{2-}	NO_3^-	NH_4^+	BC	POA	SOA	SO_4^{2-}	NO_3^-	NH_4^+	BC	POA	SOA
World	-8	84	21	0	1	2	-3	79	22	0	0	2	-4	80	21	0	0	2
AS	-7	81	21	0	2	3	-2	78	22	0	2	1	-4	80	22	0	2	0
EU	-22	101	20	0	0	0	-8	80	20	1	2	6	-17	94	20	0	1	1
NA	-8	85	21	0	0	1	1	73	21	0	4	1	8	50	17	2	9	14

Source:	LTO					
Receptor	SO_4^{2-}	NO_3^-	NH_4^+	BC	POA	SOA
AS	1	65	19	2	3	11
EU	-6	67	17	3	3	16
NA	11	18	9	6	10	45

SO_4^{2-} = sulfates	BC = black carbon
NO_3^- = nitrates	POA = primary organic aerosol
NH_4^+ = ammonium	SOA = secondary organic aerosol

Figure B.15: Population-weighted changes in individual constituents as a percentage of total $PM_{2.5}$ mass increase for each perturbation case and in each region. Particle growth factors are applied in mass calculations to account for hygroscopicity, as described in Appendix B.2.3.

Differently to previous studies on air quality impacts from aviation [1, 30], $PM_{2.5}$ in the form of secondary organic aerosols (SOA) is also considered. For the LTO perturbation scenarios, it is found that the aviation-attributable SOA share of $PM_{2.5}$ mass is between 2.4–2.8 times that of black carbon and primary organic carbon combined. Scientific understanding of the chemistry of SOA formation in the atmosphere is still limited due to its complexity [195], and the simplicity of the model used here means the precise effect of aircraft emissions on organic aerosols remains largely unresolved. However, the results suggest that SOA could be a significant component of the air quality impacts of aviation, particularly in NA. The strong nonlinearity of the NO_x-organic chemistry can change the sensitivity of SOA formation to new emissions significantly with changing background atmospheric composition [419], which poses further questions about the current and future impacts of aviation on $PM_{2.5}$.

B.4 Alternative health impact estimations

Due to the sensitivity of the health impacts estimates presented to the choice of concentration-response function (CRF), in addition to the main health impacts estimation methods described in Chapter 5, several other CRFs were applied. Tables B.10 and B.11 give the additional (marginal) premature mortality from aviation emissions in each region per additional mass of fuel burn estimated using CRFs from different sources and considering different mortality endpoints. The tables show the median estimate of the Monte-Carlo method, with uncertainty quantified by considering triangular error distributions defined by the central value and the 95% confidence intervals reported for the hazard ratio in each CRF, besides the error distributions for $PM_{2.5}$ and ozone changes as described in Section 5.2.4.

For the $PM_{2.5}$ CRF used in Chapter 5, the median estimates are 8.3% higher than the estimates using the nominal input values for all three perturbation cases. For the ozone CRF used, the median estimates are 1.4% smaller than the result from nominal values for all three perturbation cases. Tables B.10 and B.11 indicate the relative difference between median and nominal results for the other CRFs, for all of which these differences are the same (to 0.1%) for every perturbation case.

Alternative $PM_{2.5}$ CRFs lead to values between −58% and +122% the main estimate (Table B.10). The ratios between impacts of emissions of different regions range from EU/NA between 1.74–1.83, and AS/NA between 0.92–1.02. Alternative ozone CRFs lead to values between −66% and +52% the main estimate (Table B.11). The corresponding ratios between impacts of emissions of different regions range from EU/NA between 1.34–1.44, and AS/NA between 0.96–1.04.

Table B.10: Global premature mortality from $PM_{2.5}$ attributed to aviation emissions perturbations in 2005 in each region per additional mass of fuel burn calculated with various concentration-response functions [deaths·(Tg fuel)$^{-1}$]. Median estimates with 95% confidence intervals shown in parentheses. The CRF used in Chapter 5 is in italics. * Relative difference between median estimates and the results using nominal input values (average across all perturbation cases). † NCD = Noncommunicable disease, LRI = Lower respiratory infection. ‡ For this CRF, no error distribution was considered for the hazard ratio, the nominal value reported was used. The values in parentheses are the 95% confidence intervals for estimates calculated using the 25th and 75th percentile values of the hazard ratio reported for the CRF.

CRF		Region of perturbation			Ratios		
Ref.	Endpoint	AS	EU	NA	EU/NA	AS/NA	*
[114]	*NCD+LRI†*	*106 (47-193)*	*187 (84-341)*	*106 (47-193)*	*1.77*	*1.00*	*8.3%*
[115]	All-cause	127 (61-209)	215 (103-354)	124 (59-204)	1.74	1.02	9.4%
[420]	All-cause	190‡ (47-440)	322‡ (80-748)	185‡ (46-430)	1.74	1.02	9.4%
[329]	All-cause	108 (49-191)	183 (84-325)	105 (48-187)	1.74	1.02	8.8%
[329]	Cardiovascular	70 (30-132)	126 (55-239)	70 (30-132)	1.81	1.00	7.5%
[421]	All-cause	97 (44-176)	165 (75-299)	95 (43-172)	1.74	1.02	8.6%
[421]	Cardiopulmonary	120 (56-206)	207 (96-356)	117 (55-202)	1.76	1.02	9.0%
[101]	All-cause	235 (102-449)	399 (173-762)	229 (99-439)	1.74	1.02	8.9%
[101]	Cardiovascular	163 (72-303)	295 (131-548)	163 (72-302)	1.81	1.00	9.5%
[328] linear	Cardiopulmonary + lung cancer	96 (40-191)	167 (69-331)	95 (39-188)	1.76	1.02	6.1%
[328] nonlinear	Cardiopulmonary + lung cancer	45 (18-88)	89 (37-176)	49 (20-96)	1.83	0.92	6.1%
[422]	All-cause	95 (25-217)	161 (43-368)	92 (25-212)	1.74	1.02	5.5%
[422]	Cardiovascular	204 (93-364)	369 (169-659)	204 (93-364)	1.81	1.00	9.2%

Table B.11: Global premature mortality from ozone attributed to aviation emissions perturbations in 2005 in each region per additional mass of fuel burn calculated with various concentration-response functions [deaths·(Tg fuel)$^{-1}$]. Median estimates with 95% confidence intervals are shown in parentheses. The CRF used in Chapter 5 is in italics. * Relative difference between median estimates and the results using nominal input values (average across all perturbation cases).

CRF			Region of perturbation			Ratios		
Ref.	Endpoint	Ozone metric	AS	EU	NA	EU/NA	AS/NA	*
[104]	*Respiratory*	*MDA8 annual*	*193 (112-296)*	*251 (145-383)*	*185 (107-283)*	*1.35*	*1.04*	*−1.4%*
[104]	All-cause	MDA8 annual	268 (130-496)	380 (185-703)	269 (130-496)	1.42	1.00	11.4%
[115]	All-cause	24h season	109 (66-152)	164 (100-229)	113 (69-159)	1.44	0.96	0.0%
[330]	Respiratory	MDA1 season	65 (29-118)	85 (37-153)	63 (28-114)	1.34	1.03	−3.1%

B.5 Estimate of the health impacts of global aviation emissions

The study in Chapter 5 focused on calculating the human health impacts of aviation emissions over one of three regions (named AS, EU, and NA). In order to compare results with previous research, an estimation of the impacts from aviation emissions over the whole world was also performed, as described in this section.

An additional global coarse resolution (4° × 5°) simulation was performed, in which all aviation emissions were turned off altogether. Assuming linearity of the model response to aviation emissions (discussed in Appendix B.2.4) and linearity of the concentration-response functions (for simplification), the results from this coarse "zero aviation emissions" simulation was combined with the nested grid regional simulations discussed in Chapter 5 to give an estimate of the impacts from total (global) aviation emissions. This essentially means that this estimate extrapolates the impacts from the regional perturbation (nested) simulations and uses a coarse global simulation to estimate the sensitivity of impacts to emissions over "other" regions (outside AS, EU, and NA).

Impacts (I) are defined here as the increase in premature mortality from changes in ground-level fine particulate matter ($PM_{2.5}$) and ozone concentrations over the baseline simulation, in which aviation emissions were unperturbed. The impacts attributed to emissions in "other" regions are calculated as the difference between the impacts from the "zero" simulation (with the signal flipped, since emissions were removed) and the contribution from emissions over the AS, EU, and NA regions. These contributions are calculated from the simulations where the aviation emissions over those regions were perturbed by a multiplier α (Section 5.2.1 and Table 5.1), scaled so as to represent the impacts of the total amount of aviation emissions from the regions. Equation (B.4) is calculated using only results from the coarse global simulations, denoted by the C subscript.

$$I_{C,other} = -I_{C,zero} - \frac{I_{C,AS}}{\alpha_{AS} - 1} - \frac{I_{C,EU}}{\alpha_{EU} - 1} - \frac{I_{C,NA}}{\alpha_{NA} - 1} \tag{B.4}$$

The impacts from emissions in "other" regions are then added back with the impacts from the AS, EU, and NA regions calculated using the finer resolution regional simulations, denoted by the F subscript:

$$I_{total} = -I_{C,other} - \frac{I_{F,AS}}{\alpha_{AS} - 1} - \frac{I_{F,EU}}{\alpha_{EU} - 1} - \frac{I_{F,NA}}{\alpha_{NA} - 1} \tag{B.5}$$

The 95% confidence interval for these results are calculated in the same manner, but using the 2.5th or 97.5th percentile values of each impact estimate. That is, the random variables apply simultaneously to all perturbation cases, as our error quantification is related only to the CRFs and the model response to emissions.

C

Additional details on air quality impact estimations

This appendix provides further details supporting the study presented in Chapter 6. Included are the seasonal variation of aircraft-attributable impacts on ground-level air quality (Figure C.1), map of share of all-source $PM_{2.5}$ concentration due to aircraft emissions (Figure C.2), map of share of aircraft-attributable $PM_{2.5}$ due to LTO (Figure C.3), map of share of aircraft-attributable $PM_{2.5}$ due to full-flight NO_x emissions (Figure C.4, relative difference in air quality impacts of LTO emissions between different non-aviation emissions scenarios (Figure C.5, and a comparison of vertical profiles of global concentration of multiple species between simulations driven by MERRA-2 and GCAP 2.0 meteorology fields (Figure C.6).

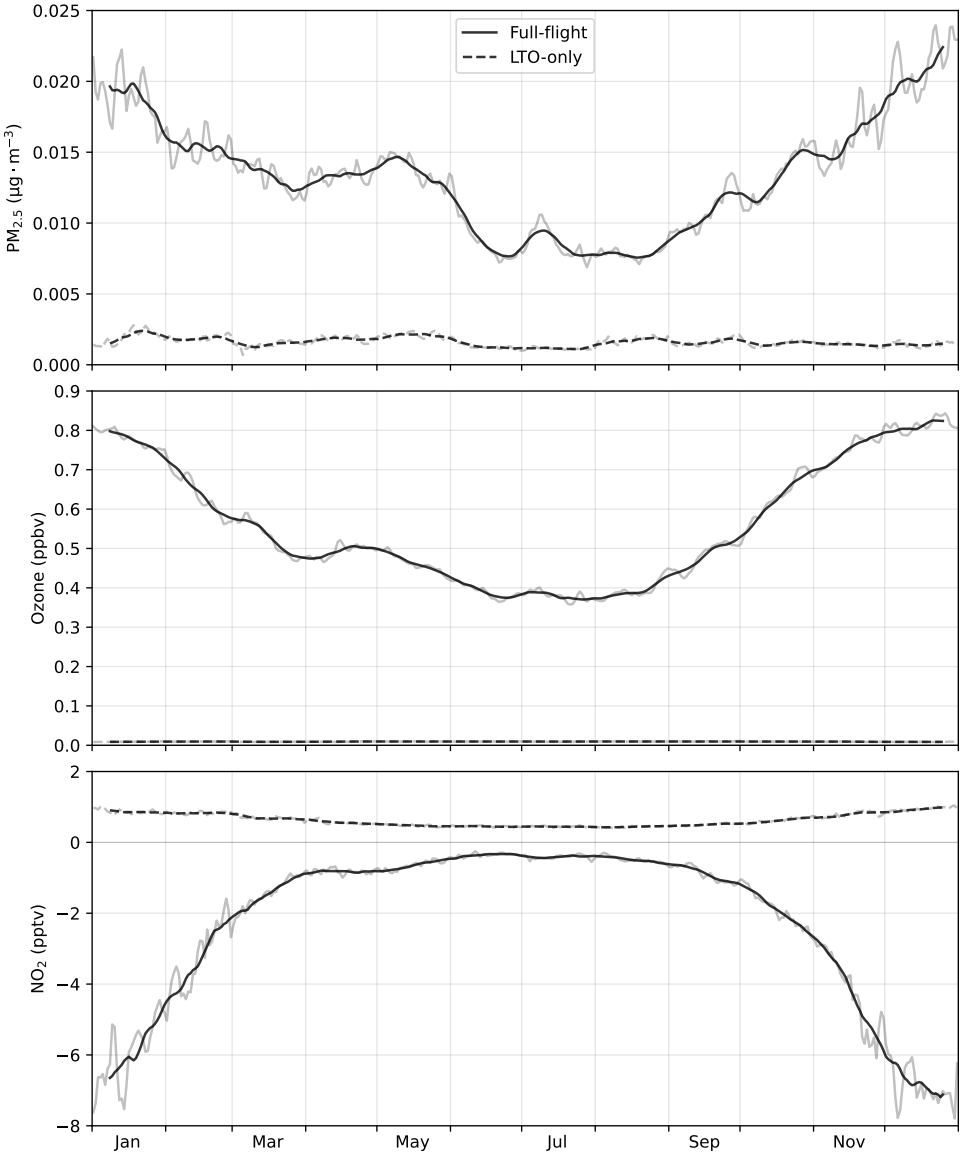

Figure C.1: Daily and 14-day area-weighted global average ground-level pollutant concentration changes attributed to 2019 full-flight and LTO-only emissions.

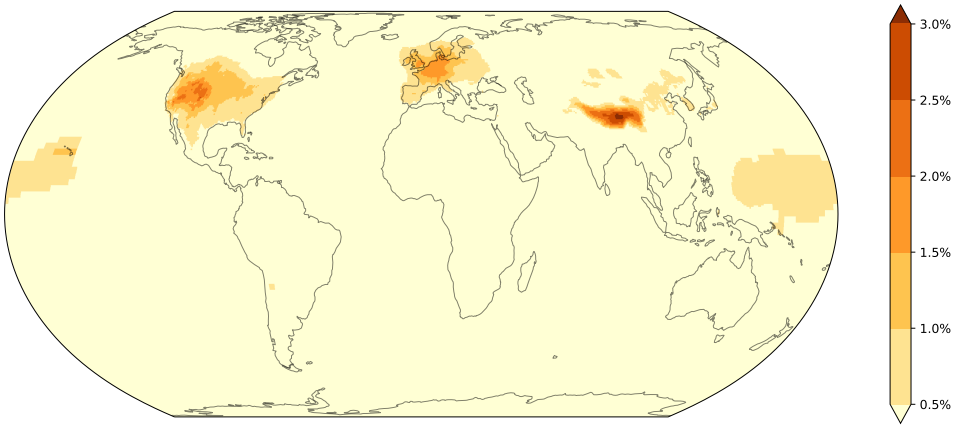

Figure C.2: Share of ground-level 2019 annual average $PM_{2.5}$ concentration due to aircraft (full-flight) emissions.

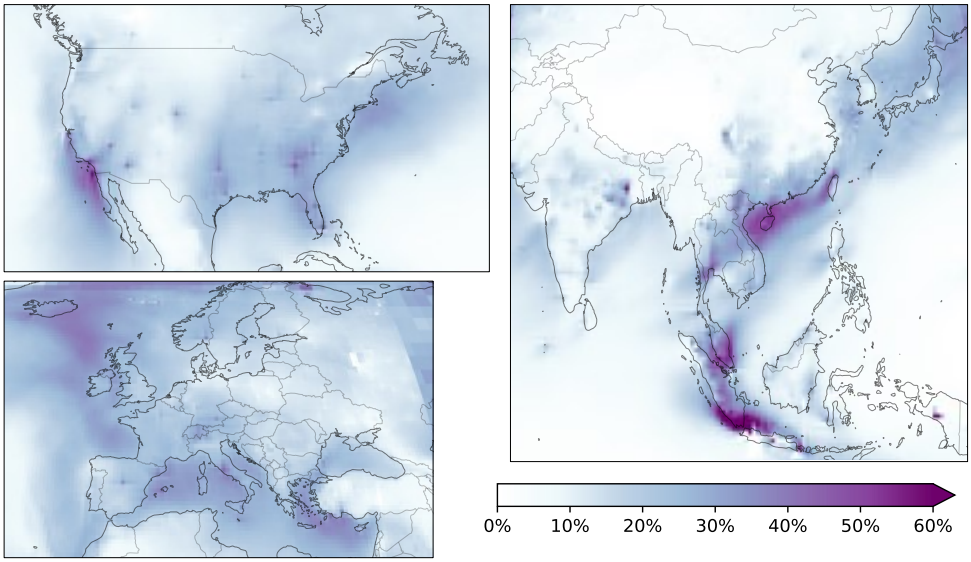

Figure C.3: Share of aircraft-attributable ground-level 2019 annual average $PM_{2.5}$ concentration due to LTO emissions.

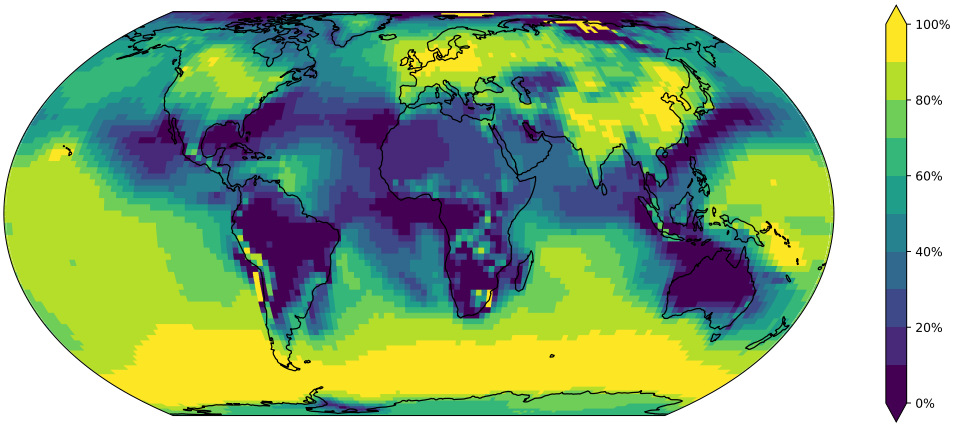

Figure C.4: Ratio of 2019 annual average $PM_{2.5}$ aircraft-attributable increases between full-flight NO_x-only and full-flight including emission of other species.

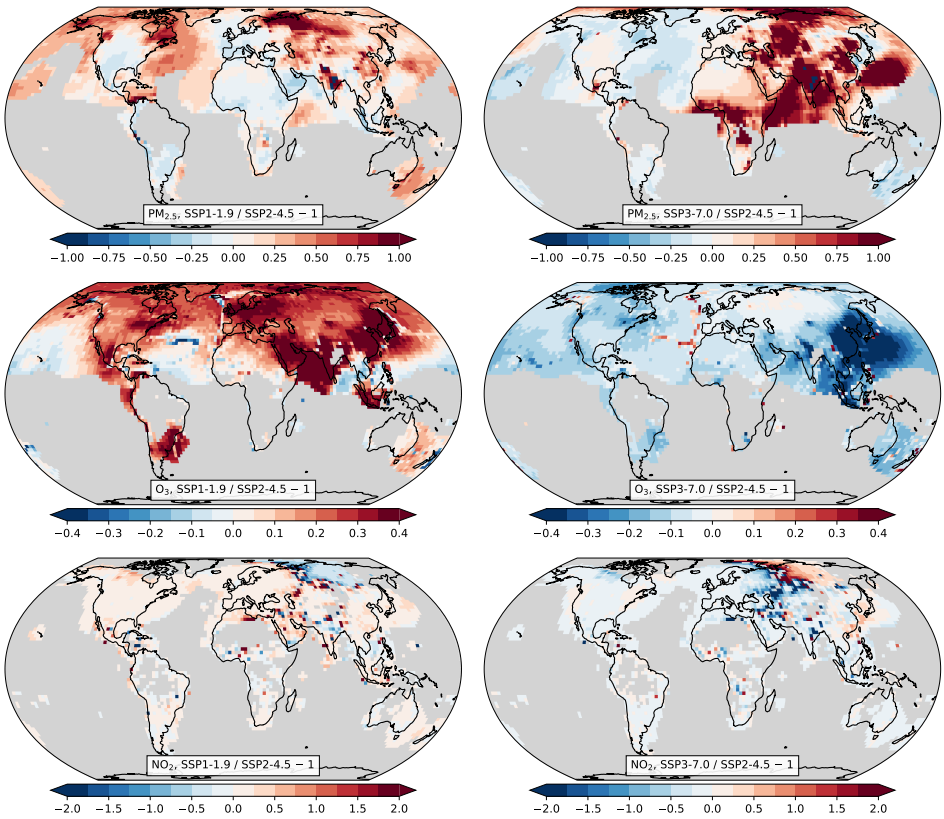

Figure C.5: Relative difference in ground-level concentrations attributable to LTO emissions in 2040 between a less polluted scenario (SSP1-1.9) or more polluted scenario (SSP3-7.0) and a more likely scenario (SSP2-4.5). Grid cells where values for SSP2-4.5 are below the 50th percentile are grayed out.

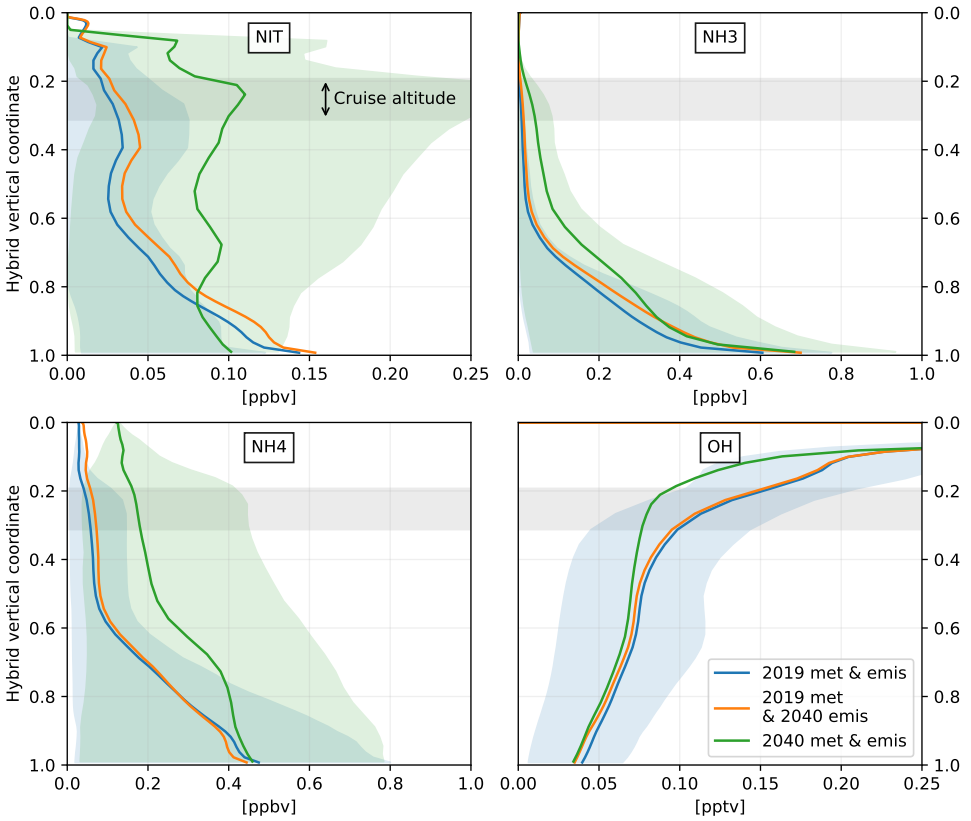

Figure C.6: Global annual average mixing ratio (dry air basis) of model tracers for inorganic nitrates (NIT), NH_3, NH_4^+, and OH per hybrid pressure vertical coordinate, which is roughly equal to the fraction of atmospheric column above that point. Comparison of 2019 meteorology from MERRA-2 against 2040 emissions and meteorology from GCAP 2.0. Shaded areas indicate the 68% range of values ($1\,\sigma$) at each vertical level for two of the three simulations. The band of "cruise altitude" indicates the altitude range where roughly 70% of full-flight aircraft NO_x emissions are released.

D

Additional details on simulations performed for nitrogen deposition

This appendix contains additional information relevant to Chapter 7, as listed below along with section numbers:

- D.1 shows the grids used for averaging over populated areas.
- D.2 shows the location of measurement stations considered.
- D.3 contains statistical summaries of the comparison between modeled and observed nitrogen deposition.
- D.4 shows the modeled spatial distribution of aviation-attributable and all-source nitrogen deposition.
- D.5 contains a table giving the change in nitrogen deposition rates per land cover class when considering the higher resolution simulations.

This appendix was originally published as Supporting Information to an article in the publication Science of The Total Environment. Please cite as shown in the list of peer-reviewed journal articles, item 4.

D.1 Populated grid cells

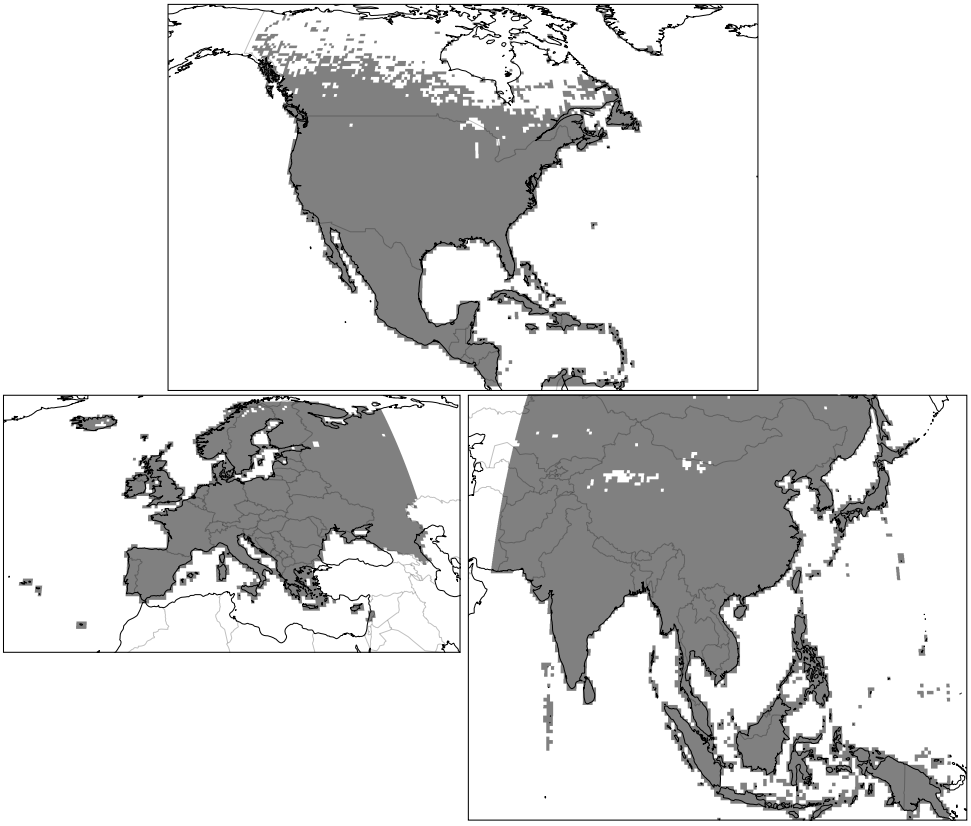

Figure D.1: Populated areas (in grey) defined as North America, Europe, and Asia for the analysis. The population map from LandScan Global 2019 is used [357].

D.2 Measurement stations used in model comparison

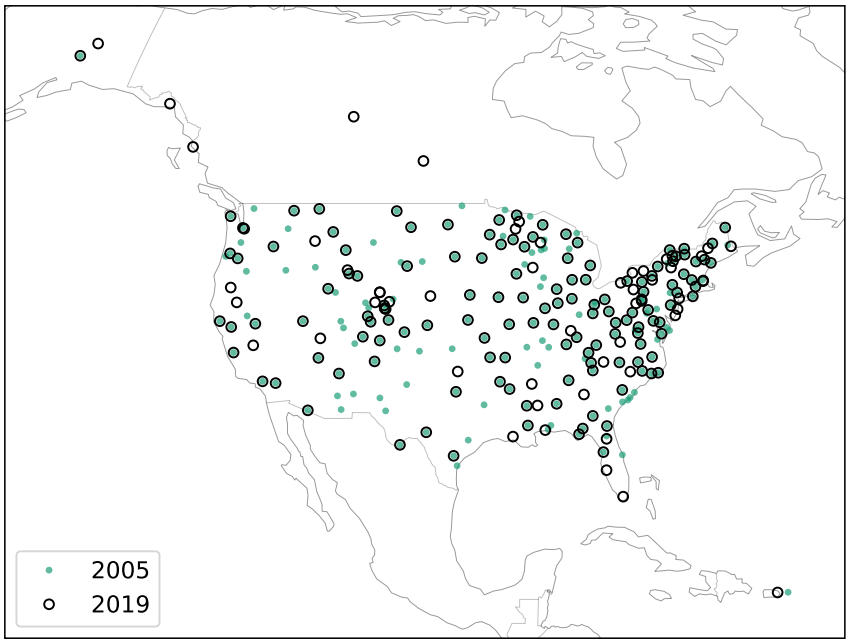

Figure D.2: NADP sites with nitrogen deposition measurements [385].

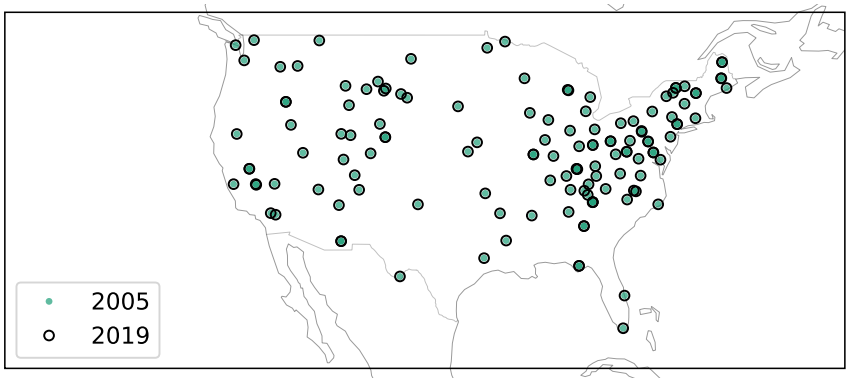

Figure D.3: CASTNET sites with nitrogen deposition measurements [390].

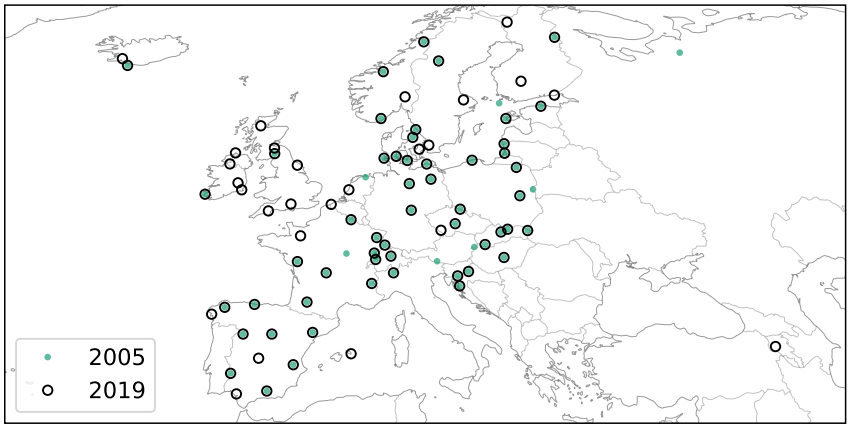

Figure D.4: EMEP sites with nitrogen deposition measurements [386, 387].

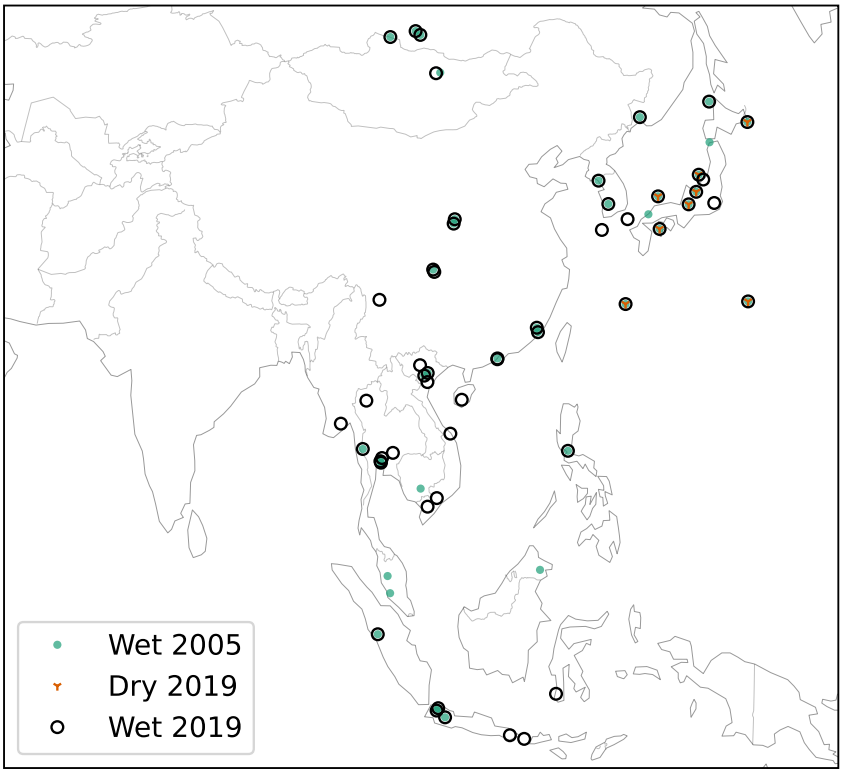

Figure D.5: EANET sites with nitrogen deposition measurements [388, 389].

D.3 Comparison of modeled N deposition with measurements

Table D.1: Comparison of modeled (M) against observed (O) [385–389] annual average $NH_3 + NH_4^+$ wet deposition rates ($kg\,N{\cdot}km^{-2}{\cdot}yr^{-1}$), per year and region.

	2005			2019		
	U.S. and Canada	Europe	Asia	U.S. and Canada	Europe	Asia
Measurement source	NADP	EMEP	EANET	NADP	EMEP	EANET
Number of stations	205	60	38	189	78	52
Mean (M)	177	295	490	210	285	692
Mean (O)	179	337	589	215	280	486
Standard deviation (M)	70.3	137	369	110	176	672
Standard deviation (O)	101	228	564	134	193	432
Mean bias	−1.91	−42.2	−99.8	−5.44	5.22	207
Mean error	51.1	123	307	57.4	97.7	334
RMS error	67.9	218	474	77.3	154	505
Normalized mean bias	−1.1%	−12.5%	−16.9%	−2.5%	1.9%	42.5%
Normalized mean error	28.6%	36.6%	52.1%	26.6%	34.9%	68.7%
Correlation coefficient	0.74	0.38	0.56	0.82	0.65	0.73
Index of agreement	0.63	0.53	0.58	0.71	0.62	0.53

Table D.2: Comparison of modeled (M) against observed (O) [385–389] annual average $HNO_3 + NO_3^-$ wet deposition rates ($kg\,N{\cdot}km^{-2}{\cdot}yr^{-1}$), per year and region.

	2005			2019		
	U.S. and Canada	Europe	Asia	U.S. and Canada	Europe	Asia
Measurement source	NADP	EMEP	EANET	NADP	EMEP	EANET
Number of stations	205	60	37	189	78	52
Mean (M)	178	206	327	132	142	419
Mean (O)	176	286	411	138	205	376
Standard deviation (M)	79.2	78.1	199	58.3	71.9	426
Standard deviation (O)	88.2	196	369	67.7	148	304
Mean bias	1.71	−80.4	−83.3	−6.13	−63	42.5
Mean error	30.4	113	201	28.2	85.6	201
RMS error	38.8	188	338	36.4	139	332
Normalized mean bias	1.0%	−28.1%	−20.3%	−4.4%	−30.8%	11.3%
Normalized mean error	17.2%	39.5%	49.0%	20.4%	41.8%	53.3%
Correlation coefficient	0.90	0.49	0.44	0.85	0.54	0.63
Index of agreement	0.79	0.51	0.55	0.73	0.52	0.58

Table D.3: Comparison of modeled (M) against observed (O) [385–389] annual average nitrogen wet deposition rates from all species ($kg\,N{\cdot}km^{-2}{\cdot}yr^{-1}$), per year and measurement source.

	2005			2019		
	U.S. and Canada	Europe	Asia	U.S. and Canada	Europe	Asia
Measurement source	NADP	EMEP	EANET	NADP	EMEP	EANET
Number of stations	205	59	37	189	77	52
Mean (M)	355	501	820	342	428	1111
Mean (O)	355	624	1008	354	487	862
Standard deviation (M)	142	213	544	160	244	1070
Standard deviation (O)	174	366	811	191	321	664
Mean bias	−0.196	−122	−188	−11.6	−58.8	249
Mean error	74.6	221	451	78.2	164	466
RMS error	95.4	341	677	102	256	714
Normalized mean bias	−0.1%	−19.6%	−18.6%	−3.3%	−12.1%	28.9%
Normalized mean error	21.0%	35.5%	44.7%	22.1%	33.6%	54.1%
Correlation coefficient	0.84	0.49	0.59	0.84	0.64	0.79
Index of agreement	0.72	0.53	0.61	0.73	0.60	0.58

Table D.4: Comparison of modeled (M) against observed (O) [389, 390] annual average NH_3 and NH_4^+ dry deposition rates ($kg\,N{\cdot}km^{-2}{\cdot}yr^{-1}$), per year and region.

	NH_3			NH_4^+		
	2005 U.S.	2019 U.S.	2019 Japan	2005 U.S.	2019 U.S.	2019 Japan
Measurement source	CASTNET	CASTNET	EANET	CASTNET	CASTNET	EANET
Number of stations	132	132	8	132	132	8
Mean (M)	69.5	123	78.9	48.4	23.5	14.2
Mean (O)	57	95	103	23.2	13.5	15.4
Standard deviation (M)	40.7	72.5	30.4	31.6	14.4	16.8
Standard deviation (O)	54	74.7	76.9	13.2	7.79	7.49
Mean bias	12.5	28	−24.3	25.2	10	−1.13
Mean error	34.6	47.5	64.1	29.6	15.4	17.8
RMS error	44.3	61.5	80.9	37.5	18.8	19.1
Normalized mean bias	21.9%	29.5%	−23.6%	108.9%	74.5%	−7.4%
Normalized mean error	60.8%	50.0%	62.2%	127.8%	114.3%	115.9%
Correlation coefficient	0.63	0.72	0.01	0.48	0.06	−0.29
Index of agreement	0.50	0.58	0.28	0.29	0.21	0.14

Table D.5: Comparison of modeled (M) against observed (O) [389, 390] annual average $HNO_3 + NO_3^-$ dry deposition rates ($kg\,N{\cdot}km^{-2}{\cdot}yr^{-1}$), per year and region.

	HNO_3			NO_3^-		
	2005 U.S.	2019 U.S.	2019 Japan	2005 U.S.	2019 U.S.	2019 Japan
Measurement source	CASTNET	CASTNET	EANET	CASTNET	CASTNET	EANET
Number of stations	132	132	8	132	132	8
Mean (M)	300	135	144	17.5	13.7	65.9
Mean (O)	242	101	32.2	30.3	27.4	13.5
Standard deviation (M)	143	59.7	119	10.8	8.47	24.2
Standard deviation (O)	140	47.4	20.9	53.7	28.3	9.55
Mean bias	58	34	112	−12.8	−13.7	52.3
Mean error	82.6	44.6	113	21.7	16.6	52.3
RMS error	104	57.4	158	57	32.3	55.5
Normalized mean bias	23.9%	33.6%	348.9%	−42.1%	−50.0%	386.5%
Normalized mean error	34.1%	44.2%	350.0%	71.7%	60.5%	386.5%
Correlation coefficient	0.81	0.64	0.12	−0.09	0.02	0.61
Index of agreement	0.67	0.53	0.16	0.41	0.43	0.13

Table D.6: Comparison of modeled (M) against observed (O) [389, 390] annual average dry and wet + dry nitrogen deposition rates from all species ($kg\,N{\cdot}km^{-2}{\cdot}yr^{-1}$), per year and region.

	Dry N			Wet + Dry N		
	2005 U.S.	2019 U.S.	2019 Japan	2005 U.S.	2019 U.S.	2019 Japan
Measurement source	CASTNET	CASTNET	EANET	CASTNET	CASTNET	EANET
Number of stations	132	132	8	132	132	8
Mean (M)	528	347	337	897	690	964
Mean (O)	494	348	165	860	692	639
Standard deviation (M)	221	136	202	353	261	577
Standard deviation (O)	267	173	95.3	399	324	280
Mean bias	34.6	−0.994	171	37.2	−1.46	324
Mean error	127	86.8	177	168	127	324
RMS error	170	123	241	216	172	512
Normalized mean bias	7.0%	−0.3%	103.5%	4.3%	−0.2%	50.7%
Normalized mean error	25.7%	24.9%	107.0%	19.6%	18.3%	50.7%
Correlation coefficient	0.78	0.70	0.45	0.85	0.85	0.72
Index of agreement	0.70	0.66	0.34	0.75	0.75	0.54

D.4 Spatial distribution of N deposition for each scenario

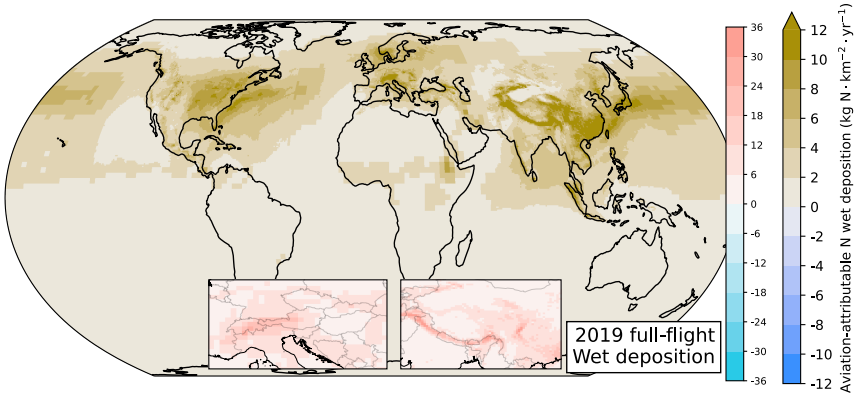

Figure D.6: Wet nitrogen deposition flux due to 2019 full-flight emissions. Inset: Alps and Tibetan plateau.

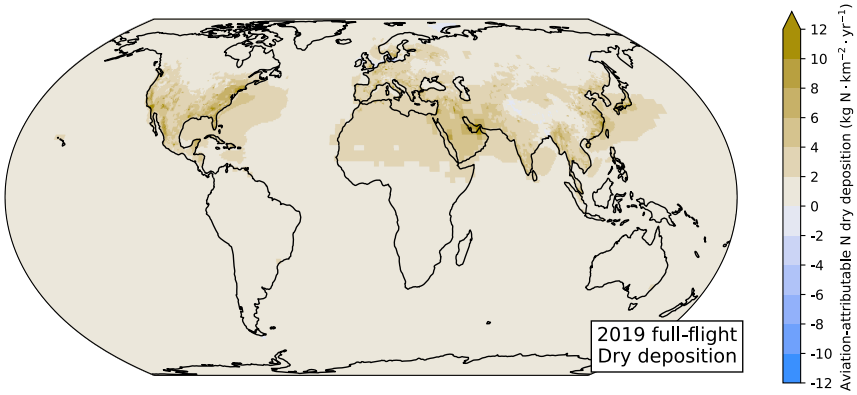

Figure D.7: Dry nitrogen deposition flux due to 2019 full-flight emissions.

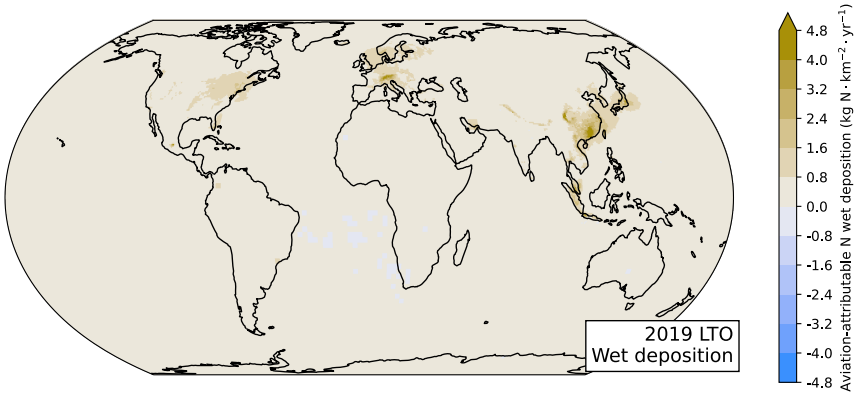

Figure D.8: Wet nitrogen deposition flux due to 2019 LTO emissions.

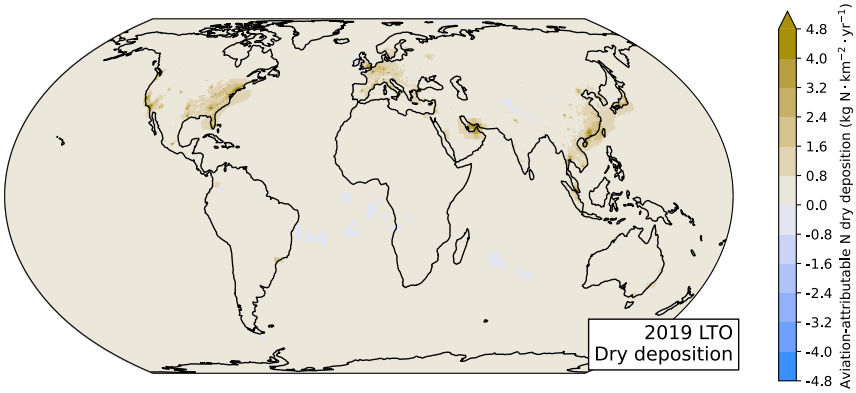

Figure D.9: Dry nitrogen deposition flux due to 2019 LTO emissions.

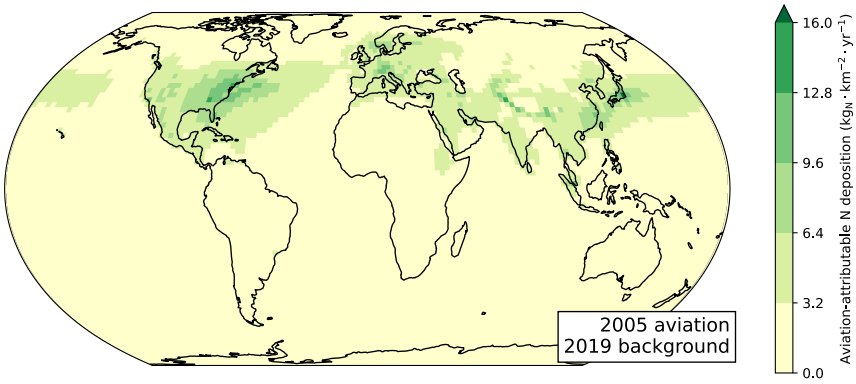

Figure D.10: Wet + dry nitrogen deposition flux due to 2005 aviation full-flight emissions. Simulation using meteorology and non-aviation emissions for 2019.

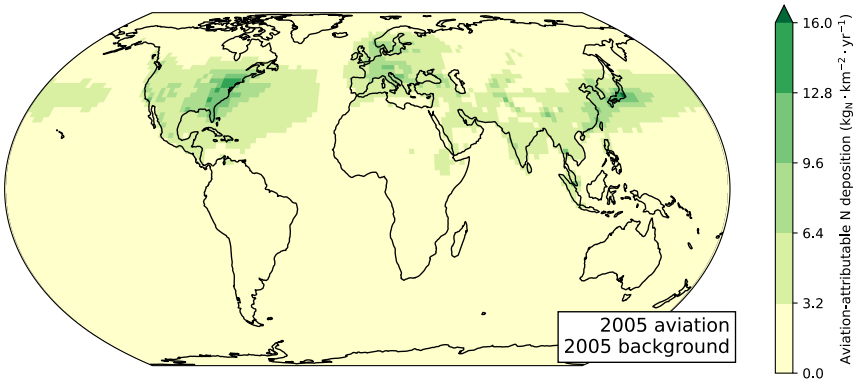

Figure D.11: Wet + dry nitrogen deposition flux due to 2005 aviation full-flight emissions. Simulation using meteorology and non-aviation emissions for 2005.

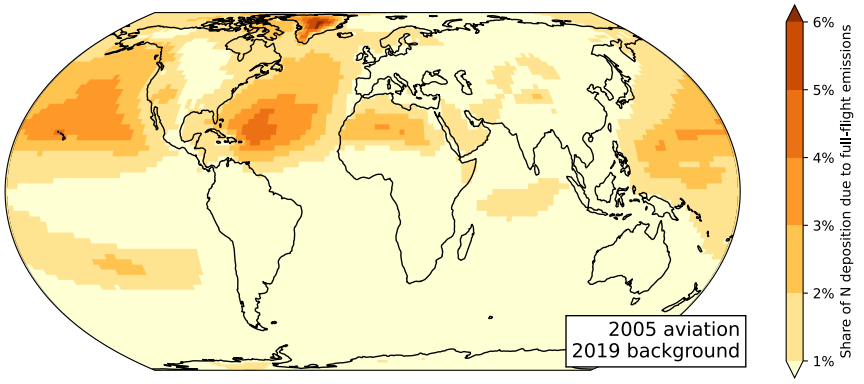

Figure D.12: Wet + dry nitrogen deposition due to 2005 aviation full-flight emissions relative to deposition from all sources. Simulation using meteorology and non-aviation emissions for 2019.

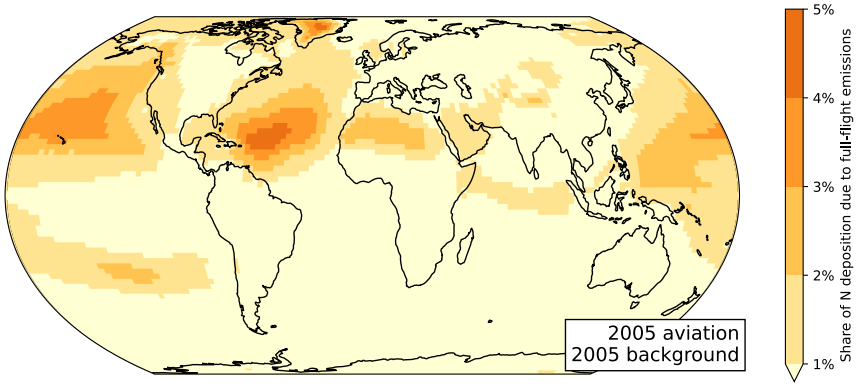

Figure D.13: Wet + dry nitrogen deposition due to 2005 aviation full-flight emissions relative to deposition from all sources. Simulation using meteorology and non-aviation emissions for 2005.

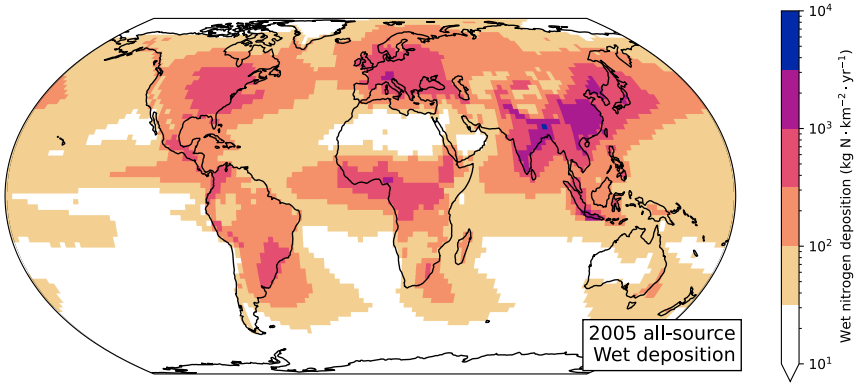

Figure D.14: Nitrogen wet deposition flux from all sources in 2005, in logarithmic scale.

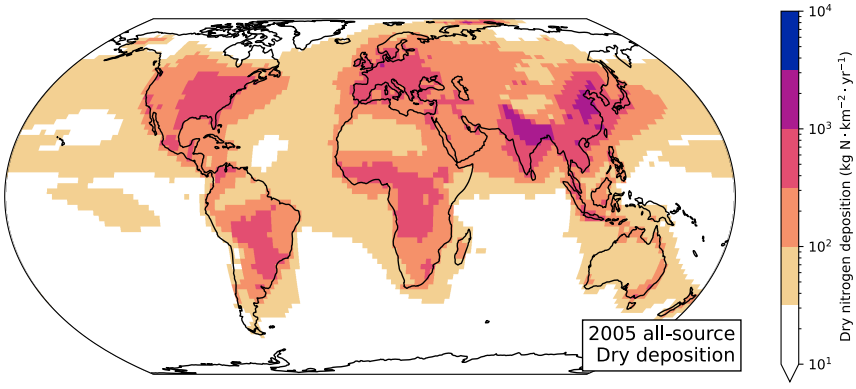

Figure D.15: Nitrogen dry deposition flux from all sources in 2005, in logarithmic scale.

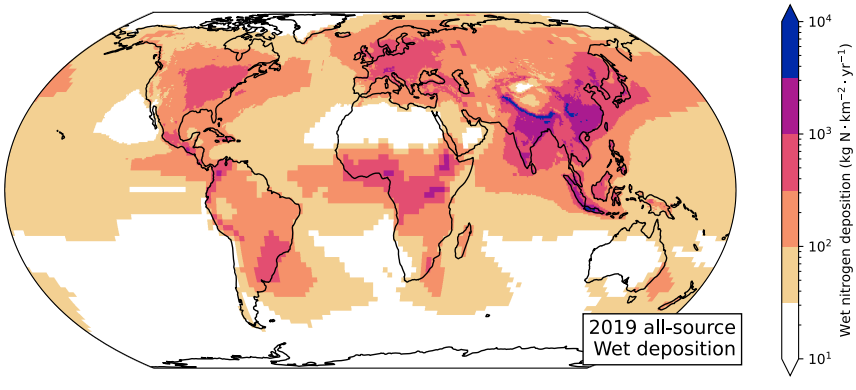

Figure D.16: Nitrogen wet deposition flux from all sources in 2019, in logarithmic scale.

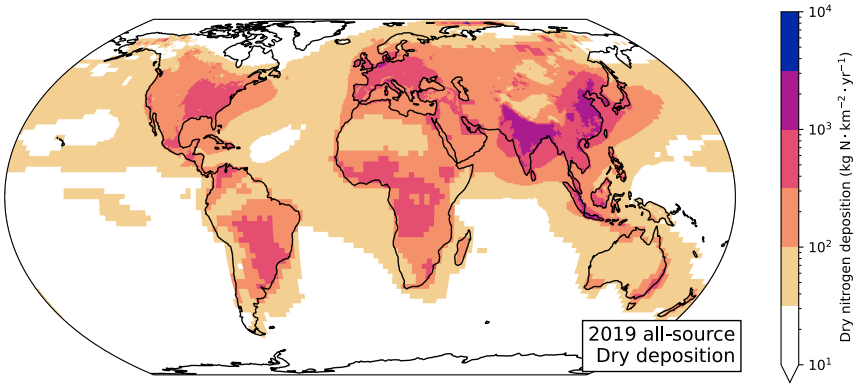

Figure D.17: Nitrogen dry deposition flux from all sources in 2019, in logarithmic scale.

D.5 Effect of model resolution on distribution of N deposition per land cover type

Table D.7: Relative change in mass of all-source and aviation-attributable nitrogen deposited in 2019 over different land cover classes after incorporating results from finer resolution nested simulations.

	Relative change in nitrogen deposition [%] $\left(\frac{\text{mass including } 0.5^\circ \times 0.625^\circ \text{ resolution results}}{\text{mass with only } 2^\circ \times 2.5^\circ \text{ resolution results}} - 1\right)$		
Land cover class	All sources	Attributable to LTO emissions	Attributable to full-flight emissions
Urban / built up	+4.2	+13.3	+1.8
Cultivated and managed vegetation	+1.0	+0.4	−2.3
Closed forest	+5.4	+6.0	+5.6
Open forest	+3.5	+4.7	+3.5
Shrubs	+0.3	−2.4	−0.9
Herbaceous vegetation	−0.9	+0.1	+2.4
Herbaceous wetland	+1.2	+0.1	+0.1
Moss and lichen	+1.9	−0.5	+2.2
Bare / sparse vegetation	−7.4	−3.0	+0.0
Snow and ice	−16.7	−1.1	+8.1
Permanent water bodies	−0.1	−4.2	−1.0
Open sea	−3.6	−5.2	−2.1
All land classes	+1.9	+2.8	+2.1
All water classes	−3.5	−5.2	−2.1
All areas	−0.3	−0.8	−0.3

Bibliography

References

[1] S. H. L. Yim, G. L. Lee, I. H. Lee, F. Allroggen, A. Ashok, F. Caiazzo, S. D. Eastham, R. Malina, and S. R. H. Barrett, *Global, regional and local health impacts of civil aviation emissions,* Environmental Research Letters **10**, 034001 (2015).

[2] R. Sausen and U. Schumann, *Estimates of the Climate Response to Aircraft CO_2 and NO_x Emissions Scenarios,* Climatic Change **44**, 27 (2000).

[3] D. S. Lee, D. W. Fahey, P. M. Forster, P. J. Newton, R. C. Wit, L. L. Lim, B. Owen, and R. Sausen, *Aviation and global climate change in the 21st century,* Atmospheric Environment **43**, 3520 (2009).

[4] M. Masiol and R. M. Harrison, *Aircraft engine exhaust emissions and other airport-related contributions to ambient air pollution: A review,* Atmospheric Environment **95**, 409 (2014).

[5] D. S. Lee, D. W. Fahey, A. Skowron, M. R. Allen, U. Burkhardt, Q. Chen, S. J. Doherty, S. Freeman, P. M. Forster, J. Fuglestvedt, A. Gettelman, R. R. De León, L. L. Lim, M. T. Lund, R. J. Millar, B. Owen, J. E. Penner, G. Pitari, M. J. Prather, R. Sausen, and L. J. Wilcox, *The contribution of global aviation to anthropogenic climate forcing for 2000 to 2018,* Atmospheric Environment **244**, 117834 (2021).

[6] G. G. Fleming, I. de Lépinay, and R. Schaufele, *Environmental Trends in Aviation to 2050,* in *ICAO Environmental Report 2022* (International Civil Aviation Organization, Montréal, 2022) pp. 24–31.

[7] International Civil Aviation Organization, *ICAO Annex 16: Environmental Protection, Volume II – Aircraft Engine Emissions*, 4th ed. (International Civil Aviation Organization, 2017).

[8] M. Gauss, I. S. A. Isaksen, D. S. Lee, and O. A. Søvde, *Impact of aircraft NO_x emissions on the atmosphere – tradeoffs to reduce the impact,* Atmospheric Chemistry and Physics **6**, 1529 (2006).

[9] V. Grewe, C. Frömming, S. Matthes, S. Brinkop, M. Ponater, S. Dietmüller, P. Jöckel, H. Garny, E. Tsati, K. Dahlmann, O. A. Søvde, J. Fuglestvedt, T. K. Berntsen, K. P. Shine, E. A. Irvine, T. Champougny, and P. Hullah, *Aircraft routing with minimal climate impact: The REACT4C climate cost function modelling approach (V1.0),* Geoscientific Model Development **7**, 175 (2014).

[10] S. Freeman, D. S. Lee, L. L. Lim, A. Skowron, and R. R. De León, *Trading off Aircraft Fuel Burn and NO_x Emissions for Optimal Climate Policy,* Environmental Science & Technology **52**, 2498 (2018).

[11] A. Skowron, D. S. Lee, R. R. De León, L. L. Lim, and B. Owen, *Greater fuel efficiency is potentially preferable to reducing NO_x emissions for aviation's climate impacts,* Nature Communications **12**, 564 (2021).

[12] J. Koo, Q. Wang, D. K. Henze, I. A. Waitz, and S. R. Barrett, *Spatial sensitivities of human health risk to intercontinental and high-altitude pollution,* Atmospheric Environment **71**, 140 (2013).

[13] J. N. Galloway, A. Bleeker, and J. W. Erisman, *The Human Creation and Use of Reactive Nitrogen: A Global and Regional Perspective,* Annual Review of Environment and Resources **46**, 255 (2021).

[14] S. Matassa, P. Boeckx, J. Boere, J. W. Erisman, M. Guo, R. Manzo, F. Meerburg, S. Papirio, I. Pikaar, K. Rabaey, D. Rousseau, J. Schnoor, P. Smith, E. Smolders, S. Wuertz, and W. Verstraete, *How can we possibly resolve the planet's nitrogen dilemma?* Microbial Biotechnology **16**, 15 (2023).

[15] A. Hazekamp, *Question for written answer E-003873/2019 to the Commission. Subject: Pollution of nature reserves in Europe due to excess nitrogen deposition,* (2019).

[16] E. Stokstad, *Nitrogen crisis threatens Dutch environment—and economy,* Science **366**, 1180 (2019).

[17] J. W. Erisman, *Setting ambitious goals for agriculture to meet environmental targets,* One Earth **4**, 15 (2021).

[18] R. L. Wayson and G. G. Fleming, *Consideration of Air Quality Impacts By Airplane Operations at or Above 3000 Feet AGL*, Tech. Rep. FAA-AEE-00-01 (Federal Aviation Administration, 2000).

[19] U.S. Environmental Protection Agency, *Control of Air Pollution From Aircraft and Aircraft Engines; Emission Standards and Test Procedures; Final Rule,* Federal Register **77**, 36342 (2012).

[20] European Parliament and the Council of the European Union, *Directive (EU) 2016/2284 - on the reduction of national emissions of certain atmospheric pollutants,* (2016).

[21] International Civil Aviation Organization, *Airport Air Quality Manual*, 2nd ed. (International Civil Aviation Organization, 2020).

[22] A. Unal, Y. Hu, M. E. Chang, M. T. Odman, and A. G. Russell, *Airport related emissions and impacts on air quality: Application to the Atlanta International Airport,* Atmospheric Environment **39**, 5787 (2005).

[23] G. Schürmann, Schäfer, C. Jahn, H. Hoffmann, M. Bauerfeind, E. Fleuti, and B. Rappenglück, *The impact of NO_x, CO and VOC emissions on the air quality of Zurich airport,* Atmospheric Environment **41**, 103 (2007).

[24] Y. Zhu, E. Fanning, R. C. Yu, Q. Zhang, and J. R. Froines, *Aircraft emissions and local air quality impacts from takeoff activities at a large International Airport,* Atmospheric Environment **45**, 6526 (2011).

[25] M. Keuken, M. Moerman, P. Zandveld, J. Henzing, and G. Hoek, *Total and size-resolved particle number and black carbon concentrations in urban areas near Schiphol airport (the Netherlands),* Atmospheric Environment **104**, 132 (2015).

[26] M. Masiol and R. M. Harrison, *Quantification of air quality impacts of London Heathrow Airport (UK) from 2005 to 2012,* Atmospheric Environment **116**, 308 (2015).

[27] I. Simonetti, S. Maltagliati, and G. Manfrida, *Air quality impact of a middle size airport within an urban context through EDMS simulation,* Transportation Research Part D: Transport and Environment **40**, 144 (2015).

[28] X. Yang, S. Cheng, J. Lang, R. Xu, and Z. Lu, *Characterization of aircraft emissions and air quality impacts of an international airport,* Journal of Environmental Sciences **72**, 198 (2018).

[29] L. Tarrasón, J. E. Jonson, T. K. Berntsen, and K. Rypdal, *Study on Air Quality Impacts of Non-LTO Emissions from Aviation*, Tech. Rep. 3 (Air Pollution Section, Norwegian Meteorological Institute (met.no); CICERO, Centre for International Climate and Environmental Research- Oslo, 2004).

[30] S. R. H. Barrett, R. E. Britter, and I. A. Waitz, *Global Mortality Attributable to Aircraft Cruise Emissions,* Environmental Science & Technology **44**, 7736 (2010).

[31] O. A. Søvde, S. Matthes, A. Skowron, D. Iachetti, L. Lim, B. Owen, Ø. Hodnebrog, G. Di Genova, G. Pitari, D. S. Lee, G. Myhre, and I. S. Isaksen, *Aircraft emission mitigation by changing route altitude: A multi-model estimate of aircraft NO_x emission impact on O_3 photochemistry,* Atmospheric Environment **95**, 468 (2014).

[32] S. D. Eastham and S. R. Barrett, *Aviation-attributable ozone as a driver for changes in mortality related to air quality and skin cancer,* Atmospheric Environment **144**, 17 (2016).

[33] M. A. Cameron, M. Z. Jacobson, S. R. H. Barrett, H. Bian, C. C. Chen, S. D. Eastham, A. Gettelman, A. Khodayari, Q. Liang, H. B. Selkirk, N. Unger, D. J. Wuebbles, and X. Yue, *An intercomparative study of the effects of aircraft emissions on surface air quality,* Journal of Geophysical Research: Atmospheres **122**, 8325 (2017).

[34] E. Terrenoire, D. Hauglustaine, Y. Cohen, A. Cozic, R. Valorso, F. Lefèvre, and S. Matthes, *Impact of present and future aircraft NO_x and aerosol emissions on atmospheric composition and associated direct radiative forcing of climate,* Atmospheric Chemistry and Physics **22**, 11987 (2022).

[35] R. H. Moore, M. Shook, A. Beyersdorf, C. Corr, S. Herndon, W. B. Knighton, R. Miake-Lye, K. L. Thornhill, E. L. Winstead, Z. Yu, L. D. Ziemba, and B. E. Anderson, *Influence of Jet Fuel Composition on Aircraft Engine Emissions: A Synthesis of Aerosol Emissions Data from the NASA APEX, AAFEX, and ACCESS Missions,* Energy & Fuels **29**, 2591 (2015).

[36] R. H. Moore, K. L. Thornhill, B. Weinzierl, D. Sauer, E. D'Ascoli, J. Kim, M. Lichtenstern, M. Scheibe, B. Beaton, A. J. Beyersdorf, J. Barrick, D. Bulzan, C. A. Corr, E. Crosbie, T. Jurkat, R. Martin, D. Riddick, M. Shook, G. Slover, C. Voigt, R. White, E. Winstead, R. Yasky, L. D. Ziemba, A. Brown, H. Schlager, and B. E. Anderson, *Biofuel blending reduces particle emissions from aircraft engines at cruise conditions,* Nature **543**, 411 (2017).

[37] T. Schripp, B. Anderson, E. C. Crosbie, R. H. Moore, F. Herrmann, P. Oßwald, C. Wahl, M. Kapernaum, M. Köhler, P. Le Clercq, B. Rauch, P. Eichler, T. Mikoviny, and A. Wisthaler, *Impact of Alternative Jet Fuels on Engine Exhaust Composition During the 2015 ECLIF Ground-Based Measurements Campaign,* Environmental Science & Technology **52**, 4969 (2018).

[38] S. Tran, A. Brown, and J. S. Olfert, *Comparison of Particle Number Emissions from In-Flight Aircraft Fueled with Jet A1, JP-5 and an Alcohol-to-Jet Fuel Blend,* Energy & Fuels **34**, 7218 (2020).

[39] C. Voigt, J. Kleine, D. Sauer, R. H. Moore, T. Bräuer, P. Le Clercq, S. Kaufmann, M. Scheibe, T. Jurkat-Witschas, M. Aigner, U. Bauder, Y. Boose, S. Borrmann, E. Crosbie, G. S. Diskin, J. DiGangi, V. Hahn, C. Heckl, F. Huber, J. B. Nowak, M. Rapp, B. Rauch, C. Robinson, T. Schripp, M. Shook, E. Winstead, L. Ziemba, H. Schlager, and B. E. Anderson, *Cleaner burning aviation fuels can reduce contrail cloudiness,* Communications Earth & Environment **2**, 1 (2021).

[40] S. T. Turnock, R. J. Allen, M. Andrews, S. E. Bauer, M. Deushi, L. Emmons, P. Good, L. Horowitz, J. G. John, M. Michou, P. Nabat, V. Naik, D. Neubauer, F. M. O'Connor, D. Olivié, N. Oshima, M. Schulz, A. Sellar, S. Shim, T. Takemura, S. Tilmes, K. Tsigaridis, T. Wu, and J. Zhang, *Historical and future changes in air pollutants from CMIP6 models,* Atmospheric Chemistry and Physics **20**, 14547 (2020).

[41] N. W. Simone, M. E. Stettler, and S. R. Barrett, *Rapid estimation of global civil aviation emissions with uncertainty quantification,* Transportation Research Part D: Transport and Environment **25**, 33 (2013).

[42] X. Liu, L. Duan, J. Mo, E. Du, J. Shen, X. Lu, Y. Zhang, X. Zhou, C. He, and F. Zhang, *Nitrogen deposition and its ecological impact in China: An overview,* Environmental Pollution **159**, 2251 (2011).

[43] L. Zhang, D. J. Jacob, E. M. Knipping, N. Kumar, J. W. Munger, C. C. Carouge, A. van Donkelaar, Y. X. Wang, and D. Chen, *Nitrogen deposition to the United States: Distribution, sources, and processes,* Atmospheric Chemistry and Physics **12**, 4539 (2012).

[44] A. Ito, G. Lin, and J. E. Penner, *Global modeling study of soluble organic nitrogen from open biomass burning,* Atmospheric Environment **121**, 103 (2015).

[45] M. Kanakidou, S. Myriokefalitakis, N. Daskalakis, G. Fanourgakis, A. Nenes, A. R. Baker, K. Tsigaridis, and N. Mihalopoulos, *Past, Present, and Future Atmospheric Nitrogen Deposition,* Journal of the Atmospheric Sciences **73**, 2039 (2016).

[46] D. Ackerman, D. B. Millet, and X. Chen, *Global Estimates of Inorganic Nitrogen Deposition Across Four Decades,* Global Biogeochemical Cycles **33**, 100 (2019).

[47] P. C. Campbell, J. O. Bash, C. G. Nolte, T. L. Spero, E. J. Cooter, K. Hinson, and L. C. Linker, *Projections of Atmospheric Nitrogen Deposition to the Chesapeake Bay Watershed,* Journal of Geophysical Research: Biogeosciences **124**, 3307 (2019).

[48] G. Bisignani, *Chapter 6: The Future is Green : Environmental initiatives, including airspace issues and the EU ETS,* in *Shaking the Skies* (LID Publishing, London, United Kingdom, 2013) pp. 129–164.

[49] International Air Transport Association, *Resolution on the indrustry's commitment to reach net zero carbon emissions by 2050,* (2021).

[50] NLR – Royal Netherlands Aerospace Centre and SEO Amsterdam Economics, *Destination 2050 : A Route To Net Zero European Aviation*, Tech. Rep. NLR-CR-2020-510 (A4E, ACI-EUROPE, ASD, CANSO, ERA, 2021).

[51] U.S. Department of Transportation, *United States Aviation Climate Action Plan,* (2021).

[52] ICAO Assembly, *Resolution A41-21: Consolidated statement of continuing ICAO policies and practices related to environmental protection — Climate change,* in *Doc 10184, Assembly Resolutions in Force (as of 7 October 2022)* (International Civil Aviation Organization, Montréal, 2022) provisional ed.

[53] Department for Transport, *Jet Zero Strategy: Delivering net zero aviation by 2050,* (2022).

[54] French Presidency of the Council of the European Union, *Déclaration de Toulouse sur le Developpement Durable et la Décarbonation de l'Aviation (Declaration on future sustainability and decarbonisation of Aviation),* (2022).

[55] D. Stradling and P. Thorsheim, *The Smoke of Great Cities: British and American Efforts to Control Air Pollution, 1860–1914,* Environmental History **4**, 6 (1999).

[56] J. H. Seinfeld and S. N. Pandis, *Atmospheric Chemistry and Physics : From Air Pollution to Climate Change*, 3rd ed. (John Wiley & Sons, Inc., Hoboken, New Jersey, 2016).

[57] World Health Organization, *WHO Global Air Quality Guidelines: Particulate Matter ($PM_{2.5}$ and PM_{10}), Ozone, Nitrogen Dioxide, Sulfur Dioxide and Carbon Monoxide* (World Health Organization, 2021).

[58] F. J. Kelly and J. C. Fussell, *Size, source and chemical composition as determinants of toxicity attributable to ambient particulate matter,* Atmospheric Environment **60**, 504 (2012).

[59] D. E. Schraufnagel, *The health effects of ultrafine particles,* Experimental & Molecular Medicine **52**, 311 (2020).

[60] N. A. H. Janssen, G. Hoek, L. M. Simic, P. Fischer, B. L. van, B. H. ten, M. Keuken, R. W. Atkinson, H. R. Anderson, B. Brunekreef, and F. R. Cassee, *Black Carbon as an Additional Indicator of the Adverse Health Effects of Airborne Particles Compared with PM_{10} and $PM_{2.5}$,* Environmental Health Perspectives **119**, 1691 (2011).

[61] F. R. Cassee, M.-E. Héroux, M. E. Gerlofs-Nijland, and F. J. Kelly, *Particulate matter beyond mass: Recent health evidence on the role of fractions, chemical constituents and sources of emission,* Inhalation Toxicology **25**, 802 (2013).

[62] H. R. Jonsdottir, M. Delaval, Z. Leni, A. Keller, B. T. Brem, F. Siegerist, D. Schönenberger, L. Durdina, M. Elser, H. Burtscher, A. Liati, and M. Geiser, *Non-volatile particle emissions from aircraft turbine engines at ground-idle induce oxidative stress in bronchial cells,* Communications Biology **2**, 90 (2019).

[63] U.S. Environmental Protection Agency, *National Primary and Secondary Ambient Air Quality Standards,* (2023).

[64] European Parliament and the Council of the European Union, *Directive 2008/50/EC of the European Parliament and of the Council of 21 May 2008 on ambient air quality and cleaner air for Europe,* (2008).

[65] OAR. US EPA, *Initial List of Hazardous Air Pollutants with Modifications,* https://www.epa.gov/haps/initial-list-hazardous-air-pollutants-modifications (2015), accessed 2023-07-17.

[66] J. Bachmann, *Will the Circle Be Unbroken: A History of the U.S. National Ambient Air Quality Standards,* Journal of the Air & Waste Management Association **57**, 652 (2007).

[67] R. R. Tucker, *Smoke Prevention in St. Louis,* Industrial & Engineering Chemistry **33**, 836 (1941).

[68] P. L. Magill, *The Los Angeles Smog Problem,* Industrial & Engineering Chemistry **41**, 2476 (1949).

[69] A. J. Haagen-Smit, *Chemistry and Physiology of Los Angeles Smog,* Industrial & Engineering Chemistry **44**, 1342 (1952).

[70] H. L. Platt, *Invisible gases: Smoke, gender, and the redefinition of environmental policy in Chicago, 1900–1920,* Planning Perspectives **10**, 67 (1995).

[71] M. Glasser, L. Greenburg, and F. Field, *Mortality and Morbidity During a Period of High Levels of Air Pollution: New York, Nov 23 to 25, 1966,* Archives of Environmental Health: An International Journal **15**, 684 (1967).

[72] Z. J. Andersen, *Chapter 7 - Air pollution epidemiology,* in *Traffic-Related Air Pollution*, edited by H. Khreis, M. Nieuwenhuijsen, J. Zietsman, and T. Ramani (Elsevier, 2020) pp. 163–182.

[73] M. L. Bell and D. L. Davis, *Reassessment of the lethal London fog of 1952: Novel indicators of acute and chronic consequences of acute exposure to air pollution.* Environmental Health Perspectives **109**, 389 (2001).

[74] M. S. Goldberg, R. T. Burnett, and D. Stieb, *A review of time-series studies used to evaluate the short-term effects of air pollution on human health,* Reviews on Environmental Health **18**, 269 (2003).

[75] R. Rückerl, A. Schneider, S. Breitner, J. Cyrys, and A. Peters, *Health effects of particulate air pollution: A review of epidemiological evidence,* Inhalation Toxicology **23**, 555 (2011).

[76] J. M. Samet, F. Dominici, F. C. Curriero, I. Coursac, and S. L. Zeger, *Fine Particulate Air Pollution and Mortality in 20 U.S. Cities, 1987–1994,* New England Journal of Medicine **343**, 1742 (2000).

[77] K. Katsouyanni, G. Touloumi, E. Samoli, A. Gryparis, A. Le Tertre, Y. Monopolis, G. Rossi, D. Zmirou, F. Ballester, A. Boumghar, H. R. Anderson, B. Wojtyniak, A. Paldy, R. Braunstein, J. Pekkanen, C. Schindler, and J. Schwartz, *Confounding and Effect Modification in the Short-Term Effects of Ambient Particles on Total Mortality: Results from 29 European Cities within the APHEA2 Project,* Epidemiology **12**, 521 (2001).

[78] J. M. Samet, S. L. Zeger, F. Dominici, F. Curriero, I. Coursac, D. W. Dockery, J. Schwartz, and A. Zanobetti, *The National Morbidity, Mortality, and Air Pollution Study. Part II: Morbidity and Mortality in the United States*, Tech. Rep. 94, Part II (Health Effects Institute, Cambridge, MA, USA, 2000).

[79] R. W. Atkinson, H. Ross Anderson, J. Sunyer, J. Ayres, M. Baccini, J. M. Vonk, A. Boumghar, F. Forastiere, B. Forsberg, G. Touloumi, J. Schwartz, and K. Katsouyanni, *Acute Effects of Particulate Air Pollution on Respiratory Admissions,* American Journal of Respiratory and Critical Care Medicine **164**, 1860 (2001).

[80] A. L. Tertre, S. Medina, E. Samoli, B. Forsberg, P. Michelozzi, A. Boumghar, J. M. Vonk, A. Bellini, R. Atkinson, J. G. Ayres, J. Sunyer, J. Schwartz, and K. Katsouyanni, *Short-term effects of particulate air pollution on cardiovascular diseases in eight European cities,* Journal of Epidemiology & Community Health **56**, 773 (2002).

[81] J. Sunyer, R. Atkinson, F. Ballester, A. L. Tertre, J. G. Ayres, F. Forastiere, B. Forsberg, J. M. Vonk, L. Bisanti, R. H. Anderson, J. Schwartz, and K. Katsouyanni, *Respiratory effects of sulphur dioxide: A hierarchical multicity analysis in the APHEA 2 study,* Occupational and Environmental Medicine **60**, e2 (2003).

[82] J. Sunyer, *The association of daily sulfur dioxide air pollution levels with hospital admissions for cardiovascular diseases in Europe (The Aphea-II study),* European Heart Journal **24**, 752 (2003).

[83] C. Liu, R. Chen, F. Sera, A. M. Vicedo-Cabrera, Y. Guo, S. Tong, M. S. Coelho, P. H. Saldiva, E. Lavigne, P. Matus, N. Valdes Ortega, S. Osorio Garcia, M. Pascal, M. Stafoggia, M. Scortichini, M. Hashizume, Y. Honda, M. Hurtado-Díaz, J. Cruz, B. Nunes, J. P. Teixeira, H. Kim, A. Tobias, C. Íñiguez, B. Forsberg, C. Åström, M. S. Ragettli, Y.-L. Guo, B.-Y. Chen, M. L. Bell, C. Y. Wright, N. Scovronick, R. M. Garland, A. Milojevic, J. Kyselý, A. Urban, H. Orru, E. Indermitte, J. J. Jaakkola, N. R. Ryti, K. Katsouyanni, A. Analitis, A. Zanobetti, J. Schwartz, J. Chen, T. Wu, A. Cohen, A. Gasparrini, and H. Kan, *Ambient Particulate Air Pollution and Daily Mortality in 652 Cities,* New England Journal of Medicine **381**, 705 (2019).

[84] A. M. Vicedo-Cabrera, F. Sera, C. Liu, B. Armstrong, A. Milojevic, Y. Guo, S. Tong, E. Lavigne, J. Kyselý, A. Urban, H. Orru, E. Indermitte, M. Pascal, V. Huber, A. Schneider, K. Katsouyanni, E. Samoli, M. Stafoggia, M. Scortichini, M. Hashizume, Y. Honda, C. F. S. Ng, M. Hurtado-Diaz, J. Cruz, S. Silva, J. Madureira, N. Scovronick, R. M. Garland, H. Kim, A. Tobias, C. Íñiguez, B. Forsberg, C. Åström, M. S. Ragettli, M. Röösli, Y.-L. L. Guo, B.-Y. Chen, A. Zanobetti, J. Schwartz, M. L. Bell, H. Kan, and A. Gasparrini, *Short term association between ozone and mortality: Global two stage time series study in 406 locations in 20 countries,* BMJ **368**, m108 (2020).

[85] P. Orellano, J. Reynoso, N. Quaranta, A. Bardach, and A. Ciapponi, *Short-term exposure to particulate matter (PM_{10} and $PM_{2.5}$), nitrogen dioxide (NO_2), and ozone (O_3) and all-cause and cause-specific mortality: Systematic review and* meta-*analysis,* Environment International **142**, 105876 (2020).

[86] P. Orellano, J. Reynoso, and N. Quaranta, *Short-term exposure to sulphur dioxide (SO_2) and all-cause and respiratory mortality: A systematic review and meta-analysis,* Environment International **150**, 106434 (2021).

[87] X.-y. Zheng, P. Orellano, H.-l. Lin, M. Jiang, and W.-j. Guan, *Short-term exposure to ozone, nitrogen dioxide, and sulphur dioxide and emergency department visits and hospital admissions due to asthma: A systematic review and meta-analysis,* Environment International **150**, 106435 (2021).

[88] K. K. Lee, N. Spath, M. R. Miller, N. L. Mills, and A. S. Shah, *Short-term exposure to carbon monoxide and myocardial infarction: A systematic review and meta-analysis,* Environment International **143**, 105901 (2020).

[89] P. Stocks, *Cancer and Bronchitis Mortality in Relation to Atmospheric Deposit and Smoke,* British Medical Journal **1**, 74 (1959).

[90] L. B. Lave and E. P. Seskin, *Air Pollution and Human Health,* Science **169**, 723 (1970).

[91] H. Ozkaynak and G. D. Thurston, *Associations Between 1980 U.S. Mortality Rates and Alternative Measures of Airborne Particle Concentration,* Risk Analysis **7**, 449 (1987).

[92] M. Bobak and D. A. Leon, *Air pollution and infant mortality in the Czech Republic, 1986-88,* The Lancet **340**, 1010 (1992).

[93] F. W. Lipfert and R. E. Wyzga, *Air Pollution and Mortality: Issues and Uncertainties,* Journal of the Air & Waste Management Association **45**, 949 (1995).

[94] M. B. Dijkema, S. F. Mallant, U. Gehring, K. van den Hurk, M. Alssema, R. T. van Strien, P. H. Fischer, G. Nijpels, C. D. Stehouwer, G. Hoek, J. M. Dekker, and B. Brunekreef, *Long-term Exposure to Traffic-related Air Pollution and Type 2 Diabetes Prevalence in a Cross-sectional Screening-study in the Netherlands,* Environmental Health **10**, 1 (2011).

[95] C. Liu, R. Chen, Y. Zhao, Z. Ma, J. Bi, Y. Liu, X. Meng, Y. Wang, X. Chen, W. Li, and H. Kan, *Associations between ambient fine particulate air pollution and hypertension: A nationwide cross-sectional study in China,* Science of The Total Environment **584–585**, 869 (2017).

[96] D. W. Dockery, C. A. Pope III, X. Xu, J. D. Spengler, J. H. Ware, M. E. Fay, B. G. Ferris, and F. E. Speizer, *An Association Between Air Pollution and Mortality in Six U.S. Cities,* The New England Journal of Medicine **329**, 7 (1993).

[97] C. A. Pope, M. J. Thun, M. M. Namboodiri, D. W. Dockery, J. S. Evans, F. E. Speizer, and C. W. Heath, *Particulate Air Pollution as a Predictor of Mortality in a Prospective Study of U.S. Adults,* American Journal of Respiratory and Critical Care Medicine **151**, 669 (1995).

[98] C. A. Pope, N. Coleman, Z. A. Pond, and R. T. Burnett, *Fine particulate air pollution and human mortality: 25+ years of cohort studies,* Environmental Research **183**, 108924 (2020).

[99] W. Cornwall, *Critics see hidden goal in EPA data access rule,* Science **360**, 472 (2018).

[100] D. J. Hicks, *Open science, the replication crisis, and environmental public health,* Accountability in Research **30**, 34 (2023).

[101] J. Lepeule, F. Laden, D. Dockery, and J. Schwartz, *Chronic Exposure to Fine Particles and Mortality: An Extended Follow-up of the Harvard Six Cities Study from 1974 to 2009,* Environmental Health Perspectives **120**, 965 (2012).

[102] C. A. Pope III, *Lung Cancer, Cardiopulmonary Mortality, and Long-term Exposure to Fine Particulate Air Pollution,* JAMA **287**, 1132 (2002).

[103] C. A. Pope, M. C. Turner, R. T. Burnett, M. Jerrett, S. M. Gapstur, W. R. Diver, D. Krewski, and R. D. Brook, *Relationships Between Fine Particulate Air Pollution, Cardiometabolic Disorders, and Cardiovascular Mortality,* Circulation Research **116**, 108 (2015).

[104] M. C. Turner, M. Jerrett, C. A. Pope, D. Krewski, S. M. Gapstur, W. R. Diver, B. S. Beckerman, J. D. Marshall, J. Su, D. L. Crouse, and R. T. Burnett, *Long-Term Ozone Exposure and Mortality in a Large Prospective Study,* American Journal of Respiratory and Critical Care Medicine **193**, 1134 (2016).

[105] B. Ostro, M. Lipsett, P. Reynolds, D. Goldberg, A. Hertz, C. Garcia, K. D. Henderson, and L. Bernstein, *Long-Term Exposure to Constituents of Fine Particulate Air Pollution and Mortality: Results from the California Teachers Study,* Environmental Health Perspectives **118**, 363 (2010).

[106] R. C. Puett, J. E. Hart, J. D. Yanosky, C. Paciorek, J. Schwartz, H. Suh, F. E. Speizer, and F. Laden, *Chronic Fine and Coarse Particulate Exposure, Mortality, and Coronary Heart Disease in the Nurses' Health Study,* Environmental Health Perspectives **117**, 1697 (2009).

[107] R. C. Puett, J. E. Hart, H. Suh, M. Mittleman, and F. Laden, *Particulate Matter Exposures, Mortality, and Cardiovascular Disease in the Health Professionals Follow-up Study,* Environmental Health Perspectives **119**, 1130 (2011).

[108] K. A. Miller, D. S. Siscovick, L. Sheppard, K. Shepherd, J. H. Sullivan, G. L. Anderson, and J. D. Kaufman, *Long-Term Exposure to Air Pollution and Incidence of Cardiovascular Events in Women,* New England Journal of Medicine **356**, 447 (2007).

[109] R. Beelen, G. Hoek, P. A. van den Brandt, R. A. Goldbohm, P. Fischer, L. J. Schouten, M. Jerrett, E. Hughes, B. Armstrong, and B. Brunekreef, *Long-Term Effects of Traffic-Related Air Pollution on Mortality in a Dutch Cohort (NLCS-AIR Study),* Environmental Health Perspectives **116**, 196 (2008).

[110] P. J. Villeneuve, S. A. Weichenthal, D. Crouse, A. B. Miller, T. To, R. V. Martin, A. van Donkelaar, C. Wall, and R. T. Burnett, *Long-term Exposure to Fine Particulate Matter Air Pollution and Mortality Among Canadian Women,* Epidemiology **26**, 536 (2015), 26511569 .

[111] D. L. Crouse, P. A. Peters, P. Hystad, J. R. Brook, A. van Donkelaar, R. V. Martin, P. J. Villeneuve, M. Jerrett, M. S. Goldberg, C. A. Pope, M. Brauer, R. D. Brook, A. Robichaud, R. Menard, and R. T. Burnett, *Ambient $PM_{2.5}$, O_3, and NO_2 Exposures and Associations with Mortality over 16 Years of Follow-Up in the Canadian Census Health and Environment Cohort (CanCHEC),* Environmental Health Perspectives **123**, 1180 (2015).

[112] R. Beelen, O. Raaschou-Nielsen, M. Stafoggia, Z. J. Andersen, G. Weinmayr, B. Hoffmann, K. Wolf, E. Samoli, P. Fischer, M. Nieuwenhuijsen, P. Vineis, W. W. Xun, K. Katsouyanni, K. Dimakopoulou, A. Oudin, B. Forsberg, L. Modig, A. S. Havulinna, T. Lanki, A. Turunen, B. Oftedal, W. Nystad, P. Nafstad, U. D. Faire, N. L. Pedersen, C.-G. Östenson, L. Fratiglioni, J. Penell, M. Korek, G. Pershagen, K. T. Eriksen, K. Overvad, T. Ellermann, M. Eeftens, P. H. Peeters, K. Meliefste, M. Wang, B. Bueno-de-Mesquita, D. Sugiri, U. Krämer, J. Heinrich, K. de Hoogh, T. Key, A. Peters, R. Hampel, H. Concin, G. Nagel, A. Ineichen, E. Schaffner, N. Probst-Hensch, N. Künzli, C. Schindler, T. Schikowski, M. Adam, H. Phuleria, A. Vilier, F. Clavel-Chapelon, C. Declercq, S. Grioni, V. Krogh, M.-Y. Tsai, F. Ricceri, C. Sacerdote, C. Galassi, E. Migliore, A. Ranzi, G. Cesaroni, C. Badaloni, F. Forastiere, I. Tamayo, P. Amiano, M. Dorronsoro, M. Katsoulis, A. Trichopoulou, B. Brunekreef, and G. Hoek, *Effects of long-term exposure to air pollution on natural-cause mortality: An analysis*

of 22 European cohorts within the multicentre ESCAPE project, The Lancet **383**, 785 (2014).

[113] M. Stafoggia, B. Oftedal, J. Chen, S. Rodopoulou, M. Renzi, R. W. Atkinson, M. Bauwelinck, J. O. Klompmaker, A. Mehta, D. Vienneau, Z. J. Andersen, T. Bellander, J. Brandt, G. Cesaroni, K. de Hoogh, D. Fecht, J. Gulliver, O. Hertel, B. Hoffmann, U. A. Hvidtfeldt, K.-H. Jöckel, J. T. Jørgensen, K. Katsouyanni, M. Ketzel, D. T. Kristoffersen, A. Lager, K. Leander, S. Liu, P. L. S. Ljungman, G. Nagel, G. Pershagen, A. Peters, O. Raaschou-Nielsen, D. Rizzuto, S. Schramm, P. E. Schwarze, G. Severi, T. Sigsgaard, M. Strak, Y. T. van der Schouw, M. Verschuren, G. Weinmayr, K. Wolf, E. Zitt, E. Samoli, F. Forastiere, B. Brunekreef, G. Hoek, and N. A. H. Janssen, *Long-term exposure to low ambient air pollution concentrations and mortality among 28 million people: Results from seven large European cohorts within the ELAPSE project,* The Lancet Planetary Health **6**, e9 (2022).

[114] R. Burnett, H. Chen, M. Szyszkowicz, N. Fann, B. Hubbell, C. A. Pope, J. S. Apte, M. Brauer, A. Cohen, S. Weichenthal, J. Coggins, Q. Di, B. Brunekreef, J. Frostad, S. S. Lim, H. Kan, K. D. Walker, G. D. Thurston, R. B. Hayes, C. C. Lim, M. C. Turner, M. Jerrett, D. Krewski, S. M. Gapstur, W. R. Diver, B. Ostro, D. Goldberg, D. L. Crouse, R. V. Martin, P. Peters, L. Pinault, M. Tjepkema, A. van Donkelaar, P. J. Villeneuve, A. B. Miller, P. Yin, M. Zhou, L. Wang, N. A. H. Janssen, M. Marra, R. W. Atkinson, H. Tsang, T. Quoc Thach, J. B. Cannon, R. T. Allen, J. E. Hart, F. Laden, G. Cesaroni, F. Forastiere, G. Weinmayr, A. Jaensch, G. Nagel, H. Concin, and J. V. Spadaro, *Global estimates of mortality associated with long-term exposure to outdoor fine particulate matter,* Proceedings of the National Academy of Sciences **115**, 9592 (2018).

[115] Q. Di, Y. Wang, A. Zanobetti, Y. Wang, P. Koutrakis, C. Choirat, F. Dominici, and J. D. Schwartz, *Air Pollution and Mortality in the Medicare Population,* New England Journal of Medicine **376**, 2513 (2017).

[116] J. Chen and G. Hoek, *Long-term exposure to PM and all-cause and cause-specific mortality: A systematic review and meta-analysis,* Environment International **143**, 105974 (2020).

[117] P. Huangfu and R. Atkinson, *Long-term exposure to NO_2 and O_3 and all-cause and respiratory mortality: A systematic review and meta-analysis,* Environment International **144**, 105998 (2020).

[118] K. Kuklinska, L. Wolska, and J. Namiesnik, *Air quality policy in the U.S. and the EU – a review,* Atmospheric Pollution Research **6**, 129 (2015).

[119] H. Boogaard, Z. J. Andersen, B. Brunekreef, F. Forastiere, B. Forsberg, G. Hoek, M. Krzyzanowski, E. Malmqvist, M. Nieuwenhuijsen, and B. Hoffmann, *Clean air in Europe for all,* Environmental Epidemiology **7**, e245 (2023).

[120] L. J. Stal, *Nitrogen Fixation in Cyanobacteria,* eLS , 1 (2015).

[121] M. M. M. Kuypers, H. K. Marchant, and B. Kartal, *The microbial nitrogen-cycling network,* Nature Reviews Microbiology **16**, 263 (2018).

[122] J. N. Galloway, F. J. Dentener, D. G. Capone, E. W. Boyer, R. W. Howarth, S. P. Seitzinger, G. P. Asner, C. C. Cleveland, P. A. Green, E. A. Holland, D. M. Karl, A. F. Michaels, J. H. Porter, A. R. Townsend, and C. J. Vörösmarty, *Nitrogen Cycles: Past, Present, and Future,* Biogeochemistry **70**, 153 (2004).

[123] J. W. Erisman, M. A. Sutton, J. Galloway, Z. Klimont, and W. Winiwarter, *How a century of ammonia synthesis changed the world,* Nature Geoscience **1**, 636 (2008).

[124] FAO, *World Fertilizer Trends and Outlook to 2022*, Tech. Rep. (FAO, Rome, 2019).

[125] OECD/FAO, *OECD-FAO Agricultural Outlook 2019-2028*, OECD-FAO Agricultural Outlook (OECD Publishing, Paris / Food and Agriculture Organization of the United Nations, Rome, 2019).

[126] International Energy Agency, *Ammonia Technology Roadmap: Towards More Sustainable Nitrogen Fertiliser Production* (OECD, 2021).

[127] D. Tian and S. Niu, *A global analysis of soil acidification caused by nitrogen addition,* Environmental Research Letters **10**, 024019 (2015).

[128] R. Bobbink, K. Hicks, J. Galloway, T. Spranger, R. Alkemade, M. Ashmore, M. Bustamante, S. Cinderby, E. Davidson, F. Dentener, B. Emmett, J.-W. Erisman, M. Fenn, F. Gilliam, A. Nordin, L. Pardo, and W. De Vries, *Global assessment of nitrogen deposition effects on terrestrial plant diversity: A synthesis,* Ecological Applications **20**, 30 (2010).

[129] M. H. Ward, R. R. Jones, J. D. Brender, T. M. De Kok, P. J. Weyer, B. T. Nolan, C. M. Villanueva, and S. G. Van Breda, *Drinking Water Nitrate and Human Health: An Updated Review,* International Journal of Environmental Research and Public Health **15**, 1557 (2018).

[130] V. H. Smith and D. W. Schindler, *Eutrophication science: Where do we go from here?* Trends in Ecology & Evolution **24**, 201 (2009).

[131] R. J. Diaz and R. Rosenberg, *Spreading Dead Zones and Consequences for Marine Ecosystems,* Science **321**, 926 (2008).

[132] D. Breitburg, L. A. Levin, A. Oschlies, M. Grégoire, F. P. Chavez, D. J. Conley, V. Garçon, D. Gilbert, D. Gutiérrez, K. Isensee, G. S. Jacinto, K. E. Limburg, I. Montes, S. W. A. Naqvi, G. C. Pitcher, N. N. Rabalais, M. R. Roman, K. A. Rose, B. A. Seibel, M. Telszewski, M. Yasuhara, and J. Zhang, *Declining oxygen in the global ocean and coastal waters,* Science **359**, eaam7240 (2018).

[133] T. C. Malone and A. Newton, *The Globalization of Cultural Eutrophication in the Coastal Ocean: Causes and Consequences,* Frontiers in Marine Science **7** (2020), 10.3389/fmars.2020.00670.

[134] J. Canadell, P. Monteiro, M. Costa, L. Cotrim da Cunha, P. Cox, A. Eliseev, S. Henson, M. Ishii, S. Jaccard, C. Koven, A. Lohila, P. Patra, S. Piao, J. Rogelj, S. Syampungani, S. Zaehle, and K. Zickfeld, *Global Carbon and other Biogeochemical Cycles*

and Feedbacks, in *Climate Change 2021: The Physical Science Basis. Contribution of Working Group I to the Sixth Assessment Report of the Intergovernmental Panel on Climate Change*, edited by V. Masson-Delmotte, P. Zhai, A. Pirani, S. Connors, C. Péan, S. Berger, N. Caud, Y. Chen, L. Goldfarb, M. Gomis, M. Huang, K. Leitzell, E. Lonnoy, J. Matthews, T. Maycock, T. Waterfield, O. Yelekçi, R. Yu, and B. Zhou (Cambridge University Press, Cambridge, United Kingdom and New York, NY, USA, 2021) pp. 673–816.

[135] T. J. Griffis, Z. Chen, J. M. Baker, J. D. Wood, D. B. Millet, X. Lee, R. T. Venterea, and P. A. Turner, *Nitrous oxide emissions are enhanced in a warmer and wetter world,* Proceedings of the National Academy of Sciences **114**, 12081 (2017).

[136] J. Nilsson, *Critical Loads for Sulphur and Nitrogen,* in *Air Pollution and Ecosystems*, edited by P. Mathy (Springer Netherlands, Dordrecht, 1988) pp. 85–91.

[137] R. E. Mason, J. M. Craine, N. K. Lany, M. Jonard, S. V. Ollinger, P. M. Groffman, R. W. Fulweiler, J. Angerer, Q. D. Read, P. B. Reich, P. H. Templer, and A. J. Elmore, *Evidence, causes, and consequences of declining nitrogen availability in terrestrial ecosystems,* Science **376**, eabh3767 (2022).

[138] The Council of the European Communities, *Council Directive 91/676/EEC of 12 December 1991 concerning the protection of waters against pollution caused by nitrates from agricultural sources,* (1991).

[139] S. Klages, C. Heidecke, B. Osterburg, J. Bailey, I. Calciu, C. Casey, T. Dalgaard, H. Frick, M. Glavan, K. D'Haene, G. Hofman, I. A. Leitão, N. Surdyk, K. Verloop, and G. Velthof, *Nitrogen Surplus—A Unified Indicator for Water Pollution in Europe?* Water **12**, 1197 (2020).

[140] Q. Zhang, Y. Li, M. Wang, K. Wang, F. Meng, L. Liu, Y. Zhao, L. Ma, Q. Zhu, W. Xu, and F. Zhang, *Atmospheric nitrogen deposition: A review of quantification methods and its spatial pattern derived from the global monitoring networks,* Ecotoxicology and Environmental Safety **216**, 112180 (2021).

[141] J. N. Galloway and E. B. Cowling, *Reflections on 200 years of Nitrogen, 20 years later,* Ambio **50**, 745 (2021).

[142] H. Kanthilanka, T. Ramilan, R. Farquharson, and J. Weerahewa, *Optimal nitrogen fertilizer decisions for rice farming in a cascaded tank system in Sri Lanka: An analysis using an integrated crop, hydro-nutrient and economic model,* Agricultural Systems **207**, 103628 (2023).

[143] P. Jaramillo, S. Kahn Ribeiro, P. Newman, O. E. Diemuodeke, T. Kajino, D. S. Lee, S. B. Nugroho, X. Ou, A. H. Strømman, and J. Whitehead, *Transport,* in *Climate Change 2022: Mitigation of Climate Change. Contribution of Working Group III to the Sixth Assessment Report of the Intergovernmental Panel on Climate Change* (Cambridge University Press, 2022) pp. Cambridge, UK and New York, NY, USA.

[144] H. Yoshimura, M. Lunter, and M. Habib, *CAEP Report on the Feasibility of a Long-Term Aspirational Goal for International Civil Aviation CO_2 Emissions reductions (LTAG),* in *ICAO Environmental Report 2022* (International Civil Aviation Organization, Montréal, 2022) pp. 379–383.

[145] International Air Transport Association, *IATA Annual Review 2023,* (2023).

[146] S. R. Turns, *An Introduction to Combustion: Concepts and Applications*, 2nd ed., McGraw-Hill Series in Mechanical Engineering (McGraw-Hill, 2000).

[147] H. I. H. Saravanamuttoo, H. Cohen, and G. F. C. Rogers, *Gas Turbine Theory*, 5th ed. (Prentice Hall, Harlow, 2001).

[148] N. Cumpsty, D. Mavris, J. Alonso, F. Catalano, C. Eyers, M. Goutines, T. Grönstedt, D. J. Hileman, A. Joselzon, I. Khaletskii, F. Ogilvie, M. Ralph, D. J. Sabnis, D. R. Wahls, and D. Zingg, *Doc 10127, Independent Expert Integrated Technology Goals Assessment and Review for Engines and Aircraft* (International Civil Aviation Organization, Montréal, 2019).

[149] C. K. Westbrook and F. L. Dryer, *Chemical kinetic modeling of hydrocarbon combustion,* Progress in Energy and Combustion Science **10**, 1 (1984).

[150] P. Glarborg, J. A. Miller, B. Ruscic, and S. J. Klippenstein, *Modeling nitrogen chemistry in combustion,* Progress in Energy and Combustion Science **67**, 31 (2018).

[151] K. Ranasinghe, K. Guan, A. Gardi, and R. Sabatini, *Review of advanced low-emission technologies for sustainable aviation,* Energy **188**, 115945 (2019).

[152] R. McKinney, A. Cheung, W. Sowa, and D. Sepulveda, *The Pratt & Whitney TALON X Low Emissions Combustor: Revolutionary Results with Evolutionary Technology,* in *45th AIAA Aerospace Sciences Meeting and Exhibit*, Aerospace Sciences Meetings (American Institute of Aeronautics and Astronautics, 2007).

[153] M. Foust, D. Thomsen, R. Stickles, C. Cooper, and W. Dodds, *Development of the GE Aviation Low Emissions TAPS Combustor for Next Generation Aircraft Engines,* in *50th AIAA Aerospace Sciences Meeting Including the New Horizons Forum and Aerospace Exposition*, Aerospace Sciences Meetings (American Institute of Aeronautics and Astronautics, Nashville, Tennessee, 2012).

[154] D. Committee, *Standard Specification for Aviation Turbine Fuels,* (2022).

[155] Ministry of Defence, *Turbine Fuel, Kerosene Type, Jet A-1; NATO Code: F-35; Joint Service Designation: AVTUR,* (2019).

[156] J. I. Hileman, P. E. Donohoo, and R. W. Stratton, *Energy Content and Alternative Jet Fuel Viability,* Journal of Propulsion and Power **26**, 1184 (2010).

[157] S. Barrett, M. Prather, J. Penner, H. Selkirk, A. Dopelheuer, G. Fleming, M. Gupta, R. Halthore, J. Hileman, M. Jacobson, S. Kuhn, R. Miake-Lye, A. Petzold, C. Roof,

U. Schumann, I. Waitz, and R. Wayson, *Guidance on the Use of AEDT Gridded Aircraft Emissions in Atmospheric Models*, Tech. Rep. (Federal Aviation Administration, Washington, DC, 2010).

[158] Z. Z. Kapadia, D. V. Spracklen, S. R. Arnold, D. J. Borman, G. W. Mann, K. J. Pringle, S. A. Monks, C. L. Reddington, F. Benduhn, A. Rap, C. E. Scott, E. W. Butt, and M. Yoshioka, *Impacts of aviation fuel sulfur content on climate and human health,* Atmospheric Chemistry and Physics **16**, 10521 (2016).

[159] P. Lobo, L. Rye, P. I. Williams, S. Christie, I. Uryga-Bugajska, C. W. Wilson, D. E. Hagen, P. D. Whitefield, S. Blakey, H. Coe, D. Raper, and M. Pourkashanian, *Impact of Alternative Fuels on Emissions Characteristics of a Gas Turbine Engine – Part 1: Gaseous and Particulate Matter Emissions,* Environmental Science & Technology **46**, 10805 (2012).

[160] L. Durdina, B. T. Brem, M. Elser, D. Schönenberger, F. Siegerist, and J. G. Anet, *Reduction of Nonvolatile Particulate Matter Emissions of a Commercial Turbofan Engine at the Ground Level from the Use of a Sustainable Aviation Fuel Blend,* Environmental Science & Technology (2021), 10.1021/acs.est.1c04744.

[161] H. Xu, Q. Fu, Y. Yu, Q. Liu, J. Pan, J. Cheng, Z. Wang, and L. Liu, *Quantifying aircraft emissions of Shanghai Pudong International Airport with aircraft ground operational data,* Environmental Pollution **261**, 114115 (2020).

[162] A. M. Starik, A. M. Savel'ev, N. S. Titova, and U. Schumann, *Modeling of sulfur gases and chemiions in aircraft engines,* Aerospace Science and Technology **6**, 63 (2002).

[163] M. T. Timko, T. B. Onasch, M. J. Northway, J. T. Jayne, M. R. Canagaratna, S. C. Herndon, E. C. Wood, R. C. Miake-Lye, and W. B. Knighton, *Gas Turbine Engine Emissions—Part II: Chemical Properties of Particulate Matter,* Journal of Engineering for Gas Turbines and Power **132**, 061505 (2010).

[164] A. Kiendler and F. Arnold, *Unambiguous identification and measurement of sulfuric acid cluster chemiions in aircraft jet engine exhaust,* Atmospheric Environment **36**, 1757 (2002).

[165] C. W. Wilson, A. Petzold, S. Nyeki, U. Schumann, and R. Zellner, *Measurement and prediction of emissions of aerosols and gaseous precursors from gas turbine engines (PartEmis): An overview,* Aerospace Science and Technology **8**, 131 (2004).

[166] T. Jurkat, C. Voigt, F. Arnold, H. Schlager, J. Kleffmann, H. Aufmhoff, D. Schäuble, M. Schaefer, and U. Schumann, *Measurements of HONO, NO, NO_y and SO_2 in aircraft exhaust plumes at cruise,* Geophysical Research Letters **38** (2011), 10.1029/2011GL046884.

[167] P. Lobo, L. Durdina, G. J. Smallwood, T. Rindlisbacher, F. Siegerist, E. A. Black, Z. Yu, A. A. Mensah, D. E. Hagen, R. C. Miake-Lye, K. A. Thomson, B. T. Brem, J. C. Corbin, M. Abegglen, B. Sierau, P. D. Whitefield, and J. Wang, *Measurement of Aircraft*

Engine Non-Volatile PM Emissions: Results of the Aviation-Particle Regulatory Instrumentation Demonstration Experiment (A-PRIDE) 4 Campaign, Aerosol Science and Technology **49**, 472 (2015).

[168] T. Schripp, B. E. Anderson, U. Bauder, B. Rauch, J. C. Corbin, G. J. Smallwood, P. Lobo, E. C. Crosbie, M. A. Shook, R. C. Miake-Lye, Z. Yu, A. Freedman, P. D. Whitefield, C. E. Robinson, S. L. Achterberg, M. Köhler, P. Oßwald, T. Grein, D. Sauer, C. Voigt, H. Schlager, and P. LeClercq, *Aircraft engine particulate matter emissions from sustainable aviation fuels: Results from ground-based measurements during the NASA/DLR campaign ECLIF2/ND-MAX,* Fuel **325**, 124764 (2022).

[169] International Civil Aviation Organization, *ICAO Aircraft Engine Emissions Databank,* (2021).

[170] R. E. George, J. A. Verssen, and R. L. Chass, *Jet Aircraft: A Growing Pollution Source,* Journal of the Air Pollution Control Association **19**, 847 (1969).

[171] S. D. Jacob and T. Rindlisbacher, *The Landing and Take-Off Particulate Matter Standards for Aircraft Gas Turbine Engines,* in *ICAO Environmental Report 2019: Aviation and Environment – Destination Green the Next Chapter* (International Civil Aviation Organization, Montréal, 2019) pp. 100–105.

[172] P. Lobo, P. D. Whitefield, and D. E. Hagen, *Measuring PM Emissions from Aircraft Auxiliary Power Units, Tires, and Brakes*, Tech. Rep. ACRP Report 97 (National Academies of Sciences, Engineering, and Medicine, Washington, D.C., 2013).

[173] Airport Authority Hong Kong, *Expansion of Hong Kong International Airport into a Three-Runway System, Environmental Impact Assessment Report (Final)*, Tech. Rep. (Airport Authority Hong Kong, 2014).

[174] M. Winther, U. Kousgaard, T. Ellermann, A. Massling, J. K. Nøjgaard, and M. Ketzel, *Emissions of NO_x, particle mass and particle numbers from aircraft main engines, APU's and handling equipment at Copenhagen Airport,* Atmospheric Environment **100**, 218 (2015).

[175] C. Xiong, V. Beckmann, and R. Tan, *Effects of Infrastructure on Land Use and Land Cover Change (LUCC): The Case of Hangzhou International Airport, China,* Sustainability **10**, 2013 (2018).

[176] B. W. Kolosz, Y. Luo, B. Xu, M. M. Maroto-Valer, and J. M. Andresen, *Life cycle environmental analysis of 'drop in' alternative aviation fuels: A review,* Sustainable Energy & Fuels **4**, 3229 (2020).

[177] L. Jing, H. M. El-Houjeiri, J.-C. Monfort, J. Littlefield, A. Al-Qahtani, Y. Dixit, R. L. Speth, A. R. Brandt, M. S. Masnadi, H. L. MacLean, W. Peltier, D. Gordon, and J. A. Bergerson, *Understanding variability in petroleum jet fuel life cycle greenhouse gas emissions to inform aviation decarbonization,* Nature Communications **13**, 7853 (2022).

[178] The Royal Society, *Net zero aviation fuels: Resource requirements and environmental impacts : Policy briefing,* (2023).

[179] V. Grewe, *Impact of Lightning on Air Chemistry and Climate,* in *Lightning: Principles, Instruments and Applications: Review of Modern Lightning Research*, edited by H. D. Betz, U. Schumann, and P. Laroche (Springer Netherlands, Dordrecht, 2009) pp. 537–549.

[180] J. H. Kroll, C. L. Heald, C. D. Cappa, D. K. Farmer, J. L. Fry, J. G. Murphy, and A. L. Steiner, *The complex chemical effects of COVID-19 shutdowns on air quality,* Nature Chemistry **12**, 777 (2020).

[181] E. M. Fujita, W. R. Stockwell, D. E. Campbell, R. E. Keislar, and D. R. Lawson, *Evolution of the Magnitude and Spatial Extent of the Weekend Ozone Effect in California's South Coast Air Basin, 1981–2000,* Journal of the Air & Waste Management Association **53**, 802 (2003).

[182] H. Slaper, G. Velders, J. Daniel, F. De Gruijl, and J. Van der Leun, *Estimates of ozone depletion and skin cancer incidence to examine the Vienna Convention achievements,* Nature **384**, 256 (1996).

[183] V. Grewe, A. Stenke, M. Ponater, R. Sausen, G. Pitari, D. Iachetti, H. Rogers, O. Dessens, J. Pyle, I. S. A. Isaksen, L. Gulstad, O. A. Søvde, C. Marizy, and E. Pascuillo, *Climate impact of supersonic air traffic: An approach to optimize a potential future supersonic fleet – results from the EU-project SCENIC,* Atmospheric Chemistry and Physics **7**, 5129 (2007).

[184] J. Zhang, D. Wuebbles, D. Kinnison, and S. L. Baughcum, *Stratospheric Ozone and Climate Forcing Sensitivity to Cruise Altitudes for Fleets of Potential Supersonic Transport Aircraft,* Journal of Geophysical Research: Atmospheres **126**, e2021JD034971 (2021).

[185] S. D. Eastham, T. Fritz, I. Sanz-Morère, P. Prashanth, F. Allroggen, R. G. Prinn, R. L. Speth, and S. R. H. Barrett, *Impacts of a near-future supersonic aircraft fleet on atmospheric composition and climate,* Environmental Science: Atmospheres **2**, 388 (2022).

[186] C. Ye, K. Lu, H. Song, Y. Mu, J. Chen, and Y. Zhang, *A critical review of sulfate aerosol formation mechanisms during winter polluted periods,* Journal of Environmental Sciences **123**, 387 (2023).

[187] P. Prashanth, S. D. Eastham, R. L. Speth, and S. R. H. Barrett, *Aerosol formation pathways from aviation emissions,* Environmental Research Communications **4**, 021002 (2022).

[188] A. S. Ansari and S. N. Pandis, *Response of Inorganic PM to Precursor Concentrations,* Environmental Science & Technology **32**, 2706 (1998).

[189] F. Paulot, P. Ginoux, W. F. Cooke, L. J. Donner, S. Fan, M.-Y. Lin, J. Mao, V. Naik, and L. W. Horowitz, *Sensitivity of nitrate aerosols to ammonia emissions and to nitrate chemistry: Implications for present and future nitrate optical depth,* Atmospheric Chemistry and Physics **16**, 1459 (2016).

[190] H. Guo, R. Otjes, P. Schlag, A. Kiendler-Scharr, A. Nenes, and R. J. Weber, *Effectiveness of ammonia reduction on control of fine particle nitrate,* Atmospheric Chemistry and Physics **18**, 12241 (2018).

[191] C. Fountoukis and A. Nenes, *ISORROPIA II: A computationally efficient thermodynamic equilibrium model for K^+–Ca^{2+}–Mg^{2+}–NH_4^+–Na^+–SO_4^{2-}–NO_3^-–Cl^-–H_2O aerosols,* Atmospheric Chemistry and Physics **7**, 4639 (2007).

[192] M. Hallquist, J. C. Wenger, U. Baltensperger, Y. Rudich, D. Simpson, M. Claeys, J. Dommen, N. M. Donahue, C. George, A. H. Goldstein, J. F. Hamilton, H. Herrmann, T. Hoffmann, Y. Iinuma, M. Jang, M. E. Jenkin, J. L. Jimenez, A. Kiendler-Scharr, W. Maenhaut, G. McFiggans, T. F. Mentel, A. Monod, A. S. H. Prévôt, J. H. Seinfeld, J. D. Surratt, R. Szmigielski, and J. Wildt, *The formation, properties and impact of secondary organic aerosol: Current and emerging issues,* Atmospheric Chemistry and Physics **9**, 5155 (2009).

[193] M. Glasius and A. H. Goldstein, *Recent Discoveries and Future Challenges in Atmospheric Organic Chemistry,* Environmental Science & Technology **50**, 2754 (2016).

[194] M. Shrivastava, C. D. Cappa, J. Fan, A. H. Goldstein, A. B. Guenther, J. L. Jimenez, C. Kuang, A. Laskin, S. T. Martin, N. L. Ng, T. Petaja, J. R. Pierce, P. J. Rasch, P. Roldin, J. H. Seinfeld, J. Shilling, J. N. Smith, J. A. Thornton, R. Volkamer, J. Wang, D. R. Worsnop, R. A. Zaveri, A. Zelenyuk, and Q. Zhang, *Recent advances in understanding secondary organic aerosol: Implications for global climate forcing,* Reviews of Geophysics **55**, 509 (2017).

[195] C. L. Heald and J. H. Kroll, *The fuel of atmospheric chemistry: Toward a complete description of reactive organic carbon,* Science Advances **6**, eaay8967 (2020).

[196] United Nations Economic Comission for Europe, *1999 Protocol to Abate Acidification, Eutrophication and Ground-level Ozone to the Convention on Long-range Transboundary Air Pollution, as amended on 4 May 2012,* (2013).

[197] F. Dentener, T. Keating, H. Akimoto, N. Pirrone, S. Dutchak, A. Zuber, Convention on Long-range Transboundary Air Pollution, United Nations, and UNECE Task Force on Emission Inventories and Projections, eds., *Hemispheric Transport of Air Pollution 2010: Part A - Ozone and Particulate Matter*, Air Pollution Studies No. no. 17-20 (United Nations, New York; Geneva, 2010).

[198] S. C. Anenberg, J. J. West, A. M. Fiore, D. A. Jaffe, M. J. Prather, D. Bergmann, K. Cuvelier, F. J. Dentener, B. N. Duncan, M. Gauss, P. Hess, J. E. Jonson, A. Lupu, I. A. MacKenzie, E. Marmer, R. J. Park, M. G. Sanderson, M. Schultz, D. T. Shindell, S. Szopa, M. G. Vivanco, O. Wild, and G. Zeng, *Intercontinental Impacts of Ozone Pollution on Human Mortality,* Environmental Science & Technology **43**, 6482 (2009).

[199] S. C. Anenberg, J. J. West, H. Yu, M. Chin, M. Schulz, D. Bergmann, I. Bey, H. Bian, T. Diehl, A. Fiore, P. Hess, E. Marmer, V. Montanaro, R. Park, D. Shindell, T. Takemura, and F. Dentener, *Impacts of intercontinental transport of anthropogenic fine particulate matter on human mortality,* Air Quality, Atmosphere & Health **7**, 369 (2014).

[200] M. G. Sanderson, F. J. Dentener, A. M. Fiore, C. Cuvelier, T. J. Keating, A. Zuber, C. S. Atherton, D. J. Bergmann, T. Diehl, R. M. Doherty, B. N. Duncan, P. Hess, L. W. Horowitz, D. J. Jacob, J.-E. Jonson, J. W. Kaminski, A. Lupu, I. A. MacKenzie, E. Mancini, E. Marmer, R. Park, G. Pitari, M. J. Prather, K. J. Pringle, S. Schroeder, M. G. Schultz, D. T. Shindell, S. Szopa, O. Wild, and P. Wind, *A multi-model study of the hemispheric transport and deposition of oxidised nitrogen,* Geophysical Research Letters **35**, L17815 (2008).

[201] C.-K. Liang, J. J. West, R. A. Silva, H. Bian, M. Chin, Y. Davila, F. J. Dentener, L. Emmons, J. Flemming, G. Folberth, D. Henze, U. Im, J. E. Jonson, T. J. Keating, T. Kucsera, A. Lenzen, M. Lin, M. T. Lund, X. Pan, R. J. Park, R. B. Pierce, T. Sekiya, K. Sudo, and T. Takemura, *HTAP2 multi-model estimates of premature human mortality due to intercontinental transport of air pollution and emission sectors,* Atmospheric Chemistry and Physics **18**, 10497 (2018).

[202] J. L. Neu, T. Flury, G. L. Manney, M. L. Santee, N. J. Livesey, and J. Worden, *Tropospheric ozone variations governed by changes in stratospheric circulation,* Nature Geoscience **7**, 340 (2014).

[203] R. G. Derwent, S. R. Utembe, M. E. Jenkin, and D. E. Shallcross, *Tropospheric ozone production regions and the intercontinental origins of surface ozone over Europe,* Atmospheric Environment **112**, 216 (2015).

[204] J. Maruhashi, V. Grewe, C. Frömming, P. Jöckel, and I. C. Dedoussi, *Transport patterns of global aviation NO_x and their short-term O_3 radiative forcing – a machine learning approach,* Atmospheric Chemistry and Physics **22**, 14253 (2022).

[205] W. W. Verstraeten, J. L. Neu, J. E. Williams, K. W. Bowman, J. R. Worden, and K. F. Boersma, *Rapid increases in tropospheric ozone production and export from China,* Nature Geoscience **8**, 690 (2015).

[206] J. Lin, D. Pan, S. J. Davis, Q. Zhang, K. He, C. Wang, D. G. Streets, D. J. Wuebbles, and D. Guan, *China's international trade and air pollution in the United States,* Proceedings of the National Academy of Sciences **111**, 1736 (2014).

[207] Q. Zhang, X. Jiang, D. Tong, S. J. Davis, H. Zhao, G. Geng, T. Feng, B. Zheng, Z. Lu, D. G. Streets, R. Ni, M. Brauer, A. van Donkelaar, R. V. Martin, H. Huo, Z. Liu, D. Pan, H. Kan, Y. Yan, J. Lin, K. He, and D. Guan, *Transboundary health impacts of transported global air pollution and international trade,* Nature **543**, 705 (2017).

[208] International Civil Aviation Organization, *ICAO 2022 Environmental Report,* (2022).

[209] A. Ashok, I. C. Dedoussi, S. H. Yim, H. Balakrishnan, and S. R. Barrett, *Quantifying the air quality-CO_2 tradeoff potential for airports,* Atmospheric Environment **99**, 546 (2014).

[210] K. Moolchandani, P. Govindaraju, S. Roy, W. A. Crossley, and D. A. DeLaurentis, *Assessing Effects of Aircraft and Fuel Technology Advancement on Select Aviation Environmental Impacts,* Journal of Aircraft **54**, 857 (2017).

[211] C. Grobler, P. J. Wolfe, K. Dasadhikari, I. C. Dedoussi, F. Allroggen, R. L. Speth, S. D. Eastham, A. Agarwal, M. D. Staples, J. Sabnis, and S. R. H. Barrett, *Marginal climate and air quality costs of aviation emissions,* Environmental Research Letters **14**, 114031 (2019).

[212] F. D. A. Quadros, M. Snellen, and I. C. Dedoussi, *Regional sensitivities of air quality and human health impacts to aviation emissions,* Environmental Research Letters **15**, 105013 (2020).

[213] E. Austin, J. Xiang, T. R. Gould, J. H. Shirai, S. Yun, M. G. Yost, T. V. Larson, and E. Seto, *Distinct Ultrafine Particle Profiles Associated with Aircraft and Roadway Traffic,* Environmental Science & Technology **55**, 2847 (2021).

[214] C. Frömming, M. Ponater, K. Dahlmann, V. Grewe, D. S. Lee, and R. Sausen, *Aviation-induced radiative forcing and surface temperature change in dependency of the emission altitude,* Journal of Geophysical Research: Atmospheres **117** (2012), 10.1029/2012JD018204.

[215] S. Matthes, L. Lim, U. Burkhardt, K. Dahlmann, S. Dietmüller, V. Grewe, A. S. Haslerud, J. Hendricks, B. Owen, G. Pitari, M. Righi, and A. Skowron, *Mitigation of Non-CO_2 Aviation's Climate Impact by Changing Cruise Altitudes,* Aerospace **8**, 36 (2021).

[216] A. Skowron, D. S. Lee, and R. R. De León, *The assessment of the impact of aviation NO_x on ozone and other radiative forcing responses – The importance of representing cruise altitudes accurately,* Atmospheric Environment **74**, 159 (2013).

[217] A. Skowron, D. S. Lee, and R. R. De León, *Variation of radiative forcings and global warming potentials from regional aviation NO_x emissions,* Atmospheric Environment **104**, 69 (2015).

[218] V. Grewe, K. Dahlmann, J. Flink, C. Frömming, R. Ghosh, K. Gierens, R. Heller, J. Hendricks, P. Jöckel, S. Kaufmann, K. Kölker, F. Linke, T. Luchkova, B. Lührs, J. Van Manen, S. Matthes, A. Minikin, M. Niklaß, M. Plohr, M. Righi, S. Rosanka, A. Schmitt, U. Schumann, I. Terekhov, S. Unterstrasser, M. Vázquez-Navarro, C. Voigt, K. Wicke, H. Yamashita, A. Zahn, and H. Ziereis, *Mitigating the Climate Impact from Aviation: Achievements and Results of the DLR WeCare Project,* Aerospace **4**, 34 (2017).

[219] B. Lührs, F. Linke, S. Matthes, V. Grewe, and F. Yin, *Climate Impact Mitigation Potential of European Air Traffic in a Weather Situation with Strong Contrail Formation,* Aerospace **8**, 50 (2021).

[220] H. Yamashita, F. Yin, V. Grewe, P. Jöckel, S. Matthes, B. Kern, K. Dahlmann, and C. Frömming, *Analysis of Aircraft Routing Strategies for North Atlantic Flights by Using AirTraf 2.0,* Aerospace **8**, 33 (2021).

[221] G. G. Fleming and I. de Lépinay, *Environmental Trends in Aviation to 2050,* in *ICAO Environmental Report 2019: Aviation and Environment – Destination Green the Next Chapter* (International Civil Aviation Organization, Montréal, 2019) pp. 17–23.

[222] F. D. A. Quadros, M. Snellen, and I. C. Dedoussi, *Recent and Projected Trends in Global Civil Aviation Fleet Average NO_x Emissions Indices,* in *AIAA SCITECH 2022 Forum*, AIAA SciTech Forum (American Institute of Aeronautics and Astronautics, 2021).

[223] V. Grewe, A. Gangoli Rao, T. Grönstedt, C. Xisto, F. Linke, J. Melkert, J. Middel, B. Ohlenforst, S. Blakey, S. Christie, S. Matthes, and K. Dahlmann, *Evaluating the climate impact of aviation emission scenarios towards the Paris agreement including COVID-19 effects,* Nature Communications **12**, 3841 (2021).

[224] International Civil Aviation Organization, *ICAO Long-Term Traffic Forecasts,* (2018).

[225] K. Dube, G. Nhamo, and D. Chikodzi, *COVID-19 pandemic and prospects for recovery of the global aviation industry,* Journal of Air Transport Management **92**, 102022 (2021).

[226] Boeing Commercial Airplanes, *Commercial Market Outlook 2020-2039,* (2020).

[227] A. H. Epstein and S. M. O'Flarity, *Considerations for Reducing Aviation's CO_2 with Aircraft Electric Propulsion,* Journal of Propulsion and Power **35**, 572 (2019).

[228] International Civil Aviation Organization, *Resolution A40-18: Consolidated statement of continuing ICAO policies and practices related to environmental protection - Climate change,* (2019).

[229] ICAO Secretariat, *Introduction to the ICAO Basket of Measures to Mitigate Climate Change,* in *ICAO Environmental Report 2019: Aviation and Environment – Destination Green the Next Chapter* (International Civil Aviation Organization, Montréal, 2019) pp. 111–115.

[230] R. A. Silva, J. J. West, J.-F. Lamarque, D. T. Shindell, W. J. Collins, G. Faluvegi, G. A. Folberth, L. W. Horowitz, T. Nagashima, V. Naik, S. T. Rumbold, K. Sudo, T. Takemura, D. Bergmann, P. Cameron-Smith, R. M. Doherty, B. Josse, I. A. MacKenzie, D. S. Stevenson, and G. Zeng, *Future global mortality from changes in air pollution attributable to climate change,* Nature Climate Change **7**, 647 (2017).

[231] I. C. Dedoussi, *Implications of future atmospheric composition in decision-making for sustainable aviation,* Environmental Research Letters **16**, 031002 (2021).

[232] X. Zhang, X. Chen, and J. Wang, *A number-based inventory of size-resolved black carbon particle emissions by global civil aviation,* Nature Communications **10**, 534 (2019).

[233] S. C. Olsen, D. J. Wuebbles, and B. Owen, *Comparison of global 3-D aviation emissions datasets,* Atmospheric Chemistry and Physics **13**, 429 (2013).

[234] B. Owen, D. S. Lee, and L. Lim, *Flying into the Future: Aviation Emissions Scenarios to 2050,* Environmental Science & Technology **44**, 2255 (2010).

[235] C. J. Eyers, P. Norman, J. Middel, M. Plohr, S. Michot, K. Atkinson, and R. A. Christou, *AERO2k Global Aviation Emissions Inventories for 2002 and 2025*, Tech. Rep. QinetiQ/04/001113 (QinetiQ, Cody Technology Park, Farnborough, Hampshire, GU14 OLX, 2004).

[236] J. Sun, H. Vû, J. Ellerbroek, and J. M. Hoekstra, *pyModeS: Decoding Mode-S Surveillance Data for Open Air Transportation Research,* IEEE Transactions on Intelligent Transportation Systems , 1 (2019).

[237] *Commission Implementing Regulation (EU) 2023/1770 of 12 September 2023 laying down provisions on aircraft equipment required for the use of the Single European Sky airspace and operating rules related to the use of the Single European Sky airspace and repealing Regulation (EC) No 29/2009 and Implementing Regulations (EU) No 1206/2011, (EU) No 1207/2011 and (EU) No 1079/2012,* (2023).

[238] Federal Aviation Administration, *Title 14: Aeronautics and Space. §91.225 Automatic Dependent Surveillance-Broadcast (ADS-B) Out equipment and use.* (2021).

[239] Z. Liu, P. Ciais, Z. Deng, R. Lei, S. J. Davis, S. Feng, B. Zheng, D. Cui, X. Dou, B. Zhu, R. Guo, P. Ke, T. Sun, C. Lu, P. He, Y. Wang, X. Yue, Y. Wang, Y. Lei, H. Zhou, Z. Cai, Y. Wu, R. Guo, T. Han, J. Xue, O. Boucher, E. Boucher, F. Chevallier, K. Tanaka, Y. Wei, H. Zhong, C. Kang, N. Zhang, B. Chen, F. Xi, M. Liu, F.-M. Bréon, Y. Lu, Q. Zhang, D. Guan, P. Gong, D. M. Kammen, K. He, and H. J. Schellnhuber, *Near-real-time monitoring of global CO 2 emissions reveals the effects of the COVID-19 pandemic,* Nature Communications **11**, 5172 (2020).

[240] A. Filippone, B. Parkes, N. Bojdo, and T. Kelly, *Prediction of aircraft engine emissions using ADS-B flight data,* The Aeronautical Journal **125**, 988 (2021).

[241] A. Filippone and B. Parkes, *Evaluation of commuter airplane emissions: A European case study,* Transportation Research Part D: Transport and Environment **98**, 102979 (2021).

[242] B. Wang, J. Li, C. Li, and D. Wu, *A Method for Computing Flight Operation Fuel Burn and Emissions Based on ADS-B Trajectories,* Journal of Aeronautics, Astronautics and Aviation **52**, 183 (2020).

[243] J. Sun and I. Dedoussi, *Evaluation of Aviation Emissions and Environmental Costs in Europe Using OpenSky and OpenAP,* Engineering Proceedings **13**, 5 (2021).

[244] J. Sun, J. M. Hoekstra, and J. Ellerbroek, *OpenAP: An Open-Source Aircraft Performance Model for Air Transportation Studies and Simulations,* Aerospace **7**, 104 (2020).

[245] S. L. Baughcum, S. C. Henderson, and T. G. Tritz, *Scheduled Civil Aircraft Emission Inventories for 1976 and 1984: Database Development and Analysis*, Tech. Rep. NASA CR-4722 (Langley Research Center, Hampton, Virginia, 1996).

[246] S. L. Baughcum, T. G. Tritz, S. C. Henderson, and D. C. Pickett, *Scheduled Civil Aircraft Emission Inventories for 1992: Database Development and Analysis*, Tech. Rep. NASA CR-4700 (Langley Research Center, 1996).

[247] A. Mortlock and R. Van Alstyne, *Military, Charter, Unreported Domestic Traffic and General Aviation 1976, 1984, 1992, and 2015 Emission Scenarios*, Tech. Rep. NASA/CR-1998-207639 (Langley Research Center, Hampton, Virginia, 1998).

[248] D. J. Sutkus, S. L. Baughcum, and D. P. DuBois, *Scheduled Civil Aircraft Emission Inventories for 1999: Database Development and Analysis*, Tech. Rep. NASA CR-2001-211216 (National Aeronautics and Space Administration, Washington, D.C., 2001).

[249] S. C. Henderson, U. K. Wickrama, S. L. Baughcum, J. J. Begin, F. Franco, D. L. Greene, and D. S. Lee, *Aircraft Emissions: Current Inventories and Future Scenarios,* in *Aviation and the Global Atmosphere*, edited by J. E. Penner, D. H. Griggs, J. Dokken, and M. McFarland (Intergovernmental Panel on Climate Change, Cambridge, UK, 1999) pp. 290–331.

[250] B. Y. Kim, G. G. Fleming, J. J. Lee, I. A. Waitz, J.-P. Clarke, S. Balasubramanian, A. Malwitz, K. Klima, M. Locke, C. A. Holsclaw, L. Q. Maurice, and M. L. Gupta, *System for assessing Aviation's Global Emissions (SAGE), Part 1: Model description and inventory results,* Transportation Research Part D: Transport and Environment **12**, 325 (2007).

[251] M. E. Stettler, A. M. Boies, A. Petzold, and S. R. Barrett, *Global Civil Aviation Black Carbon Emissions,* Environmental Science & Technology **47**, 10397 (2013).

[252] J. T. Wilkerson, M. Z. Jacobson, A. Malwitz, S. Balasubramanian, R. Wayson, G. Fleming, A. D. Naiman, and S. K. Lele, *Analysis of emission data from global commercial aviation: 2004 and 2006,* Atmospheric Chemistry and Physics **10**, 6391 (2010).

[253] D. Lee, A. Graham, C. Fichter, L. L. Lim, and D. Dimitriu, *Allocation of International Aviation Emissions from Scheduled Air Traffic – Present Day and Historical (Report 2 of 3)*, Tech. Rep. CATE-2005-3(C)-2 (Centre for Air Transport and the Environment, Manchester, UK, 2005).

[254] TAKS, MVA Consultancy, NLR, QinetiQ, and DLR, *Study on AViation and Economic Modelling (SAVE)*, Tech. Rep. (European Aviation Safety Agency, 2010).

[255] D. K. Wasiuk, M. A. H. Khan, D. E. Shallcross, and M. H. Lowenberg, *A Commercial Aircraft Fuel Burn and Emissions Inventory for 2005–2011,* Atmosphere **7**, 78 (2016).

[256] U.S. Environmental Protection Agency, *EPA Technical Report on Aircraft Emissions Inventory and Stringency Analysis*, Tech. Rep. (U.S. Environmental Protection Agency, Washington, D.C., 2020).

[257] B. Graver, D. Rutherford, and S. Zheng, *CO_2 Emissions from Commercial Aviation: 2013, 2018, and 2019*, Tech. Rep. (International Council on Clean Transportation, Washington, DC, 2020).

[258] K. Seymour, M. Held, G. Georges, and K. Boulouchos, *Fuel Estimation in Air Transportation: Modeling global fuel consumption for commercial aviation,* Transportation Research Part D: Transport and Environment **88**, 102528 (2020).

[259] M. Strohmeier, X. Olive, J. Lübbe, M. Schäfer, and V. Lenders, *Crowdsourced air traffic data from the OpenSky Network 2019–2020,* Earth System Science Data **13**, 357 (2021).

[260] OpenFlights, *Airport and airline data,* https://openflights.org/data.html, accessed 2020-06-19.

[261] OurAirports, *Open data @ OurAirports,* https://ourairports.com/data/, accessed 2021-01-10.

[262] V. Mouillet, *User Manual for the Base of Aircraft Data (BADA) Revision 3.15*, Tech. Rep. EEC Technical/Scientific Report No. 19/03/18-45 (EUROCONTROL Experimental Centre, Brétigny-sur-Orge, France, 2019).

[263] Swiss Federal Office of Civil Aviation (FOCA), *FOCA Aircraft Piston Engine Database,* https://www.bazl.admin.ch/bazl/en/home/fachleute/regulation-und-grundlagen/umwelt/schadstoffemissionen/triebwerkemissionen/zusammenfassender-bericht–anhaenge-und-datenblaetter.html, accessed 2021-05-10.

[264] U.S. Environmental Protection Agency, Office of Air and Radiation, *Procedures for Emission Inventory Preparation - Volume IV: Mobile Sources*, Tech. Rep. EPA420-R-92-009 (U.S. Environmental Protection Agency, 1992).

[265] M. Stettler, S. Eastham, and S. Barrett, *Air quality and public health impacts of UK airports. Part I: Emissions,* Atmospheric Environment **45**, 5415 (2011).

[266] F. D. A. Quadros, M. Snellen, J. Sun, and I. Dedoussi, *openAVEM (Open Aviation Emissions),* 4TU.ResearchData (2022).

[267] J. Watterson, C. Walker, and S. Eggleston, *Revision to the Method of Estimating Emissions from Aircraft in the UK Greenhouse Gas Inventory*, Tech. Rep. netcen/ED47052 (Netcen, 2004).

[268] R. Gelaro, W. McCarty, M. J. Suárez, R. Todling, A. Molod, L. Takacs, C. A. Randles, A. Darmenov, M. G. Bosilovich, R. Reichle, K. Wargan, L. Coy, R. Cullather, C. Draper, S. Akella, V. Buchard, A. Conaty, A. M. da Silva, W. Gu, G.-K. Kim, R. Koster, R. Lucchesi, D. Merkova, J. E. Nielsen, G. Partyka, S. Pawson, W. Putman, M. Rienecker, S. D. Schubert, M. Sienkiewicz, and B. Zhao, *The Modern-Era Retrospective Analysis for Research and Applications, Version 2 (MERRA-2),* Journal of Climate **30**, 5419 (2017).

[269] B. Kim, G. Fleming, S. Balasubramanian, A. Malwitz, J. Lee, J. Ruggiero, I. Waitz, K. Klima, V. Stouffer, D. Long, P. Kostiuk, M. Locke, C. Holsclaw, A. Morales, E. McQueen, and W. Gillete, *System for Assessing Aviation's Global Emissions (SAGE), Version 1.5, Technical Manual*, Tech. Rep. FAA-EE-2005-01 (Federal Aviation Administration, 2005).

[270] A. Agarwal, R. L. Speth, T. M. Fritz, S. D. Jacob, T. Rindlisbacher, R. Iovinelli, B. Owen, R. C. Miake-Lye, J. S. Sabnis, and S. R. H. Barrett, *SCOPE11 Method for Estimating Aircraft Black Carbon Mass and Particle Number Emissions,* Environmental Science & Technology **53**, 1364 (2019).

[271] U.S. Department of Transportation, *Aviation Environmental Design Tool (AEDT), Technical Manual, Version 3d*, Tech. Rep. DOT-VNTSC-FAA-21-06 (U.S. Department of Transportation, March-2021).

[272] J. Peck, O. O. Oluwole, H.-W. Wong, and R. C. Miake-Lye, *An algorithm to estimate aircraft cruise black carbon emissions for use in developing a cruise emissions inventory,* Journal of the Air & Waste Management Association **63**, 367 (2013).

[273] International Air Transport Association, *Airline Industry Economic Performance - April 2021 - Data tables,* (2021).

[274] C. A. Wells, P. D. Williams, N. K. Nichols, D. Kalise, and I. Poll, *Reducing transatlantic flight emissions by fuel-optimised routing,* Environmental Research Letters **16**, 025002 (2021).

[275] V. Mouillet, *Model Accuracy Summary Report for the Base of Aircraft Data (BADA) Revision 3.15*, Tech. Rep. EEC Technical/Scientific Report No. 19/03/18-48 (EUROCONTROL Experimental Centre, 2019).

[276] P. Friedlingstein, M. O'Sullivan, M. W. Jones, R. M. Andrew, J. Hauck, A. Olsen, G. P. Peters, W. Peters, J. Pongratz, S. Sitch, C. Le Quéré, J. G. Canadell, P. Ciais, R. B. Jackson, S. Alin, L. E. O. C. Aragão, A. Arneth, V. Arora, N. R. Bates, M. Becker, A. Benoit-Cattin, H. C. Bittig, L. Bopp, S. Bultan, N. Chandra, F. Chevallier, L. P. Chini, W. Evans, L. Florentie, P. M. Forster, T. Gasser, M. Gehlen, D. Gilfillan, T. Gkritzalis, L. Gregor, N. Gruber, I. Harris, K. Hartung, V. Haverd, R. A. Houghton, T. Ilyina, A. K. Jain, E. Joetzjer, K. Kadono, E. Kato, V. Kitidis, J. I. Korsbakken, P. Landschützer, N. Lefèvre, A. Lenton, S. Lienert, Z. Liu, D. Lombardozzi, G. Marland, N. Metzl, D. R. Munro, J. E. M. S. Nabel, S.-I. Nakaoka, Y. Niwa, K. O'Brien, T. Ono, P. I. Palmer, D. Pierrot, B. Poulter, L. Resplandy, E. Robertson, C. Rödenbeck, J. Schwinger, R. Séférian, I. Skjelvan, A. J. P. Smith, A. J. Sutton, T. Tanhua, P. P. Tans, H. Tian, B. Tilbrook, G. van der Werf, N. Vuichard, A. P. Walker, R. Wanninkhof, A. J. Watson, D. Willis, A. J. Wiltshire, W. Yuan, X. Yue, and S. Zaehle, *Global Carbon Budget 2020,* Earth System Science Data **12**, 3269 (2020).

[277] International Energy Agency, *Oil Information 2020*, Tech. Rep. (International Energy Agency, 2020).

[278] I. A. Waitz, S. P. Lukachko, and J. J. Lee, *Military Aviation and the Environment: Historical Trends and Comparison to Civil Aviation,* Journal of Aircraft **42**, 329 (2005).

[279] A. Ashok, H. Balakrishnan, and S. R. Barrett, *Reducing the air quality and CO_2 climate impacts of taxi and takeoff operations at airports,* Transportation Research Part D: Transport and Environment **54**, 287 (2017).

[280] G. S. Koudis, S. J. Hu, A. Majumdar, R. Jones, and M. E. Stettler, *Airport emissions reductions from reduced thrust takeoff operations,* Transportation Research Part D: Transport and Environment **52**, 15 (2017).

[281] K. G. Kyprianidis and E. Dahlquist, *On the trade-off between aviation NO_x and energy efficiency,* Applied Energy Clean, Efficient and Affordable Energy for a Sustainable Future, **185**, 1506 (2017).

[282] J. P. Abrahamson, J. Zelina, M. G. Andac, and R. L. Vander Wal, *Predictive Model Development for Aviation Black Carbon Mass Emissions from Alternative and Conventional Fuels at Ground and Cruise,* Environmental Science & Technology **50**, 12048 (2016).

[283] International Air Transport Association, *Air Cargo Market Analysis - May 2021,* (2021).

[284] International Air Transport Association, *IATA Annual Review 2020,* (2020).

[285] International Air Transport Association, *Airline Industry Economic Performance - December 2019 - Report,* (2019).

[286] R. Teoh, Z. Engberg, M. Shapiro, L. Dray, and M. Stettler, *A high-resolution Global Aviation emissions Inventory based on ADS-B (GAIA) for 2019–2021,* EGUsphere , 1 (2023).

[287] M. Strohmeier, M. Smith, V. Lenders, and I. Martinovic, *The Real First Class? Inferring Confidential Corporate Mergers and Government Relations from Air Traffic Communication,* in *2018 IEEE European Symposium on Security and Privacy (EuroS P)* (2018) pp. 107–121.

[288] J. Sun, J. M. Hoekstra, and J. Ellerbroek, *Estimating aircraft drag polar using open flight surveillance data and a stochastic total energy model,* Transportation Research Part C: Emerging Technologies **114**, 391 (2020).

[289] European Parliament and the Council of the European Union, *Directive (EU) 2023/958 of the European Parliament and of the Council of 10 May 2023 amending Directive 2003/87/EC as regards aviation's contribution to the Union's economy-wide emission reduction target and the appropriate implementation of a global market-based measure (Text with EEA relevance),* (2023).

[290] V. Grewe, S. Matthes, and K. Dahlmann, *The contribution of aviation NO_x emissions to climate change: Are we ignoring methodological flaws?* Environmental Research Letters **14**, 121003 (2019).

[291] D. S. Lee, M. R. Allen, N. Cumpsty, B. Owen, K. P. Shine, and A. Skowron, *Uncertainties in mitigating aviation non-CO_2 emissions for climate and air quality using hydrocarbon fuels,* Environmental Science: Atmospheres (2023), 10.1039/D3EA00091E.

[292] C. S. Dorbian, P. J. Wolfe, and I. A. Waitz, *Estimating the climate and air quality benefits of aviation fuel and emissions reductions,* Atmospheric Environment **45**, 2750 (2011).

[293] J. J. Berton and M. D. Guynn, *Multi-Objective Optimization of a Turbofan for an Advanced, Single-Aisle Transport,* Journal of Aircraft **48**, 1795 (2011).

[294] J. Faber, D. Greenwood, D. Lee, M. Mann, P. Mendes de Leon, D. Nelissen, B. Owen, M. Ralph, J. Tilston, A. van Velzen, and G. van de Vreede, *Lower NO_x at Higher Altitudes - Policies to Reduce the Climate Impact of Aviation NO_x Emission*, Tech. Rep. 08.7536.32 (CE Delft, Delft, 2008).

[295] C. J. Miller, P. Prashanth, F. Allroggen, C. Grobler, J. S. Sabnis, R. L. Speth, and S. R. H. Barrett, *An environmental cost basis for regulating aviation NO_x emissions,* Environmental Research Communications **4**, 055002 (2022).

[296] S. Arrowsmith, D. S. Lee, B. Owen, J. Faber, L. van Wijngaarden, O. Boucher, A. Celikel, R. Deransy, J. Fuglestvedt, J. Laukia, M. Tronstad Lund, R. Sausen, M. Schaefer, A. Skowron, S. Stromatas, and A. Watt, *Updated Analysis of the Non-CO2 Climate Impacts of Aviation and Potential Policy Measures Pursuant to EU Emissions Trading System Directive Article 30(4)*, Tech. Rep. (European Union Aviation Safety Agency, Cologne, Germany, 2020).

[297] International Civil Aviation Organization, *ICAO Annex 16: Environmental Protection, Volume III – Aeroplane CO_2 Emissions*, 1st ed. (International Civil Aviation Organization, Montréal, 2017).

[298] D. Rutherford, *Fuel Burn of New Commercial Jet Aircraft: 1960 to 2019*, Tech. Rep. (International Council on Clean Transportation, Washington, DC, 2020).

[299] F. D. A. Quadros, M. Snellen, J. Sun, and I. C. Dedoussi, *Global Civil Aviation Emissions Estimates for 2017–2020 Using ADS-B Data,* Journal of Aircraft **59**, 1394 (2022).

[300] International Civil Aviation Organization, *Post-COVID-19 Forecasts Scenarios*, Tech. Rep. (International Civil Aviation Organization, 2021).

[301] International Civil Aviation Organization, *Presentation of 2019 Air Transport Statistical Results,* (2020).

[302] B. Graver and D. Rutherford, *Low-Cost Carriers and U.S. Aviation Emissions Growth, 2005 to 2019*, Tech. Rep. (International Council on Clean Transportation, Washington, DC, 2021).

[303] L. Dray, *An analysis of the impact of aircraft lifecycles on aviation emissions mitigation policies,* Journal of Air Transport Management Selected Papers from the 15th Air Transport Research Society Conference, Sydney, 2011, **28**, 62 (2013).

[304] International Civil Aviation Organization, *Final Report of the Independent Expert Operational Goals Group (IEOGG)*, Tech. Rep. Doc 10021 (International Civil Aviation Organization, Montréal, 2014).

[305] EUROCONTROL, *Network Operations Report 2022*, Tech. Rep. (EUROCONTROL, 2023).

[306] C. J. Hedges, L. L. Sundstrom, J. Navarrete, H. Vagnerova, E. P. Delaney, N. Barnes, J. Correro, A. Purcell, R. R. Hadley, L. A. Krugler, E. C. Lu, A. G. Stash, S. A. Syed, T. Cuddy, W. Gillette, and C. Gerencher, *Alternative Jet Fuels Emissions - Quantification Methods Creation and Validation Report*, Tech. Rep. ACRP 02-80 (Booz Allen Hamilton, McLean, Virginia, 2019).

[307] D. S. Lee, G. Pitari, V. Grewe, K. Gierens, J. E. Penner, A. Petzold, M. J. Prather, U. Schumann, A. Bais, T. Berntsen, D. Iachetti, L. L. Lim, and R. Sausen, *Transport impacts on atmosphere and climate: Aviation,* Atmospheric Environment Transport Impacts on Atmosphere and Climate: The ATTICA Assessment Report, **44**, 4678 (2010).

[308] M. A. Delucchi, J. J. Murphy, and D. R. McCubbin, *The health and visibility cost of air pollution: A comparison of estimation methods,* Journal of Environmental Management **64**, 139 (2002).

[309] E. A. Ainsworth, *Understanding and improving global crop response to ozone pollution,* The Plant Journal **90**, 886 (2017).

[310] M. R. Ashmore, *Assessing the future global impacts of ozone on vegetation,* Plant, Cell and Environment **28**, 949 (2005).

[311] P. J. Wolfe, S. H. Yim, G. Lee, A. Ashok, S. R. Barrett, and I. A. Waitz, *Near-airport distribution of the environmental costs of aviation,* Transport Policy **34**, 102 (2014).

[312] E. M. Leibensperger, L. J. Mickley, D. J. Jacob, and S. R. Barrett, *Intercontinental influence of NO_x and CO emissions on particulate matter air quality,* Atmospheric Environment **45**, 3318 (2011).

[313] M. Woody, B. Haeng Baek, Z. Adelman, M. Omary, Y. Fat Lam, J. Jason West, and S. Arunachalam, *An assessment of Aviation's contribution to current and future fine particulate matter in the United States,* Atmospheric Environment **45**, 3424 (2011).

[314] The International GEOS-Chem User Community, *Geoschem/geos-chem: GEOS-Chem 12.6.1,* (2019).

[315] S. D. Eastham, D. K. Weisenstein, and S. R. H. Barrett, *Development and evaluation of the unified tropospheric–stratospheric chemistry extension (UCX) for the global chemistry-transport model GEOS-Chem,* Atmospheric Environment **89**, 52 (2014).

[316] P. S. Kim, D. J. Jacob, J. A. Fisher, K. Travis, K. Yu, L. Zhu, R. M. Yantosca, M. P. Sulprizio, J. L. Jimenez, P. Campuzano-Jost, K. D. Froyd, J. Liao, J. W. Hair, M. A. Fenn, C. F. Butler, N. L. Wagner, T. D. Gordon, A. Welti, P. O. Wennberg, J. D. Crounse, J. M.

St. Clair, A. P. Teng, D. B. Millet, J. P. Schwarz, M. Z. Markovic, and A. E. Perring, *Sources, seasonality, and trends of southeast US aerosol: An integrated analysis of surface, aircraft, and satellite observations with the GEOS-Chem chemical transport model,* Atmospheric Chemistry and Physics **15**, 10411 (2015).

[317] R. M. Hoesly, S. J. Smith, L. Feng, Z. Klimont, G. Janssens-Maenhout, T. Pitkanen, J. J. Seibert, L. Vu, R. J. Andres, R. M. Bolt, T. C. Bond, L. Dawidowski, N. Kholod, J.-i. Kurokawa, M. Li, L. Liu, Z. Lu, M. C. P. Moura, P. R. O'Rourke, and Q. Zhang, *Historical (1750–2014) anthropogenic emissions of reactive gases and aerosols from the Community Emissions Data System (CEDS),* Geoscientific Model Development **11**, 369 (2018).

[318] A. van Donkelaar, R. V. Martin, W. R. Leaitch, A. M. Macdonald, T. W. Walker, D. G. Streets, Q. Zhang, E. J. Dunlea, J. L. Jimenez, J. E. Dibb, L. G. Huey, R. Weber, and M. O. Andreae, *Analysis of aircraft and satellite measurements from the Intercontinental Chemical Transport Experiment (INTEX-B) to quantify long-range transport of East Asian sulfur to Canada,* Atmos. Chem. Phys. , 16 (2008).

[319] E. A. Marais and C. Wiedinmyer, *Air Quality Impact of Diffuse and Inefficient Combustion Emissions in Africa (DICE-Africa),* Environmental Science & Technology **50**, 10739 (2016).

[320] M. Li, Q. Zhang, D. G. Streets, K. B. He, Y. F. Cheng, L. K. Emmons, H. Huo, S. C. Kang, Z. Lu, M. Shao, H. Su, X. Yu, and Y. Zhang, *Mapping Asian anthropogenic emissions of non-methane volatile organic compounds to multiple chemical mechanisms,* Atmospheric Chemistry and Physics **14**, 5617 (2014).

[321] M. Crippa, D. Guizzardi, M. Muntean, E. Schaaf, F. Dentener, J. A. van Aardenne, S. Monni, U. Doering, J. G. J. Olivier, V. Pagliari, and G. Janssens-Maenhout, *Gridded emissions of air pollutants for the period 1970–2012 within EDGAR v4.3.2,* Earth System Science Data **10**, 1987 (2018).

[322] S. Arunachalam, B. Wang, N. Davis, B. H. Baek, and J. I. Levy, *Effect of chemistry-transport model scale and resolution on population exposure to $PM_{2.5}$ from aircraft emissions during landing and takeoff,* Atmospheric Environment **45**, 3294 (2011).

[323] S. R. H. Barrett, S. H. L. Yim, C. K. Gilmore, L. T. Murray, S. R. Kuhn, A. P. K. Tai, R. M. Yantosca, D. W. Byun, F. Ngan, X. Li, J. I. Levy, A. Ashok, J. Koo, H. M. Wong, O. Dessens, S. Balasubramanian, G. G. Fleming, M. N. Pearlson, C. Wollersheim, R. Malina, S. Arunachalam, F. S. Binkowski, E. M. Leibensperger, D. J. Jacob, J. I. Hileman, and I. A. Waitz, *Public Health, Climate, and Economic Impacts of Desulfurizing Jet Fuel,* Environmental Science & Technology **46**, 4275 (2012).

[324] S. Sillman, *The use of NO_y, H_2O_2, and HNO_3 as indicators for ozone-NO_x-hydrocarbon sensitivity in urban locations,* Journal of Geophysical Research **100**, 14175 (1995).

[325] E. A. Bright, P. R. Coleman, and A. L. King, *LandScan Global 2005,* (2006).

[326] World Health Organization, *Global Health Estimates 2015: Deaths by Cause, Age, Sex, by Country and by Region 2000-2015* (World Health Organization, Geneva, 2016).

[327] Boeing Commercial Airplanes, *Commercial Market Outlook 2019-2038,* (2019).

[328] B. D. Ostro, *Outdoor Air Pollution: Assessing the Environmental Burden of Disease at National and Local Levels* (World Health Organization, Protection of the Human Environment, Geneva, 2004).

[329] G. Hoek, R. M. Krishnan, R. Beelen, A. Peters, B. Ostro, B. Brunekreef, and J. D. Kaufman, *Long-term air pollution exposure and cardio- respiratory mortality: A review,* Environmental Health **12**, 43 (2013).

[330] M. Jerrett, R. T. Burnett, C. A. Pope, K. Ito, G. Thurston, D. Krewski, Y. Shi, E. Calle, and M. Thun, *Long-Term Ozone Exposure and Mortality,* New England Journal of Medicine **360**, 1085 (2009).

[331] J. Holt, N. E. Selin, and S. Solomon, *Changes in Inorganic Fine Particulate Matter Sensitivities to Precursors Due to Large-Scale US Emissions Reductions,* Environmental Science & Technology **49**, 4834 (2015).

[332] I. C. Dedoussi, S. D. Eastham, E. Monier, and S. R. H. Barrett, *Premature mortality related to United States cross-state air pollution,* Nature **578**, 261 (2020).

[333] M. Sharmina, O. Y. Edelenbosch, C. Wilson, R. Freeman, D. E. H. J. Gernaat, P. Gilbert, A. Larkin, E. W. Littleton, M. Traut, D. P. van Vuuren, N. E. Vaughan, F. R. Wood, and C. Le Quéré, *Decarbonising the critical sectors of aviation, shipping, road freight and industry to limit warming to 1.5–2°C,* Climate Policy **21**, 455 (2021).

[334] B. Jones and B. C. O'Neill, *Spatially explicit global population scenarios consistent with the Shared Socioeconomic Pathways,* Environmental Research Letters **11**, 084003 (2016).

[335] S. KC and W. Lutz, *The human core of the shared socioeconomic pathways: Population scenarios by age, sex and level of education for all countries to 2100,* Global Environmental Change **42**, 181 (2017).

[336] L. Feng, S. J. Smith, C. Braun, M. Crippa, M. J. Gidden, R. Hoesly, Z. Klimont, M. van Marle, M. van den Berg, and G. R. van der Werf, *The generation of gridded emissions data for CMIP6,* Geoscientific Model Development **13**, 461 (2020).

[337] Core Writing Team, *Climate Change 2023: Synthesis Report. Contribution of Working Groups I, II and III to the Sixth Assessment Report of the Intergovernmental Panel on Climate Change*, Tech. Rep. (IPCC, Geneva, Switzerland, 2023).

[338] K. M. Bendtsen, E. Bengtsen, A. T. Saber, and U. Vogel, *A review of health effects associated with exposure to jet engine emissions in and around airports,* Environmental Health **20**, 1 (2021).

[339] K. Riley, R. Cook, E. Carr, and B. Manning, *A systematic review of the impact of commercial aircraft activity on air quality near airports,* City and Environment Interactions **11**, 100066 (2021).

[340] M. C. Woody, H. W. Wong, J. J. West, and S. Arunachalam, *Multiscale predictions of aviation-attributable $PM_{2.5}$ for U.S. airports modeled using CMAQ with plume-in-grid and an aircraft-specific 1-D emission model,* Atmospheric Environment **147**, 384 (2016).

[341] L. P. Vennam, W. Vizuete, K. Talgo, M. Omary, F. S. Binkowski, J. Xing, R. Mathur, and S. Arunachalam, *Modeled Full-Flight Aircraft Emissions Impacts on Air Quality and Their Sensitivity to Grid Resolution: Aircraft Emissions Impacts on Surface AQ,* Journal of Geophysical Research: Atmospheres **122**, 13,472 (2017).

[342] J. Zhang, Y. Jiang, Y. Wang, S. Zhang, Y. Wu, S. Wang, C. P. Nielsen, M. B. McElroy, and J. Hao, *Increased Impact of Aviation on Air Quality and Human Health in China,* Environmental Science & Technology (2023), 10.1021/acs.est.3c05821.

[343] M. Z. Jacobson, J. T. Wilkerson, A. D. Naiman, and S. K. Lele, *The effects of aircraft on climate and pollution. Part II: 20-year impacts of exhaust from all commercial aircraft worldwide treated individually at the subgrid scale,* Faraday Discussions **165**, 369 (2013).

[344] H. Lee, S. C. Olsen, D. J. Wuebbles, and D. Youn, *Impacts of aircraft emissions on the air quality near the ground,* Atmospheric Chemistry and Physics **13**, 5505 (2013).

[345] H. Morita, S. Yang, N. Unger, and P. L. Kinney, *Global Health Impacts of Future Aviation Emissions Under Alternative Control Scenarios,* Environmental Science & Technology **48**, 14659 (2014).

[346] D. Phoenix, A. Khodayari, D. Wuebbles, and K. Stewart, *Aviation impact on air quality present day and mid-century simulated in the Community Atmosphere Model (CAM),* Atmospheric Environment **196**, 125 (2019).

[347] M. Righi, J. Hendricks, and S. Brinkop, *The global impact of the transport sectors on the atmospheric aerosol and the resulting climate effects under the Shared Socioeconomic Pathways (SSPs),* Earth System Dynamics **14**, 835 (2023).

[348] K. Riahi, D. P. van Vuuren, E. Kriegler, J. Edmonds, B. C. O'Neill, S. Fujimori, N. Bauer, K. Calvin, R. Dellink, O. Fricko, W. Lutz, A. Popp, J. C. Cuaresma, S. Kc, M. Leimbach, L. Jiang, T. Kram, S. Rao, J. Emmerling, K. Ebi, T. Hasegawa, P. Havlik, F. Humpenöder, L. A. Da Silva, S. Smith, E. Stehfest, V. Bosetti, J. Eom, D. Gernaat, T. Masui, J. Rogelj, J. Strefler, L. Drouet, V. Krey, G. Luderer, M. Harmsen, K. Takahashi, L. Baumstark, J. C. Doelman, M. Kainuma, Z. Klimont, G. Marangoni, H. Lotze-Campen, M. Obersteiner, A. Tabeau, and M. Tavoni, *The Shared Socioeconomic Pathways and their energy, land use, and greenhouse gas emissions implications: An overview,* Global Environmental Change **42**, 153 (2017).

[349] U.S. Environmental Protection Agency and Federal Aviation Administration, *Recommended Best Practice for Quantifying Speciated Organic Gas Emissions from Aircraft Equipped with Turbofan, Turbojet, and Turboprop Engines*, Tech. Rep. EPA-420-R-09-901 (U.S. Environmental Protection Agency, 2009).

[350] The International GEOS-Chem User Community, *Geoschem/GCClassic: GEOS-Chem 13.3.3,* (2021).

[351] L. T. Murray, E. M. Leibensperger, C. Orbe, L. J. Mickley, and M. Sulprizio, *GCAP 2.0: A global 3-D chemical-transport model framework for past, present, and future climate scenarios,* Geoscientific Model Development **14**, 5789 (2021).

[352] B. C. O'Neill, C. Tebaldi, D. P. van Vuuren, V. Eyring, P. Friedlingstein, G. Hurtt, R. Knutti, E. Kriegler, J.-F. Lamarque, J. Lowe, G. A. Meehl, R. Moss, K. Riahi, and B. M. Sanderson, *The Scenario Model Intercomparison Project (ScenarioMIP) for CMIP6,* Geoscientific Model Development **9**, 3461 (2016).

[353] R. L. Miller, G. A. Schmidt, L. S. Nazarenko, S. E. Bauer, M. Kelley, R. Ruedy, G. L. Russell, A. S. Ackerman, I. Aleinov, M. Bauer, R. Bleck, V. Canuto, G. Cesana, Y. Cheng, T. L. Clune, B. I. Cook, C. A. Cruz, A. D. Del Genio, G. S. Elsaesser, G. Faluvegi, N. Y. Kiang, D. Kim, A. A. Lacis, A. Leboissetier, A. N. LeGrande, K. K. Lo, J. Marshall, E. E. Matthews, S. McDermid, K. Mezuman, L. T. Murray, V. Oinas, C. Orbe, C. Pérez García-Pando, J. P. Perlwitz, M. J. Puma, D. Rind, A. Romanou, D. T. Shindell, S. Sun, N. Tausnev, K. Tsigaridis, G. Tselioudis, E. Weng, J. Wu, and M.-S. Yao, *CMIP6 Historical Simulations (1850–2014) With GISS-E2.1,* Journal of Advances in Modeling Earth Systems **13**, e2019MS002034 (2021).

[354] M. Kelley, G. A. Schmidt, L. S. Nazarenko, S. E. Bauer, R. Ruedy, G. L. Russell, A. S. Ackerman, I. Aleinov, M. Bauer, R. Bleck, V. Canuto, G. Cesana, Y. Cheng, T. L. Clune, B. I. Cook, C. A. Cruz, A. D. Del Genio, G. S. Elsaesser, G. Faluvegi, N. Y. Kiang, D. Kim, A. A. Lacis, A. Leboissetier, A. N. LeGrande, K. K. Lo, J. Marshall, E. E. Matthews, S. McDermid, K. Mezuman, R. L. Miller, L. T. Murray, V. Oinas, C. Orbe, C. P. García-Pando, J. P. Perlwitz, M. J. Puma, D. Rind, A. Romanou, D. T. Shindell, S. Sun, N. Tausnev, K. Tsigaridis, G. Tselioudis, E. Weng, J. Wu, and M.-S. Yao, *GISS-E2.1: Configurations and Climatology,* Journal of Advances in Modeling Earth Systems **12**, e2019MS002025 (2020).

[355] R. J. Park, D. J. Jacob, B. D. Field, R. M. Yantosca, and M. Chin, *Natural and transboundary pollution influences on sulfate-nitrate-ammonium aerosols in the United States: Implications for policy,* Journal of Geophysical Research: Atmospheres **109** (2004), 10.1029/2003JD004473.

[356] P. O'Rourke, S. Smith, A. Mott, H. Ahsan, E. Mcduffie, M. Crippa, Z. Klimont, B. Mcdonald, S. Wang, M. Nicholson, R. Hoesly, and L. Feng, *CEDS v_2021_04_21 Gridded emissions data,* (2021).

[357] A. Rose, J. McKee, K. Sims, E. Bright, A. Reith, and M. Urban, *LandScan Global 2019,* (2020).

[358] World Health Organization, *Global Health Estimates 2019: Deaths by Cuase, Age, Sex, by Country and by Region, 2000-2019* (World Health Organization, Geneva, 2020).

[359] C. A. Arter, J. J. Buonocore, C. Moniruzzaman, D. Yang, J. Huang, and S. Arunachalam, *Air quality and health-related impacts of traditional and alternate jet fuels from airport aircraft operations in the U.S.* Environment International **158**, 106958 (2022).

[360] U.S. Environmental Protection Agency, *Integrated Science Assessment for Particulate Matter*, Tech. Rep. EPA/600/R-19/188 (U.S. Environmental Protection Agency, Research Triangle Park, NC, 2019).

[361] A. Mohegh, D. Goldberg, P. Achakulwisut, and S. C. Anenberg, *Sensitivity of estimated NO_2-attributable pediatric asthma incidence to grid resolution and urbanicity,* Environmental Research Letters **16**, 014019 (2020).

[362] S. Szopa, V. Naik, B. Adhikary, P. Artaxo, T. Berntsen, W. D. Collins, S. Fuzzi, L. Gallardo, A. Kiendler-Scharr, Z. Klimont, H. Liao, N. Unger, and P. Zanis, *Short-Lived Climate Forcers,* in *Climate Change 2021: The Physical Science Basis. Contribution of Working Group I to the Sixth Assessment Report of the Intergovernmental Panel on Climate Change* (Cambridge University Press, Cambridge, UK, 2021) pp. 817–922.

[363] H. Fagerli, S. Tsyro, J. E. Jonson, Á. Nyíri, Gauss, D. Simpson, P. Wind, A. Benedictow, H. Klein, A. Mortier, W. Aas, A.-G. Hjellbrekke, S. Solberg, S. M. Platt, K. E. Yttri, K. Tørseth, S. Gaisbauer, K. Mareckova, B. Matthews, S. Schindlbacher, C. Sosa, M. Tista, B. Ullrich, R. Wankmüller, T. Scheuschner, R. Bergström, L. Johanson, J.-P. Jalkanen, S. Metzger, H. A. C. D. van der Gon, J. J. P. Kuenen, A. J. H. Visschedijk, L. Barregård, P. Molnár, and L. Stockfelt, *Transboundary Particulate Matter, Photo-Oxidants, Acidifying and Eutrophying Components*, Tech. Rep. EMEP Report 1/2019 (Meteorologisk institutt (Norwegian Meteorological Institute), 2019).

[364] U. Schumann and H. Huntrieser, *The global lightning-induced nitrogen oxides source,* Atmospheric Chemistry and Physics **7**, 3823 (2007).

[365] B. A. Nault, J. L. Laughner, P. J. Wooldridge, J. D. Crounse, J. Dibb, G. Diskin, J. Peischl, J. R. Podolske, I. B. Pollack, T. B. Ryerson, E. Scheuer, P. O. Wennberg, and R. C. Cohen, *Lightning NO_x Emissions: Reconciling Measured and Modeled Estimates With Updated NO_x Chemistry,* Geophysical Research Letters **44**, 9479 (2017).

[366] C. D. Holmes, T. H. Bertram, K. L. Confer, K. A. Graham, A. C. Ronan, C. K. Wirks, and V. Shah, *The Role of Clouds in the Tropospheric NO_x Cycle: A New Modeling Approach for Cloud Chemistry and Its Global Implications,* Geophysical Research Letters **46**, 4980 (2019).

[367] E. E. McDuffie, D. L. Fibiger, W. P. Dubé, F. Lopez Hilfiker, B. H. Lee, L. Jaeglé, H. Guo, R. J. Weber, J. M. Reeves, A. J. Weinheimer, J. C. Schroder, P. Campuzano-Jost, J. L. Jimenez, J. E. Dibb, P. Veres, C. Ebben, T. L. Sparks, P. J. Wooldridge, R. C. Cohen, T. Campos, S. R. Hall, K. Ullmann, J. M. Roberts, J. A. Thornton, and S. S. Brown, *$ClNO_2$ Yields From Aircraft Measurements During the 2015 WINTER Campaign and*

Critical Evaluation of the Current Parameterization, Journal of Geophysical Research: Atmospheres **123**, 12,994 (2018).

[368] E. E. McDuffie, D. L. Fibiger, W. P. Dubé, F. Lopez-Hilfiker, B. H. Lee, J. A. Thornton, V. Shah, L. Jaeglé, H. Guo, R. J. Weber, J. Michael Reeves, A. J. Weinheimer, J. C. Schroder, P. Campuzano-Jost, J. L. Jimenez, J. E. Dibb, P. Veres, C. Ebben, T. L. Sparks, P. J. Wooldridge, R. C. Cohen, R. S. Hornbrook, E. C. Apel, T. Campos, S. R. Hall, K. Ullmann, and S. S. Brown, *Heterogeneous N_2O_5 Uptake During Winter: Aircraft Measurements During the 2015 WINTER Campaign and Critical Evaluation of Current Parameterizations,* Journal of Geophysical Research: Atmospheres **123**, 4345 (2018).

[369] R. N. C. Latimer and R. V. Martin, *Interpretation of measured aerosol mass scattering efficiency over North America using a chemical transport model,* Atmospheric Chemistry and Physics **19**, 2635 (2019).

[370] V. Shah, D. J. Jacob, J. M. Moch, X. Wang, and S. Zhai, *Global modeling of cloud water acidity, precipitation acidity, and acid inputs to ecosystems,* Atmospheric Chemistry and Physics **20**, 12223 (2020).

[371] M. Chin, R. B. Rood, S.-J. Lin, J.-F. Müller, and A. M. Thompson, *Atmospheric sulfur cycle simulated in the global model GOCART: Model description and global properties,* Journal of Geophysical Research: Atmospheres **105**, 24671 (2000).

[372] H. Liu, D. J. Jacob, I. Bey, and R. M. Yantosca, *Constraints from 210Pb and 7Be on wet deposition and transport in a global three-dimensional chemical tracer model driven by assimilated meteorological fields,* Journal of Geophysical Research: Atmospheres **106**, 12109 (2001).

[373] H. M. Amos, D. J. Jacob, C. D. Holmes, J. A. Fisher, Q. Wang, R. M. Yantosca, E. S. Corbitt, E. Galarneau, A. P. Rutter, M. S. Gustin, A. Steffen, J. J. Schauer, J. A. Graydon, V. L. S. Louis, R. W. Talbot, E. S. Edgerton, Y. Zhang, and E. M. Sunderland, *Gas-particle partitioning of atmospheric Hg(II) and its effect on global mercury deposition,* Atmospheric Chemistry and Physics **12**, 591 (2012).

[374] R. Sander, *Compilation of Henry's law constants (version 4.0) for water as solvent,* Atmospheric Chemistry and Physics **15**, 4399 (2015).

[375] Q. Wang, D. J. Jacob, J. A. Fisher, J. Mao, E. M. Leibensperger, C. C. Carouge, P. Le Sager, Y. Kondo, J. L. Jimenez, M. J. Cubison, and S. J. Doherty, *Sources of carbonaceous aerosols and deposited black carbon in the Arctic in winter-spring: Implications for radiative forcing,* Atmospheric Chemistry and Physics **11**, 12453 (2011).

[376] Q. Wang, D. J. Jacob, J. R. Spackman, A. E. Perring, J. P. Schwarz, N. Moteki, E. A. Marais, C. Ge, J. Wang, and S. R. H. Barrett, *Global budget and radiative forcing of black carbon aerosol: Constraints from pole-to-pole (HIPPO) observations across the Pacific,* Journal of Geophysical Research: Atmospheres **119**, 195 (2014).

[377] M. L. Wesely, *Parameterization of surface resistances to gaseous dry deposition in regional-scale numerical models,* Atmospheric Environment (1967) **23**, 1293 (1989).

[378] Y. Wang, D. J. Jacob, and J. A. Logan, *Global simulation of tropospheric O_3-NO_x -hydrocarbon chemistry: 1. Model formulation,* Journal of Geophysical Research: Atmospheres **103**, 10713 (1998).

[379] L. Zhang, S. Gong, J. Padro, and L. Barrie, *A size-segregated particle dry deposition scheme for an atmospheric aerosol module,* Atmospheric Environment **35**, 549 (2001).

[380] J. A. Fisher, D. J. Jacob, Q. Wang, R. Bahreini, C. C. Carouge, M. J. Cubison, J. E. Dibb, T. Diehl, J. L. Jimenez, E. M. Leibensperger, Z. Lu, M. B. J. Meinders, H. O. T. Pye, P. K. Quinn, S. Sharma, D. G. Streets, A. van Donkelaar, and R. M. Yantosca, *Sources, distribution, and acidity of sulfate–ammonium aerosol in the Arctic in winter–spring,* Atmospheric Environment **45**, 7301 (2011).

[381] E. W. Emerson, A. L. Hodshire, H. M. DeBolt, K. R. Bilsback, J. R. Pierce, G. R. McMeeking, and D. K. Farmer, *Revisiting particle dry deposition and its role in radiative effect estimates,* Proceedings of the National Academy of Sciences **117**, 26076 (2020).

[382] L. Jaeglé, V. Shah, J. A. Thornton, F. D. Lopez-Hilfiker, B. H. Lee, E. E. McDuffie, D. Fibiger, S. S. Brown, P. Veres, T. L. Sparks, C. J. Ebben, P. J. Wooldridge, H. S. Kenagy, R. C. Cohen, A. J. Weinheimer, T. L. Campos, D. D. Montzka, J. P. Digangi, G. M. Wolfe, T. Hanisco, J. C. Schroder, P. Campuzano-Jost, D. A. Day, J. L. Jimenez, A. P. Sullivan, H. Guo, and R. J. Weber, *Nitrogen Oxides Emissions, Chemistry, Deposition, and Export Over the Northeast United States During the WINTER Aircraft Campaign,* Journal of Geophysical Research: Atmospheres **123**, 12,368 (2018).

[383] H. Weng, J. Lin, R. Martin, D. B. Millet, L. Jaeglé, D. Ridley, C. Keller, C. Li, M. Du, and J. Meng, *Global high-resolution emissions of soil NO_x, sea salt aerosols, and biogenic volatile organic compounds,* Scientific Data **7**, 148 (2020).

[384] L. T. Murray, D. J. Jacob, J. A. Logan, R. C. Hudman, and W. J. Koshak, *Optimized regional and interannual variability of lightning in a global chemical transport model constrained by LIS/OTD satellite data,* Journal of Geophysical Research: Atmospheres **117** (2012), 10.1029/2012JD017934.

[385] National Atmospheric Deposition Program, *National Trends Network,* https://nadp.slh.wisc.edu/networks/national-trends-network/, accessed 2022-07-12.

[386] A.-G. Hjellbrekke and A. M. Fjæraa, *Data Report 2005 Acidifying and Eutrophying Compounds and Particulate Matter*, Tech. Rep. EMEP/CCC-Report 1/2007 (EMEP Co-operative Programme for Monitoring and Evaluation of the Long-range Transmission of Air Pollutants in Europe, Kjeller, Norway, 2007).

[387] A.-G. Hjellbrekke, *Data Report 2019 Particulate Matter, Carbonaceous and Inorganic Compounds*, Tech. Rep. EMEP/CCC-Report 1/2021 (EMEP Co-operative Programme for Monitoring and Evaluation of the Long-range Transmission of Air Pollutants in Europe, Kjeller, Norway, 2021).

[388] Network Center for EANET, *Data Report on the Acid Deposition in the East Asian Region 2005*, Tech. Rep. (Acid Deposition Monitoring Network in East Asia (EANET), 2006).

[389] Network Center for EANET, *Data Report 2019*, Tech. Rep. (Acid Deposition Monitoring Network in East Asia (EANET), 2020).

[390] U.S. Environmental Protection Agency, *CASTNET - Download Data,* https://java.epa.gov/castnet/clearsession.do, accessed 2022-07-12.

[391] M. Buchhorn, B. Smets, L. Bertels, B. D. Roo, M. Lesiv, N.-E. Tsendbazar, M. Herold, and S. Fritz, *Copernicus Global Land Service: Land Cover 100m: Collection 3: Epoch 2019: Globe,* (2020).

[392] European Environment Agency, *Natura 2000 End 2019 - Shapefile,* (2020).

[393] M. van Loo, *Quantifying the Impact of Aviation Emissions on Global Nitrogen Deposition*, Ph.D. thesis, Delft University of Technology, Delft (2021).

[394] L. Liu, W. Xu, X. Lu, B. Zhong, Y. Guo, X. Lu, Y. Zhao, W. He, S. Wang, X. Zhang, X. Liu, and P. Vitousek, *Exploring global changes in agricultural ammonia emissions and their contribution to nitrogen deposition since 1980,* Proceedings of the National Academy of Sciences **119**, e2121998119 (2022).

[395] F. Dentener, J. Drevet, J. F. Lamarque, I. Bey, B. Eickhout, A. M. Fiore, D. Hauglustaine, L. W. Horowitz, M. Krol, U. C. Kulshrestha, M. Lawrence, C. Galy-Lacaux, S. Rast, D. Shindell, D. Stevenson, T. Van Noije, C. Atherton, N. Bell, D. Bergman, T. Butler, J. Cofala, B. Collins, R. Doherty, K. Ellingsen, J. Galloway, M. Gauss, V. Montanaro, J. F. Müller, G. Pitari, J. Rodriguez, M. Sanderson, F. Solmon, S. Strahan, M. Schultz, K. Sudo, S. Szopa, and O. Wild, *Nitrogen and sulfur deposition on regional and global scales: A multimodel evaluation,* Global Biogeochemical Cycles **20** (2006), 10.1029/2005GB002672.

[396] L. F. Schulte-Uebbing, A. H. W. Beusen, A. F. Bouwman, and W. de Vries, *From planetary to regional boundaries for agricultural nitrogen pollution,* Nature **610**, 507 (2022).

[397] F. Paulot, D. J. Jacob, and D. K. Henze, *Sources and Processes Contributing to Nitrogen Deposition: An Adjoint Model Analysis Applied to Biodiversity Hotspots Worldwide,* Environmental Science & Technology **47**, 3226 (2013).

[398] Y. Zhao, L. Zhang, Y. Pan, Y. Wang, F. Paulot, and D. K. Henze, *Atmospheric nitrogen deposition to the northwestern Pacific: Seasonal variation and source attribution,* Atmospheric Chemistry and Physics **15**, 10905 (2015).

[399] J. Sun, J. S. Fu, and K. Huang, *Organic nitrates and other oxidized nitrogen compounds contribute significantly to the total nitrogen depositions in the United States,* Proceedings of the National Academy of Sciences **113**, E4433 (2016).

[400] X.-Y. Liu, K. Koba, L. A. Koyama, S. E. Hobbie, M. S. Weiss, Y. Inagaki, G. R. Shaver, A. E. Giblin, S. Hobara, K. J. Nadelhoffer, M. Sommerkorn, E. B. Rastetter, G. W. Kling, J. A. Laundre, Y. Yano, A. Makabe, M. Yano, and C.-Q. Liu, *Nitrate is an important nitrogen source for Arctic tundra plants,* Proceedings of the National Academy of Sciences **115**, 3398 (2018).

[401] M. Kanakidou, S. Myriokefalitakis, and K. Tsigaridis, *Aerosols in atmospheric chemistry and biogeochemical cycles of nutrients,* Environmental Research Letters **13**, 063004 (2018).

[402] Boeing, *Boeing: Commercial,* https://www.boeing.com/commercial/#/orders-deliveries, accessed 2022-01-20.

[403] Airbus, *Orders and deliveries,* https://www.airbus.com/en/products-services/commercial-aircraft/market/orders-and-deliveries, accessed 2022-01-20.

[404] CFM International, *Fleet Statistics,* https://www.cfmaeroengines.com/engines/fleet-statistics/, accessed 2022-01-20.

[405] Planespotters, *Planespotters.net,* http://www.planespotters.net, accessed 2022-01-20.

[406] ICF, *Airbus A330 market update and review,* https://www.icf.com/insights/transportation/airbus-a330-aircraft-analysis, accessed 2022-01-20.

[407] M. Kenney, C. Fowler, M. Ratte, P. Sanford, P. Pringle, C. Sequeira, and N. Didyk, *Aviation Emissions and Air Quality Handbook, Version 3, Update 1*, Tech. Rep. DOT/FAA/AEE/2015-01 (Federal Aviation Administration, 2015).

[408] National Academies of Sciences, Engineering, and Medicine, *Handbook for Evaluating Emissions and Costs of APUs and Alternative Systems* (The National Academies Press, Washington, D.C., 2012) p. 22797.

[409] R. L. Wayson, G. G. Fleming, and R. Iovinelli, *Methodology to Estimate Particulate Matter Emissions from Certified Commercial Aircraft Engines,* Journal of the Air & Waste Management Association **59**, 91 (2009).

[410] T. Reynolds, *Analysis of Lateral Flight Inefficiency in Global Air Traffic Management,* in *The 26th Congress of ICAS and 8th AIAA ATIO* (American Institute of Aeronautics and Astronautics, Anchorage, Alaska, 2008).

[411] United Nations, *UNSD — Methodology, Standard country or area codes for statistical use (M49),* https://unstats.un.org/unsd/methodology/m49/, accessed 2021-07-16.

[412] H. Bian and M. J. Prather, *Fast-J2: Accurate Simulation of Stratospheric Photolysis in Global Chemical Models,* Journal of Atmospheric Chemistry **41**, 281 (2002).

[413] J. Mao, D. J. Jacob, M. J. Evans, J. R. Olson, X. Ren, W. H. Brune, J. M. S. Clair, J. D. Crounse, K. M. Spencer, M. R. Beaver, P. O. Wennberg, M. J. Cubison, J. L. Jimenez, A. Fried, P. Weibring, J. G. Walega, S. R. Hall, A. J. Weinheimer, R. C. Cohen, G. Chen,

J. H. Crawford, C. McNaughton, A. D. Clarke, L. Jaeglé, J. A. Fisher, R. M. Yantosca, P. L. Sager, and C. Carouge, *Chemistry of hydrogen oxide radicals (HO_x) in the Arctic troposphere in spring,* Atmospheric Chemistry and Physics **10**, 5823 (2010).

[414] S. J. Pai, C. L. Heald, J. R. Pierce, S. C. Farina, E. A. Marais, J. L. Jimenez, P. Campuzano-Jost, B. A. Nault, A. M. Middlebrook, H. Coe, J. E. Shilling, R. Bahreini, J. H. Dingle, and K. Vu, *An evaluation of global organic aerosol schemes using airborne observations,* Atmospheric Chemistry and Physics **20**, 2637 (2020).

[415] W. Trivitayanurak, P. J. Adams, D. V. Spracklen, and K. S. Carslaw, *Tropospheric aerosol microphysics simulation with assimilated meteorology: Model description and intermodel comparison,* Atmospheric Chemistry and Physics **8**, 3149 (2008).

[416] F. Yu and G. Luo, *Simulation of particle size distribution with a global aerosol model: Contribution of nucleation to aerosol and CCN number concentrations,* Atmospheric Chemistry and Physics **9**, 7691 (2009).

[417] G. P. Chossière, R. Malina, A. Ashok, I. C. Dedoussi, S. D. Eastham, R. L. Speth, and S. R. H. Barrett, *Public health impacts of excess NO_x emissions from Volkswagen diesel passenger vehicles in Germany,* Environmental Research Letters **12**, 034014 (2017).

[418] X. Jin, A. M. Fiore, L. T. Murray, L. C. Valin, L. N. Lamsal, B. Duncan, K. F. Boersma, I. D. Smedt, G. G. Abad, K. Chance, and G. S. Tonnesen, *Evaluating a Space-Based Indicator of Surface Ozone-NO_x-VOC Sensitivity Over Midlatitude Source Regions and Application to Decadal Trends,* Journal of Geophysical Research: Atmospheres **122**, 10,439 (2017).

[419] Y. Zhao, R. Saleh, G. Saliba, A. A. Presto, T. D. Gordon, G. T. Drozd, A. H. Goldstein, N. M. Donahue, and A. L. Robinson, *Reducing secondary organic aerosol formation from gasoline vehicle exhaust,* Proceedings of the National Academy of Sciences **114**, 6984 (2017).

[420] U.S. Environmental Protection Agency, Office of Air and Radiation, *The Benefits and Costs of the Clean Air Act from 1990 to 2020 - Final Report - Rev. A*, Tech. Rep. (U.S. Environmental Protection Agency, 2011).

[421] D. Krewski, M. Jerrett, R. T. Burnett, R. Ma, E. Hughes, Y. Shi, M. C. Turner, C. A. Pope III, G. Thurston, E. E. Calle, and M. J. Thun, *Extended Follow-Up and Spatial Analysis of the American Cancer Society Study Linking Particulate Air Pollution and Mortality*, Tech. Rep. HEI Research Report 140 (Health Effects Institute, Boston, Mass., U.S.A., 2009).

[422] C. A. Pope, M. Ezzati, J. B. Cannon, R. T. Allen, M. Jerrett, and R. T. Burnett, *Mortality risk and $PM_{2.5}$ air pollution in the USA: An analysis of a national prospective cohort,* Air Quality, Atmosphere & Health **11**, 245 (2018).

Acknowledgments

It is a great lie that a PhD thesis has a single author. Any accomplishments achieved in these years of research are not just mine, but shared by a host of people that contributed—scientifically and otherwise.

I am immensely grateful to my supervisors and (co)promotors, Mirjam and Irene, for believing in me, supporting me along the entire way, always with a positive attitude and ready to offer help whenever needed. I started the project without much previous experience in atmospheric sciences, but their guidance made it for a smooth transition, giving me confidence in the work we have done. I consider both not just good role models for my scientific career, but also great people that inspire me to be a better person all-around. Working with you was a pleasure.

Many thanks also go to *all* my colleagues at ANCE. Among others and in no particular order, I would like to thank: Lisette for the kindness, Kathrin for the companionship, Irina for the cheerfulness, Roberto for the laughs, Bieke for the positivity, Rebekka voor de vertaling, Salil for the enthusiasm, Jurriaan for the Snelius Tech Tips, Anique for the cake recipe, Pratik for the okra, Jin for the pastel de nata, and Colin for showing that it is possible to finish a PhD with more people in your family than you started with. It goes without saying, but the discussions within our group on modeling aviation and air quality are also very appreciated, irrespectively of any eventual food offerings along the way.

During these four years I also had the pleasure to interact with a number of MSc students, including Jeff, Harry, and Lidia. As well as work more closely with Jaime, Marijn, Liesbeth, and Rick. Marijn's work also served as an essential precursor for the study in Chapter 7.

This thesis made heavy use of a number of openly available tools. My work would not have been possible without the GEOS-Chem model and the international community that keeps it at the bleeding edge of scientific knowledge. Likewise, I am grateful to the OpenSky Network and the countless volunteers that maintain it as a transparent resource for the public good. Particular thanks go to Junzi for his efforts in ADS-B processing, which contributed to Chapter 3.

But if the covers of theses had space for another author, mine would certainly read *Joselyn*. Through thick and thin, always by my side during this adventure, sharing all the challenges and joys of moving across continents in search of a better life; thank you for all the love and for the sacrifices you have made which allowed this accomplishment to be a reality. Likewise, no matter how bad a day I had, knowing that Dasi and Aurora were waiting for me at home always made everything alright. Finally, I would like to thank all of my family and friends, in Brazil and elsewhere, for not only putting up with me, but also for shaping me into who I am and getting me to where I stand.

Flávio
Delft, December 2023

Curriculum Vitæ

Flávio Domingos de Azevedo Quadros

1990/03/13 Born in São Paulo, Brazil

Education

2005–2007 Secondary Education
Colégio Albert Sabin
São Paulo, Brazil

2008–2014 Bachelor of Science in Mechanical Engineering
Escola Politécnica da Universidade de São Paulo
São Paulo, Brazil

2015–2018 Master of Science (M.Sc.) in Aeronautical and Mechanical Engineering
Instituto Tecnológico de Aeronáutica
São José dos Campos, Brazil
Thesis: Swirl Injection of Gaseous Oxygen in a Lab-Scale Paraffin Hybrid Rocket Motor
Promotor: Prof. dr. P. T. Lacava

2019–2023 Doctor of Philosophy (Ph.D.) in Aerospace Engineering
Delft University of Technology
Thesis: Global impacts of aircraft emissions on air quality and nitrogen deposition
Promotors: Prof. dr. ir. M. Snellen and Dr. I. C. Dedoussi

Professional Experience

2014–2015	Mechanical Engineer TESIS Engenharia e Gestão de Programas de Qualidade, Meio Ambiente e Inovação São Paulo, Brazil
2013–2014	Trainee in Mechanical Engineering TESIS Engenharia e Gestão de Programas de Qualidade, Meio Ambiente e Inovação São Paulo, Brazil

List of Publications

Peer-reviewed journal articles

6. **F. D. A. Quadros**, R. Nelen, M. Snellen, I. C. Dedoussi, *Global air quality impacts of aviation in 2019 and 2040 under different scenarios*, Manuscript in preparation.

5. N. Bellouin, M. Bickel, U. Burkhardt, Y. Cohen, I. Dedoussi, M. Dollner, J. Fuglestvedt, A. Gettelman, K. Gierens, V. Grewe, J. Hahofer, D. Hauglustaine, J. Hendricks, Z. Kanji, B. Kärcher, M. Krämer, D. Lee, R. R. de Leon, Y. Li, U. Lohmann, M. Lund, J. Maruhashi, S. Matthes, R. Paoli, J. Penner, A. Petzold, J. Quaas, **F. Quadros**, M. Righi, B. Samset, A. Skowron, E. Terrenoire, M. Tesche, S. Unterstrasser, C. Voigt, B. Weinzierl, *Assessment of the uncertainty in the effective radiative forcing of aviation: nitrogen oxide emissions, contrail cirrus formation, and aerosol-cloud interactions*, Manuscript in preparation.

4. **F. D. A. Quadros**, M. van Loo, M. Snellen, I. C. Dedoussi, *Nitrogen deposition from aviation emissions*, Science of The Total Environment **858**, 159855 (2023).

3. **F. D. A. Quadros**, M. Snellen, I. C. Dedoussi, *Global Civil Aviation Emissions Estimates for 2017–2020 Using ADS-B Data*, Journal of Aircraft **59**, 6, 1394–1405 (2022).

2. **F. D. A. Quadros**, M. Snellen, I. C. Dedoussi, *Regional sensitivities of air quality and human health impacts to aviation emissions*, Environmental Research Letters **15**, 10, 105013 (2020).

1. **F. D. A. Quadros**, P. T. Lacava, *Swirl Injection of Gaseous Oxygen in a Lab-Scale Paraffin Hybrid Rocket Motor*, Journal of Propulsion and Power **35**, 5, 896–905 (2019).

Conference papers and presentations

6. **F. D. A. Quadros**, M. Snellen, I. C. Dedoussi, *Present-day and next mid-century estimates of global aviation impacts on air quality*, GCE2: 2nd Regional GEOS-Chem Europe User's Meeting, London, UK, 14–16 Aug 2023.

5. I. C. Dedoussi, **F. D. A. Quadros**, *Modeling aviation's air quality impacts over time in the context of the changing atmospheric composition*, EGU General Assembly 2023, Vienna, Austria, 24–28 Apr 2023, EGU23-14938.

4. **F. D. A. Quadros**, M. Snellen, I. C. Dedoussi, *Global aviation emissions and their air quality impacts in 2019*, TSAS2022: Towards Sustainable Aviation Summit, Toulouse, France, 18–20 Oct 2022.

3. **F. D. A. Quadros**, M. Snellen, I. C. Dedoussi, *Recent and Projected Trends in Global Civil Aviation Fleet Average NO_x Emissions Indices*, AIAA SciTech 2022 Forum, San Diego, CA, USA & Virtual, 3–7 Jan 2022.

2. **F. D. A. Quadros**, M. Snellen, J. Sun, I. C. Dedoussi, *Viability of OpenSky data to estimate global aviation emissions*, 9th OpenSky Symposium, Brussels, Belgium, 18–19 Nov 2021.

1. **F. D. A. Quadros**, M. Snellen, I. C. Dedoussi, *Regional sensitivities of air quality to aviation emissions*, 3rd ECATS Conference, Online, 13–15 Oct 2020.